Fakultät für Maschinenwesen

Lehrstuhl für Carbon Composites

Process Control in Compression Molding of Composites

Paul Bockelmann

Vollständiger Abdruck der von der Fakultät für Maschinenwesen
der Technischen Universität München zur Erlangung des akademischen Grades eines

Doktor-Ingenieurs

genehmigten Dissertation.

<div>

Vorsitzender: Prof. Dr. Carlo L. Bottasso

Prüfer der Dissertation:

          1. Prof. Dr.-Ing. Klaus Drechsler

          2. Prof. Dr.-Ing. Udo Lindemann

</div>

Die Dissertation wurde am 04.11.2016 bei der Technischen Universität München einge-
reicht und durch die Fakultät für Maschinenwesen
am 16.05.2017 angenommen.

Technische Universität München
Fakultät für Maschinenwesen
Lehrstuhl für Carbon Composites
Boltzmannstraße 15
D-85748 Garching bei München

Tel.: + 49 (0) 89 / 289 – 15092
Fax.: + 49 (0) 89 / 289 – 15097
Email: info@lcc.mw.tum.de
Web: www.lcc.mw.tum.de

Acknowledgments

I am deeply indebted to several people who have supported me in the course of crafting this thesis and contributed to its development. I am very grateful to Prof. Klaus Drechsler for his supervision and in particular for providing the freedom to pursue my own goals. He also maintained this attitude when there was a shortage of funding during the early stage of my work. Likewise, Elisabeth Ladstätter and Swen Zaremba allowed for enough rope to hang myself.

The notion of industrial wet compression molding was shaped early by VOITH Composites that briefly collaborated with me in the beginning of my work. For this direction and for his idea of collaboration that put me in the fortunate position to work at the LCC, I am grateful to Dr. Lars Herbeck. The origin of the idea that led to the development of carrier-integrated pressing (CIP) was initially ignited by Daniel Häffelin, during a warm spring day in the courtyard of our university. He consistently motivates me to this day and did everything in his power to find industrial partners for my project. I would also like to thank all of my other colleagues from the institute for showing me the basics of composites and saving me from killing myself in the workshop.

The research of this thesis would not have been conducted if Dekumed and Toyota Boshoku had not agreed to invest into the development of CIP. Namely Robert Meier, Wolfgang Raffelt, Oliver Hierl, Roland Öffner, Daniel Hummel, Michael Belohlavek, Daniel Richter, Tayfun Buzkan and Oliver Kern contributed greatly to the success of our research project. Likewise did the Bavarian Research Foundation, who granted funding for our research project, in particular Reiner Donaubauer and Robert Zitzlsperger. In the project's final stages, Dr. Felix Grimm and Peter Kunzelmann of Infiana supported the industrial validation of CIP by customizing polymer films to our needs - thank you very much.

I would also like to express my gratitude to many colleagues at TUM, LMU and Fraunhofer FIL who always gave a helping hand. In particular, Teresa Huppmann and Vera Seitz for letting me fall in love with their thermoforming machine, Daniel Rumschöttel for repeatedly sneaking in overnight jobs on his 3D-printer, Andrea Hohmann for introducing me to Gabi (several times) and Severin Filser for letting me abuse his wicked fluorescent microscope that usually allows researchers to do important things.

I am particularly indebted to Prof. Amaresh Chakrabarti who let me visit his lab in Bangalore, India and who has taught me invaluable things about how to conduct proper research - he is, by the way, responsible for my obsession to formulate research questions. The Bavarian Research Foundation also made this stay possible (but somehow scrapped the indiviual funding program somewhen afterwards...).

Abstract

Wet compression molding (WCM) of continuous fiber-reinforced composites is an alternative to resin transfer molding (RTM) to produce parts of low complexity and smaller dimensions in high volumes. Despite its benefits of a shorter process chain and fast part curing because of through-thickness impregnation, it has hitherto not been subject to scientific studies. Although it is particularly relevant in all other liquid composite molding processes, there are no insights into matrix flow in WCM.

This thesis hypothesizes from literature of associated processes that matrix flow through fibers and the need to stabilize materials for automation conflicts with matrix pre-application onto the fiber materials. Based on this hypothesis, the thesis proposes a principle solution for spacial separation of matrix and fiber material with storage of the matrix inside cavities of a carrier. From this principle, a process and prototyping tool is designed in which the carrier is an integrative part to improve matrix flow and material stabilization. Hence, the new compression technology is named carrier-integrated pressing (CIP).

Matrix flow in plates produced by WCM and CIP was studied with a newly developed evaluation method that allows to trace the distribution of matrix with fluorescent photography and microscopy. Experiments conducted within design of experiments (DoE) studies lend evidence to the hypothesis of matrix pre-application, matrix flow control and material stabilization. It was found that fluorescent matrix flow was highly heterogeneous in WCM with low initial flow in through-thickness direction. Distribution was much more compact with good control of the flow in CIP. In complex parts, gravity governed matrix dislocation prior to final compression for both processes.

The proposed carrier-integration was validated for parts on an industrial-scale production system designed according to the initial prototype system. The industrial system served as a basis for a life cycle assessment and -costing study, from which it is concluded that despite additional carrier input and higher matrix expense, CIP can compete with WCM and provides the same advantages as WCM compared to RTM. For suitable part geometries, CIP may even reduce costs and CO_2 emissions because draping with the carrier can reduce scrap of fibers.

Kurzfassung

Nasspressen (NP) von endlosfaserverstärkten Kunststoffen ist eine Alternative zum Resin Transfer Molding (RTM), um Bauteile geringerer Komplexität und Größe in großen Stückzahlen herzustellen. Obwohl NP Vorteile einer kürzeren Prozesskette und schneller Bauteilhärtung aufgrund von Tränkung der Fasermatten in Dickenrichtung bietet, wurde dies bisher wissenschaftlich nicht untersucht. Auch wenn der Harzfluss besonders relevant für andere Verfahren dieser Art ist, bestehen kaum Erkenntnisse über Fließvorgänge beim NP.

Gegenstand dieser Arbeit ist die von der Literatur verwandter Verfahren abgeleitete Hypothese, dass der Harzfluss und die für die Automatisierung notwendige Materialstabilisierung mit der Aufbringung des flüssigen Harzes auf das Fasermaterial konfligiert. Darauf basierend wird eine Prinziplösung erarbeitet, die es erlaubt das flüssige Harz von den trockenen Fasern durch einen mit Speicherkaviäten versehenen Träger zu trennen. Ausgehend von dieser Prinziplösung wird ein Produktionsprozess definiert und ein entsprechendes Pressenwerkzeug entworfen. Der Träger spielt hierbei eine entscheidende Rolle, woraus die Bezeichnung der neuen Technologie, trägerintegriertes Pressen (TIP), folgt.

Der Harzfluss bei der Produktion von Plattenlaminaten mittels NP und TIP wurde mit Hilfe einer eigens entwickelten Methode untersucht. Diese ermöglichte es, durch Fluoreszenzfotographie und -mikroskopie die Harzverteilung sichtbar zu machen. Experimente, die im Rahmen von Studien zur Versuchsplanung (DoE) durchgeführt wurden, stützten die Hypothese hinsichtlich des Konflikts zwischen Harzauftrag, Flusskontrolle und Materialstabilisierung. Die Experimente erlaubten Rückschlüsse auf einen hochgradig heterogenen Matrixfluss im NP mit einem geringen Anteil an initialer Tränkung in Dickenrichtung. TIP zeigte hingegen eine kompaktere Fluoreszenzharzverteilung und entsprechende Flusskontrolle durch die Trägerkavitäten. Im Falle von Bauteilen komplexer Geometrie dominierte jedoch die Schwerkraft den Harzfluss kurz vor der finalen Kompaktierung.

Die vorgeschlagene Trägerintegration wurde für ein Demonstratorbauteil auf einem Produktionssystem im Industriemaßstab, welches auf dem initial genutzen Prototypensystem basiert, validiert. Die Industrieanlage diente als Basis für eine Lebenszyklus- und Kostenanalyse, deren Ergebnisse darauf schließen lassen, dass trotz des zusätzlichen Trägermaterials und eines höheren Harzverbrauchs TIP mit NP konkurrieren kann und die gleichen Vorteile gegenüber RTM bietet. Bei geeigneten Bauteilgeometrien könnte TIP sogar Kosten und CO_2-Emissionen reduzieren, da die Drapierung mittels des Trägers Faserverschnitt einspart.

Contents

Nomenclature

Symbol	Unit	Designation
α	–	Degree of cure
α_f	°	Fiber angle
A_m	mm^2	Area of fluorescent matrix
A_{fl}	mm^2	Area of fluorescent phase
A_{roi}	mm^2	Area of region of interest
α	–	Degree of cure
c	w-%	Concentration of fluorescent marker in matrix
η	$mPas$	Viscosity
m_f	g	Mass of fiber stack
φ	–	Fiber volume content
$\vec{K}$	$1/mm$	Permeability
l_{fl}	mm	Edge length of fluorescent phase
p	bar	Pressure
p_c	bar	Maximum pressure inside tool cavity
Q^2	–	Goodness of model prediction
Q_{1b}	–	Fluorescent area ratio on plate bottom
Q_{1t}	–	Fluorescent area ratio on plate top
Q_{2b}	–	Fluorescent edge length ratio on plate bottom
Q_{2t}	–	Fluorescent edge length ratio on plate top
Q_{3b}	–	Fluorescent centroid shift on plate bottom
Q_{3t}	–	Fluorescent centroid shift on plate top
R^2	–	coefficient of determination
S	–	Saturation of HSV color model
$\vec{s}$		Vector between initial and final fluorescent centroid
σ_t	N/mm	Compressive stress
T_g	K	Glass transition temperature
T_{g0}	K	Glass transition temperature of uncured resin
t_h	s	Heating time in tool
t_{pa}	s	Pre-application time of matrix
T_r	°C	Temperature of resin
T_t	°C	Temperature of tool
$\vec{v}$	mm/s	Velocity
V_r	mm^3	Resin volume

V_f	mm^3	Fiber volume
v_p	mm/s	Press velocity
x_f	mm	X-coordinate of centroid of fiber stack
x_m	mm	X-coordinate of centroid of fluorescent matrix
y_f	mm	Y-coordinate of centroid of fiber stack
y_m	mm	Y-coordinate of centroid of fluorescent matrix
Z_i	-	Criteria for objectives of benefit analysis

Abbreviations

Abbreviation	Designation
ADP	Abiotic resource depletion
CFRP	Carbon fiber-reinforced plastic
CCD	Charged-Coupled Device
CIP	Carrier-Integrated Pressing
CMOS	Complementary metal-oxide-semiconductors
FEM	Finite element method
FVC	Fiber volume content
GWP	Global warming potential
LCA	Life cycle assessment
LCC	Life cycle costing
LCI	Life cycle inventory
LCM	Liquid composite molding
NCF	Non-crimp fabric
PFS	process-flow simultion
ROI	Region of interest
RTM	Resin transfer molding
SMC	Sheet molding compound
TC	Technical conflict
TCM	Technical cost modelling
TETP	Terrestrial ecotoxicity potential
TRIZ	Theoriya resheniya izobretatel'skikh zadatch
WCM	Wet compression molding

List of Figures

List of Tables

1 Introduction

If new technologies are developed today, two major drivers shape the design process. Firstly, consumers demand that this technology improves their lifes. And secondly, it should require minimal amounts of resources to do so. Still, data[1] suggest that a country's human development index, which considers gross domestic product, average life expectancy and level of education, is higher for a person that consumes more energy. In contrast, German records show that energy intensity continuously decreases since 1990[2]. To offset energy consumption in the long term, design must couple technological progression of industrialized societies with the pursuit of highest possible sustainability [1, p. 1012]. This is especially important in the field of mobility, as ever more humans travel, goods are shipped and an increasing amount of resources are spent to manufacture and operate the respective means of transportation. In 2012, approximately 28 % of total energy consumed has been used to fuel transport and it is likely that this figure will not change for the next 25 years [2, p. 606]. Thus, mobility is considered as an integrative part on the consumption side of energy use in a system where electrical energy from renewable sources is extracted, stored and utilized [3, p. 26]. Providing the backbone of manufacturing in many countries, the industrial sector, is a major consumer itself [2, p. 606] and will be subject to structural shifts implied by electromobility [4, p. 67]. Besides battery technology, propulsion systems and charging infrastructure, light construction materials are being developed to provide the systemic paradigm shift towards sustainable energy use [4, p. 69]. In particular, anisotropic properties of materials that help to reduce part weight by abolishing slack material and automated manufacturing that is capable to process these materials are needed [5, p. 8].

Traditional structural materials like steel and aluminum are mechanically anisotropical. Both have been considerably improved in recent years along with their processing techniques and design rules [6, p. 129-133]. In fact, products in general are overwhelmingly more often than not made from homogeneous plastics, aluminum or steel, since material behavior is isotropic which makes both engineering and manufacturing easier. However, manufacturing itself is undergoing considerable change. Economies of scope gain momentum and fabrication is increasingly digitized, both of which make production processes more flexible. Furthermore, new materials allow engineers to tailor their products according to multiple needs [7, p. V]. The goal is to industrially process material structures that are environmental-centric and heterogenic in nature [8, p. 4], much like natural structures grown according to external loads, e.g. [9, p. 14] [10, p. 2].

---

[1] Obtained from www.gapminder.com; Last accessed on 05-01-2015.

[2] Obtained from www.bmwi.de; Last accessed on 05-01-2015; energy intensity=primary energy consumption/gross domestic product.

The principle of load-adapted structural design is inherent in fiber composites where fiber filaments are embedded in a stabilizing matrix. Mechanical properties of the resulting material is to a large part determined by length, orientation and degree of waviness of the fibers. These features open up an unparalleled design space where material structure can be conceived according to external loads or other functionalities [11, p. 6-17]. The possibility to piece together a product structure by aligning single fibers offers the designer flexibility to create parts with adapted properties down to their local details.

This design flexibility however is not yet matched by automated manufacturing processes that have long been cultivated for isotropic, homogeneous matter, predominantly based on subtraction. Fiber composite materials on the other hand are ultimately generated along with forming of the respective part they make up and their anisotropic properties influence behavior in production [12, p. 173] [13, p. 5]. Hence, a production process is difficult to control which leads to poor process robustness and automation. The latter, however, is considered a necessity to further industrialize manufacturing of advanced composites. Liquid composite molding (LCM) processes are favored to suit automation by many e.g. [14, p. 493] [15, p. 20] [16, p. 63]. This process family refers to processes in which dry fibrous structure is formed to near net-shape of the final part and impregnated with liquid duroplastic matrix [17, p. 77].

Although LCM technology has been advanced for many years after having been conceived as potentially suitable for mass production of complex parts [17, p. 77], it has only been achieved recently to be used for actual production of higher volumes by BMW [18, p. 39]. The firm started shipping its electric vehicle i3 in late 2013, which features a so-called "life module" made by only two LCM process variants, resin transfer molding (RTM) and wet compression molding (WCM) [19, p. 41].

RTM is a closed-mold variant of LCM in which draping of dry fibers into a so-called preform and its impregnation with liquid resin are subsequent process steps. This separation makes it possible to produce large and complex parts, because the preform can be broken into several less complex sub-preforms. These are then draped and mutually placed into one RTM mold in which they are consolidated into a single composite part by injecting and curing liquid duroplast [20, p. 223]. Despite subsequent steps, draping and impregnation are intertwined, which, in particular for complex parts, renders the process chain complex and unreliable [21, p. 5] [22, p. 564].

The only other industrially realized automated process for continuous fibers, WCM, partially superimposes drape and impregnation. The process is relatively inexpensive but suffers from poor process robustness. As its short and long-fiber equivalent

[23, p. 14], planar continuous dry fiber material is superficially wetted with liquid matrix. The wet stack is then shaped, compacted and cured during one press stroke. Superimposing drape and impregnation impacts production in two ways. Firstly, it helps to reduce mold occupancy time and number of coupled processes [19, p. 43]. Secondly, resin flow impregnates fibers mainly in through-thickness direction, which means the flow path is shortened compared to RTM. Therefore, resin can still permeate dense fiber materials [23, p. 14] and cycle time, which heavily depends on curing time [24, p. 4], can be reduced to under 5 minutes [25, p. 13].

On the downside, simultaneous draping and impregnation prohibits sound control of the matrix flow, which is critical in RTM processing [26, p. 25] [27, p. 439]. Preponed resin application leads to an undefined resin location prior to pressing. During compression, excessive resin atop of the stack, partially dry areas of the fiber material and progressive deformation of the fibers produce a highly heterogeneous permeability distribution within the mold cavity. In line with arguments of adverse permeability heterogeneity due to saturation and drape in LCM, described by [28, p. 985] and [21, p. 59] respectively, poor process robustness and thus, poor part quality are expected.

And indeed, industrially, series manufacturing based on the discussed LCM variants often lacks the robustness and firms generally have a low degree of experience compared to other production processes. Both not only makes economical production difficult but further complicates the product design process [29, p.495-505]. Non-ideal design of parts are the result, e.g. geometrical shapes that induce fiber deflections in draping or quality issues due to inhomogeneous matrix flow.

Given these problems connected with material flow in pressing, an alternative approach is proposed, hereafter referred to as carrier-integrated pressing (CIP). CIP is based on spacial separation of resin and fiber material with storage of the resin in proximity of its final curing location. This functionality shall be provided by a carrier that stores duroplastic matrix in macroscopic cavities and supports fiber material. The cavities collapse during closing of the tool and resin flows from its storage location into the fibers in through-thickness direction. It is hypothesized that this impregnation mechanism allows better flow control compared to WCM.

In order to investigate research questions connected to the proposed process principle, an adequate process, tool and carrier design shall be identified and realized first. Therefore, this thesis draws on the procedural model proposed by Lindemann [30, p. 47], to design a prototype production system based on the process principle. At the core of this design phase lie the following questions:

1.1 How to design a production system based on the proposed principle solution, including carrier material, physical principle of storing resin, tooling and process definition?

1.2 How to eliminate resin storage cavities during pressing to prevent carrier wrinkles?

Using the resulting prototype production system, laminates are pressed which are examined to investigate the flow situations of WCM and CIP processes. Defined portions of processed matrix are marked with fluorescent pigments to trace and quantify the flow of this matrix mass via computerized image segmentation of macrophotographs and micrographs taken under ultraviolet light. Herewith, the following research questions that are immediately associated with the different process principles of WCM and CIP are answered:

2.1 How does matrix flow through fiber material in WCM and CIP?

2.2 How is cavity elimination linked to matrix flow?

2.3 Is a more homogeneous matrix flow in press processes associated with better part quality?

2.4 How does draping disturb matrix flow in WCM and CIP?

To expand the relevance of the designed carrier-integration beyond its prototype status, the CIP process is further validated on an industrial-scale production system. Linked to such an industrial use are balancing questions regarding environmental and cost performance. As described at the outset of this thesis, environmental impacts and costs do play a major role in manufacturing, in particular for energy-intensive material like CFRP. The conceived process, CIP, decreases fiber input and increases matrix input due to the draping mechanism provided by the carrier. Furthermore, carrier material is an additional input into manufacturing compared to WCM and RTM. Thus, the third part of this thesis is dedicated to the following question:

3. How does a composite production based on CIP impact the environment and costs per part compared to RTM and WCM?

Aligned to the research questions, the aggregated content of the document is structured in chapters which form the architecture of the thesis.

Chapter 2 introduces the reader to previous industrial and scientific work on composite processing and material properties. The characteristics of part design, resin flow and fiber draping behavior as well as material properties are discussed. The chapter further outlines why this work is new and relevant to academia and industry.

The purpose and approach of this thesis is outlined in Chapter 3. Important process functions are derived from literature and conflicting requirements with respective functions are discussed. Herewith, a polylemma of conflicts in traditional WCM processes is derived that is used as a framework for the purpose of this thesis and the design phase to conceive an improved process.

A comprehensive description of the systematic design process is given in Chapter 4, in order to define an improved compression molding process and to build a functional prototype of respective production system. The prototype allows to select an appropriate carrier material and to prove that the designated process qualitatively works (research questions 1.1 and 1.2).

Investigation of how matrix flows through fiber material and how this can be controlled in CIP in comparison to WCM (research question 2.1-2.4) is presented in Chapter 5. It first describes the development of the investigation method using a fluorescent tracer and subsequently exhibits results from experimental trials. The chapter closes with the interpretation of results to conclude the associated research questions.

Carrier-use is further investigated on an industrial-scale production system in Chapter 6 in order to expand the validated findings from earlier chapters onto part sizes relevant to the industry.

To shed more light on the question of whether or not environmental impact and costs per part are improved if a CIP-based production for composite parts is run in comparison to WCM and RTM (research question 3), a life cycle analysis (LCA) combined with costing analysis is performed in Chapter 7.

Finally, in Chapter 8, the pieces of initial process design, description of matrix flow and draping as well as environmental and cost potentials of an industrial production line are drawn together in conclusion. Further work is suggested, so that some of the ideas generated in this thesis may be put into practice.

2 The Industrialization of Processes for Advanced Fiber Composites[1]

In this thesis, advanced fiber composites refer to plastics reinforced with fibers that extend through the entire part [32, p. 138]. This material class provides the highest lightweight potential of CFRP and may enter price sensitive markets if an industrialization of production processes is achieved [33, p. 5]. This is difficult because fiber orientation and architecture for continuous fibers are easily disturbed during automated manipulation. Disturbances influence product qualities in two major ways. Firstly, distortion of fibers may degrade the mechanical performance of a composite. Secondly, a subsequent process step, impregnation with liquid resin for instance, can be influenced, which might lead to additional defects. That has not been the case in the past when manual placement of preimpregnated fiber mats, or prepregs, was almost exclusively practiced. Thus, one important obstacle today is to translate material- and process knowledge needed to manually craft a composite part into automated processes. This results in a multiplicity of processes and associated materials that are available now, including thermoplastic matrices and LCM. The latter is preferred for medium to high volume productions due to its relatively low material costs, ability to produce complex geometries and high potential for automation [15, p. 20] [34, p. 3]. The process is divided into two basic steps. The dry fibrous structure is deformed into a threedimensional part shape, generally called draping, and the fibers are impregnated by liquid resin which subsequently cures and stabilizes the embedded fibers. A threedimensional construct of dry fibers, referred to as preform, is often produced before impregnation. It may consist of different materials that were processed with respective automated textile machines. Non-crimp and woven fabrics for shell structures, braids for hollow sections and knits for local reinforcements can be used to tailor the reinforcing fiber structure for LCM in an automated manner.

Due to their relevance for the formation of an CFRP industry, discussion in following sections is limited to LCM processes. The working principles of fiber composites are presented first, where fiber architecture plays an important role. This determines, alongside with the impregnation process used, which semi-finished fiber material is processed. Both, process and semi-finished materials, are discussed in the subsequent section. In that light it is also important to discuss the role of pro-cessing in design of respective LCM parts, since it strongly influences the producibility of parts.

---

[1] Sections 2.1, 2.2 and 2.3 are based on work by the author previously published in [31, p. 877-904] and [29, p. 495-505]

2.1 Principles of Advanced Fiber Composites

Nature routinely composes material properties of one heterogenous material by a combination of multiple homogeneous materials and adapts product form to its loads. Bamboo, for example, is extremely solid, light and flexible because its walls consist of orientated fibers embedded in pulp and form a hollow stem core [9, p. 14]. Similarly, CFRP offer a high stiffness to weight ratio by combining mechanically capable reinforcing fibers with an embedding, stabilizing polymer matrix. The interface between fibers and matrix represents the third component of the composite. Only if the interface is free of defects, mechanical loads can be transferred without propagating cracks and thus the composite can function properly [35, p. 209]. In addition to load transfer, the matrix fixates the fiber's orientation within the composite, protects fibers from environmental conditions and defines a part's outward shape.

Besides benefits for lightweight design, CFRP can be used to tailor specific part functions in regard to its application in ways rivaling materials can not [11, p. 1-6]. For example, composites show a brittle failure due to their fiber reinforcement and, thus, consume more energy compared to metallic parts when used as automobile crash structures. In such cases, crash forces can be adjusted by reinforcement architecture and designed to be constant. Another example is local use of different resin systems within one composite part to combine certain physical properties [36, p. 3]. This and a multiplicity of other properties can be designed by appropriate selection, geometry and processing of fiber reinforcements and matrix systems. Considering mechanical behavior of a part however, the reinforcement plays the biggest role.

2.1.1 Effect and Use of Fiber Reinforcement

The effect of reinforcement of a composite is determined by material characteristics, the amount as well as length, orientation and stretch of fibers. Alongside the part properties desired, available production technology must be considered when fiber material is selected because LCM processing strongly influences the determinants of the reinforcement effect.

Material selection is often driven by a part's strength or stiffness properties in combination with material costs. While low-cost glass fibers are suitable for parts under relatively low load, aramide is very tough and thus appropriate for impact stress. Fibers made out of carbon are among the most expensive materials but offer the highest strength and therefore weight savings. Carbon fibers are available in different quality grades, high modulus, high tenacity and high strength providing

elastic moduli of 50-100 GPa and a maximum tensile strength of 500 MPa [35, p. 43].

The amount of fibers that are embedded in the matrix to form the composite is an important design criterion and is indicated by the fiber volume content φ (FVC). It corresponds to the ratio of fiber volume V_f to the sum of V_r and matrix volume V_f in a laminate according to equation (2-1).

$$\varphi = \frac{V_f}{V_r + V_f} \tag{2-1}$$

The mechanical performance of a laminate increases with higher FVC and a given fiber material and architecture. Geometrically, a maximum FVC of 0,907 is achievable with unidirectional, uniformly stacked carbon fiber laminate [11, p. 2-11]. However, the FVC of physical laminates is considerably lower and is determined by process mechanics, fiber architecture of semi-finished material as well as fiber diameter. In particular automated LCM processes that comprise preforming and impregnation limit FVC to around 0.5 [11, p. 4-27]. Automated preforming depends on good handling properties of the fibers so that the stabilizing mechanism, crossing rovings, stitching or binder, reduces FVC of the preform. Successful impregnation benefits from the reduction, and sometimes depends on it, since the permeability of the preform is increased alongside with it [37, p. 6].

Fiber length is an important parameter in regard to mechanical performance. It is mainly classified in short fibers (0.1-1 mm), long fibers (1-50 mm) and continuous fibers. The latter extend through the entire dimension of the part in the respective fiber direction. With increasing fiber length lower forces have to be redirected between fiber ends by the surrounding matrix. Hence, the matrix, which has a much lower elastic modulus than fibers, is strained less and the composite is stronger. [32, p. 138] [38, p. 165]

This work limits itself mainly on application of continuous fibers as current efforts to advance industrialization in composites focus on these high-performance materials [34, p. 5]. In this regard, the fiber's strong anisotropy of mechanical properties is a major concern. In longitudinal fiber direction, stiffness and strength are much higher than in lateral direction. In fact, accumulated microscopic deviations of fiber orientation lead to a rapid macroscopic degradation of achievable strength (Figure 2-1 A). In combination with a relatively soft polymer matrix, material properties of the entire part are strongly heterogenic depending on the direction considered [11, p. 2-8]. Since mechanical parts are almost always subject to polyaxial loads, fibers within a laminate have to be oriented in multiple directions. This is achieved by stacking multiple plies with different fiber orientation. Hence, it is possible to

generate composite laminates that behave isotropically under loads (Figure 2-1 B). One part may be assembled from stacks of different fiber direction and thus possesses locally varying mechanical properties (Figure 2-1 C).
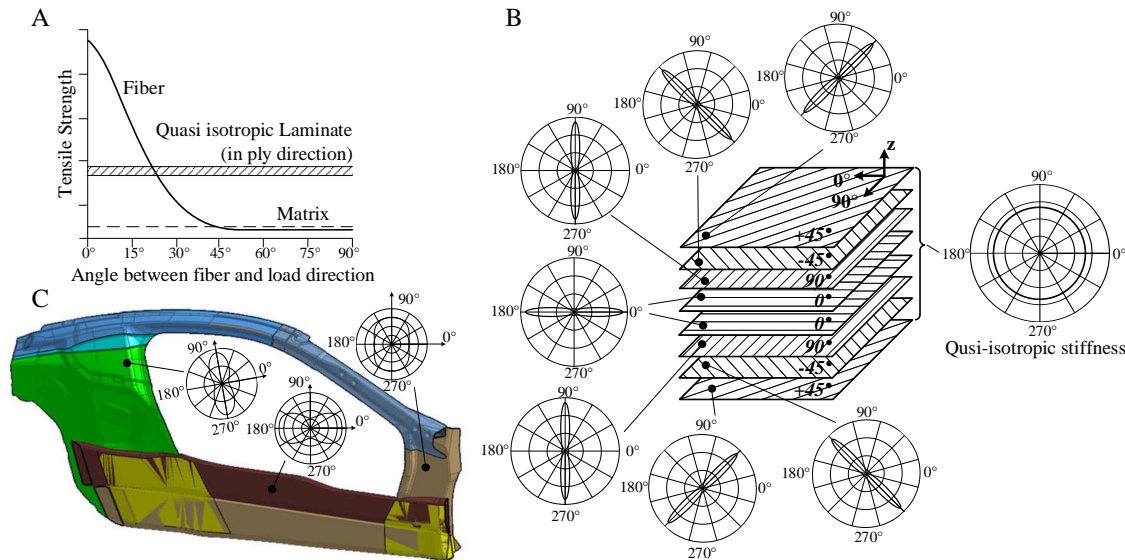
Figure 2-1 Fiber orientation as a design parameter of CFRP parts. Loss of tensile strength under angled loading of fibers (A) (adapted from [35, p. 8]). Resulting stiffness of laminate from addition of stiffnesses of single plies (B). Fiber architecture in sideframe of BMW i8 (C) (adapted from [20, p. 223])

Stiffness of quasi-isotropically reinforced parts (Figure 2-1 B) is independent from the considered part direction, which responds uniformly under load. The biggest drawback in this case is that not the entire potential for lightweight design can be exploited [32, p. 246]. The quasi-isotropic stack is designed according to the highest load, even if it only appears locally. All other part areas provide a higher mechanical performance than necessary for operational loads at the respective part location. Excessive material can be mitigated effectively by local adaption of fiber orientation and amount according to expected loads. Figure 2-1 C, which is supplemented by respective polar diagramms of stiffness, shows a CAD model of BMW i8 sideframe. This part is known to be made from joining multiple small preforms, socalled "sub-preforms", with different fiber directions [20, p. 223]. Besides reduced part weight and improved mechanical behavior, this procedure yields benefits for production by RTM. Smaller, less complex sub-preforms can be automatically draped, whereas one large structure would need manual assistance in production. In addition, part regions can be varied in their macroscopic shape and type of preforming method that best suits mechanical functionality. The A-pillar, for instance, is designed as a hollow part that can be efficiently preformed by braiding [20, p. 223].

Material exploitation can be further promoted by locally adapted laminate thickness induced by reinforcements. Ideally, these parts are thicker along the line of

forces, while part sections apart from these paths are thinner. Respective manufacturing processes are currently inefficient, since material throughput decreases with the need to orientate and position locally adapted fibers [39, p. 14]. Until current efforts in the field, e.g. from Compositence[2] or Cevotec[3], become integrated in a fully-automated production, manufacturing of high part volumes is achieved on expense of material exploitation and, thus, part weight.

2.1.2 Functions and Properties of Polymer Matrices

Although fibers overwhelmingly influence the mechanical performance of composite laminates, general functionality can only be achieved in combination with an appropriate matrix material. Matrices are selected according to their adherence properties with fibers and sizing, toughness in respect to dynamical loads, temperature and chemical resistance, electric properties as well as behavior under time-dependent loads [11, p. 2-17]. On the other hand, processing characteristics are very important for defect-free embedding of fibers into the polymer matrix. In respect to LCM processing, impregnation of dry fibers with liquid resin is described by pressure-induced flow of a viscous, Newton fluid through porous media [28, p. 981]. Darcy's law is considered the basis for any computation of impregnation processes [40], equation (2-2),

$$\vec{v} = -\frac{\vec{K}}{\eta}\nabla P, \tag{2-2}$$

where $\vec{v}$ is the flow velocity, $\vec{K}$ the permeability of the porous media, η the fluid viscosity and ∇P is the pressure difference on the fluid.

Polymers that can be used as a matrix for CFRP materials consist of long-chain macro molecules that are the product from chemical reaction of single molecules (polycondensation, polyaddition and polymerization). Resulting polymers can be classified in three distinct groups thermosets, thermoplastics and elastomers. While thermoset and elastomer plastics irreversibly cure during the chemical reaction, thermoplastic molecules build interlocking loops. Thus, thermoplastic polymers can be reversibly melted and consolidated under heat.

Thermosets are liquid in uncured state in dependence of their uncured glass transition temperature T_{g0} and exothermally cure when mixed with a catalytic hardener under temperature. During this chemical reaction molecules become longer and

---

form fixed junctures. An important parameter for processing is matrix viscosity, which is effected by temperature and by the polymer's current degree of cure α [21, p. 49]. Likewise, temperature also influences curing rate $\dot{\alpha}$. These superimposed effects lead to a parabolic viscosity progression over time (Figure 2-2).
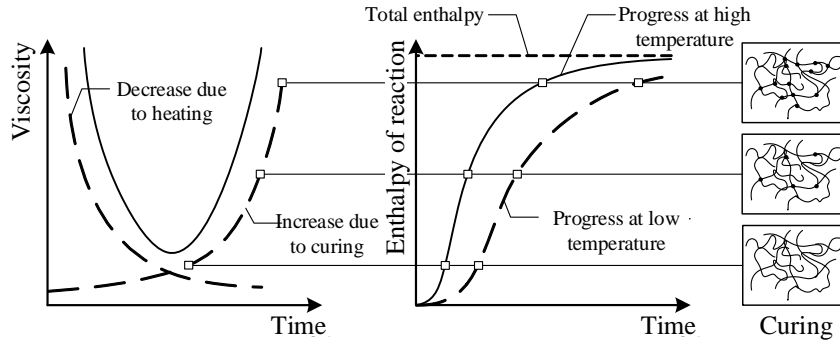
Figure 2-2 Qualitative correlation between viscosity (adapted from [21, p. 49]), enthalpy of reaction and time during curing of thermosets

Enthalpy of reaction is a measure of degree of cure α which by definition reaches one when the maximum enthalpy change has occured within the reactive system [35, p. 80]. The glass transition temperature T_g depends on the degree of cure and is linked to mechanical properties of a polymer [32, p. 100]. Thus, it is an important factor for design of curing progression during production processes as well as an important aspect of matrix selection.

The link between degree of cure, viscosity and temperature and its role in LCM processing becomes apparent when considering Equation (2-2). In order to facilitate processing, the matrix viscosity is to be minimized, which can only be done by increasing the temperature in case of epoxy resins. However, as the matrix curing progresses faster under higher temperatures, it is important to find the point in time when viscosity is relatively low to initiate flow processing. Impregnation must be completed before gel point, which describes the first appearance of a macroscopic molecule with infinite molecular weight [35, p. 76]. Subsequently, the matrix location within the fibrous structure remains the same but curing progresses its T_g until demolding. Thus, the link between impregnation time before gel point and subsequent curing determines cycle time in processing.

Cycle time in LCM can be minimized when impregnation is completed as fast as possible, which is also connected to permeability K of the fibrous structure, Equation(2-2). Permeability of a dry fiber material describes its porosity and therefore the ease with which a protruding fluid can flow through. K mainly depends on fiber architecture, compaction pressure, FVC and state of impregnation [28, p. 988]. These dependencies mean that K changes significantly during processing steps of LCM. For instance, if areal fiber mats like weaves or non-crimp fabrics

are used that are deformed into the three dimensional part geometry, single fibers are spatially shifted and thus permeability is altered [21, p. 5]. Hence, highly heterogenic permeability distributions result, which influence how flow progression during impregnation occures and may ultimately lead to porosities or dry spots [27, p. 438-439].

2.2 Liquid Composite Molding of Advanced Fiber Composites

CFRP as used for mechanical parts are only generated in the primary manufacturing process. Hence, material properties strongly depend on process parameters as well as design of geometry to be produced [12, p. 173] [41, p. 423]. In fact, microscopic quality of LCM parts is often influenced by macroscopic design features, such as radii. This is the case because in LCM draping of dry fiber materials and their impregnation with liquid resin are strongly interlocked. Therefore, it is important to integrate requirements regarding fiber processing and matrix processing during setup of LCM. A multiplicity of process routes regarding application of liquid, thermoset resin exist. The different processes are best classified via their material flow, Figure 2-3.
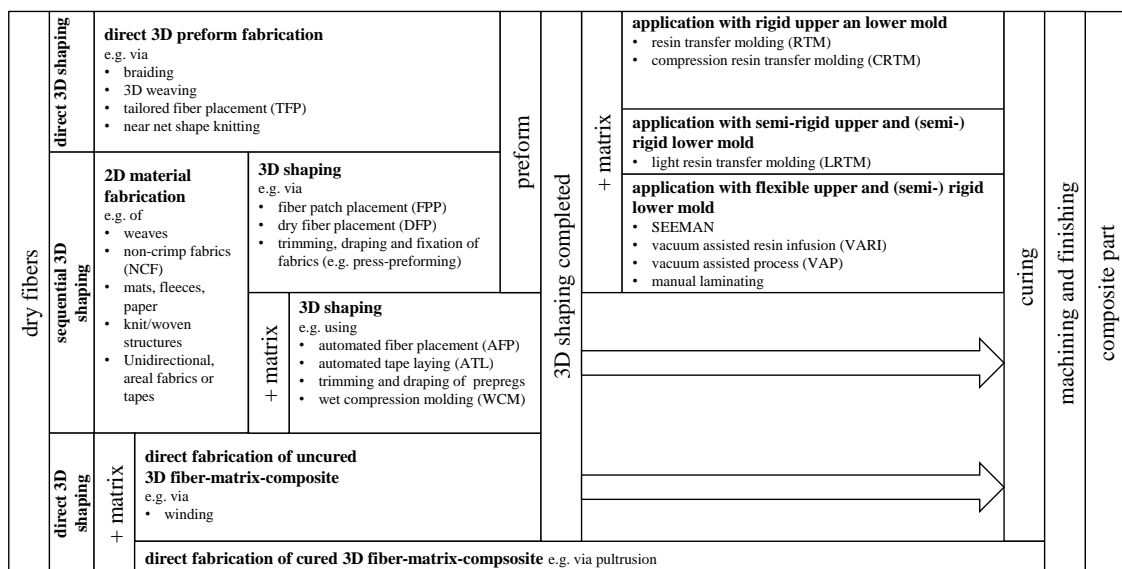
Figure 2-3 Material flow oriented process overview of liquid molding processes for manufacture of composite parts. Sequence runs from left to right (adapted from lecture materials of "Production technologies for composite parts", TUM, 2014)

Definition of LCM is somewhat imprecise, but traditionally refers to the preform route with subsequent matrix application, depicted in Figure 2-3. Here, matrix flow

through fibers is initiated by a pressure difference. WCM which only optionally uses a preform and otherwise processes flat fabric cut-outs, is considered to belong to LCM, too. In that light, industrial LCM processes as being subject to this thesis are RTM and WCM.

All process variants include three distinct steps of manufacture: shaping of dry fibers, impregnation of dry fibers with liquid matrix and curing of matrix. One closed-mold variant of LCM, RTM, separates shaping and impregnation which accommodates complex fiber alignment on the one hand and subsequent impregnation on the other. Each process step can be optimized for properties and behavior of materials at hand. However, these steps, draping and impregnation, are intertwined, in particular for continuous fiber-reinforcements [21, p. 5]. This renders the process chain complex and in many cases unreliable [22, p. 564].

The only other industrially realized automated LCM process for continuous fibers, WCM [20, p. 223] [19, p. 41], partially superimposes drape and impregnation when no preform is used. This thesis focuses on compression processes based on through-thickness impregnation of dry fiber material with liquid matrix und superimposed draping as depicted in Figure 2-4 B.
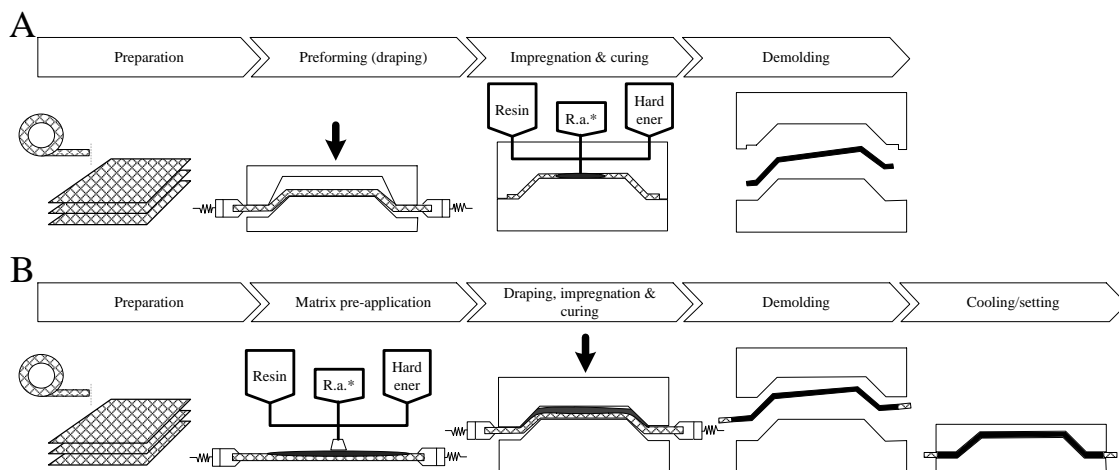
Figure 2-4 Examplary processing procedure of RTM (A) and WCM (B). The main difference is the superposition of draping and impregnation of WCM, whereas RTM performs both steps sequentially

WCM is a relatively inexpensive process based on pre-applicating liquid matrix superficaly on planar continuous dry fiber material. The wet stack is then shaped, compacted and cured during one press stroke [42, p. 14]. Superimposing drape and impregnation impacts production in two ways. Firstly, it helps to reduce mold occupancy time and number of coupled processes [19, p. 43]. Secondly, resin flow impregnates fibers mainly in through-thickness direction, which means the flow path is shortened compared to RTM. Therefore, resin can still permeate dense fiber materials [42, p. 14] and cycle time, which heavily depends on curing time

[24, p. 4], can be reduced to around 3 minutes[4]. On the other hand, RTM is used when more complex, integral parts are to be manufactured that may consist of several subpreforms as shown in Figure 2-1, C.

In both cases, RTM and WCM, fiber materials play an important role, since they determine processing to a large extent, especially for continuous fibers. Fiber orientation and architecture are determined by the type of semi-finished material, which can be limited by the process capabilities. Whereas WCM is currently mostly dependent on areal fiber materials, RTM proves to be more flexible in this regard, as it may produce hollow parts as well. However, preforming processes become more capable of combining different semi-finished materials of which the most commonly used are displayed in Figure 2-5.

	Plain weave	Twill weave	Satin weave	Biax. NCF	UD* fabric	Biax. braid	UD tape	Random fiber mat
		Areal semi-finished materials from continuous fibers				**Direct preforming**	**Tapes**	**Short/Long fiber mats**
Scheme								
Reinforcing direction								
Mech. performance	-	+	++	++	++	-	++	--
Draping	0	+	++	0	++	++	-	++
Handling	+	0	-	++	+	+	+	++
Processing	Preforming/ LCM	Preforming/ LCM	Preforming/ LCM	Preforming/ LCM	Prepreg placement	Braiding/ LCM	Tape placement dry/prepreg	Wet compression molding
Application	Simple, low performance parts	Visible parts	Complex, high performance parts	Highest performance, automotive/ aerospace	Manual placement aerospace, sports	Complex hollow parts	Areal, high performance parts, aerospace	Low performance parts, recycled fibers

* UD=Unidirectional

Figure 2-5 Overview of the most commonly used fiber materials for fiber composites and their properties, typical manufacturing processes and applications

Basically, fiber materials are available as continuous fibers in stretched (roving, non-crimp fabrics or NCF, and tapes) or undulating state (braids, weaves) and as discontinuous long or short fibers in random mats [43, p. 5]. Fabrics displayed

---

[4]Personal interview with practitioner from industry on 2015-09-14

can be produced in different variants regarding fiber orientation, areal weights and stitching. The latter is important for automation, since constant and reproducible part properties must be guaranteed over the entire process chain. This is only possible if fiber position remains constant, so that positioned fibers are stabilized. While fibers in weaves intersect and lock themselves, fiber bundles in NCF have to be held in place by stitching. In automotive, mostly NCF are used due to their mechanical properties that do not suffer from fiber undulations found in weaves and due to their comparably low price. However, sews in NCF hinder fiber movement that is necessary during draping [44]. NCF come with three different sew types - chain, tricot and tricot/chain. In that order, drapability increases and handability of respective semi-finished material decreases.

2.3 The Role of Processing in Design of Liquid Composite Molding Parts[5]

Beyond costing aspects hindering realization of LCM parts that are discussed elsewhere, e.g. [34] [33], industrial application suffers from more wide-ranging problems connected to part design. The current state of technological knowledge seems to be sufficient to reliably establish economical LCM products of high quality while tapping the full mechanical potential of fiber reinforcement. However, within the context of LCM-processing, the realization process of products often obstructs successful results.

Holistic part development must always consider three aspects: selection of the material from which a part should be made, design of the part geometry and determination of the production process that can reliably convert raw material into the final part shape. Considering part development for LCM, process selection is already determined. However, raw materials to be used are not merely selected from available materials. Their properties are altered within the molding process itself and therefore process parameters, curing cycle etc., determine the properties of the resulting composite. Additionally, the production process is strongly influenced by part geometry due to fiber orientations and resin flow paths. Thus, the nature of the problem is not solely selection but interdepending adjustment of geometrical design, process parameters and material properties.

From the process point of view, this connection among geometry, process and material within LCM processes was subject experimental investigations before, e.g. [26, p. 25-33]. Equally well established are fundamentals of structural design with com-

---

[5]This section is based on work by the author previously published in [29, p.495-505]

posites. Exploitation of the mechanical potential of a composite based on the fiber's anisotropy has been subject of various publications, including [32]. Regarding the methodological aspects of development, material and process selection within the scope of engineering problems are widely discussed. Ashby et. al. give an overview on selection strategies that lead to a set of possible materials through evaluation based on requirements [45, p. 21-56]. No strategy explicitly supports the possibility to adapt part design and works only if interference of all aspects is completely determined. Methodology-focused research on composite part development with regard to the actual manufacturing technology is very scarce. There is a consensus that the principles of concurrent engineering apply to the development of composite parts. In 1990, Gandhi et. al. proposed a manufacturing-process-driven design methodology for composite components [46, p. 238]. This methodology starts - after establishment of specifications - with parallel material selection and part geometry. Considerations of manufacturing constraints iteratively follow thereafter. In the same decade, Potter proposes a refinement of design strategies by concurrency, iterative nature and abstraction of the design problem through a procedure of connected loops [12, p. 174]. He discusses departmental structures that could hinder consistent cost monitoring and states that integration of all needed disciplines - most notably manufacturing - is a prerequisite to avoid quality, yield or cost problems during production.

As the current state of technological knowledge seems to be sufficient to reliably establish economical, mechanically adequate LCM products, it is not clear, why low material exploitation, problems in fiber impregnation and uneconomic products are still often characteristic for the design of LCM composites. It is assumed, that contextual aspects in development are at work as described Maffin's contextual framework which serves as an initial theoretical framework. Qualitative case study research after Eisenhardt [47] and Patton [48] was applied for personal interviews with experts from selected industries and academia [29].

The interview results confirm the assumption that the technological context of LCM projects plays a major role on how well their outcome is. Currently, industrial use of LCM technology is undergoing a process of technological exploration which is associated with terms like "search, variation, risk taking, experimentation, play, etc." [49, p. 71]. Furthermore, this learning process relates to product and process alike and amplifies the already strong concurrency. Both have to be advanced simultaneously in order to cater to the assumed requirements but also suffer from a lack of experience. The focus of technical learning, however, has to be differentiated: While firms operating in the automotive sector are mostly concerned with expanding the production throughput, those in the aerospace sector emphasize on the predictability of quality, e.g. in simulation, as it is currently the standard

in prepreg technology. OEM-supplier partnerships, particularly in the automotive sector, are strongly shaped by the situation of technical learning. Collaboration is often complicated by unclear or inappropriate requirement formulation as well as a lack of explicit integration of the supplier into part development. In consequence, product features and geometries derived from traditional technologies pose difficulties in fiber alignment (preforming) as well as in resin flow processing during LCM.

As firms aim to mitigate risks of the learning phase, projects usually focus on material substitution of single parts rather than systems or complete products. Thus, project variables, e.g. available installation space, are often not ideal, as the new lightweighting technology has to adapt to the existing product. In result, the part design is already pre-existing to a great extend which does not only restrict the basic geometric design but also interferes with development strategies employed. This results in a what Maffin calls "product-focused approach" [50, p. 319] rather than an "process-focused" design, advocated by academia as more optimal [51, p. 130] [52] [30, p. 47] [53, p. 45]. Product-orientation leads to a trial and error optimization of a design conjecture, rather than scientific reasoning from first principles and systematic solution finding. Therefore, accumulation and reuse of past experiences, in particular concerning flow processing using LCM, is inhibited and so are standardization and knowledge transfer to facilitate new projects. The lack of knowledge is especially severe concerning compression molding processes where almost no academic literature regarding process design is published so far.

3 Purpose and Approach of Thesis

Any technical system can be described as a network of interacting functions that are linked to flow of energy, material and signal [51, p. 170]. Drawing on this framework, this thesis interprets compression molding of advanced composites as a superposition of material flows that initiate matrix impregnation and draping of fiber materials. This superposition yields benefits of reduced mold occupancy, a short process chain and fast, through-thickness impregnation but does not come without compromises. The key function, pre-application of matrix onto fibers, which allows the superposition, conflicts with the need to control material flows. Control of flow, either of matrix into fiber material or fiber material into the cavity, is important in other LCM variants such as RTM, as it is associated with the resulting part quality. Flow control is commonly facilitated when the respective semi-finished materials are stabilized. In the light of WCM processes however, traditional techniques for stabilization, e.g. preforming with binder or solidifying matrix, undermine some of the benefits of compression molding. Thus, the conflicting needs to pre-applicate matrix, control its flow and stabilize material form a polylemma, which will be derived from discussion of functions in the following sections. Herein, it becomes evident that the established polylemma is hypothetical, as it is based on literature of connected fields applied to the subject of compression molding.

3.1 Functional Description of LCM Processes

The flow of liquid resin through porous media is a combination of inter-roving macroscopic and intra-roving microscopic flow [54, p. 838]. Driving forces are external pressure gradients and capillary forces. In RTM, these forces and the resulting flow types should be balanced in order to prevent inhomogeneous flow fronts that are prone to form laminate defects [55, p. 2106] [56, p. 1860]. Another issue in LCM is racetracking [57], where some sections of the flow front progress faster than others due to heterogenic permeabilities. Areas between racing flow fronts are often left dry which renders respective parts as scrap.

Many have proposed active control systems of flow sensors and versatile vents to homogenize flow front propagation during mold filling [58–61]. Others have shown that closing patterns of tooling components either rigid or flexible can be used to steer resin flow [62] [16]. One WCM process solidifies a resin layer on the tool's surface to provide homogeneous flow in through-thickness direction during pressing [63]. In resin bulk infusion, fiber compaction and resin flux can be controlled individually, since resin is contained in a separate chamber [64].

Thus, from the combined liturature on resin flow in LCM processes, it is concluded, that "*control matrix flow*" to obtain a uniform resin flow during mold filling is an important functionality of LCM processes.

Process parameters, which are also linked to mold filling influence part quality as well. Evacuation of the mold and increasing resin pressure effectively reduce voids inside the laminate. This results from reduced pressure inside trapped air and added pressure of surrounding matrix that promotes further resin penetration [26, p. 25] [65, p. 1028]. While in RTM resin pressure builds up by inflowing resin against resistance from sealed mold, pressure in WCM must be established by compressing excessively applied resin. Since fiber mats exceed the part cavities for draping support (Figure 2-4), flow resistance has to be generated by compressing the fabric along the cavity circumference. This also makes mold evacuation complex, so that usually WCM is applicated without vacuum support despite its benefits. In order to incorporate vacuum assistance and resin pressure as important aspects of processing into development, the functions "*establish vacuum tightness over press stroke*" and "*establish matrix tightness*" are defined.

During the press stroke in WCM, deformation of planar fiber mats or draping superimposes impregnation. Draping of dry fabrics has been subject to many studies, since it determines fiber orientation and therefore mechanical properties of the part. Deformation mechanisms of multiaxial NCF include rotation, sliding and compaction of the fiber tows [66, p. 249]. In particular, shearing of tows in different layers during deformation determines how well the stack can be shaped [67, p. 104]. In order to allow controlled shear, tensile forces have to be introduced into fibers, e.g. by blank holders [68, p. 2270]. Increasing blank holder forces reduce unintended asymmetrical fiber angles as well as in-plane and out-of-plane buckling [69, p. 366]. In diaphragm and double-diaphragm forming, which was initially developed for shaping thermoplastic composites, forces onto the composite are generated by layers of elastic material [70, p. 460]. This concept can be transferred to form dry fabrics as well [71]. An alternative process, Film RTM, combines thermoforming of thermoplastic films with draping of NCF. It employs tensile forces by viscoelastic extension of molten films to generate normal forces and thus, via friction, tension onto the fabric [72]. In all cases, shear and plastic or elastic elongation of films under tension has to be guaranteed in order to drape films into complex shapes.

Independent from its physical realization as discussed before, the function "*transfer tensional forces to fabric*" is essential to allow good draping results of continuous fiber materials.

3.2 Polylemma of Superimposed Draping and Impregnation of Automated Wet Compression Molding

As discussed in previous sections, two overarching mechanisms in LCM processing systems determine the final part quality - draping and mold filling. These mechanisms are superimposed by WCM processes to tap major benefits for production. In addition, automation of WCM has to be dexterous enough to handle limp fibers and liquid resin. Precisely that is not self-evident, even for separated processing of the two materials as present in RTM [13, p. 20]. Transport of dry fabrics is addressed in ongoing research and development of several gripper systems that temporarily fixate fibers through different physical mechanisms [73, p. 301] [74, p. 691]. While research is focused on handling of dry fiber textiles in regard to minimize its impact on fiber destortion, no literature is available for material transport in WCM. When matrix is superficially pre-applied on fiber mats for short through-thickness impregnation, flow mechanisms described in Section 3.1 can lead to a mostly areal distribution of matrix atop dense fiber materials, similar to the injection stage of compression RTM [75, p. 2528]. Due to a low permeability of rovings perpendicular to their longitudinal direction [76, p. 104] in carbon fiber NCF it is expected that the bulk of matrix forms a film on top of the stack. Only a smaller share sinks into the fiber bundles in through-thickness direction. If a liquid film on top is formed, the matrix is prone to dislocation under material transport due to its inertia. Furthermore, without any stabilization matrix flow during compression is subject to an inhomogeneous initial position and may become highly heterogeneous in nature due to a heterogenic permeability distribution (Figure 3-1).
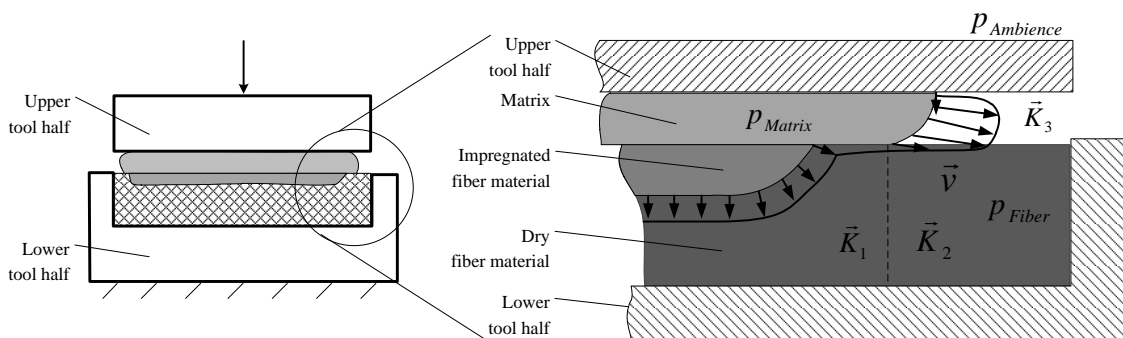
Figure 3-1 Hypothetical flow situation in WCM. The velocity $\vec{v}$ of the matrix flow front is heterogenic due to heterogenic permeability distribution

Compression of the fiber and matrix material initiates the impregnating flow of matrix through the initially dry fibers. Depending on the initial state of materials before compaction and distribution of fibers and matrix inside the mold, the

flow front is shaped according to the present permeability distributions. However, regarding process robustness and impregnation quality, a more homogeneous flow front is favored.

To achieve a more homogeneous flow front and a defined initial position of matrix some processes stabilize the applied matrix in order to control its position prior and during impregnation of the textile. This is usually achieved by cooling the matrix to increase its viscosity or applicate a matrix that solidifies at room temperature [16, p. 64] [77, p. 79] [63, p. 1]. One RTM variant, gap impregnation process, controls matrix flow by closing the tool in a wedge-shaped kinematic [78]. However, the process also seperates impregnation from fiber draping and stabilizes the preform shape with commonly used epoxy or thermoplastic binder [13, p. 43].

It becomes evident that although the materials at hand provide beneficial freedom in part design by their limpness and liquid state, modern production systems need to fixate the components to be able to process them. If WCM as introduced superimposes drape and impregnation to reap the benefits of a shorter process chain, the position of the pre-applied resin during handling and initiated matrix flow during compression are critical. A temporary stabilization of the state of materials as traditionally practiced partially undermine the benefits. Thus, the requirements of short matrix flow path, high impregnation quality and clean and secure handling of semi-finished materials depend on functions that cause conflicts regarding position of the matrix and the state of semi-finished materials (Figure 3-2).
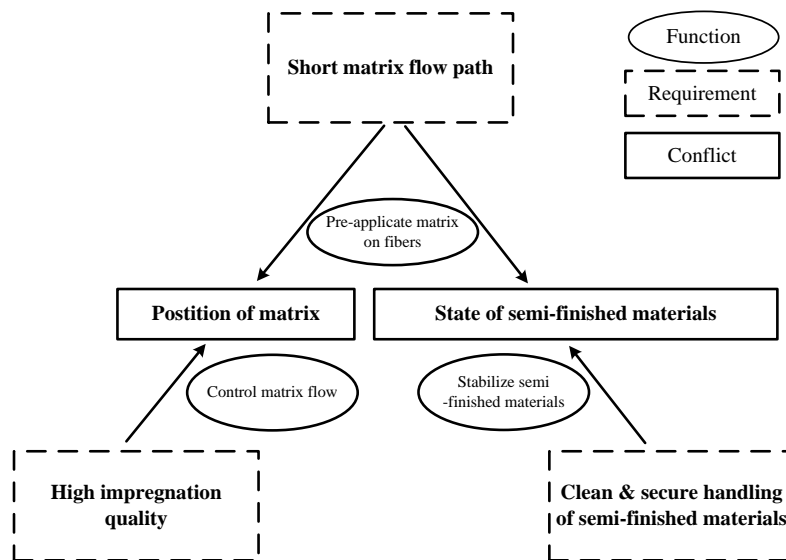
Figure 3-2 Polylemma of conflicts of automated WCM that stem from superimposed drape and impregnation

Providing a possible solution to the polylemma is subject to this thesis. It furthermore aims to better understand and improve material flow in WCM processes, as

academic research in this field has not been published so far. Thus, the remainder of this thesis is clustered into three parts. First, an alternative process to solve the polylemma is designed. In a second step, this alternative process and WCM are investigated regarding their characteristics of matrix flow. Lastly, both processes are studied in a life cycle assessment (LCA) and costing analysis in comparison to RTM in order to evaluate their performances in circumstances of an industrialized production.

4 Design Of Carrier-Integration Pressing[1]

Wet compression molding of advanced composites, as introduced in Chapter 2 and elaborated in Chapter 3 has not been subject to available academic literature. In particular, matrix flow in through-thickness impregnation and mechanisms of matrix pre-application have hitherto not been discussed. As this thesis argues, conflicts between matrix pre-application, flow control and secure handling of semi-finished materials arise. Based on this polylemma, the author proposes an alternative impregnation process, carrier-integrated pressing (CIP), to solve the conflicts in order to possibly improve material flow in compression molding processes. The proposed solution results from a spacial separation of liquid matrix and fibers with storage of the matrix in proximity to its subsequent curing location. Physical embodiment of this approach is a carrier structure with storage cavities.

In this chapter, further design and concrete emboniment of tools and materials that are based on the principle solution are presented, followed by a validation of the developed process.

4.1 Principle Solution of Polylemma and Connected Goals of Design

Superimposed drape and impregnation for WCM in the context of automation leads to conflicting functions regarding the location of resin and the state of materials. Solving these conflicts might provide critical advancement of WCM in terms of material flow in reference to high laminate qualities, process robustness and easy automation. In order to prevent inhomogeneous resin location and still allow pre-application, defined storage over space and time of matrix is preferable. To enable controlled matrix flow in through-thickness direction, two aspects are important. Firstly, matrix should be distributed across the projected area of fiber material dependent on the required mass in each location to prevent high inplane flow resulting from pressure gradients. Secondly, resin should first contact the fiber material when flow is triggered on purpose, in order to allow for full evacuation of air from the fibrous structure and a defined location of matrix prior to pressing. In order to be able to securely handle pre-applied matrix, it must be stabilized in its intended

---

[1]Parts of this chapter have been previously presented by the author at the Second International Symposium on Automated Composites Manufacturing, Montreal, Canada, 04-23-2015

location. For this purpose, three physical principles known from literature [16, p. 64] [79, p. 406] [80, p. 2] may be exploited:

- Viscosity increase by cooling

- Viscosity increase by partial cure

- Containment by form, gravity and/or capillary forces

Based on spacial separation of resin and fibers by one of the principles, simultaneous handling of both materials should be supported. Cooling temporarily stabilizes the matrix but requires non-isothermal tooling or a separation of cooling and heating in two separate steps. Both is undesirable in the context of automated series production as advocated by the industry. Drawing on the reactive behavior of a resin system for partial cure with subsequent liquefaction severely limits the selection of available resin systems. Furthermore, no current B-staging resin is known to the author that meets cycle time requirements of around three minutes. In the light of modern series production that relies on isothermal processing and fast-curing resin sytems, resin containment inside cavities within a planar carrier structure that also supports the fiber material is proposed to be able to solve the functional polylemma (Figure 4-1).
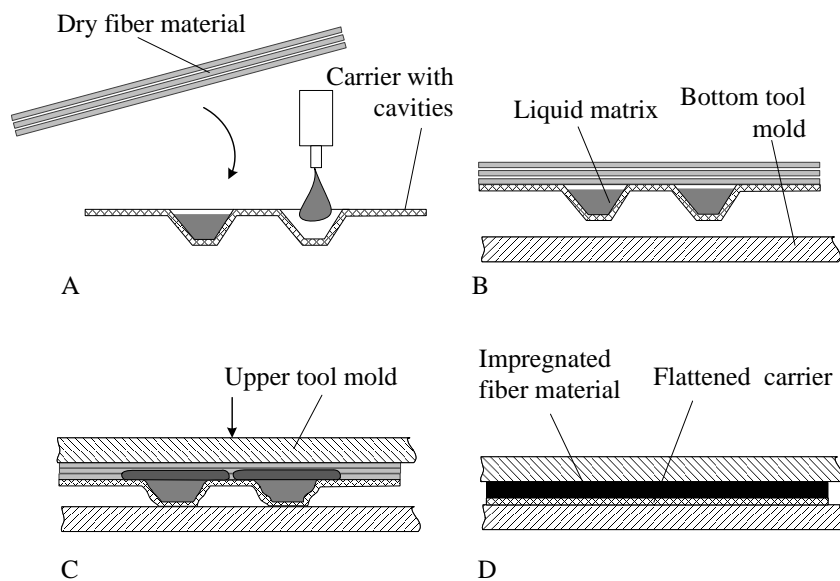
Figure 4-1 Principle solution for spacial separation of matrix and fiber material with storage of the matrix in proximity of its final curing location. A: Preparation of material outside of tool; B: Insertion of the material blank into tool; C: Impregnation by cavity deformation; D: Curing and bonding of carrier

The principle solution from Figure 4-1 revolves around use of a carrier with cavities, still independent from the physical embodiment. The carrier allows controlled storage of matrix in relation to the fiber material subsequent to pre-application.

The matrix does not contact the fiber material in that state. The release of matrix from storage cavities is initiated when cavities are deformed. In this stage, continuous compaction drives matrix flow until the final part thickness is reached. After complete compression, cavities are leveled out and the carrier shall bond to the laminate during resin cure, which reduces scrap in production and allows to functionalize the part surface depending on the properties of the carrier for added part value.

In applying the carrier, both semi-finished materials, matrix and fibers, are still separated and stabilized. Yet, pre-application of matrix is not disturbed by the stabilization of materials and preparation can be performed outside of press. Due to the defined storage of matrix close to its subsequent curing location, it can be hypothesized that matrix flow is of higher homogeneity compared to WCM, Figure 4-2.
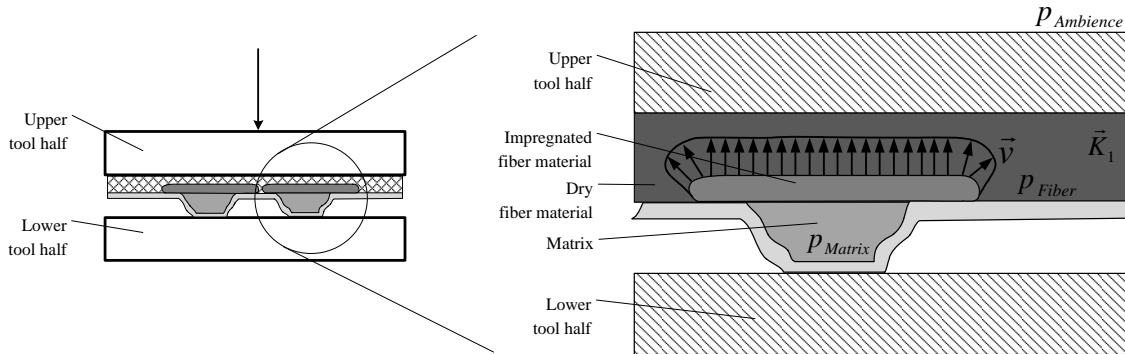
Figure 4-2 Hypothetical flow situation in CIP. The velocity $\vec{v}$ of the matrix flow front is more homogeneous due to a more uniform permeability distribution and a defined location in reference to the fiber material prior to compaction

The shape and flow direction of the flow front is only depicted principally, as it is dependent on the shape of the matrix cavities and the functional principle of their elimination. However, it is expected that resin flow is primarily directed in through-thickness direction of the laminate during continuous compaction of the material and only flows in lateral direction between storage cavities.

In addition to the main functions that should be fulfilled by CIP derived from literature in Section 3.1, the proposed carrier use suggests the introduction of three additional functions. Considering the main physical principle, "*store/eject resin*" is associated with the carrier. Carrier functionality after production is generated by the functions "*attach carrier to laminate*" and "*functionalize part surface*".

With additional functions attributed to the principle of carrier use in CIP, in total eight functions represent the abstract description of the technology proposed. In relation to these functions and within the context of industrial series manufactur-

ing, the following questions that guide the process and tool design are phrased:

1.1 How to design a production system based on the proposed principle solution, including carrier material definition, physical principle of storing resin, draping mechanism and a respective tooling?

1.2 How to eliminate resin storage cavities during pressing to prevent carrier wrinkles?

The questions are answered first prescriptively, as the work elaborates on the functions defined earlier to establish a theoretical description of the process and a rough design for the tool drawing on an adequate design methodology. Design and cavity elimination are evaluated in experimental trials after definitive design and manufacturing of the tool.

4.2 Design Methodology

This work explores the feasibility of a novel matrix processing principle in industrial production of composites. Thus, it is prescriptive in nature with a descriptive study of the realized tooling system for assessment of process functionality [81, p. 15]. The underlying methodology for development of the principle idea into an integrative tool, process and carrier design is based on the Munich Procedural Model (MPM), proposed by Lindemann [30, p. 47] (Figure 4-3). This methodology is used, since it comprehensively supports early stages as well as evaluation of design and sufficiently specifies single methods to be applied in each stage of development. The first two stages, plan and analyze goal, have been completed with the literature review to identify functions and their analysis to identify the functional polylemma, which led to the proposed principle solution in Figure 4-1. Stage 3 and 4, structure problem and establish solution ideas, are dedicated to the theoretical description and specification of the process. Based on the weighting of functions according to their importance for the overall functionality of the system, the conceptual design of the tool is conceived using TRIZ[2]. To identify the carrier best suitable for the process, experimental draping trials with dry materials are performed. The overall functionality is evaluated in wet trials using the best suitable carrier material. Methods, outcomes and references for each stage of the MPM are listed in Table 4-1.

---

[2]Theoriya resheniya izobretatel'skikh zadatch (Engl.: Inventive problem solving)
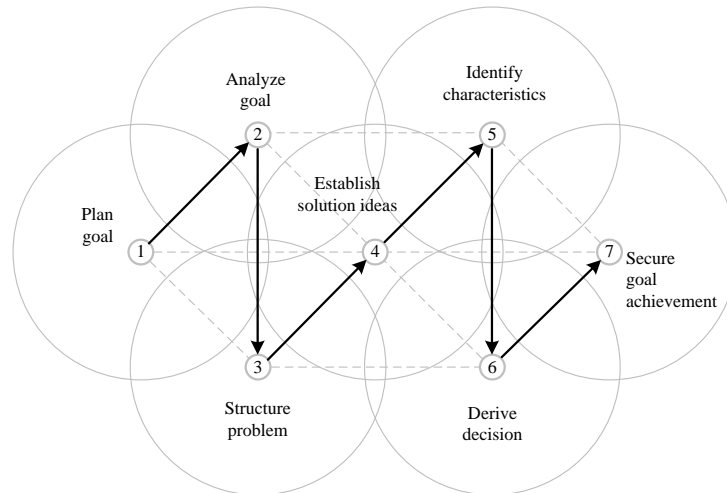
Figure 4-3 Munich procedural model (MPM) adapted from [30, p. 47]. Black arrows mark the sequence of procedure for the design of CIP

Table 4-1 Applied design methods, outcomes and reference that have been used in the work for every stage of the MPM

MPM Stage	Method	Outcome	Reference
1	Literature review	Functional representation	[51]
2	Functional analysis	Principle solution	
3	Effect analysis/Portfolio	Weighted functions	[51]
4	TRIZ	Solved technical conflict	[82, 83]
5	Dry experiments	Draping quality	
6	Benefit analysis	Choose carrier material	[30]
7	Wet experiments	Functionality evaluation	

In the following, the stages structure problem and establish solution ideas are presented within a theoretical part of the chapter. All succeeding stages based on experiments are discussed in separate sections with additional information on materials and methods used for the specific stage. Interpretative remarks with hypotheses formulation based on theoretical and practical results conclude the study.

4.3 Theoretical Design of Carrier-Integrated Pressing

To gain a theoretical understanding of the overall system, the single functions identified in literature review are set into relation to each other. Thus, the importance of each function in regard to the overall system is evaluated and allows subsequent focus on the most critical functions in design. This method, effect analysis [30, p. 76-77], produces a functional portfolio of CIP.

Hypothetical effects of one function on another were discussed and rated in the development team that consisted of one researcher, one industrial process engineer, one automotive part design engineer and one development engineer of resin dosing machines. The resulting effect matrix of the eight identified functions is depicted in Table A-1. The corresponding portfolio is derived when active and passive sum are plotted on abscissa and ordinate respectively, Figure 4-4. Criticality, computed by multiplying passive and active sum, is represented by the diameter of spheres. Hyperbolas of constant criticality are inserted for orientation.
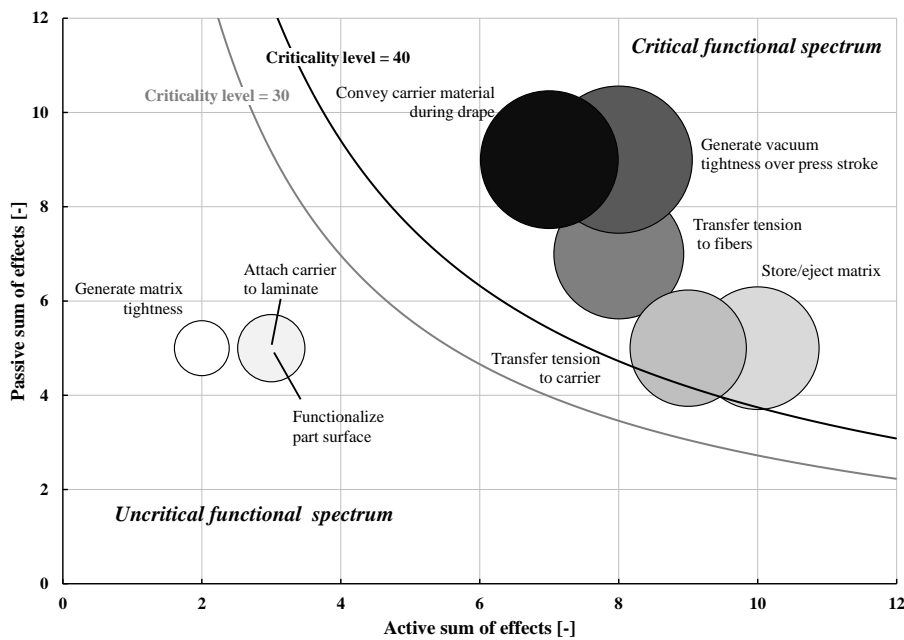
Figure 4-4 Portfolio diagram of functions for CIP based on data of effect analysis in Table A-1. Sphere size represents criticality of functions

Functions regarding carrier bonding to the laminate effect others weakly. Their physical or chemical properties required for bonding are not thought to necessarily interact with physical or chemical properties needed for draping or impregnation. Although resin tightness of the mold is required for good impregnation properties after cure, it does not influence the impregnation flow as such.

Functions located in the critical spectrum (Figure 4-4, top right) are all connected to the draping and impregnation mechanisms executed by the press stroke. During the stroke, the tool transitions from open to closed state in a linear kinematic movement, executing the critical functions simultaneously. The most critical function, "*Generate vacuum tightness over press stroke*" is interacting with other critical functions strongly, as it potentially determines the overall structure of the tool. The individual elements of the tool have to fulfill other functions as well, which can lead to strong interaction.

Tools for CFRP processing are usually sealed with steady state sealings, compacted between two parallel tool surfaces. The sealing element, typically silicone rubber, does not need to seal the tooling over press stroke, as in most cases the liquid matrix is injected into the tool cavity after closing. Thus, silicone sealings do only allow stroke of a few millimeter at best. For compression molding, this would only be sufficient if draping complexity is very low and thus deformation due to press stroke is negligible. It becomes evident that the function "*Generate vacuum tightness over press stroke*" yields the following technical conflict (TC):

If press stroke is large, draping complexity is high, but vacuum tightness is poor.

This conflict has been subject to previous developments, partially from other industries. Inflatable or non-inflatable tube sealings[3] allow a larger functional range of motion than massive sealings but are still not sufficient for larger strokes. In another concept, the cavity mold for actuation sits inside a second, static mold, which can be evacuated [65, p. 1029]. This functional separation might be economic for smaller molds but is too costly in comparison to unsealed WCM tools for large parts. On the other hand, overlapping tool walls used in long fiber wet compression molding [84, p. 335] may only be an option if tolerances are large and the remaining gap can be sealed by a dynamic silicone sealing. The sealing function in series production, however, is undermined when matrix repeatedly contacts the sealing material. Dynamic sealings between overlapping tool walls are successfully used in sheet metal compound (SMC) tools that can be evacuated for A-class surface parts[4]. In this case, the sealings are only burdened mechanically, since the matrix in SMC material is highly viscous and does not protrude into the tool gap. This is not the case for CIP in which low viscous matrix is processed.

Concluding from available sealing technology, no ready-made solution can be applied to solve the conflict. In such cases, Lindemann suggests to apply TRIZ to solve problems with contradicting parameters [30, p. 317]. Two parameters are contradicting if the improvement of one impairs the other, and vice versa [85, p. 92]. This state can be tested by negating the above stated TC:

If press stroke is small, draping complexity is low, but vacuum tightness is good.

---

[3]www.technix-rubber.com; Last accessed on 01-23-2016

[4]After personal interview with head of production of a fabricator of SMC tools on 04-28-2014

This inverted TC is valid as well, as the deformation path of some sealings allow for a few millimeters of press stroke, leading to low draping complexity. However, as the processes considered in this thesis should drape high complexity shapes, the first TC is considered in TRIZ.

The concrete technical parameters of the tool are draping complexity and vacuum tightness. For each parameter, several different abstractions[5] exist. The abstract parameters

- shape,

- adaptability or

- structural complexity

are selected to substitute draping complexity. Vacuum tightness is replaced by

- reliability or

- energy loss.

Combinations of the respective conflicting abstract parameters are associated with with abstract solution principles suggested by the TRIZ contradiction matrix. Concrete solutions applicable to the technical environment at hand are derived from proposed principles. An overview of concrete solutions found based on the suggested principles is presented in Table 4-2.

Of all proposed principles, three are deemed capable of effectively solving the TC:

- Principle 17: New dimension

- Principle 10: Prior action

- Principle 24: Mediator, intermediary

The combination of these principles provide a set of concrete solutions promoting each other. Principle 17 leads to the approach that the generation of air tightness can be separated from resin tightness, as specified in solution 17.2. The separation can be spacial and temporal in nature and is embodied by solution 10.4, drawing on principle 10. In this solution, a sealing frame or blank holder prepones vacuum sealing before draping and impregnation. The blank holder retains the carrier, which acts as mediator after principle 24. Both concrete solutions 24.1 and 24.2 can be applied. The carrier material can mediate the tensile forces onto the fibers for draping and it can seal the tool. Using the carrier material as a sealing element allows to spatially separate the resin-flooded part cavity from all other silicone sealings.

---

[5]According to TRIZ contradiction matrix,
www.innovation-triz.com/TRIZ40/TRIZ_Matrix.xls; Last accessed on 01-25-2016

Table 4-2 Result of search for solution to the technical conflict "*If press stroke is large, draping complexity is high, but vacuum tightness is poor*" by reference to the TRIZ contradiction matrix

Abstract parmeters	Innovative principle	Concrete realization
	14: spheroidality, curvilinearity	?
Improving feature: shape Worsening feature: reliability	10: prior action	10.1: prepone draping: preform
		10.2: prepone sealing: carrier bagging
		10.3: prepone impregnation: wet fibers
		10.4: prepone vacuumation: sealing frame
		10.5: prepone vacuumation: overlapping tool halves
	34: rejection and regeneration	34.1: use carrier material for sealing
		34.2: self-draping carrier, e.g. vacuumized bagging
	17: new dimension	17.1: new dimension: tool housed in vacuum boxing
		17.2: separate actions: Stepwise sealing
		17.3: more movements: Sealing, draping and then pressing
Improving feature: adaptability Worsening feature: reliability	35: transformation of the physical and chemical states of an object	?
	13: functional inversion	?
	8: counterweight, levitation	?
	24: mediator, intermediary	24.1: use carrier material for draping
		24.2: use carrier for sealing
Improving feature: structural complexity Worsening feature: reliability	13: functional inversion	?
	35: transformation of the physical and chemical states of an object	?
	1: segmentation	1.1: segmentation of carrier in area for draping and area for sealing
		1.2: segmentation of fiber material to substitute mechanical requirements of 3D shape with local reinforcements
Improving feature: shape Worsening feature: energy loss	14: spheriodality, curvilinearity	?

For further conceptual embodiment of the relevant TRIZ solutions, several designs are conceived for the functions which are primarily fulfilled by the mechanical tool structure (Table 4-3).

The favored combination of solutions for each function is marked with a link in Table 4-3. Solution 24.1 is the hypothetical mechanism for draping under tensioned films which has been experimentally shown to work in Film RTM [72]. In this variant, tensile forces are thought to be transferred onto fiber material by clamping it between the upper tool wall and the carrier during carrier deformation. It potentially enables to safe fiber scrap produced from conventional clamping and resin sealing systems in which the planar fiber material has to be drawn to the outside of the tool in order to fix clampings. Apart from the draping solution, all other single solutions favored are the most secure design options found by applying TRIZ, in regard to different possible carrier materials and thicknesses which are not yet

Table 4-3 Morphological box with conceptual embodiment design variants for the functions to be specified by tool design from Figure 4-4. Variants are either directly derived from concrete solutions of TRIZ (labeled with numbers originated in Table 4-2) or additional variations found for the same functions (labeled with letters)

Generate vacuum tightness over press stroke	Transfer tension to fibers/carrier	Convey carrier material during drape	Generate matrix tightness
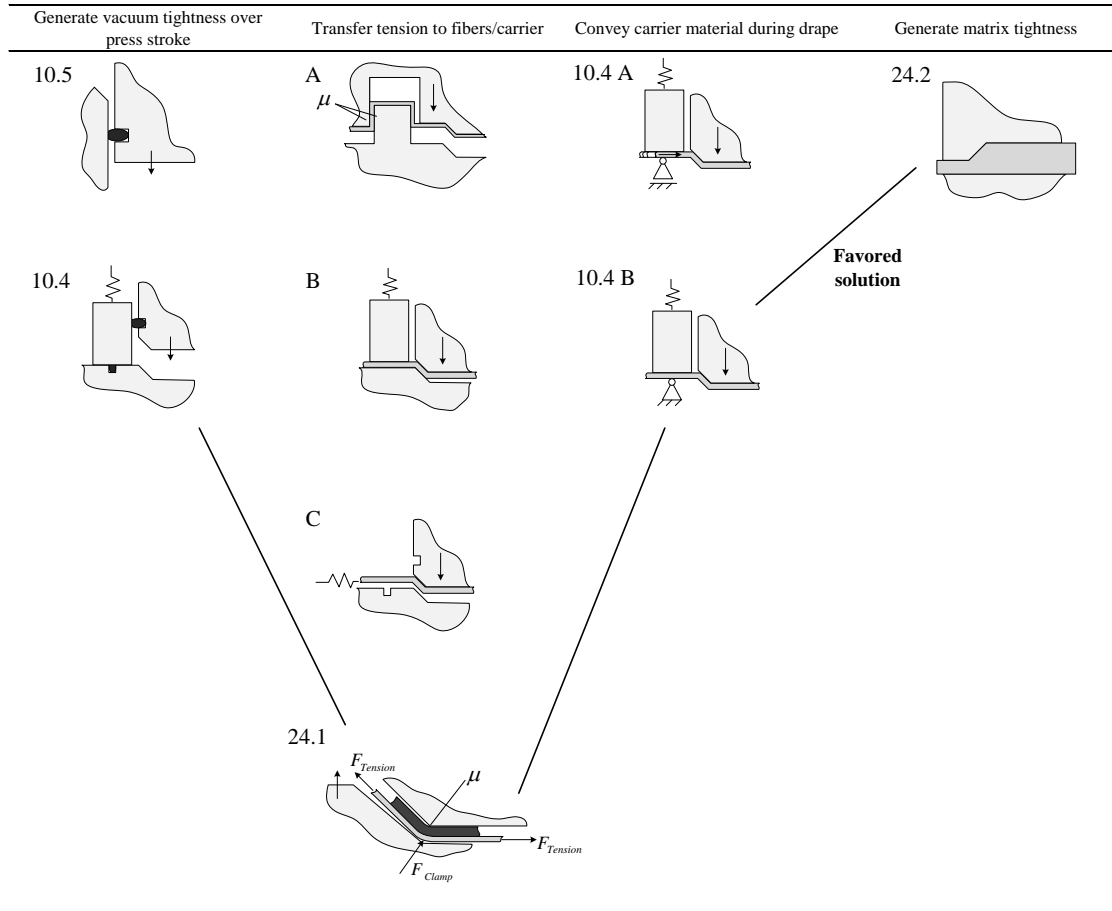
determined. The synthesis of the preferred solution from the morphological box is shown in Figure 4-5.

Detail A.1 in Figure 4-5 specifies how carrier integration prevents matrix contact with the sealing which provides a big benefit regarding tool design, since it can apply conventional silicone sealings without high maintenance effort. The carrier serves as a sealing between resin-flooded regions within the part cavity above the carrier and dry regions outside the pinch-off area. The dynamic sealings are placed inside the dry section. Furthermore, the vacuum bores are placed between carrier pinch-off and dynamic sealings. They hereby allow to evacuate the part cavity without risking resin to flood the vacuum bores. Vacuum sealing 1 is implemented as a dynamical sealing, since this design allows for guaranteed sealing independent from the carrier material or its thickness, in contrary to static sealings displayed in solution 10.4 in Table 4-3. An air- and resin-tight carrier splits the cavity into
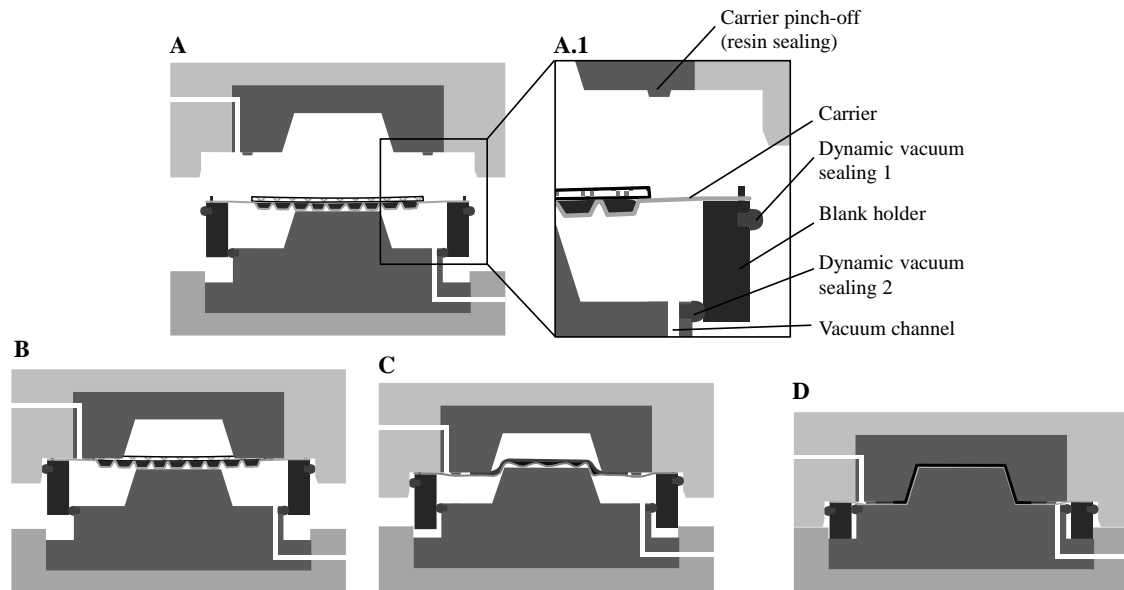
Figure 4-5 Conceptual design of tool and process sequence for CIP. Carrier with applied resin and fiber material is positioned on blank holder (A); Tool is closed until both dynamic sealings (A.1) are effective and cavity areas above and below the carrier can be evacuated (B); Tool is further closed after evacuation initiating draping and impregnation by deformation of carrier (C); Tool is completely closed for curing (D) and carrier pinch-off seals the cavity against resin flow (A.1)

an upper and lower part. Therefore, upper and lower vacuum bores are present in the conceptual design.

The conceptual design phase is concluded with the conceptual tool embodiment for all functions and its respective process flow depicted in Figure 4-5. Further concretization includes concrete embodiment design of the tool and specification of the carrier. The latter has to be specified regarding its basic material and shape. A decision will be made based on experimental trials. Therefore, suitable materials are classified in a material framework with respect to physical properties that determine the main functions, within the material section for experimental trials. The concrete embodiment of the tool based on the concept derived is presented in the following section.

4.4 Concrete Tool Design for Carrier-Integrated Pressing
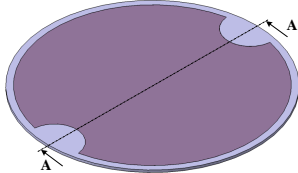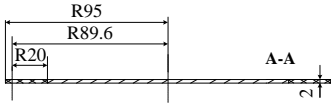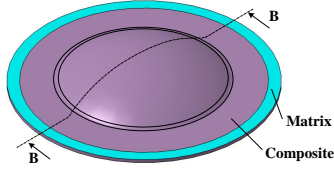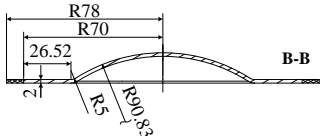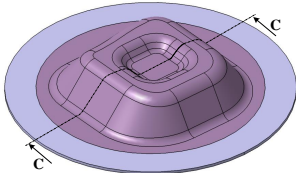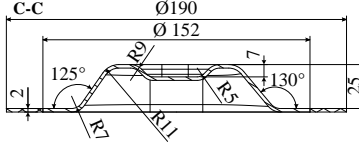
Concrete embodiment of the tool concept from Section 4.3 must be simple and robust, so that the additional complexity due to vacuum technology in comparison to common WCM tools is still reasonable. In order to allow for different parts to be manufactured on the same tool system, exchangeable cavity inserts shall be used

and outer tool dimensions must not be greater than 550 mm to allow mounting on a PEI Vacuum 1000 heating press (100 t). In order to increase the likelihood of robust operation, only standard components for sealing and guiding functions shall be used. The tool designed should be able to be equipped with carriers that are up to 5 mm thick. Embodiment design in this case progresses stepwise from the concrete definition of inner to outer structure. Thus, part cavity definition is derived first before blank holder and, lastly, tool base is designed.

A default application for WCM are automotive parts, which are mostly made from thin, formed sheets with FVC ranging from $0.5 - 0.55$ and mostly contain $300\,\mathrm{g/m^2}$ fabrics. FVC values of $0.53 - 0.55$ are achieved when carriers with $0.05 - 0.15\,\mathrm{mm}$, respectively, are used within a 2 mm thick cavity and six plies of fabric.

Requirements for the cavity design differ dependent of each research section. In order to investigate matrix flow in depth, a plate tool is the most simple geometry producible, as the matrix flow here is not influenced by draping. On the other hand, the conceptual design assumes that the fabric can be draped due to the deformation of the carrier. In order to test this, a tool of complex geometry must be available, too. Lastly, a tool of medium complexity is used for the initial evaluation of the overall functionality of CIP. All designs conceived are presented in Figure 4-4.

Table 4-4 Part layouts for press tool in regard to research sections

Plate	Spherical shell	Complex part
Fiber mass: 43.5 g	Fiber mass: 27.7 g	Fiber mass: 45.8 g
Matrix mass: 49.5 g	Matrix mass: 35.7 g	Matrix mass: 50.8 g
Initial stack diameter: 180 mm	Initial stack diameter: 140 mm	Initial stack diameter: 180 mm

The cavity in which the composite is processed must be sealed against matrix discharge by compressing the carrier in circumference of the parts (Solution 24.2 in Table 4-3). However, the thickness of the carrier is not defined yet. Thus, a tapered edge that reduces the cavity height to 0.5 mm is combined with a silicone sealing of 10 mm diameter to allow for fluctuations of carrier height. Beyond the the pinch-off

edge, the cavity insert contains a circumfering matrix catch tank, in case matrix is involuntarily discharged from the cavity (Detail A in Figure 4-6).

The blank holder prepones evacuation of the cavity prior to draping the material. Therefore, it has to stay in the top dead end position when the tool is open and slide down during tool closure (Scene C in Figure 4-5). The carrier and composite material must not touch the lower cavity surface in the top dead end. The blank holder therefore has a sliding path of 50 mm and exceeds the cavity surface of the complex tool of around 25 mm. In addition, the blank holder has to tightly clamp the carrier to prevent it from sliding through. This variant has been chosen (10.4 B in Table 4-3) because it provides easier process control than a sliding carrier. In order to maintain a position in top dead end and clamp the carrier, the blank holder is equipped with three gas springs SN2800-42-S (Strack[6]) with stroke, a stroke length of 50 mm and 650 N force each.
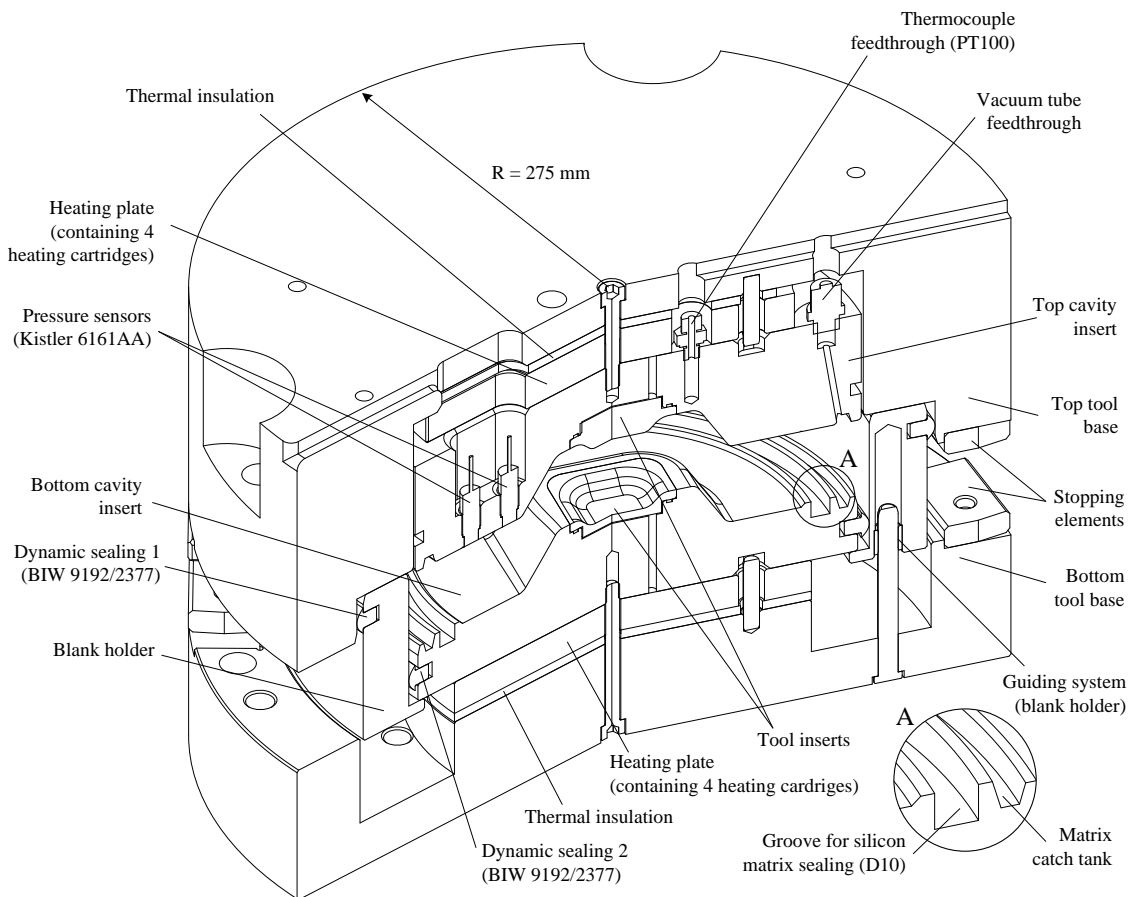
Figure 4-6 Concrete tool design for carrier-integrated pressing depicted in semi closed state (as scene B, Figure 4-5). The cavity inserts can be switched between three different cavity designs: plate, spherical cup and complex insert (depicted)

---

[6]Page 2.3.60 in http://www.strack.de/_files/media_gross/GDF.pdf; Last accessed on 01-27-2016

Since the operational temperature of the springs is limited to $80\,°C$, an internal heating system is installed. Internal heating allows the system to selectively heat the cavity in which the matrix cures under temperatures from $80 - 130\,°C$. Other parts of the tool, such as the blank holder and the tool body are only secondarily heated due to radiation, since they are shielded against the heating plate with a fiber glass insulation. In order to selectively heat the cavity, a heating plate which contains four heating cartridges is installed beneath and above the bottom and top cavity insert, respectively. Cartridges used are HLP 120087 and 125087 (Tuerk+Hillinger[7]) which are $12.5\,mm$ thick, $80\,mm$ long and provide $200\,W$ of heating power. For dynamic sealing between the moving blank holder and the inner cavity, as well as between blank holder and top tool half, dynamic sealings of BIW are installed. The sealings are used in SMC press tools[8] and thus, work under frictional load in high volume processing.

The overall geometry of the tool is circular ($550\,mm$ in diameter), since the basic structure of parts can be produced by turning to reduce manufacturing costs. All parts except supplied components are made from aluminum (EN AW 7075), which offers sufficient lifetime, is cheaper to machine and faster to heat than steel.

4.5 Experimental Determination of Carrier Material for Carrier-Integrated Pressing[9]

In order to complete the design phase of the thesis, the carrier material has to be determined and the theoretical process and tool design evaluated. Both aspects are investigated within experimental trials in two steps. First, dry draping experiments are performed with a selection of potentially suitable carrier materials. The best carrier material regarding process functionality is used in the second set of experiments, wet pressings, in which the overall functionality is initially evaluated.

---

[7]Page 9 in http://www.tuerk-hillinger.de/fileadmin/media/pdfs/HLP-5.0.pdf; Last accessed on 01-27-2016

[8]After personal interview with head of production of a fabricator of SMC tools on 04-28-2014

[9]This section is based on the term project "Experimental Characterization of Materials for Carrier-Integrated Pressing in Automated Composite Manufacturing" written by Anja Nieratschker, TU München, 2015, supervised by Paul Bockelmann

4.5.1 Experimental Setup and Materials for Carrier Material Definition

To evaluate possible carrier materials, a benefit analysis based on data from dry draping experiments and estimations is conducted. Experiments are run on the circular aluminum tool manufactured according to the design specified in section 4.4. Experimentation focuses on carrier properties that influence draping of a planar stack of NCF, thermoplastic binder and the planar carrier into a spherical shell geometry shown in Table 4-4.

NCF material to be used is selected based on its draping behavior. Fabrics with an areal weight of $300\,\mathrm{g/m^2}$ are available in three different stitch types - tricot, warp and tricot-warp. Shear trials with a pictureframe test are performed according to the methods described by Lomov [86]. Herewith, the stitching with the lowest deformation resistance and therefore the best draping behavior is identified, Figure 4-7.
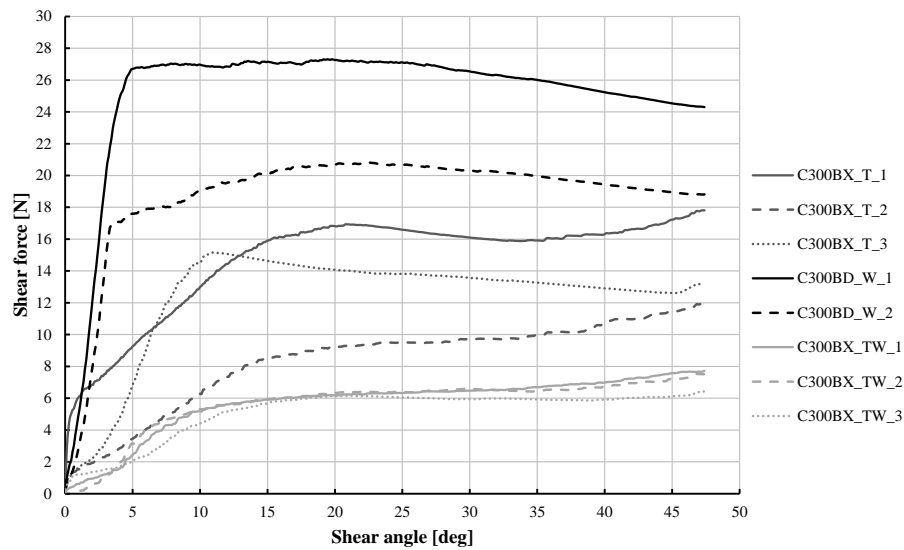
Figure 4-7 Shear force development over shear angle for NCF with different stitching (T = tricot; W = warp; TW = tricot-warp). C300BX or BD specifies the material type, carbon fiber material and fiber layout, biaxial (BX) or bidirectional (BD) with $300\,\mathrm{g/m^2}$

C300BX_TW shows the lowest shear resistance, due to its loose stitching. This matches findings of others [87, p. 144-165] [88, p. 32] who investigated shear in biaxial glass NCF and unidirectional carbon NCF with tricot-warp stitching, respectively. Additionally, in both cases a slight increase in shear forces can be seen at $50\,^\circ$. The shear resistance after that point rapidly increases, which indicates that the locking angle is reached. Thus, self-locking does not allow further deformation. The fiber material to be used in all experimental trials is CB300BX with tricot-

warp stitch consisting of 24K Tenax STS fibers of supplier Hacotech (data sheet is attached in A-1).

Relevant carrier materials for trials are selected regarding their principle qualitative properties that are expected to impact draping and matrix storage as well as ejection. The main property that determines draping behavior is believed to be the type of conveyance of carrier material: elastic deformation, plastic deformation, straightening of cavities or sliding in reference to the blank holder. Storing and ejecting matrix is influenced by the type of storage principle. Storage by gravitation and form using macroscopic cavities or storage based on capillary forces of microscopic cavities are possible. Materials considered in the study are elastic polymer film (Stretch-Vac 250, datasheet in A-4), inelastic polymer film (prototype film $50\,\mu m$ film of Infiana Group), non-fixed fibers (suction fleece for composite processing), knob paper ($100\,g/m^2$ kraft paper, Vereinigte Papierwarenfabriken GmbH) and fixed fibers (nap core material), Table 4-5.

Table 4-5 Systematic classification of carrier material properties in regard to the functions "drape fiber materials" and "store/eject matrix"

General material type	Exemplary carrier	Material conveyance to drape carrier				Store/eject matrix	
		Elastic	Plastic	Straigthening	Translation	Gravitation/Form	Capillary
Inelastic polymer	Polypropylen film*		X			X	
Elastic polymer	Silicon film*	X				X	
	Polyurethan film* **	X		X		X	
Paper	Tissue paper**		X	X			X
	Knob paper*		X	X		X	X
Non-fixed fibers	Suction fleece		X	X			X
	Peel ply				X	(X)	X
Fixed fibers	Nap core	(X)	X	X		X	(X)

* planar shape; **shape includes macroscopic cavities

The tool is isothermally heated to $130\,°C$ and opened before each experiment to allow access for material insertion. Each carrier is placed on the blank holder in a tensioned state, fixed by four cylindrical pins. A circular stack of NCF with a diameter of 140 mm is assembled with a stacking sequence of $[0°\,/90°, +/-\,45°, +/-45°]_s$. Thermoplastic binder fabric ABE 003 (Tec Web) with a processing temperature of $127-143\,°C$ is placed between each ply. The stack is then placed concentrically on the carrier in reference to the circular blank holder. In that state, the tool is closed with a velocity of 3 mm/s until a nominal cavity thickness of 2 mm is reached, held 30 s to activate the binder and then opened with 3 mm/s for extraction of the formed dry material and carrier.

From the extracted parts, data for the benefit analysis are obtained using visual and physical inspection, computerized image segmentation, fiber angle measurement using the Profactor sensor [89] and estimations to evaluate benefit criteria. Evaluated criteria concretely represent functions depicted in Figure 4-4, Table 4-6.

Table 4-6 Objectives of carrier materials evaluated in dry draping experiments

	Evaluation criteria	Represented function	Measured / Estimated
Z11	Technical criteria		
Z111	Flexibility of the carrier material		
Z1111	Number of wrinkles	Convey carrier material during drape	Visual inspection
Z1112	Number of ruptures		Visual inspection
Z112	Increased part weight by carrier	Attach carrier to laminate	Estimation
Z113	Transfer tension to fibers		
Z1131	Deviation of fiber angle	Transfer tension to fiber material	Profactor sensor
Z1132	Deviation from target geometry		Profactor sensor
Z114	Seal tool with carrier	Generate resin tightness	Physical inspection
Z115	Storing/ejection of resin on carrier		
Z1151	Defined position of resin on the carrier	Store/eject resin	Estimation
Z1152	Forming of cavities into carrier		Estimation
Z1153	Elimination of cavities		Estimation
Z12	Economic criteria		
Z121	Material costs [€/m²]		Purchasing price
Z122	Processing costs		Physical inspection (resin tightness)

Each objective is weighted in an objectives tree after Pahl [51, p. 110-123] according to criticality of the respective function, Figure 4-8.

In order to combine different criteria within an overall benefit value, points are awarded between zero and four to each criterion with four representing ideal. Criteria that are measured, such as fiber angle deviations, are translated to benefit points regarding a linear function between best and poorest results. When the benefit of criteria must be estimated, points are directly awarded.

Visual inspection is manually performed to count the number of wrinkles and ruptures of each carrier. Wrinkles within a carrier result in poor part surface on the carrier side or lead to preform wrinkling. No wrinkles and ruptures are awarded four points, with point reduction relative to severity of wrinkling and thinning. Complete ruptures are evaluated with zero points.

Matrix tightness of a carrier material is estimated manually. If a carrier is matrix tight, it is supposed that no matrix contacts the lower mold, which reduces processing costs because this mold half does not need to be cleaned or prepared. Thus, this carrier earns four points for reduced processing costs, otherwise zero points are given.

Added part weight by carrier material is estimated from the areal weight of a carrier material and the ability of the carrier to be impregnated by resin. The more porous and the thicker a carrier is, the higher the added weight is in addition to
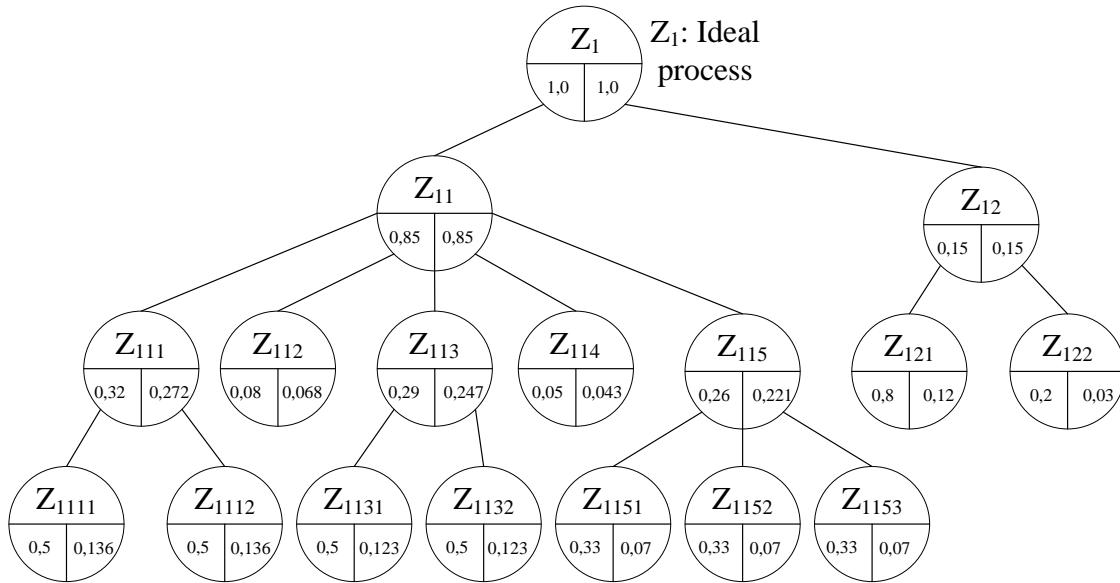
Figure 4-8 Objectives tree for the evaluation of carrier material. Objective names are given in Table 4-6, left numbers indicate the global weighting factor of an objective, the right number the relative weighting factor inside each group of sub-objectives

the carrier's weight. Points are awarded regarding a linear function between the highest and lowest weight increase.

The capability of a carrier to store and eject matrix is estimated from physical inspection and manual trials of how well storage cavities can be formed into the base material and how well these cavities can be eliminated during pressing in regard to wrinkles. This criterion also includes how well defined the position of applied matrix on the carrier is.

The criterion "Transfer tensions to fibers" (Z_{113}) mainly considers the draping quality provided by the carrier. The quality of draped fibers is determined by the deviation of fiber angles from a target angle and the deviation of the macroscopic geometry of the draped fibrous structure from the cavity geometry. Fiber angles are measured with the F-scan software from images acquired using the Profactor fiber sensor after [89]. Data are then exported to Matlab to plot histograms of angle distribution. The mean over each histogram's standard distribution is computed from data of three trials per carrier as a measure of fiber angle deviation due to draping, Figure 4-9.

Fiber angles from trials produced with elastic polyurethane film can not be measured, since the fiber material is displaced during demolding because the carrier clings to the lower mold. Hence, results are estimated based on results from the silicone film. Standard deviations extracted from the histograms (Scene D in Figure 4-9) are again translated into the point scale by means of a linear function between smallest (best) and highest (worst) standard deviation.
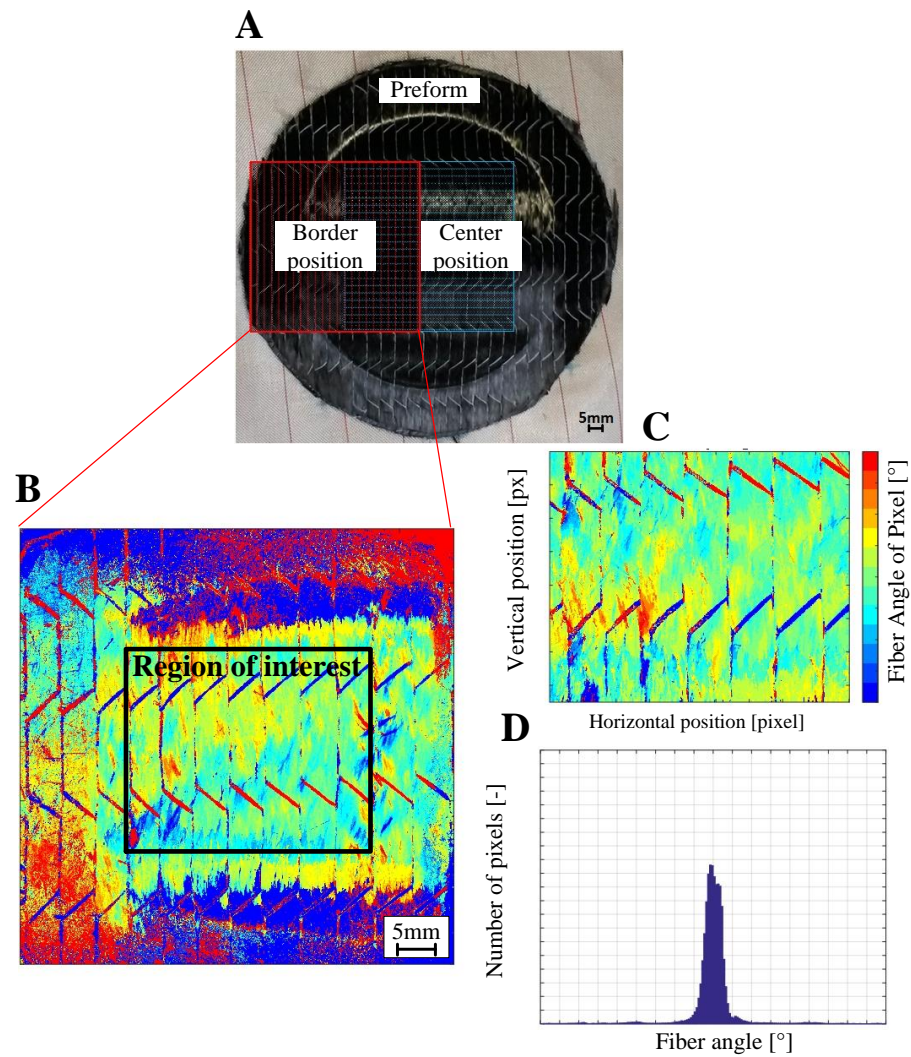
Figure 4-9 Measurement of fiber angle deviation of dry fibers to evaluate draping quality of carriers. An image is taken from a border or center position of a draped preform (A) with the fiber angle sensor (Profactor). Its software computes a false color image in reference to fiber angles (B). The region of interest (C) is analyzed in Matlab and the fiber angle distribution is plotted in a histogram (D) with its respective standard distribution

Deviation of macroscopic geometry is measured from images using Halcon 11, a software for image recognition. The boundary of the spherical section is isolated from the image, smoothed and fitted with a circle. Difference between the radii of the fitted circles and the ideal radius of 90.83 mm is obtained as a measure of the macroscopic draping quality, Figure 4-10.
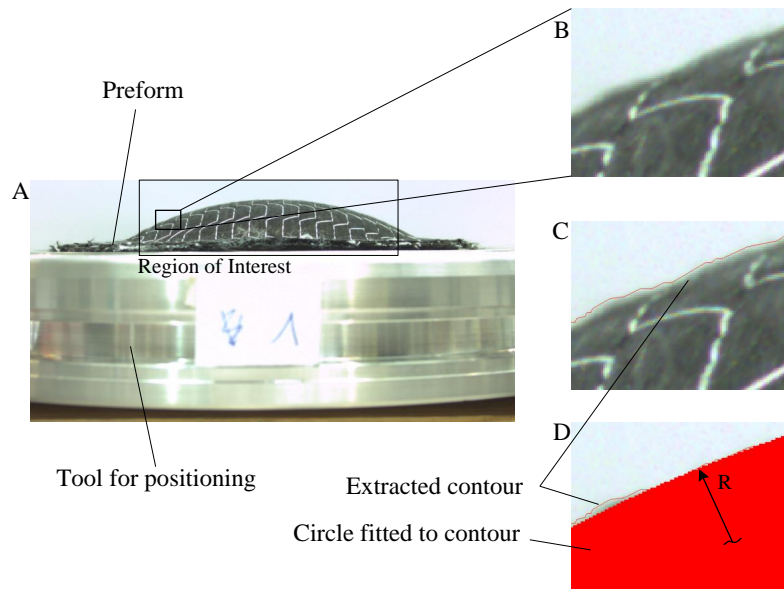
Figure 4-10 Measurement of macroscopic geometry quality of draped dry fiber material. An image from a positioned preform is acquired (A, B). The boundary of the fiber material is extracted (C) within the region of interest and a circle is fitted to the extracted contour (D) with Halcon 11

4.5.2 Results of Dry Draping Experiments for Carrier Material Definition

Carriers consisting of fixed fibers, like paper, generally show a low tendency to wrinkle during draping of the given geometry. Varying results are obtained in regard to ripping - knob paper ruptured in every experiment although deformation consumed the initially existing knobs, while tissue paper was not affected. Non-fixed fibers showed excellent draping behavior in regard to wrinkling but were subject to ruptures or thinning. Polymer films showed, independent from their elastic or plastic properties, no rips. Wrinkles were primarily formed by the plastic film, while the elastic film performed better.

Only fiber-based carriers are subject to notable resin impregnation that increases part weight in addition to carrier weight itself. It is assumed that the density of the material determines resin uptake. Thus, the share of resin in knob paper ($154\,\mathrm{g/m^2}$; $2.7\,\mathrm{g}$ added part weight by carrier) made from Kraft paper is estimated to be $7\,\%$.

Peel ply (86 g/m²; 6.7 g added part weight by carrier) is assumed to uptake 5 % of resin. Absorption by tissue paper (55.6 g/m²; 0.86 g added part weight by carrier) and suction fleece (146 g/m²; 2.25 g added part weight by carrier) is estimated to be 10 % and 20 %, respectively.

Complete air tightness that facilitates tool sealing can only be guaranteed by plastic films to their porosity which earn four points. Suction fleece seems to provide the possibility to acting as a sealing when compressed (two points) whereas other fixed or non-fixed fiber-based carrier show little or no capabilities for sealing.

To define a position of matrix on the carrier, macroscopic cavities which provide this functionality by form/weight are considered best. Thus, all carriers made from polymer films are expected to allow a highly defined positioning (four points). Due to its porosity, knob paper and nap cores provide additional storage capability by capillary forces which are expected to worsen the definition of matrix position (three points). Storage by capillary is considered less ideal, thus suction fleece and tissue paper were evaluated with two points. Peel ply proves to leak resin shortly after deposition and is awarded one point.

In order create macroscopic storage cavities, initially flat material has to be deformed. All polymer films, excluding silicone, show good forming capabilities, for instance by thermoforming. Non-fixed fibers may primarily be formed in their textile processes but are subsequently not easily deformable. Nap core materials can be formed in a deep drawing process with subsequent stabilization with resin [90], but the process is costly and inflexible compared to thermoforming of films. Non-fixed fibers, such as peel ply, can be formed but do not maintain the imposed shape without additional stabilization.

In order to avoid wrinkling of the carrier walls, and thus wrinkling of the fiber material, cavities have to be eliminated effectively during the process. Carriers drawing on capillary forces to store resin are compressed without wrinkling. Macroscopic cavities of fixed fibers however are prone to wrinkling, as are silicone and polypropylene film, since cavity walls are displaced, not compensated. Elastic polyurethane films, however, generally show almost no wrinkling.

Material costs are obtained from quotes of available materials. Nap cores are most expensive, since they are to date only produced in low volume with special material requirements. Knob paper is used for packaging and is the cheapest material. Between those extremes a linear function $y_{c,i} = -0.61x_{c,i} + 4.24$ is constructed for point evaluation, with $y_{c,i}$ being the awarded points between zero and four and $x_{c,i}$ the costs (index c) of the considered material i in € .

Differences in draping quality of the carriers are only minimal and depend on the sensor position. Highest fiber deviations of fiber angle distributions are obtained in

the border region. Standard deviation is calculated from three trials of each position and carrier, except nap cores, Figure 4-11. This core material is theoretically evaluated, since they are available in sizes which are too small for practical trials.
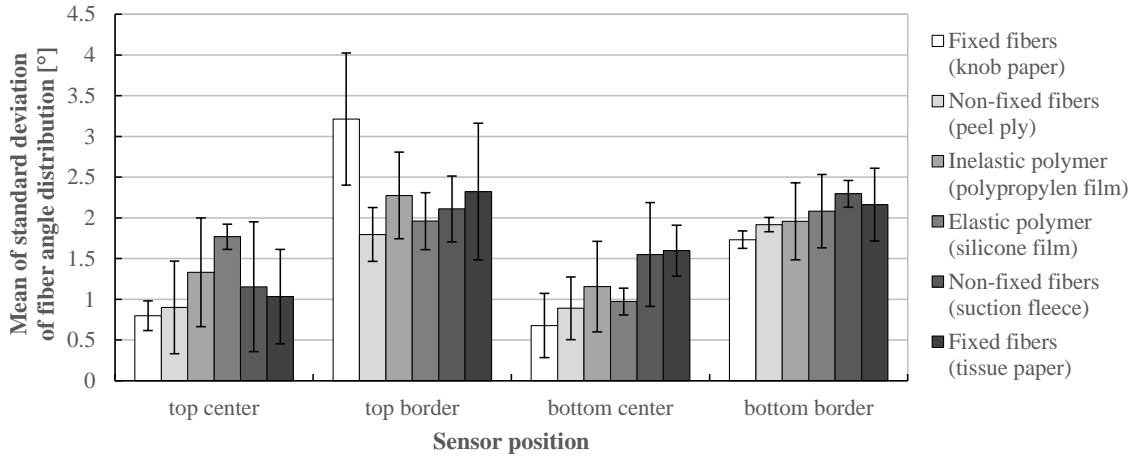
Figure 4-11 Mean of standard deviation of fiber angle distribution as a measure of draping quality (number of trials per carrier and sensor position n=3; error bars depict standard deviation

Objective values are computed using the sum of means of each sensor position. Best results shows the peel ply (5.5°), which is evaluated with four points, worst performance shows the suction fleece with 7.11°, which is evaluated with zero points. Other benefit values $y_{d,i}$ for draping quality d are computed using the resulting linear function $y_{d,i} = -1.3x_{d,i} + 11.18$ with $x_{d,i}$ being the sum of means of standard deviation of material i.

Macroscopic deviation of the shaped dry fiber geometry are computed in percent of deviation from the ideal radius. Non fixed fibers show relatively little deviation, fixed fibers result in highest deviations. Elastic silicone film performs better than polypropylene film with the lowest overall standard deviation from three experiments, Figure 4-12. Nap cores are not tested, since no sufficient carrier sizes are available.

Best and worst results represent four and zero points, respectively. All other benefit scores $y_{g,i}$ are derived using the linear function $y_{g,i} = -0.392x_{g,i} + 6.353$ with $x_{g,i}$ being the average geometric deviation g of material i.

Measurements and initial point evaluation of criteria are assembled in the objectives measurement matrix, Table A-2. From that outset, all measurements are transferred to points within the objectives value matrix, Table A-3. Finally, points are weighted according to the target system within the benefit value matrix, Table A-4. From the latter, a graphic representation, the benefit portfolio after Rinza [91, p. 118], is constructed from Table A-3 and A-4 for sub-criteria Z_{111}-Z_{115}, Z_{121} and Z_{122}, Figure 4-13.
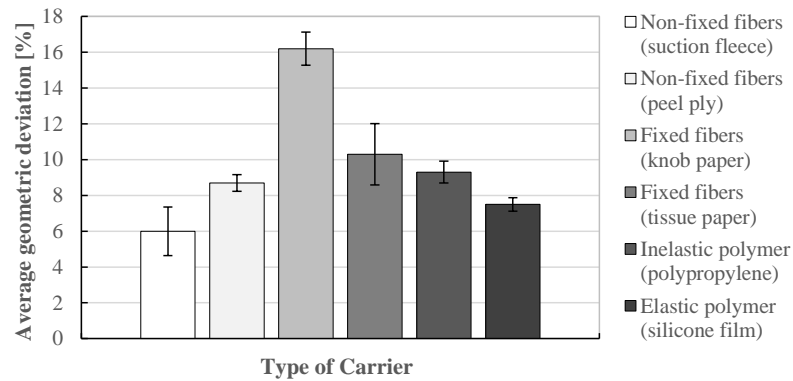
Figure 4-12 Average macroscopic deviation of spherical section of shaped dry fibers from planned geometry (error bars depict standard deviation from number of trials n=3)

Polymer films perform best among the carriers tested. Within this material class, elastic films provide the highest benefit values for the objective of this study. The polyurethane film outperforms silicone only slightly, since it is much easier to be fitted with cavities using thermoforming. Results for fixed and non-fixed fibers do not show a clear tendency for the material classes. Tissue paper is best among both, while nap cores perform poorest. The latter was evaluated without press experiments, since dimensions of sample materials were too small. Due to their use in complex sandwich parts it was assumed their drapability is good and they do not add much weight to parts. Material costs and the capability to store matrix were both evaluated poorly.

4.5.3 Conclusion of Carrier Material Definition

In order to find the optimal carrier material, the benefit value of several exemplary carriers regarding the fulfilment of functions in Figure 4-4 was studied. The properties of materials studied were abstracted and classified into inelastic and elastic polymer, fixed and non-fixed fibers. For each class, a minimum of one exemplary carrier was found and evaluated in practical draping trials on a prototype tool.

Although all carriers produced good preforms, some carrier structures were destroyed during the process. Fiber carriers showed thinning or even ruptures. Regarding draping behavior, no significant differences were identified in fiber angle measurements (Figure 4-11), since the geometry was simple and no high fiber deflections were found. However, standard deviations over three trials per carrier were much higher for fixed than non-fixed fibers or polymer films. It is assumed that this was caused by higher friction between fibrous carrier material and the dry carbon NCF.
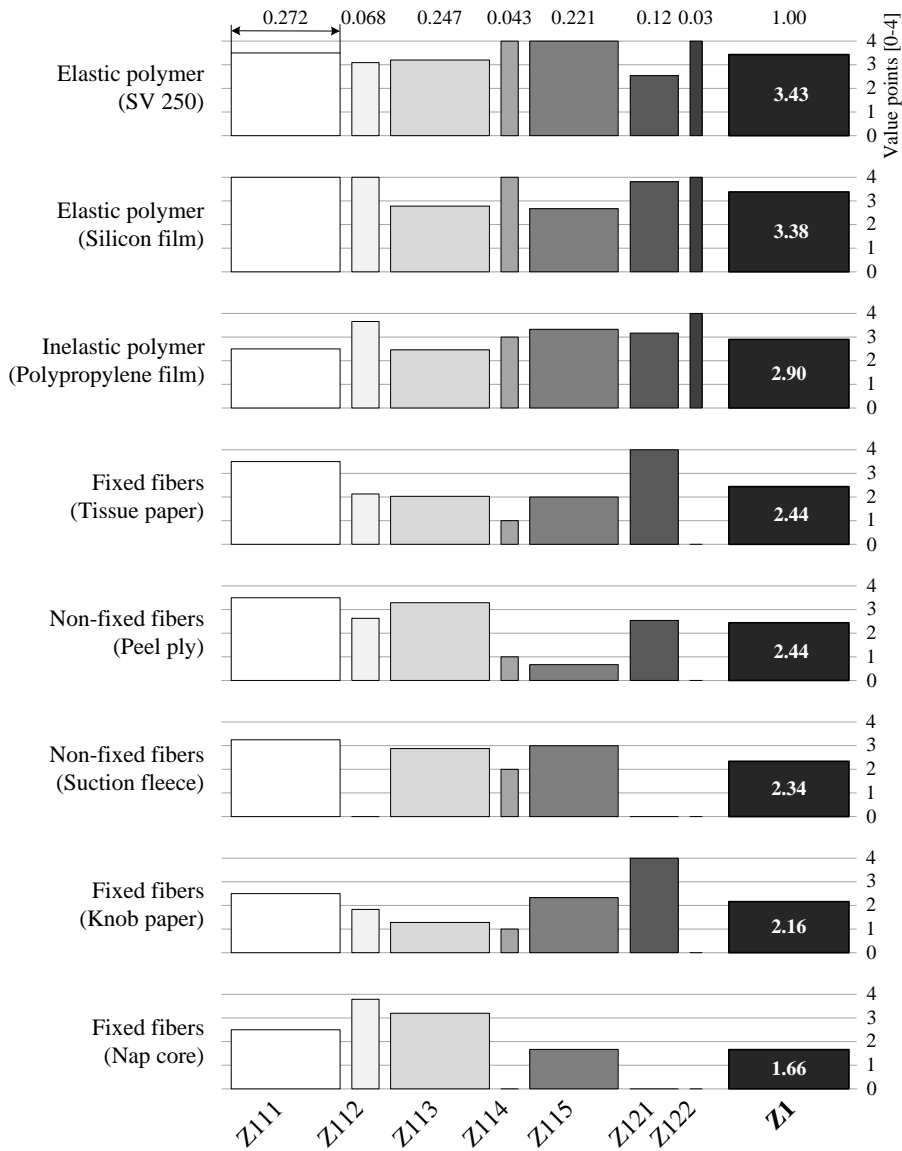
Figure 4-13 Benefit portfolio of carrier materials for CIP

In regard to macroscopic geometry deviation from the cavity shape, suction fleece and silicone film produced best results, possibly due to their good shape adaptivity and low friction between NCF and carrier.

For theoretic discussions considering tool sealing, storage and ejection of matrix and cost aspects, air and resin tight films are estimated to provide the highest benefits. It is hypothesized that capillary effects, which are absent in the polymer films considered, lead to a non-defined position of the matrix on the carrier. Polymer films, except for silicone, can be deformed easily to provide carrier cavities by thermoforming. Fixed or non-fixed fibers are more difficult to be formed and stabilized.

The polyurethane film SV 250 could not be analysed in dry draping trials because it melted under the temperature needed for binder activation. Despite that, it is assumed to produce good draping results due to the same elastic behavior as silicone film. Elastic behavior in that case appears to be very important, as it drastically reduces wrinkles which occur in trials with polyproplyene film. It is likely that due to the absence of normal forces between the blank holder and the cavity, the carrier starts to buckle under pressure forces generated through shear in draping. This effect is known from metal deep drawing, Figure 4-14.
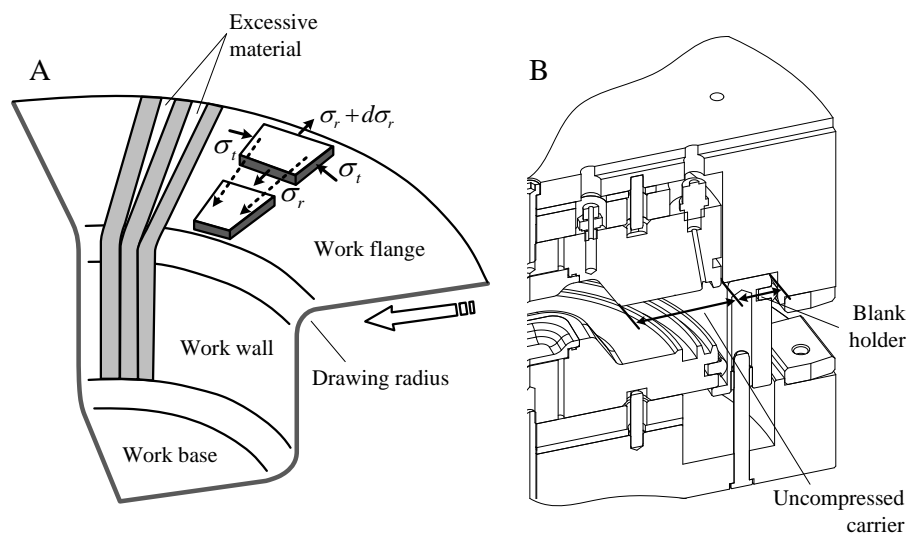
Figure 4-14 Wrinkling in work flange during deep drawing due to compressive stress (A; adapted from [92, p. 197-200]). Between blank holder and the area of deformation inside the CIP tool remains a free length in which the carrier is uncompressed, which could lead to buckling (B)

Buckling in deep drawing of metal blanks occurs due to the compressive stress σ_t that follows the compression of material that flows from outer to inner sections of the flange. In case of the CIP tooling, there is a free length between blank holder and cavity in which the carrier is not compressed. It is assumed that due to elastic properties, the carrier inside the tool is more pre-stretched than inelastic films. Thus, compressive stress during draping is superimposed by tensile stress during pre-stretching. This results in fewer wrinkles.

In the light of the dry draping results, the elastic polymer film SV250 (Stretch-Vac 250, datasheet in A-4) is used for further wet experiments to initially evaluate the overall functionality of CIP design in the next section.

4.6 Experimental Process Validation of Carrier-Integrated Pressing

The goal of the initial evaluation of CIP design is to investigate to what degree the functions on which the tool and process design for CIP were grounded (Figure 4-4) are fulfilled by the current design. Evaluation is performed qualitatively to guarantee usability of the tool and process. More detailed, quantified investigations of matrix flow control is presented in the next chapter, based on this initial validation. The validation consists of two separate aspects. Firstly, carrier thermoforming and subsequent pressings are arranged and optimized to result in spherical laminates of good quality. Secondly, complex laminates are produced to qualitatively validate the function "*transfer tension to fibers*" by the elastic carrier film.

4.6.1 Overall Process Evaluation

In order to use a carrier film with cavities for matrix storage, films have to be shaped into their intended geometry. Deformation of thermoplastic films is most suitably done by thermoforming as defined by Schwarzmann [93, p. 1]. This concept is applied to forming of carriers from SV 250, a thermoplastic polyurethane film, using a manually operated thermoforming machine, KFG 37 (Illig), Figure 4-15.

Heating of SV 250 on KFG 37 is performed at $350\,^{\circ}\text{C}$ for $10\,\text{s}$ before forming, which leads to a good trade-off between reproduction of the tool geometry and high enough thickness of cavity walls for their stability. After thermoforming, carriers are stored at $-18\,^{\circ}\text{C}$ in order to prevent the reversion of cavity forming in consequence of creeping [94, p. 52-53].

Suitable cavity geometry and arrangement for forming and CIP processing are identified in experimental trials, requiring a tool for each design. The basic aspect of cavity geometry is the volume needed to store the entire mass of matrix for a respective part geometry and volume or mass of fiber material. For the initial trials for wet pressings of spherical parts, a manually machined tool is used. For complex and plate parts, 3D printed tools are derived, Figure 4-7.

Conical cavities are used for initial evaluation of the overall functionality. To produce parts of complex and plate geometry, cavity sizes were changed and required re-engineering of cavities. Thus, hexagonal and conic section design are developed. The first allowed seamless tiling of the carrier but thermoforming of the films did not result in good geometry replication due to sharp edges of the hexagon cavities. The latter, conic section design, proved to be a good trade-off between geometry replication and tiling of the carrier. Both designs need many vacuum vents to al-
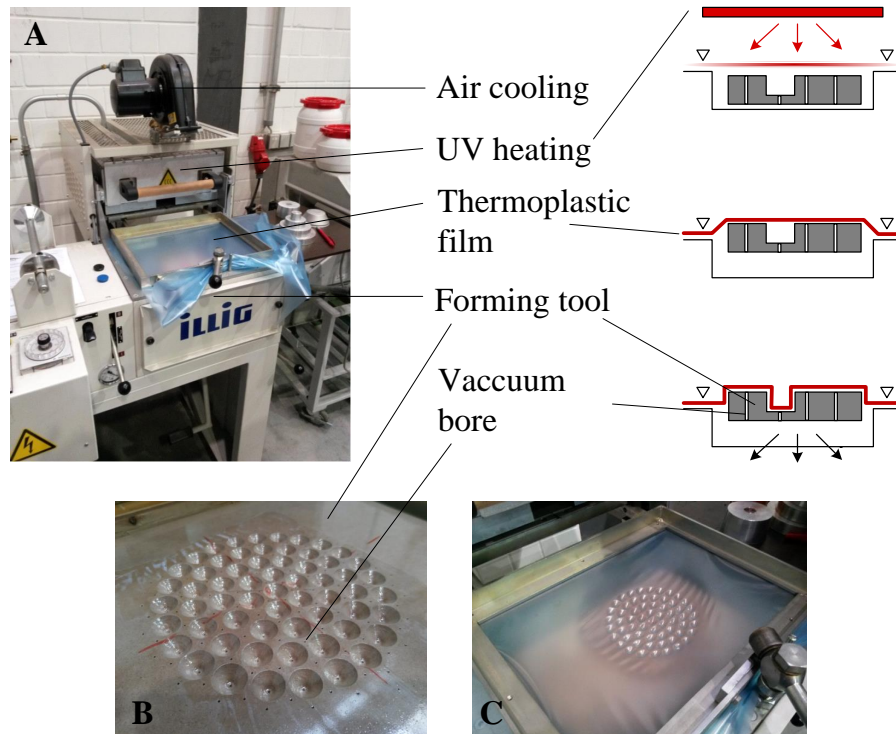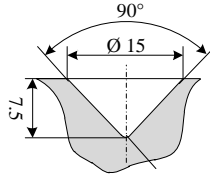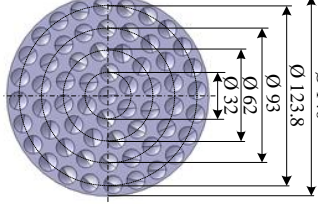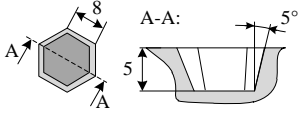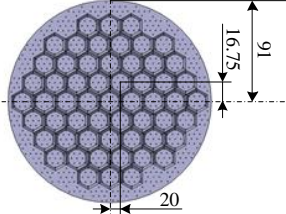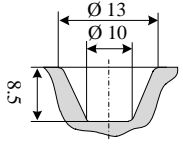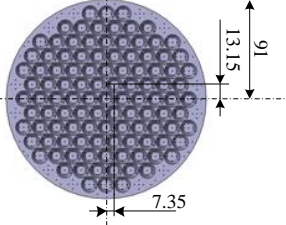
Figure 4-15 Thermoforming of SV 250 to produce carriers with cavities for matrix storage. KFG
37 with equipped film and tool (A); Formed film on tool with cavities (B); Formed
film after demolding (C)

low for sufficient forming of the film into the tool cavities. Thus, the tools were
additively manufactured on a Stratasys Objet 30 prime from high temperature
RGD525 polymer. No vents need to be drilled because they are already formed
during printing.

For the initial press experiments, the tool is preheated to 100 °C and a thermo-
formed carrier, stored at −18 °C, is placed onto the blank holder in a stretched
state, held by four pins. The fiber material stack is prepared similar to stacks for
the dry experiments (Section 4.5.1) but without binder material. A mass of 60 g
of reactive matrix XB3585/XB3458 is dosed by a custom-made three component
dosing machine (Dekumed) into a paper cup containing 1.5 g internal release agent
Wuertz PAT-657/BW. Temperatures for the resin and hardener are set to 60 °C
and 25 °C, respectively. The dosed matrix and release agent are mixed manually for
15 s and are then distributed into the cavities of the carrier inside the opened tool.
After matrix distribution which requires approximately 30 s, the prepared fiber
stack is placed onto the carrier concentrically to the blank holder. Subsequently,
the tool is closed with a velocity of 3 mm/s until the carrier is clamped between
the blank holder and the top tool body (Scene B in Figure 4-5). The tool cavity is
evacuated to approx. 2 mbar before the tool is closed to final part thickness with

Table 4-7 Tools for thermoforming of carrier cavities

Cavity design	Fundamental geometry	CAD model	Specification
Cone	$90°$, Ø 15, 7.5	Ø 140, Ø 123.8, Ø 93, Ø 62, Ø 32	Number of cavities: 61 Matrix mass per cavity: 0.5738 g Total matrix mass: 35 g Fiber mass: 27.71 g Parts used for: sphere Film elasticity correction: 0.0
Hexagon	8, A-A:, A, A, 5°, 5	91, 16.75, 20	Number of cavities: 57 Matrix mass per cavity: 1.67 g Total matrix mass: 95 g Fiber mass: 45.8 g Parts used for: complex part Film elasticity correction: 0.5
Conic section	Ø 13, Ø 10, 8.5	91, 13.15, 7.35	Number of cavities: 109 Matrix mass per cavity: 1.04 g Total matrix mass: 113.23 g Fiber mass: 45.8 g Parts used for: complex/plate Film elasticity correction: 0.5

3 mm/s. The part is cured within the heated cavity for 3.5 min before the tool is opened and the part is demolded.

Functionality of the process and tooling is qualitatively evaluated based on visual inspection of pressed laminates and micrographs, Figure 4-16.

After initial experimentation with the preparation procedure and press velocity, visually appealing laminates with attached carriers were produced with the method prescribed above. Vacuum could be generated inside the tool and remained below 2 mbar over the entire press stroke. Draping and impregnation were possible using the SV 250 film which was found to bond to the matrix above 60 °C tool temperature. Cavities used for initial matrix storage were almost completely eliminated after pressing (Scene B.2 and D.3 in Figure 4-16). Almost no wrinkles from the storage cavities were found after pressing. It must be assumed that cavities are not primarily eliminated due to normal forces during compression but that polymer molecules that are stretched and stabilized during thermoforming rearrange under heat, which conforms to creeping behavior of thermoplasts [94, p. 52-53]. Micrographs show good quality of the pressed laminates (Scene D.1-D.3 in Figure 4-16) with low void content and densely packed fibers. In optical analysis of the micrographs performed with the Stream Motion software (Olympus) a FVC of 53 % was determined, which matched the theoretical FVC.
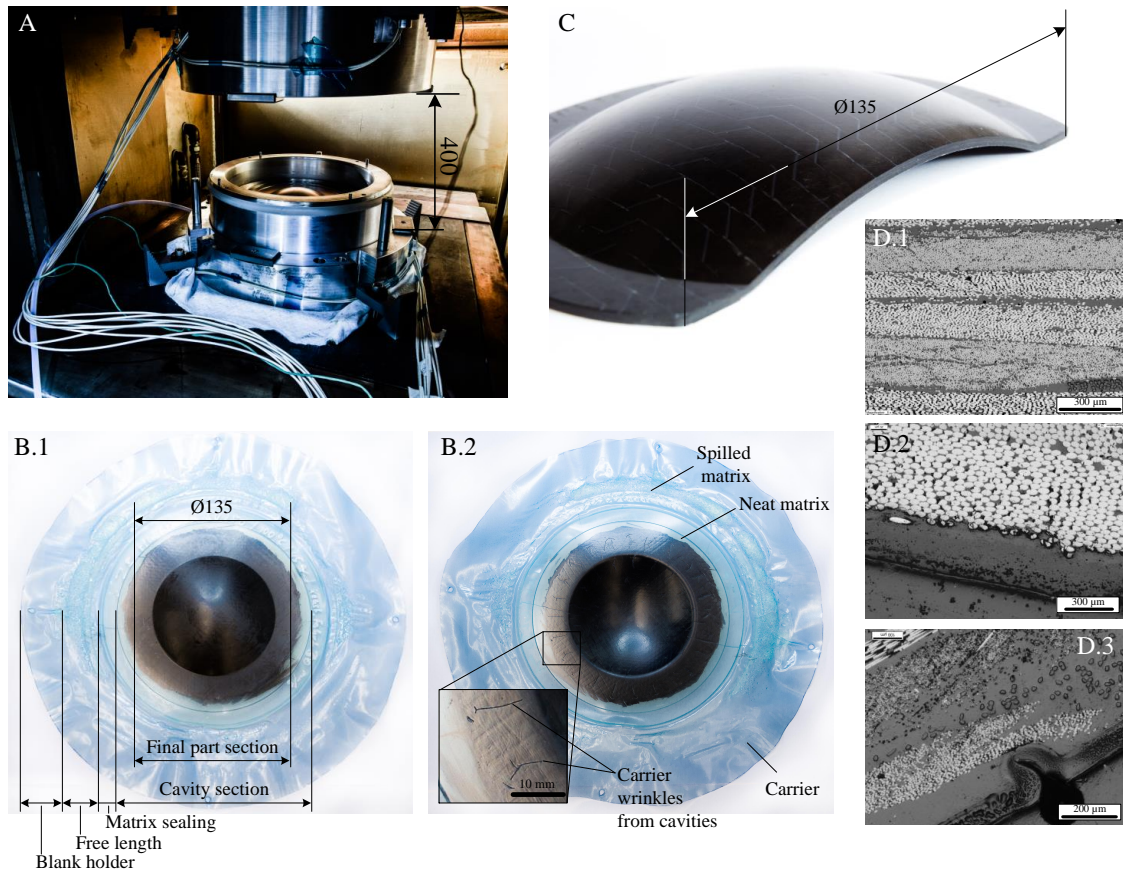
Figure 4-16 Tool system before material insertion (A) and pressed laminate with attached carrier film (top B.1; bottom/carrier side B.2); Pressed laminate after trimming with carrier film bonded to its bottom surface (C); Micrograph from section representative for part (D.1), carrier film bonded to laminate (D.2) and wrinkle in carrier film as residue from matrix storage cavity (D.3)

The findings of the initial press trials indicate that the process and tool design derived for CIP were qualitatively functional. However, carrier use for draping must be considered for more complex parts in order to allow for a confident assessment of that critical functionality.

4.6.2 Evaluation of Fiber Material Draping

Fiber material draping due to carrier film deformation is the most critical function of the process and follows the assumption that fiber material is clamped between the carrier stretched during tool closing and the upper tool wall (solution 24.1 in Table 4-3). The resulting frictional forces act as tensioning forces under which the fiber material can slide into the cavity without wrinkling. To test the functionality, the complex part geometry (Table 4-4) is pressed. In order to guarantee constant process condition, a clamping frame for the carrier is introduced. On the one hand,

the frame preserves a constant carrier tension on its circumference. On the other hand, all materials for pressing can be prepared outside of the press and only inserted with the frame prior to pressing.

To manually prepare the carrier outside of press, the carrier is stretched by a pre-tensioning frame by four spring loaded clamps (spring rate of approximately $5\,\mathrm{N/mm}$) holding a square blank on its corners. The uniformly tensioned carrier is positioned on an aluminum clamping frame with the thermoformed cavity concentric to the rim of the ring. A compliment top ring is snapped onto the bottom ring by means of embedded magnets in both rings. Two adjacent magnet pairs are embedded to reject each other. Thus, the top ring centers itself while it is snapped onto the bottom ring. The carrier is then clamped between the two rings, fixated by magnetic force. Finally, the overlapping edges of the carrier are trimmed.

Subsequent material preparation and pressing are performed according to the press method for spherical parts with matrix and NCF masses adjusted for the complex geometry (Table 4-7) and the exception of the tool closing velocity. It was found that a closing velocity of $5\,\mathrm{mm/s}$ produced good laminates and led to less matrix discharge from the cavity during pressing.

Fiber paths within the complex geometry are expected to be strongly influenced by the replicated part geometry. If draping of the fiber material works properly under carrier use, fiber paths do not show wrinkles but follow the the part geometry as expected. Complex parts that were produced after the method described previously showed no wrinkles, despite theoretical shear angles of the draped NCF that are close to the locking angle of the material at approximately $50\,^{\circ}$, Figure 4-17.

Shearing angles of the fabric peak in part corners and in the flanges for $0/90\,^{\circ}$ and $+/-45\,^{\circ}$ layers, respectively. Pressed laminates show fiber deflections in the draped $0/90\,^{\circ}$ layer that qualitatively correspond with deflections predicted by the kinematic draping simulation and do not show wrinkles. Furthermore, several parts produced under the same conditions showed similar fiber path distributions.

Fiber paths and geometry of pressed laminates indicate that the draping functionality of CIP with use of carrier works. It is therefore assumed that the process generally allows production of complex parts.

4.7 Conclusion of Design of Carrier-Integrated Pressing

Design of CIP focussed on how a production system can be conceived from the principle solution of carrier use as a means to store and eject resin (Figure 4-1).
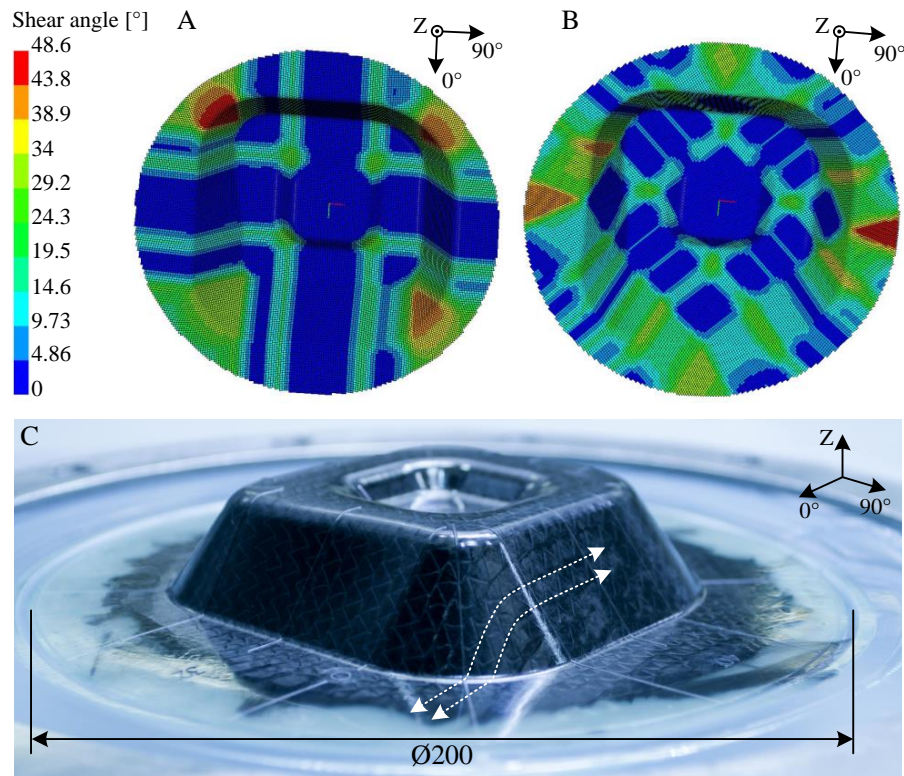
Figure 4-17 Theoretical shear angle distribution of $0/90°$ (A) and $+/-45°$ layers (B) according to kinematic draping simulation of the complex part geometry. Fiber paths after draping do not show wrinkles that may originate from insufficient fiber tension during draping and part does not show geometrical flaws (C)

The design procedure was guided by MPM based on functions derived from a literature review on LCM processing and included selected methods for each design step. The importance of derived functions were estimated in an effect analysis and showed that the most critical function at the early stage of design was "*Generate vacuum tightness over press stroke*". A technical conflict between vacuum tightness and press stroke was solved by drawing on the TRIZ construct and solutions were derived from the principles of new dimension, prior action and mediator. Considering a new dimension was realized by separating air and matrix tightness. This separation in combination with preponing an action, led to the solution of using a blank holder. The blank holder clamps the carrier and seals the tool with dynamic silicone sealings. The third principle, mediator, was applied to the carrier. It acts as a mediator of tensile forces onto the fiber material for drape and shields sensible sealing elements from reactive matrix.

The most beneficial carrier material regarding fulfillment of the derived functions was selected by a benefit analysis based on dry draping experiments. It was found that thermoplastic elastic films perform best. Macroscopic cavities can be easily

thermoformed into the carrier and wrinkles during draping are effectively reduced by elastic pre-tension.

Finally, the design of tool, carrier and process was evaluated in wet experiments within two steps. Firstly, a spherical part of low complexity was successfully produced and showed that the process definition, carrier layout and tool work as intended. Secondly, a highly complex part was pressed, which qualitatively showed that the carrier is capable of acting as a mediator of tensile forces onto the fabric to allow for good draping of the material. Even under manual material preparation, a defined matrix storage inside the thermoformed cavities is possible. For both parts a process setup was found that showed no dry spots, major impregnation flaws or fiber wrinkling due to poor draping. In addition, storage cavities produced only minor wrinkles. It is assumed that creeping of thermoplastic molecules stretched during thermoforming is increased under the heat during processing. This would lead to a partial elimination of the cavities prior to final compaction.

CIP was shown to work manually but was derived in the light of industrial processing. The principles known from WCM do also apply to CIP. This includes industrially established supply of semi-finished materials and their preparation outside of the press tool. All functions of the CIP tool itself, in particular the dynamic sealing and blank holder concept, as well as further part treatment with bonded film do not impair the classical chain of compression molding processes, Figure 4-18.
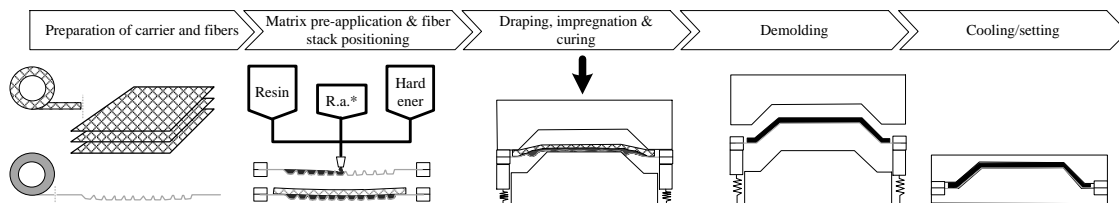
Figure 4-18 Industrial process chain of CIP (*R. a.= release agent). Carrier film with cavities is supplied on roll, similar to the fiber material used. Thermoforming of the carrier film is performed after film extrusion, as industrially realized for production of air cushion film[10]

The combination of production system, carrier material and process setup qualitatively work as intended to solve the polylemma of conflicts of automated WCM (Figure 3-2). All requirements short matrix flow path, high impregnation quality and clean and secure handling of semi-finished materials seem to be fulfilled by the existing production system. The conflict between pre-application of matrix and stabilization of semi-finished materials could be solved with the macroscopic cavities that store matrix close to its intended curing location without contacting the fiber material. However, it remains unclear if the conflict between matrix pre-application and controlled matrix flow is solved by the new process. Although good parts were produced with the new process, initial experiments of WCM, where a

carrier film without cavities was used and the matrix was pre-applicated onto the fibers, showed no indications of a minor quality.

With the current process design the prerequisites for industrial production of CFRP parts with CIP are given. However, on a production-scale view, it is not clear how process design, process parameters and the production technology interact compared with the traditional high-volume processes RTM and, in particular, WCM. Precisely, it remains to be investigated if reduced fiber input due to the draping mechanism of CIP can offset increased matrix consumption and additional use of carrier in terms of costs and environmental impacts.

5 Matrix Flow in Compression Molding Processes

No information on matrix flow in WCM processes has been published so far and the conflict between pre-applied matrix and controlled matrix flow during pressing hypothesized in this thesis (Figure 3-2) has not been tested. Since matrix pre-application itself is considered a prerequisite, the matrix flow and its control influenced by the initial position of the matrix after pre-application is of interest. In this regard, different hypothetical flow situations for WCM and CIP have been formulated (Figure 3-1 for WCM and Figure 4-2 for CIP). Furthermore, the process parameters certainly influence the flow, too. Both aspects lead to the following question that lies at the heart of this chapter:

2.1 How does matrix flow through fiber material in WCM and CIP?

Because matrix position and its flow during pressing are linked, cavity elimination has to be taken into account with the following question:

2.2 How is cavity elimination linked to matrix flow?

Matrix flow and its control have been closely linked to part quality in RTM processing and thus it is important to ask for both process types, WCM and CIP:

2.3 Is a more homogeneous matrix flow in press processes associated with better part quality?

Questions 2.1-2.3 are strongly influenced by process parameters of the respective process. In order to answer them more universally, changing process parameters within design of experiment studies for WCM and CIP are considered. The studies are conducted experimentally with the tooling system developed in Chapter 4, on which plates are produced for both WCM and CIP. In case of WCM, a film without cavities is used and the matrix is pre-applied on top of the fiber stack.

Since industrial processes usually produce parts of complex shapes, flow situations under drape should be considered in addition to the plate studies. It is assumed that the flow is governed by gravity when draping begins. Therefore, the following

question is framed in regard to flow situations under draping :

2.4 How does draping disturb matrix flow in WCM and CIP?

This question will be investigated with a fixed set of process parameters for WCM and CIP with which plates as well as a complex parts are producible. No parameter variation is taken into account.

Since the questions shall be answered by evidence from press experiments performed on the developed tooling, an appropriate method to visualize matrix flow has to be defined. As existing experiments are not suitable for compression molding, a new method has to be developed. Material and process parameters have to be monitored regarding their variability, since materials are prepared and the press is controlled manually. The new method for matrix flow analysis and the visual monitoring method are based on the same principle and will be presented in the next section. The experimental setup, materials and their preparation methods for the press experiments are specified subsequently. The results section does not only include results regarding matrix flow but also analysis of material preparation and press parameters to secure low variability. The chapter closes with conclusions drawn from the experimental results in regard to the framed research questions.

5.1 Development of Visualization Methods to Investigate Matrix Flow[1]

In processing of composites, materials are continuously dislocated from an initial position to their final position. Thus, it is obvious to use visual analysis of photos or videos to research the intermediate flow, especially for matrix flow. However, information on matrix flow in processes are difficult to obtain. While some investigated flow during compaction of prepreg materials with computer tomography (CT) [95], others used transparent tools to trace the effects of flow with cameras, either on a macroscopic [78, p. 9] or microscopic scale [96]. Camera-tracing even allows to continuously monitor flow throughout the entire process which is not the case with CT pictures. Centea and Hubert still visualized the progression of the matrix during compression via time-dependent disruption of the slow vacuum bagging process [95, p. 595]. However, both alternatives are generally unsuitable to study flow in compression molding, since transparent tool walls deform under

---

[1]This section is based on the term project "Entwicklung und Anwendung einer makroskopischen Analysemethode zur Charakterisierung des Harzflusses in Nasspressverfahren" written by Johannes Maierhofer, TU Munich, 2015, supervised by Paul Bockelmann

pressures of $5 - 50$ bar experienced in WCM and CIP. Matrix flow cannot be traced selectively in CT without altering the processing properties. This is the case because different phases in CT pictures are distinguished based on the density of the respective material. Since the flow in compression molding is much faster than in common prepreg consolidation and the matrix is of low viscosity, disruption of the press process would result in unintended flow generated by the disruption. Furthermore, no flow from individual carrier cavities can be monitored, an important aspect to evaluate flow in CIP. However, if the density of the mass of matrix to be monitored would be altered to allow its recognition in CT images, the viscosity will also be changed and with it the flow properties.

Given the challenges of previous visualization methods in the context of compression molding, only the initial and final position of a defined mass of matrix distinguishable from the rest of the matrix shall be analyzed. These points in the process chain represent mechanically relatively steady states, which facilitates their visual analysis. In consequence however, the flow in between these two states cannot be characterized directly but only via a qualitative interpolation by the results of the two states. The initial position of matrix in WCM and CIP is visually controlled because application of matrix and fiber stack is performed manually. Analysis of the final position of the matrix to be traced is used to investigate the research questions in this chapter.

Because only a fraction of matrix shall be used to investigate flow from one carrier cavity or position on top of the fiber mat, visual appearance of the respective matrix mass to be traced is altered with a fluorescent marker. Fluorescence has been used before in studies concerning material distribution, e.g. behavior of filler particles in vacuum bag infusion [96], self-repair of composites [97] or deposited colloid tracers in silica sand [98]. In all cases, fluorescent particles or phases allow better identification and quantification of the fluorescent matter on photographs or video. This is the case, because the contrast between fluorescent and non-fluorescent phases is stronger, which facilitates computerized image analysis. In the impregnation studies of this chapter, fluorescent marker allows to quantify material preparation and matrix distribution after pressing. Both methods are developed in regard to the needs of the processes and are consecutively presented in the following.

One important prerequisite for the use of fluorescent pigments to distinguish a certain mass of matrix is that the viscosity of the matrix system must not be altered. This is necessary, because the flow properties of the entire matrix, dyed and non-dyed, should be equal to avoid distortion of the impregnation process under investigation. In order to examine the behavior of a marked matrix system,

viscosity measurements are performed on a MCR 302 rheometer[2] (Anton Paar) with conic plate system with a diameter of 25 mm. The process is run gap-regulated with a constant gap of 0.048 mm. The matrix system investigated is XB3585/XB3458 (Huntsman; Appendix A-3) with 3 w-% regarding XB3585 of internal release agent PAT-657/BW (Wuertz). An appropriate shear rate of 700 1/s is determined for further experiments from rheological tests of non-fluorescent matrix at 25° (Scene A in Figure 5-1). This is adequate because at this shear rate no shear-thinning is induced, which is the case at faster rotation.

Because a fast-curing matrix system is prepared manually for the experiments, conditions of measurements need to be constant. Therefore, the following preparation routine is followed. A mass of 50 g XB3585/PAT-657/BW is dosed in a paper cup and the corresponding mass of 9.22 g XB3458 is filled in a syringe. The hardener is injected into the paper cup and the compound is mixed manually for 15 s with a wooden scoopula. A volume of 25 µl is transferred into the aluminum cup mounted to the rheometer using a pipette. The rheometer is pre-closed to a gap of 30 mm prior to matrix insertion, so that the time between hardener injection and the start of measurement is 86 s for all experiments.

For experiments with fluorescent matrix, EpoDye is applied into the XB3585/PAT-657/BW compound, heated to 60 °C and manually stirred with a wooden scoopula for 2 min. The fluorescent compound is pre-heated to 60 °C before the XB3458 hardener is injected and rheological measurements are performed as previously described.
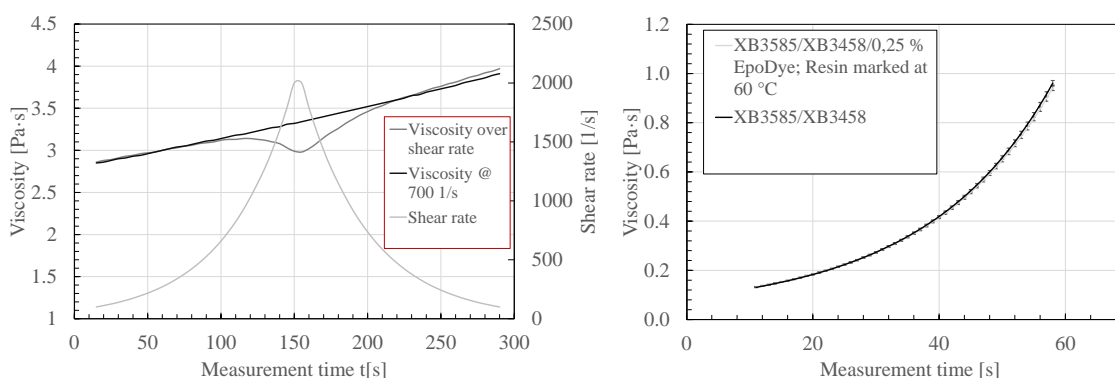
Figure 5-1 Rheological examination of the matrix with and without 0.25 w-% of EpoDye. Results from non-fluorescent matrix under shear sweep from 100-2000 1/s at 25 °C (A). Viscosity progression of non-fluorescent and fluorescent matrix at 700 1/s and 80 °C with $n = 3$ experiments per matrix type (B).

Graph B in Figure 5-1 shows that matrix viscosity is not altered when EpoDye powder is mixed into the pure XB3585 at 60 °C under manual stirring. Other

---

[2] www.anton-paar.com/corp-en/products/details/mcr-rheometer-series; Last accessed on 02-23-2016

experiments showed higher viscosity of matrix that has been dyed with EpoDye in XB3585 at room temperature or when fluorescent pigments are mixed into the hardener. In these cases the pulver particles are not fully diluted, so that the solids within the matrix increase viscosity compared to the non-marked matrix.

From the rheological measurements it is concluded that EpoDye can be used to mark the matrix for experimentation without altering its flow properties. All experiments that are described in this chapter are performed with fluorescent matrix that has been prepared under the presented circumstances to allow for equal flow properties of marked and non-marked matrix.

5.1.1 Quality Control of Manual Matrix and Fiber Application

The materials used in CIP and WCM are prepared manually outside of the press tool and thus facilitate quality control via an overhead camera. For matrix pre-application in particular the amount and the position of the pre-applied matrix on the carrier or the fabric are important. The amount can only be specified by an area A_m on photographs, the position is computed via the deviation of areal centroid coordinates x_m, y_m from the origin of a reference coordination system. The same values for the fiber stack A_f, x_f, y_f are complemented by control of the fiber angle α_m between fiber direction and reference coordinate system.

The reference system is defined by the inner edge of the aluminum rings that clamp the carrier. To this circle the overhead camera, UI-3580ML-C-HQ (Imaging Development Systems GmbH; 1/2 ” CMOS-sensor with 4.92 megapixel), is referenced. The lens of the camera is adjusted concentrically to the clamp ring underneath and is controlled by uEye Cockpit software. Pictures are taken after each preparation step carrier clamping, matrix pre-application and fiber stack application. The latter two pictures are segmented within a Matlab script to identify geometrical control criteria for the manual prepared materials, Figure 5-2.

Fluorescent matrix appears yellowish on the pictures taken with the overhead camera. Thus, it can be segmented from other matter on the picture by Matlab via HSV[3] values of each pixel. Via canny edge detection algorithm the outer edge of the conglomeration of fluorescent pixels is determined and all pixels enclosed by this edge are counted as fluorescent matrix. This avoids misinterpretation of light reflections on the fluorescent matrix that produce HSV color values, which do not fit the value range of the fluorescent phase. Subsequently, the pixels that are recognized as fluorescent matter are added and multiplied with a conversion factor into

---

[3]HSV color model, which describes a color of a combination of hue (H), saturation (S) and value (V)
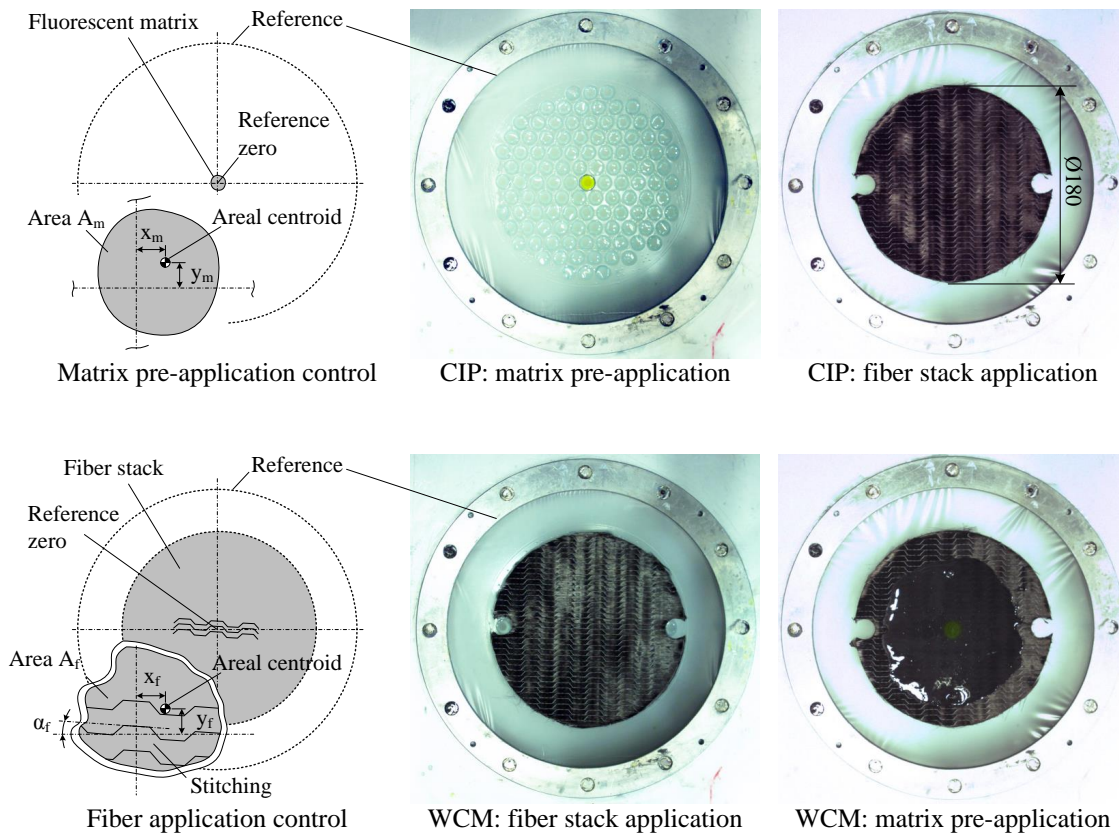
Figure 5-2 Geometrical control criteria for matrix pre-application (A_m, x_m, y_m) and fiber application (A_f or m_f, x_f, y_f, α_f) computed by image segmentation in Matlab from camera pictures of each preparation step (middle and right; notches in fiber stacks are not captured by image segmentation algorithm in Matlab)

an area A_m of fluorescent matrix. The centroid of A_m is computed in reference to a coordinate system with its origin set in the center of a circle fitted to the inner edge of the clamp ring which serves as a reference.

In principle, the same procedure applies to the analysis of fiber application. In addition to the fiber area A_f, or the respective fiber mass m_f, and the areal centroid coordinates x_f and y_f of the stack, the fiber angle α_f of the top NCF ply is detected. The angle is generated by the reference coordinate system and a straight line fitted to the warp section of the tricot-warp stitching, since it runs parallel to the fiber direction.

5.1.2 Tracing Matrix Flow by Fluorescent Photography

In order to study matrix flow in compression molding processes, this thesis proposes to detect the spatial distribution of individual resin accumulations via fluorescence markers to draw conclusions about the flow of the marked resin during pressing. Thus, the final state of the flow process is interpreted by computer-aided analysis of

digital images. The images have to provide criteria that are quantifiable in regard to matrix flow. Two criteria are seen as describing the quality of the flow. Firstly, the spatial distribution of the marked matrix mass and, secondly, its path between initial and final location, Figure 5-3.
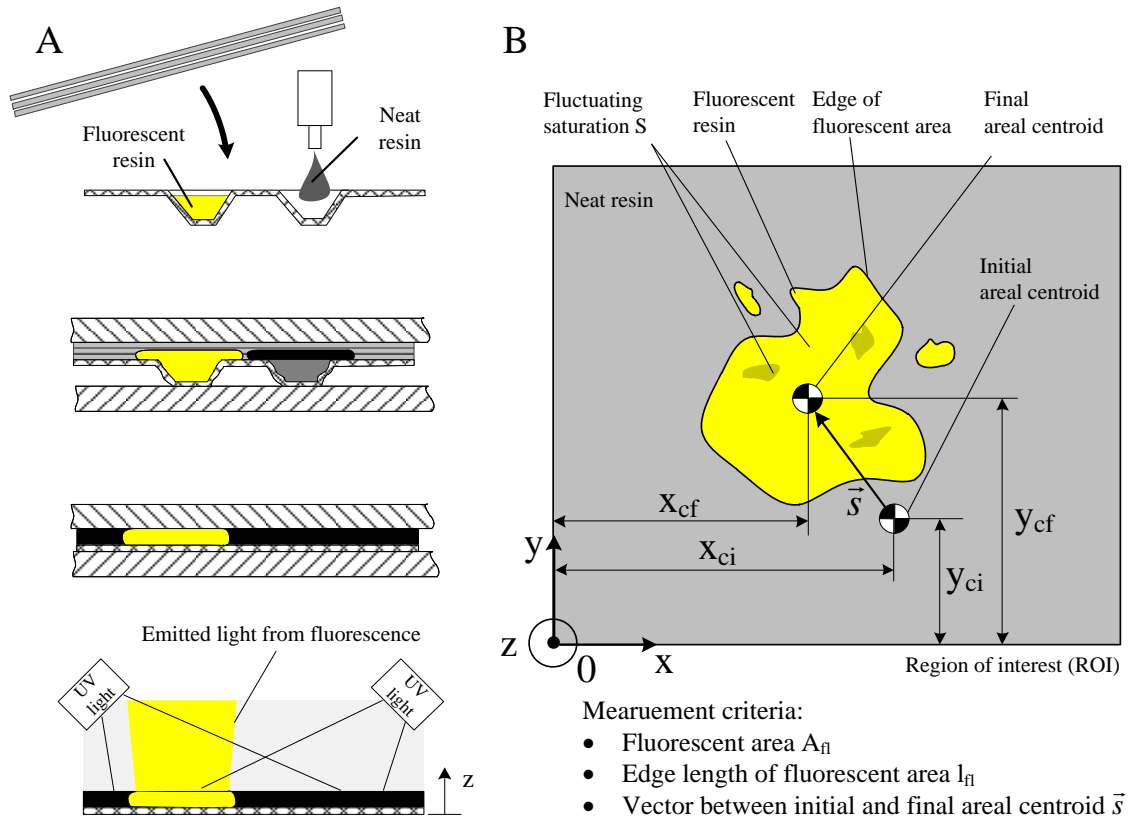
Figure 5-3 Processing principle (A) and criteria to quantify matrix flow regarding distribution and flow path of fluorescent resin (B). Resin distribution is described by fluorescent area A_{fl} and its edge length l_{fl}, vector $\vec{s}$ represents the flow path between centroids defined by initial (x_{ci}, y_{ci}) and final coordinates (x_{cf}, y_{cf})

The criteria derived in Figure 5-3 to describe compactness and flow of fluorescent matrix are converted to quality parameters Q_1-Q_3, which provide quantitative values regarding the matrix flow. The parameters Q_1 and Q_2 set the respective criteria in reference to the entire region of interest (roi). The third parameter computes the absolute value of the position vectors for initial and final areal centroids.

$$Q_1 = \frac{A_{fl}}{A_{roi}} \qquad\qquad Q_1 \in \ [0;1] \qquad\qquad (5\text{-}1)$$

$$Q_1 = \text{Ratio of fluorescent area}$$
$$A_{fl} = \text{Fluorescent area}$$
$$A_{roi} = \text{Area of ROI}$$

$$Q_2 = \frac{l_{fl}}{l_{roi}} \qquad\qquad Q_2 \in \quad [0; \infty] \qquad\qquad (5\text{-}2)$$

$$Q_2 = \text{Ratio of edge length}$$
$$l_{fl} = \text{Edge length of } A_{fl}$$
$$l_{roi} = \text{Edge length of } A_{roi}$$

$$Q_3 = mean(|\vec{s}_i|) = mean(|\vec{s}_{cf} - \vec{s}_{ci}|) \quad Q_3 \in \quad \mathcal{R} \qquad\qquad (5\text{-}3)$$
$$= \sqrt{(x_{cf} - x_{ci})^2 + (y_{cf} - y_{ci})^2}$$

$$\vec{s}_{ci} = \text{Position vector of initial areal centroid}$$
$$\vec{s}_{cf} = \text{Position vector of final areal centroid}$$

The derived quality parameters are computed from digital images, following the construct of computerized image processing discussed elsewhere [99, p. 13]. To allow quantification of properties, essential steps are image acquisition, segmentation in objects of interest, their classification as well as extraction of important properties. In the following, realization of these steps are discussed, divided in image acquisition, establishment of a fluorescence model and image processing.

Image Acquisition Two types of sensors can be used for digital image acquisition complementary metal-oxide-semiconductors (CMOS) or charged-coupled-device-sensors (CCD) [99, p. 197-201]. CCD are still often used in scientific studies because they are very photosensitive and provide images consisting of pixels that were recorded at the exact same point in time due to a global shutter. CMOS sensors work with a rolling shutter that can distort images of high velocity scenes. However, both sensors provide comparable image quality and thus are both used in image recognition for process control [100, p. 172]. Due to lower cost [100, p. 371], better availability in digital single lens reflex (DSLR) cameras and the need to photograph static scenes in sufficient lighting, this work uses a CMOS sensor integrated in an EOS 7D DSLR (Canon).

In order to compare the results from each digital image, camera settings remain constant for all parts. The EOS 7D is operated with a 17-40 L USM lens at a focal distance of 40 mm with an f13.0 aperature and 10 s exposure time. Exposure time is evaluated as suitable in the next paragraph, the fluorescent model. The white balance is set to sunshine and the Iso-photosensitivity remains at 100, the lowest

value, to minimize image noise. The camera-integrated chip converts the RAW images into JPG format, which is directly usable for image processing.

Constant camera settings are only applicable if the light situation remains the same for all parts, too. Thus, part orientation in reference to the light sources is kept constant with an alignment rig, Figure 5-4.
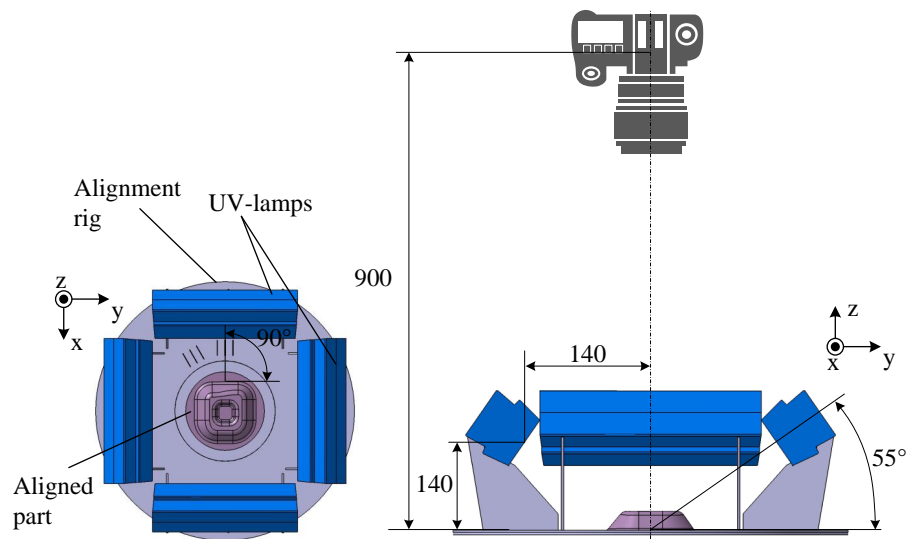
Figure 5-4 Set-up for digital image acquisition using a DSLR camera with CMOS sensor

The rig allows precise manual alignment of the parts to be photographed, both of complex and plate geometry, within the center of the rig. The camera position is fixated on a tripod and the image is concentrically adjusted above the part via the orientation grid on the camera screen and respective marks on the base plate of the alignment rig.

Furthermore, the rig carries four identical UV-lamps, LF-106S (Uvitec)[4] which emit light of a wavelength of 254 nm and intensity of 710 µW/cm^2. Fluorescence is defined as the emission of electromagnetic radiation by a molecule with fluorescent properties due to excessive energy induced by an absorbed photon [101, p. 296]. Fluorescent light appears to be red-shifted in reference to the absorbed light [101, p. 299]. It was found that light of 254 nm excites the fluorescent pigment, C.I. yellow 43, in the plastic dye Epodye (Struers) to emit light within the human visual spectrum. Longer exciting wavelengths resulted in excessive relaxation due to internal conversion, quenching, intersystem crossing or chemical reaction that suppressed fluorescence [101, p. 297-300], presumably by adjacent carbon fibers.

---

[4]http://www.uvitec.co.uk/products/uvilitetlc/index.html; Last accessed on 02-18-2016

Fluorescence Model for Saturation   In order to establish a model that characterizes saturation in reference to the fluorescence, the color space which defines each color in the image has to be introduced. To facilitate image segmentation of the distributed fluorescent matrix, this work draws on the HSV color model. The model describes each color in the same way the human conscience perceives it, differentiating the parameters hue, saturation and value [99, p. 54-55]. Hue is independent from saturation and value, which simplifies image segmentation [102, p. 325], since no superposition of different shades of colors occur. That means, when the fluorescent matrix mixes with neat matrix, only brightness and saturation are changed, while hue stays constant. This independence of parameters is reflected by the cylindrical coordinates of the color model. It consists of a radius around the white center axis for saturation (S), an angle for hue (H) and value (V) on a vertical axis[5].

Higher concentrations of fluorescent pigments decrease saturation, which is described by a smaller radius. In order to correlate both parameters positively, the following inversion of saturation is introduced:

$$S = 1 - S^\star \qquad\qquad S \in \quad [0; 1] \qquad\qquad\qquad (5\text{-}4)$$

$$S = \text{Saturation}$$

$$S^\star = \text{Saturation in HSV color model}$$

Furthermore, the exposure time of the camera has the same effect on the saturation as the fluorescence concentration. Longer exposure to light increases the white content and would thus decrease saturation. The proposed inversion leads to a positive correlation.

Both parameters, fluorescence concentration and exposure time are linked with inverted saturation and value by experiments in which the entire matrix of the part is dyed with fluorescent marker. In the experiments, the resin component is dyed with fluorescence concentrations between $0.250\,\%$ and $0.016\,\%$ and further processed to produce parts of complex geometry. Photographs of the parts are taken using the alignment rig, Figure 5-4 with exposure time set to 5, 10 and 15 s, Figure 5-5.

Saturation is strongly influenced by concentration of the fluorescent marker, while value stays approximately constant over all concentrations tested. All exposure times are within the range of both saturation and value, thus no over- or underexposure leads to loss of information. The curves for 10 s exposure time show

---

[5]https://commons.wikimedia.org/wiki/File:HSV_cylinder.jpg
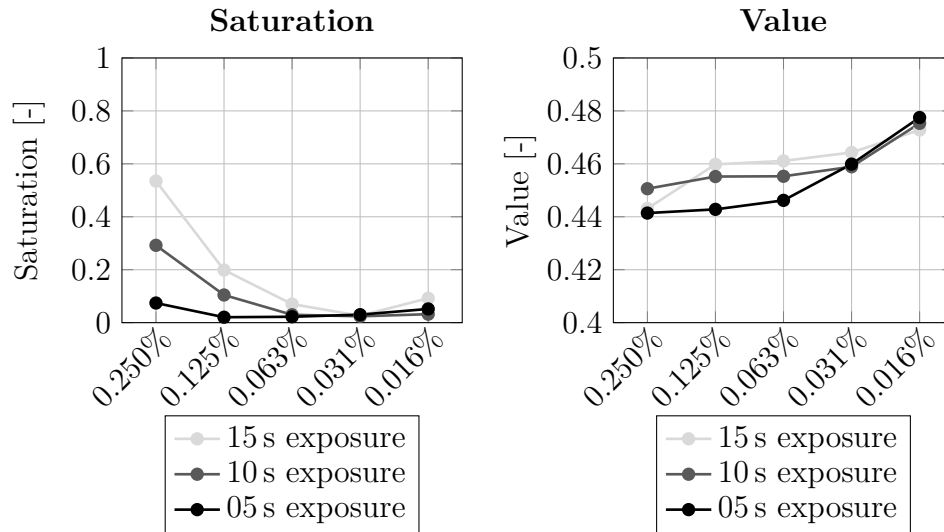
Figure 5-5 Dependency of saturation and value on fluorescence concentration and exposure time in image acquisition

consistent results over a wide range without danger of information loss and thus this exposure time is used for all further experiments. It is important to note, however, that below 0.03 % of concentration, no fluorescence is detected in the images.

To consistently analyse produced parts, a case differentiation has to be defined regarding the part areas. To produce complex parts, fibers are draped into the cavity, which produces areas of pure matrix at the part edges (Figure 4-17). Since the matrix in this area is translucent, fluorescent matrix shines through from underneath the part surface. This is not the case in regions of the part that contain fiber material. Thus, regions of pure matrix appear more saturated than fiber regions, even without a difference in fluorescent concentration.

For 10 s exposure the saturation relates to the fluorescent marker concentration within the fiber region according to Figure 5-6.

The lowest concentration tested, 0.016 %, cannot be measured correctly any more and must be excluded in order to fit a valid curve to the experiments. Thus, the following fit applies to results in fiber region of the part:

$$S_f(c) = 2.37 \cdot c - 0.07 \tag{5-5}$$

$$S_f = \text{Saturation}$$
$$c = \text{Concentration of fluorescent marker}$$
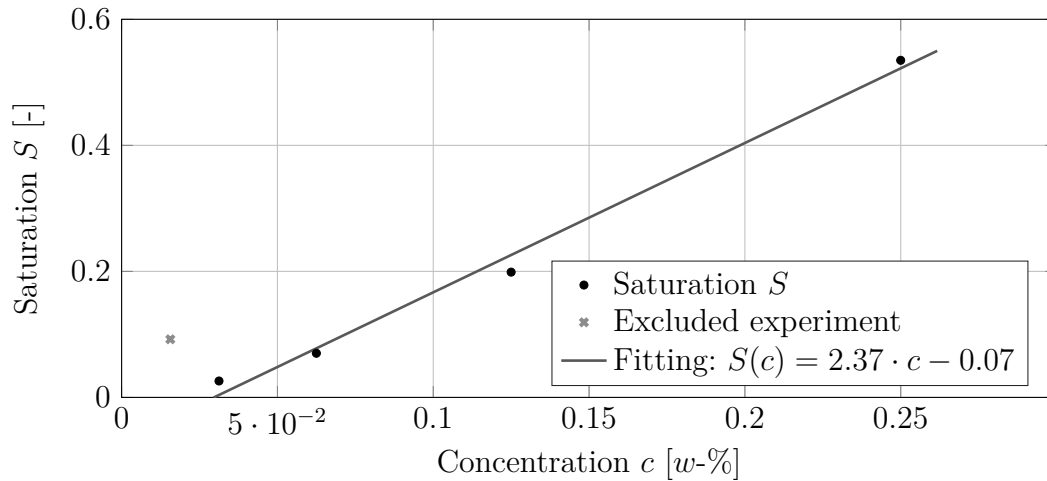
Figure 5-6 Relation between saturation S and concentration c of fluorescent marker in fiber region. Concentration of fluorescent marker is specified in weight-% of resin component

Within the pure matrix region of the part, the saturation S in dependence of marker concentration c follows a curve with a higher slope due to the accumulation of fluorescence within the translucent material, Figure 5-7.
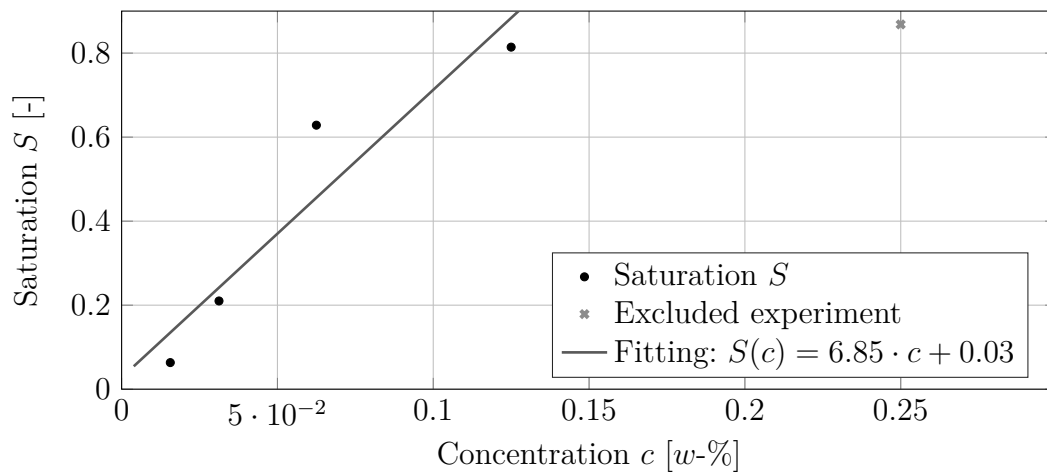
Figure 5-7 Relation between saturation S and concentration c of fluorescent marker in pure matrix region. Concentration of fluorescent marker is specified in weight-% of resin component

Due to the accumulation of fluorescent marker in pure matrix, a maximum saturation is reached at approximately $0.125\,\%$ concentration. No further increase in saturation can be detected. Thus, for higher concentrations, as in the excluded experiment, a maximum saturation of 0.85 is assumed, leading to the following differentiation of functions for the saturation in pure matrix regions:

$$S_{m1}(c) = 6.85 \cdot c + 0.03 \qquad \text{for } c \leq 0.125 \qquad\qquad (5\text{-}6)$$
$$S_{m2}(c) = 0.85 \qquad\qquad\quad \text{for } c > 0.125$$
$$S = \text{Saturation}$$
$$c = \text{Concentration of fluorescent marker}$$

In order to complete the fluorescence model needed for image processing, the hue spectrum which applies to the segmentation of the fluorescent phase is to be determined. Thus, the reference part with $0.125\,\%$ fluroescent marker is analyzed regarding the hue histogram it produces, Figure 5-8.
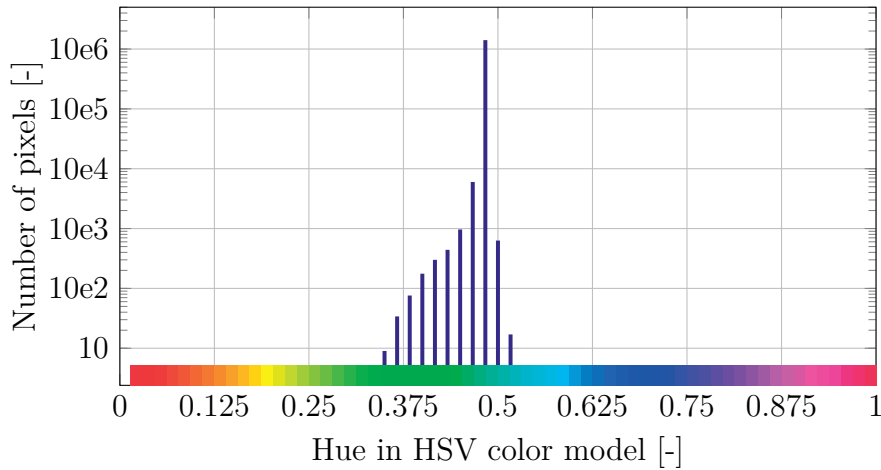
Figure 5-8 Histogram of hue in HSV color model for reference part with a concentration of fluorescent marker of $0.125\,\%$ and $10\,\text{s}$ exposure

The color spectrum in the histogram corresponds to the actual hue values. All other reference parts show a similar hue distribution. Thus, for all following analyses, hue values that are associated with fluorescence are set between 0.25 and 0.5.

Image Processing   Digital images acquired with the DSLR-camera are processed drawing on algorithms from the Image Processing Toolbox in Matlab to compute the quality parameters defined in Equations 5-1 to 5-3. The relation between concentration of fluorescent marker and saturation as well as the hue spectrum of fluorescence are embedded in the algorithms.

After the conversion of the RGB images into HSV color model, the fluorescent phase of the image is segmented and further processed. Two manual segmentation steps are performed, first to select the entire part as ROI and second, to separate fiber region and pure matrix region for the fluorescence model. All further processing

is automatically performed by the Matlab routine, Figure 5-9. The results from image processing are manually organized in Excel for further analysis.
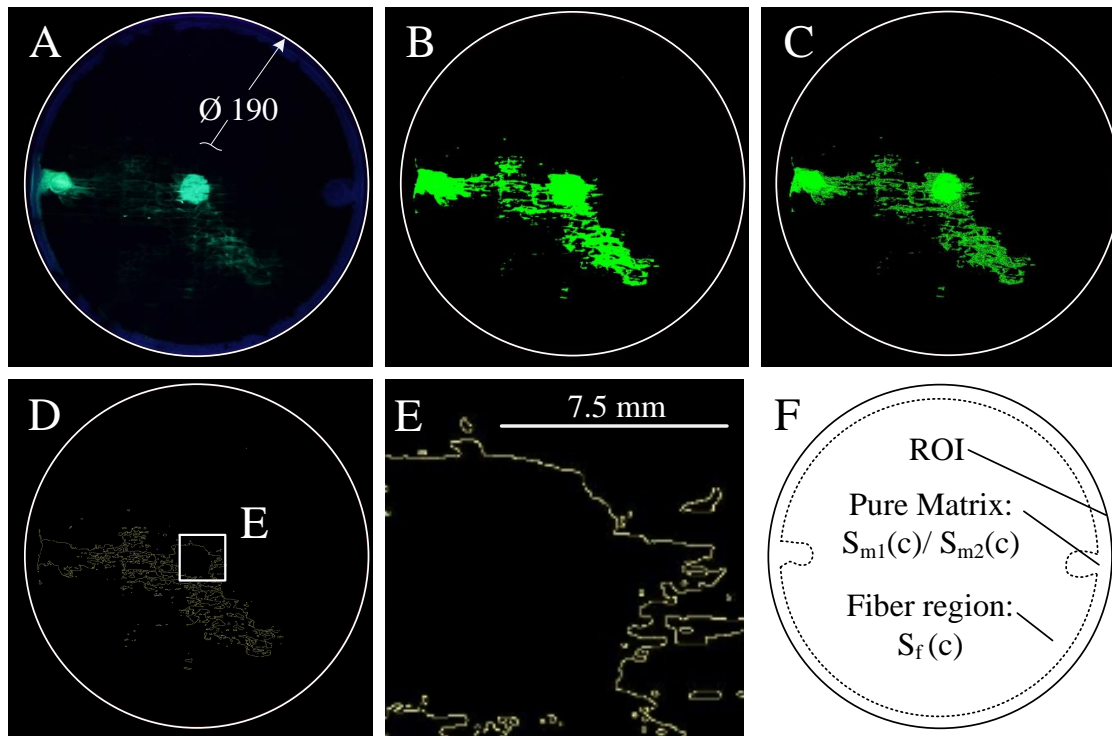
Figure 5-9 Matlab routine for image segmentation to compute quality parameter of matrix flow, exemplary demonstrated at compression molded plate. Transformation of image into HSV color model (A), fluorescence recognition via hue to calculate Q_1 (B), weighting of fluorescent region via concentration c to compute the areal centroid for Q_3(C), edge detection of fluorescent regions via Canny-algorithm using hue to determine Q_2 (D/E), exemplary manual segmentation of fiber region and pure matrix region in one part to correct concentration of fluorescent marker (F)

5.1.3 Tracing Matrix Flow by Fluorescent Microscopy

While the fluorescent photography is limited to assess matrix flow on part surface in x and y direction, microscopy of laminate sections shows the matrix distribution in the cross section of a laminate. The fluorescence phase can be used again to distinguish the marked matrix from the rest in order to quantify matrix distribution.

Fluorescence microscopy is particularly important in examination of biological specimen, since selective detection of small concentrations of matter with good signal-to-background ratio is possible [103, p. 902]. While in biology often naturally available green fluorescent proteins are used as a marker in fixed or living cells [103, p.903], epoxy matrix marked with Epodye can be excited with 254 nm by fluorescence microscopes as well.

To compare the results of all specimen with one another, samples are cut from a defined position of the pressed plates. The samples are embedded into epoxy matrix before beeing polished on a planar grinding machine with a minimum grain size of 3 µm and chemically etched in a last step. Digital micrographs are recorded using the ApoTome 2 fluorescence microscopy (Carl Zeiss Microscopy) to automatically stitch single images recorded with a magnification of 2.5 to one overview. The exposure time is set according to the region of maximum brightness in each sample in order to avoid loss of information. All micrographs are manually trimmed to an area of 1200x150 pixel to account for comparability of quality measurements that are based on the amount and distribution of fluorescent pixels. The Matlab routine developed in Section 5.1.2 is adapted to recognize fluorescent pixels based on their value within the HSV color mode. Value thresholds are set to 150 and 5000 upon manual trials and analysis of results. The principle of analysis is depicted in Figure 5-10.
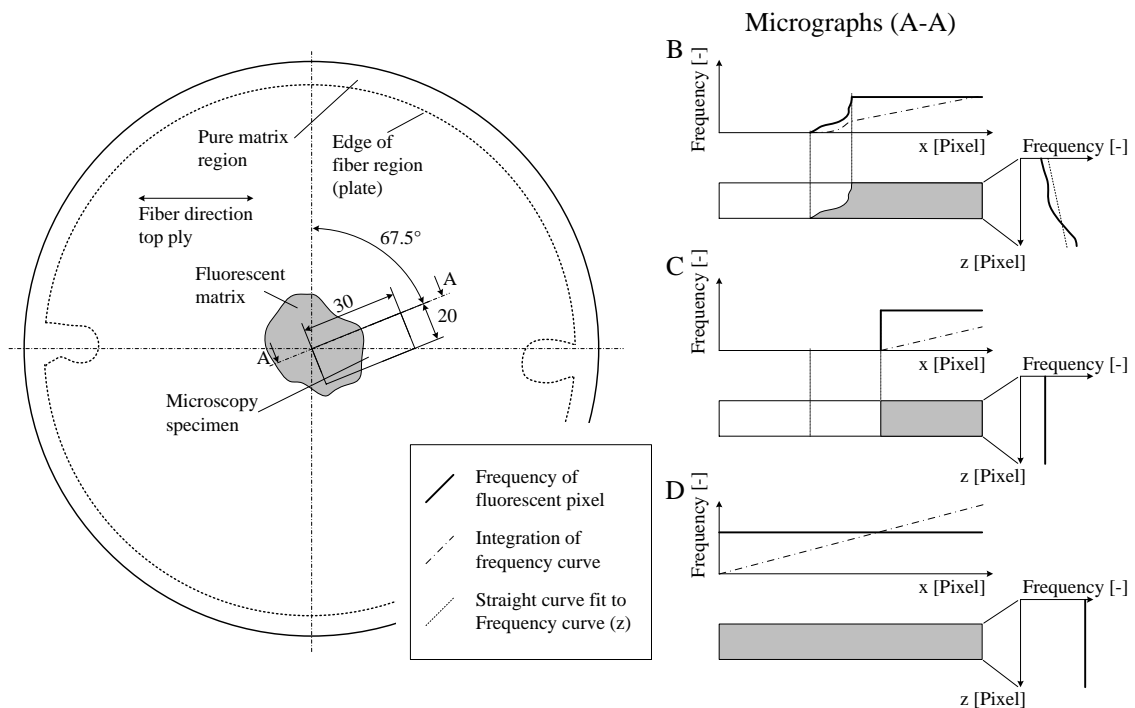
Figure 5-10 Principle of matrix flow analysis via fluorescent microscopy. Specimen are cut from the same central region of parts under an angle of 67.5 ° to the fiber direction of the top ply. From micrographs (A-A) the frequency of fluorescent pixels can be computed for the x and z direction. Quality parameters are the maximum value of the integral of frequency in x direction and slope of the fitted straight curve in z plot (B). Hypothetical plots for extreme results (C: ideal, D: worst) show different magnitudes of the quality parameters, magnitudes are not true to scale

The compactness of marked resin is again the foundation to define the quality parameters within the micrographs. The more compact the fluorescent matrix flows from its initial position to its final position, the more localized the marked matrix

is distributed in the micrograph. When the transition from fluorescent to non-fluorescent area is defined, the frequency of fluorescent pixels over z direction the micrograph is constant (scene C in Figure 5-10). When the fluorescent phase is localized, the frequency curve begins at higher x values and its integral amounts to a final value which is smaller than in a sample with more widely distributed resin (e.g. scene D in Figure 5-10). The same relation applies to the plot in z direction, where the integral of the frequency curve has a lower value than a widely distributed fluorescent phase. If the progression in z direction is ideally homogenous, the slope of the straight line is zero (Scence C in Figure 5-10). The straight line is tilted, which means the slope has a negative or positive value when the flow front of the marked matrix is heterogenically distributed over the part thickness (Scene B in Figure 5-10).

5.2 Experimental Setup, Materials and Methods for Investigation of Matrix Flow

The research to be conducted is experimental in nature. In the following, the method portfolio is assembled in regard to the research questions before single methods are specified in detail, Figure 5-11.

WCM and CIP are technical systems which are subject to process parameters and disturbances regarding the dependent variables. In particular, process parameters are assumed to produce different matrix flow results. Thus, major influence parameters of both processes should be varied. To study the influences of parameters in complex technical systems with a minimum of experiments, design of experiments (DoE) is a common procedure [104, p. 6].

Two independent DoE plans for WCM and CIP in connection with the method of fluorescent photography form the base of the study. Analysis of fluorescent photography and fluorescent microscopy, subjective visual evaluation of elimination of carrier cavities as well as fiber angle measurements provide quantitative data of the dependent variables in the DoE. Research question 2.1 and 2.2 are answered comprehensively in the light of parameter variation through the DoE results.

WCM and CIP parts that show good and poor results regarding the matrix flow are selected for void measurements in micrographs and three point bending tests to investigate research question 2.3. Results are complemented by findings of fiber angle measurements from the DoE studies.

Research question 2.4 is investigated in a second, smaller study in which fluorescent photography is used to quantify matrix flow in plates as well as in the $32°$ and $40°$

WCM   CIP

RQ 2.1: How does matrix flow through fiber material for WCM and CIP?

Design of experiments

RQ 2.2: How is cavity elimination linked to matrix flow?

45 experiments for 15 parameter combinations

15 experiments for 3 parameter combinations

Fluorescent photography

Fluorescent microscopy

Fiber angle measurement (Profactor)

Subjective visual evaluation of cavity elimination

Optical void/fiber volume content measurement from micrographs

RQ 2.3: Does type of matrix flow influence part quality?

Three point bending

RQ 2.4: How does draping disturb matrix flow in WCM and CIP?

18 single experiments for plate, 32° and 40° incline

Fluorescent photography

Figure 5-11 Portfolio of methods selected to investigate research questions 2.1-2.4

inclines of the complex part. All parts in this study are produced with the same parameter set, both for WCM and CIP, in order to allow for comparability.

In the following, all methods used for each research question are specified in detail, except the previously developed methods of fluorescent photography (Section 5.1.2) and microscopy (Section 5.1.3).

5.2.1 Design of Experiments for Wet Compression Molding

In case of WCM matrix is pre-applied on the fiber material directly. It is assumed that the degree to which the fluorescent matrix sinks into the fibers influences its distribution after pressing. The more the matrix sinks in, the less it is prone to be dislocated from its initial location during pressing. Thus, the matrix temperature, determined by the temperature of the resin component T_r, and the pre-application time t_{pa} are defined as process parameters. During pressing, the press velocity of the tool v_p is assumed to influence the dislocation of the matrix film that is atop

the fiber stack. From all three parameters, particularly T_r is assumed to yield non-linear results. This is likely, because the degree to which the matrix sinks into the fibers depends on the viscosity, which is influenced by temperature and the onset of cure with non-linear effects, Figure 2-2. For non-linear correlations, at least three factor steps are required, which are structured in quadratic DoE plans [104, p. 37].

To allow for quadratic correlations, a central-composite-design is used for the DoE structure. This plan is a combination of linear cube-design with an additional center point and circumscribed points orthogonal to the faces of the cube, so-called "star points" [104, p. 39]. When three factors, T_r, t_{pa} and v_p, with three levels each shall be investigated and each parameter combination is run three times to statistically validate the experiments, a full factorial design would require $n = 3^3 \cdot 3 = 81$ experiments [104, p. 6]. Thus, a reduced design that requires 15 single experiments and with replicates 45 is used. It applicates a star distance of 1.8309, in order to guarantee the plan is rotatable and orthogonal [104, p. 38-39], Figure 5-12.

Experiments	T_r [°C]	v_p [mm/s]	t_{pa} [s]
1, 18, 35	35	3.5	5
2, 19, 36, 52*	54	3.5	5
3, 20, 37	35	9	5
4, 21, 38	54	9	5
5, 22, 39	35	3.5	15
6, 23, 40	54	3.5	15
7, 24, 41	35	9	15
8, 25, 42	54	9	15
9, 26, 43	27.11	6.25	10
10, 27, 44, 53*	61.89	6.25	10
11, 28, 45	44.5	1.22	10
12, 29, 46	44.5	11.29	10
13, 30, 47	44.5	6.25	0.85
14, 31, 48	44.5	6.25	19.15
15, 16, 17	44.5	6.25	10

*Repeated experiments
Experiments 32-34 and 49-51 are additional repetitions of the central point, which is only covered in 3 experiments in total

Figure 5-12 Design of experiments for WCM based on central-composite-design with variation of the parameters resin temperature T_r, pre-application time t_{pa} and pressing velocity v_p and a star distance of 1.8309. The plan will be run with two replicates of each point, the center point will also be subject to three experiments in total

Parameter combinations of the cube have been screened in previous trials. The extreme parameter combinations of the star points have been tested before the study and are viable, which means the star distance can be maintained as proposed. Trials are randomized according to the DOE software Modde 10.1[6], which is used for the study.

---

[6]www.umetrics.com

Subject to the DoE is the process to produce plates, Scene A in Figure 5-13. A circular stack of 180 mm from CB300BX NCF (Hactotech; Appendix A-1) with ply sequence $[0°/90°, +/- 45°, +/-45°]_s$ is assembled manually from machine-cut plies using an angle template. The carrier film SV 250 without cavities is fixed in stretched state with the clamping ring, as introduced in Section 4.6.2. The prepared fiber stack is concentrically placed on the carrier film (Scene B in Figure 5-13), using a placement template. The matrix system with resin XB3585 and hardener XB3458 (Huntsman; Appendix A-3) is to be used for all experiments. XB3585 is prepared in batches with 3 w-% internal release agent PAT-657/BW (Wuertz), either non-marked or with 0.25 w-% EpoDye in reference to the pure XB3585 mass. To prepare the matrix system for manual application, two paper cups are equipped with 50 g XB3585/PAT-657/BW and 20 g fluorescent XB3585/PAT-657/BW from the prepared batches, respectively. Both are heated to the temperature T_r of the respective experiment in an oven. Two syringes are filled with 9.22 g and 3.67 g XB3458 for the neat and marked resin. Both hardener masses are injected into the paper cups with pre-heated resin simultaneously (time $t = 0$). Both compounds are mixed manually with wooden scoopulas for 15 s before manual pre-application on the NCF stack. Both matrix types, neat and fluorescent, are dosed simultaneously. A volume of 7 ml of fluorescent matrix is taken into a syringe and expelled on the NCF within the central ring of the dosing template, while the neat matrix is pre-applicated around the central ring directly from the cup, Figure 5-13.
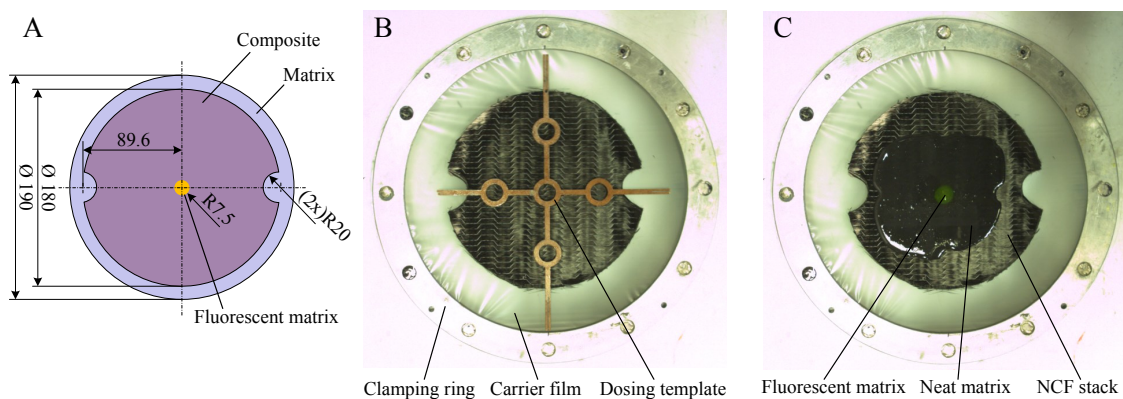
Figure 5-13 Manual material preparation for WCM experiments. Part to be produced in experiments with fluorescent matrix (A), concentric placement of NCF stack on clamped carrier film with aligned template for the dosing of fluorescent matrix (B), initial distribution of fluorescent and neat matrix after dosing on top of the NCF stack (C). Circular cutouts on both sides of the NCF are needed for positioning pins inside the tool and do not fulfill any other function regarding the process

The rings of the dosing template with a radius of 7.5 mm sit on the fiber materials and no matrix can flow in or out of the ring. The wall thickness of the rings is 1 mm, to minimize interference with the pre-applied matrix. The pre-application time t_{pa}, a parameter to be varied within the DoE, is measured from the point in time when

the fluorescent matrix is expelled from the syringe onto the NCF. During t_{pa} of the respective experiment, the neat matrix is applied but the dosing template is left in place. When t_{pa} expires, the template is removed and the clamping ring with all materials is inserted into the tool.

The tool is heated to $T_t = 100\,°C = $ const. and closed to a position of $122.22 \pm 1.63\,$mm so that the material can still be manually inserted after preparation. The closing velocity for the first closing step to reach the evacuation stage is set to $5\,$mm/s. After material is inserted into the tool, it is closed for $11.98 \pm 1.63\,$s to the evacuation stage at $10.13 \pm 2.08\,$mm. At this stage, the cavity is evacuated for $9.98 \pm 1.42\,$s to under $10\,$mbar, before the the tool is closed completely with v_p for the respective experiment. The part is cured for $150\,$s before demolding. All produced parts are cured for $60\,$min at $115\,°C$ to fully cure the matrix before they are stored protected from any sun or artificial light to avoid premature bleaching of the fluorescent marker. After each experiment, the tool cavity is cleaned with Isopropanol and the tool is again pre-closed to its initial position for the subsequent experiment.

Fluorescent photography and fiber angle measurements are performed for both sides, top and bottom, of all parts. Thus, all three experiments of each point within the DoE can be analyzed, since the parts are not destructed. Fiber angles are measured with the Profactor sensor similar to Figure 4-9. The quantifying parameter for the fiber angle distributions is the kurtosis fiber angle distribution [105, p. 19] in the region of interest of one measurement. For the measurement after Thumfart [89], the Profactor sensor is positioned concentrically on the plate using a template. From the initially acquired image, a ROI of 1200x1600 pixel, centered on the initial image, is selected for quantification using Matlab. Angles from the sewing threads are omitted from the measurements.

For fluorescent microscopy only one experiment of each point is analyzed, since this test procedure needs specimen that are extracted from the plates. Specimen for microscopy are prepared from experiments 3, 6, 15, 22, 26, 28, 30, 31, 35, 36, 38, 41, 42, 46 and 53 (Figure 5-12).

Void content and FVC in laminates are measured optically from micrographs produced by traditional reflected-light microscopy using the same samples that were extracted for the fluorescent microscopy. Images of 5x magnification are acquired on a BX41 microscope (Olympus) and Stream Motion software of three different representative regions of each specimen. Each image of 2048x1532 pixel is segmented into a predefined set of three ROI of 1500x470 pixel each. The distinction between fibers, matrix and voids is controlled manually for each measurement according to subjective inspection of the phases in the respective micrograph, Figure 5-14.
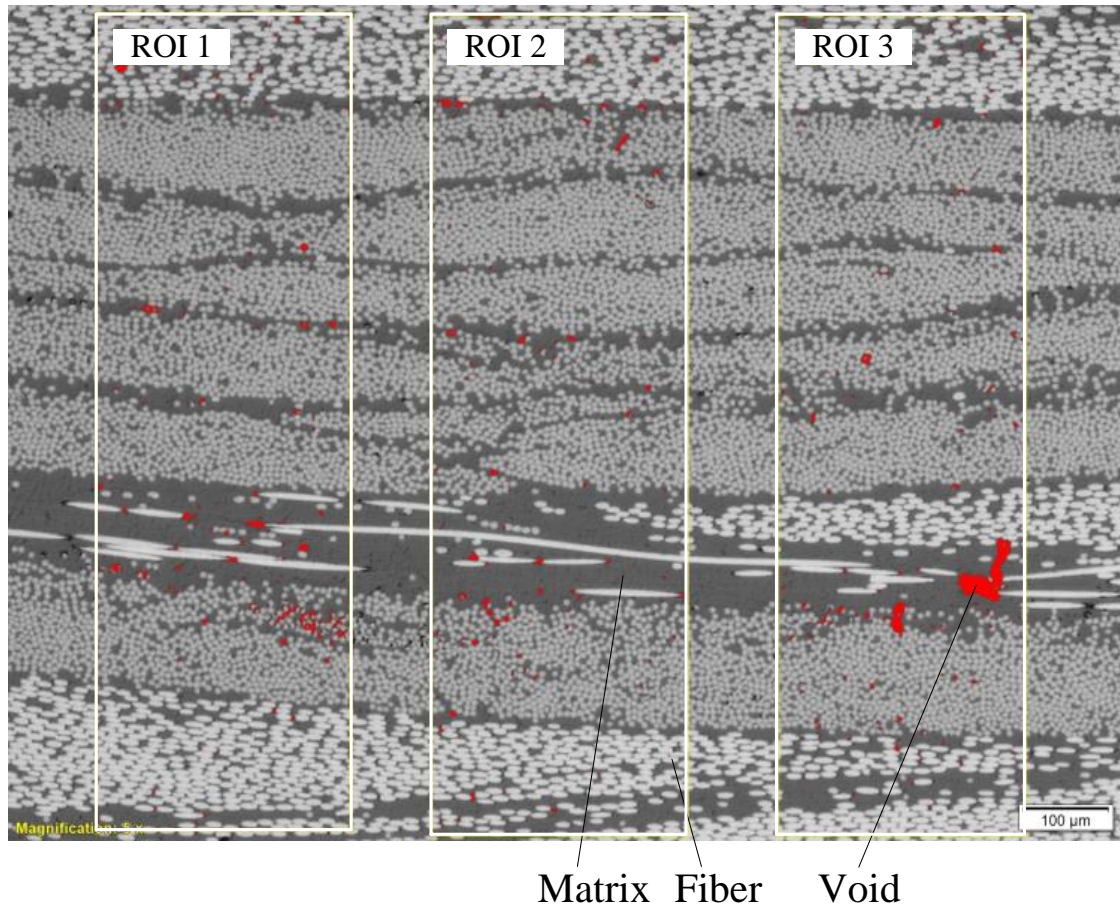
Figure 5-14 Optical void (A) and fiber volume content (B) measurements from micrographs. Region 2 of experiment 28 of the WCM DoE (Figure 5-12) with 0.72 % void content and a FVC of 52.44 % is exemplarily depicted

The computed quality parameters, the kurtosis of fiber angles from both sides of the plate, results from fluorescent microscopy and normal reflective microscopy are fed into the DoE plan in Modde for further analysis.

5.2.2 Design of Experiments for Carrier-Integrated Pressing

From the initial process evaluation in Section 4.6.1, it was hypothesized that carrier cavity elimination is not primarily achieved by mechanical compaction of the cavities when the tool closes, but by rearrangement of stretched polymer molecules under heat. This assumption is supported by preliminary trials, which show no strong influence of the tool closing velocity v_p on the impregnation results on fluorescent photographs but a direct relation to the temperature history of the carrier film during processing. This is critical because several process influences from the tool, the matrix inside the cavities and the preparation routine superimpose each other:

$$
T_c = f \begin{pmatrix} \begin{pmatrix} T_{tt} & t_a & T_r \\ T_{bt} & t_h \\ h & \alpha \\ v_p \end{pmatrix} \end{pmatrix}
\quad
\begin{array}{lcl}
\text{with} & & \\
T_{tt} & = & \text{Tool temperature top} \\
T_{bt} & = & \text{Tool temperature btm} \\
h & = & \text{Distance film-btm tool} \\
v_p & = & \text{Press velocity} \\
\alpha & = & \text{Degree of cure} \\
t_a & = & \text{Resin application time} \\
t_h & = & \text{Heating time at h} \\
T_r & = & \text{Resin temperature}
\end{array}
$$

Due to strongly interrelated parameters, especially with the exothermic reaction of the matrix, the system may become unstable, causing non-reproducible results. To allow for a stable process, most parameters are held constant while only the tool temperature $T_t = T_{tt} = T_{bt}$ and the heating time inside the tool t_h are varied. Due to the strong possible interrelations between uncontrolled and controlled parameters, a full factorial plan with a center point is selected for the DoE, Figure 5-15.

Experiments	t_h [s]	T_t [°C]
1, 6, 11	5	60
2, 7, 12	35	60
3, 8, 13	5	100
4, 9, 14	35	100
5, 10, 15	20	80
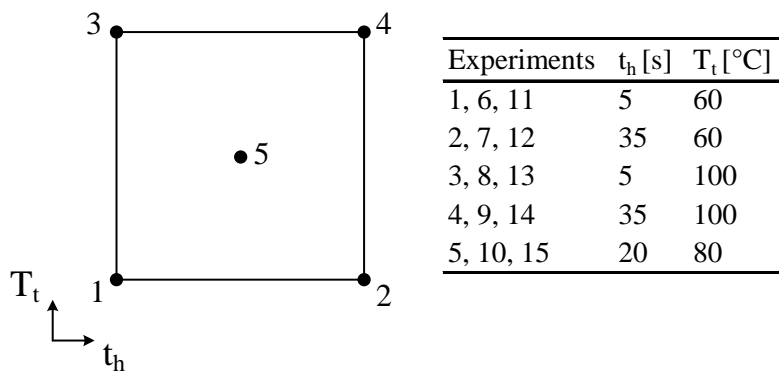
Figure 5-15 Design of experiments for CIP based on a full factorial design with variation of the parameters tool temperature T_t and heating time inside of the tool t_h. The plan will be run with two replicates of each point, the center point will also be subject to three experiments in total

Both parameters, T_t and t_h, are independent and can be controlled well. All other controllable parameters are set constant for all experiments. The influence of curing under exothermic reaction is treated as a result of the controlled parameters and thus, is assumed to be reproducible. Non-linear effects of the varied process parameters can still be traced, since the center point is included in the experiments. All points will be replicated twice, hence 15 experiments in total are planned. Randomization of the experiments is performed as proposed by Modde.

The experimental procedure follows the one for WCM experiments, described in Section 5.2.1 in principle. The carrier which was previously thermoformed with the conic section tool (Table 4-7) as described in Section 4.6.1 and stored at $-18\,°\text{C}$

is fixed in the clamping ring with its cavities concentric to the ring. Seven *ml* of fluorescent matrix is applied into the cavity in the center, while the neat matrix is poured into the cavities manually from a paper cup, starting from the inside and spiraling outward (Figure 5-2). The prepared fiber stack is concentrically positioned on the carrier without the template in order to save time during preparation.

The tool is heated to the tool temperature T_t of the respective experiment and closed to a position of $152.69 \pm 0.87\,\text{mm}$, so that the material can still be manually inserted after preparation. The closing velocity for the first closing step to reach the evacuation stage is set to $5\,\text{mm/s}$. After material is inserted into the tool, it is closed for $12.94 \pm 0.44\,\text{s}$ to the heating stage at $24.31 \pm 0.63\,\text{mm}$. At this stage, the heating time t_h prescribed by the DoE is held, while the cavity is evacuated to under $10\,\text{mbar}$. After t_h expires, the tool is closed completely with $v_p = 5\,\text{mm/s} = \text{const.}$ for all experiments. The curing cycle of $150\,\text{s}$ and for $60\,\text{min}$ at $115\,^\circ\text{C}$ after demolding is the same as for the WCM parts. Fully cured parts are also stored protected from light. After each experiment, the tool cavity is cleaned with Isopropanol and the tool is again pre-closed to its initial position for the subsequent experiment.
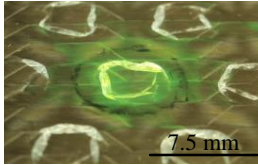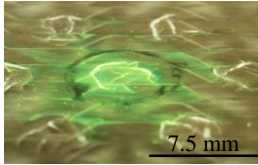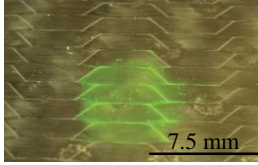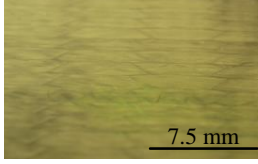
Fluorescent photography and fiber angle measurements are performed for all experiments of all points as previously described for WCM in Section 5.2.1. Fiber angles from the bottom side of the parts, however, produce invalid results, since in some parts, carrier wrinkles are so strong that the underlying fibers can not be analyzed optically. Thus, only the top side of the plates can be characterized for CIP.

How well the carrier cavities are eliminated is evaluated for all experiments and all points. The carrier wrinkles or other imperfections are subjectively evaluated by independent visual inspection of three persons that are not involved in the project. The evaluators award points between zero and ten according to a given exemplary chart, Table 5-1. For each plate the independently awarded points are averaged for the final quantification.

As for the WCM experiments specimen for fluorescent microscopy are only extracted from experiments 1, 8, 12, 14 and 15 (Figure 5-15). The void content and FVC of these experiments are also measured in traditional reflective light microscopy according to the method exemplary described in Figure 5-14.

All quantified parameters from fluorescent photography, fiber angle measurements of the top side, the quality of cavity elimination, fluorescent microscopy and reflective light microscopy are entered into the DoE plan in Modde for analysis.

Table 5-1 Evaluation chart for subjective, semi-quantiative evaluation of carrier cavity elimination in CIP from visual inspection

Points	Description	Exemplary example
0	**Not acceptable** Massive wrinkling, ruptures, air pockets	
1		
2	**Poor quality** Clear wrinkles from cavity walls that indent the laminate	7.5 mm
3		
4		
5	**Medium quality** Reduced wrinkles from cavity walls, low indents in laminate	7.5 mm
6		
7		7.5 mm
8	**Good quality** No wrinkles, only slight marks of cavity base, slight keying	
9		
10	**Ideal quality** No imperfections of surface from film identifyable	7.5 mm

5.2.3 Three-Point-Bending for Evaluation of Part Quality

In order to evaluate the part quality to investigate research question 2.3, optical void measurements from micrographs are complimented by three point bending. Specimen of two parts that showed the poorest and best results in the DoE study are tested. For WCM, experiment 7 and 24 show the poorest flow results, experiments 23 and 40 the best. In regard to CIP, experiments 3 and 13 were selected for the poorest results, experiments 4 and 9 as representative for the best. Prior to the tests of these experiments, reference plates produced by WCM were tested to investigate, if EpoDye has an influence on the mechanical performance and to initially quantify the influence of the vacuum used in the process. Reference plates are all produced according to the parameter combination specified in the central point of the DoE (Figure 5-12). Ref 1 is produced with a vacuum level of 200 mbar inside the cavity and non-fluorescent matrix. Ref 2 refers to a part with full vacuum inside the cavity and non-fluorescent matrix and Ref 3 is produced under full vacuum and a matrix with 0.25 w-% EpoDye.

Three point bending tests are performed according to specifications of DIN EN ISO 14125 [106]. According to the standard, a width of the bottom supports of 80 mm is selected for specimen geometry of 100x15x2 mm of material class IV. Radius of the supports is selected to 2 ± 0.2 mm for the specimen thickness and tests are run with 5 mm/s. Five specimen are extracted with fiber angles of the top and bottom ply perpendicular to the longitudinal axis of the specimen from the center of the plates. Due to slight deformation of the tooling system under high compaction pressures, the thickness of all specimen tested is 2.32 ± 0.13 mm, which does not comply with the standard but is assumed to be precise enough. The quantifying parameter from the testing is the maximum bending stress.

5.2.4 Experimental Set-up for Complex Parts

Single WCM and CIP experiments for visualization of matrix flow under draping are performed to investigate research question 2.4. The distribution of fluorescent matrix after superimposed impregnation and draping during manufacturing of the complex part (Table 4-4) is to be quantified in the same way as previously described in Section 5.2.1 and 5.2.2 for the plate geometry. Two positions for fluorescent matrix are selected according to the slope of the respective part section, one part wall of 32° slope and one less steep wall of 40° slope, Figure 5-16.

Material preparation for the experiments is conducted similar to the preparation for pressings of the plate geometry. However, the total mass of matrix to be dosed is 50.8 g (42.4 ml) from which 7 ml are fluorescent matrix. The stack is designed with the same ply sequence of [0° /90°, +/- 45°, +/-45°]$_s$ as for the plate geometry and has an initial diameter of 180 mm.

In previous trials, a combination of process parameters was determined to manufacture parts of good quality in both process variants, WCM and CIP, and for both geometries, plate and complex parts. In consequence, the resin temperature T_r of 44.5 °C, pre-application time t_{pa} of 10 s and pressing velocity v_p of 6.25 mm/s are selected according to the center point of the DoE plan for WCM (Figure 5-12). The parameters t_h and T_t are set to 5 s and 100 °C, respectively. The tool closing procedure is performed as described previously in Section 5.2.2.

Three experiments per slope of the part and process variant, WCM and CIP, are performed to allow for a minimum of statistical validity. The parts are analyzed with fluorescent photography, according to the method developed in Section 5.1.2 and compared with results from plates pressed with the same parameter combination in WCM and CIP.
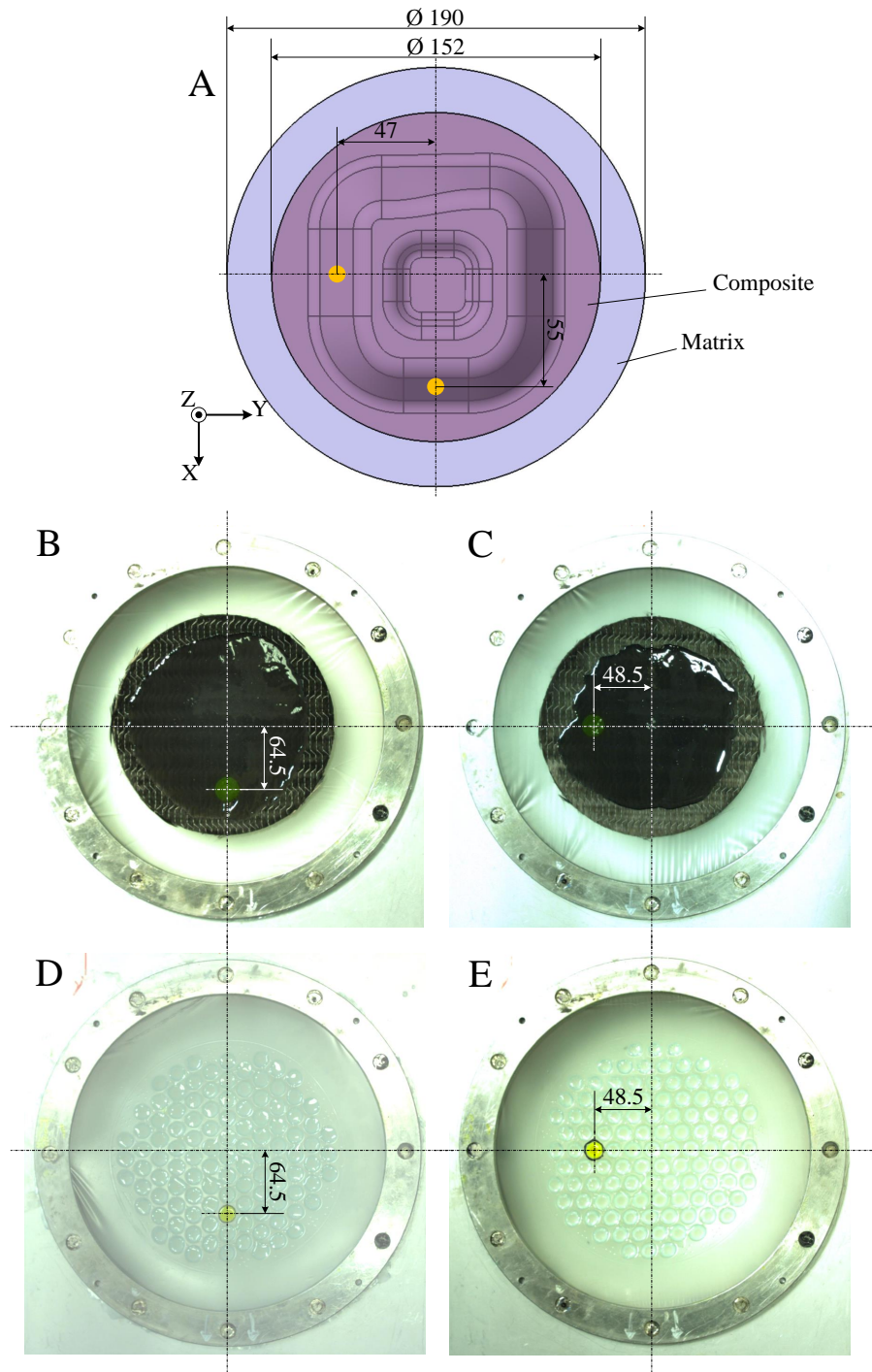
Figure 5-16 Manual material preparation for WCM and CIP manufacturing of complex parts. Part to be produced in experiments with fluorescent matrix (A), initial distribution of fluorescent and neat matrix after dosing on top of the NCF stack for WCM of fluorescent matrix at 32 ° slope (B) and 40 ° slope (C) of the part, initial distribution of fluorescent and neat matrix after dosing in carrier cavities for CIP of fluorescent matrix at 32 ° slope (D) and 40 ° slope (E) of the part

5.3 Results on Matrix Flow Studies in Compression Molding Processes

In the following the results are presented from experiments conducted to investigate research questions 2.1-2.4. The first two questions are jointly investigated within the DoE studies for plate pressings in WCM and CIP. Herein, the results from quality control of manual material preparation are presented first. Subsequently, significant parameters and quality of model fit are outlined and significant and valid responses are depicted.

5.3.1 Quality Control of Manual Preparation of Materials

In both cases, WCM and CIP, materials were prepared manually and controlled via image analysis as shown in Figure 5-2. Controlled parameters were area A_m of fluorescent matrix, its areal centroid values x_m, y_m, fiber mass m_f and its centroid coordinates x_f and y_f as well as the fiber angle α_f of the top NCF ply, Figure 5-17.

All quality control parameters indicate a sufficient accuracy of material preparation. The centroid coordinates of fluorescent matrix as well as the fiber stack showed a positive shift from the target value of $0\,mm$ with a standard deviation with up to $1.4\,mm$ in the magnitude of the average deviation. This deviation of maximally $3\,mm$ from the target value is assumed to not inhibit the reproducibility and comparability of experiments.
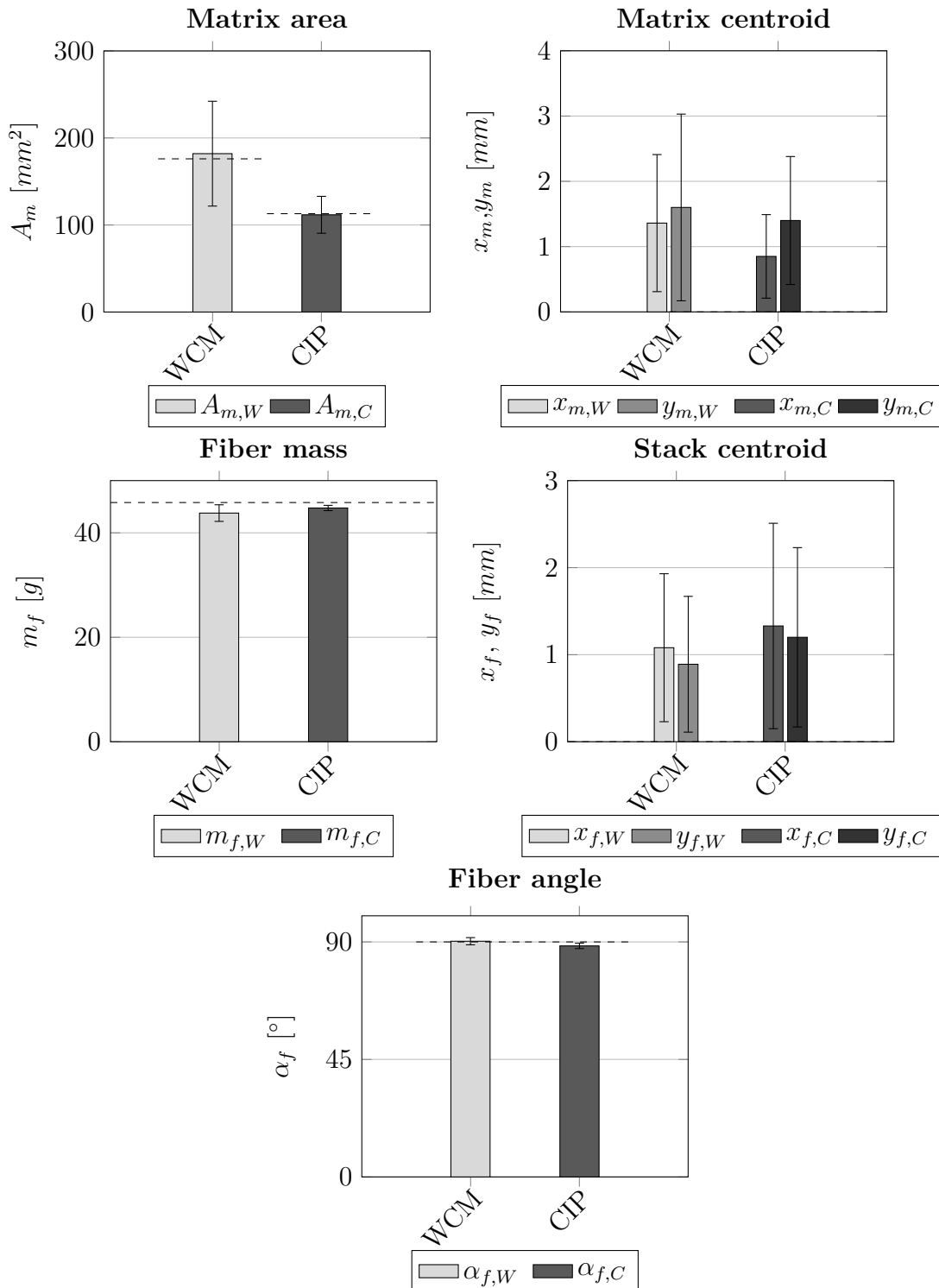
Figure 5-17 Quality parameters of manual material preparation from all DoE experiments for WCM (index W) and CIP (index C). Dashed lines mark target values

5.3.2 Results from Design of Experiments Studies

The results for the DoE experiments of both processes, WCM and CIP, include all quality parameters defined in Section 5.1 and 5.2. From fluorescent photography Q_1-Q_3 for top and bottom side of the part provide the main source of results. From fluorescent microscopy the integral of fluorescent pixel in x-direction I_x and the slope of the straight curve fit in z-direction m_z (Figure 5-10) are analyzed. The fiber angle distribution is described by the kurtosis k_α for both part sides and the cavity pressure p_c for WCM experiments is added to the statistical analysis, since it is assumed to indicate part quality. In CIP no significant pressure differences in the experiments were detected. However, assessment of cavity elimination Q_{ce} from carriers (Table 5-1) complement the DoE results for this process variant.

Results for WCM and CIP are presented separately. Both sections contain a visual representation of the flow results of extreme cases, best and poorest flow results, from fluorescent photography and microscopy. For WCM, results from fiber angle measurements and for CIP the best and poorest elimination of carrier cavities complement the respective extreme results. Subsequently, the complete results from the DoE study are presented.

Using Modde 10.1 software, it is first assessed how well the obtained data in dependence of the process parameters fit to a theoretical model within the DoE (coefficient of determination R^2) and how well this model predicts new data (Q^2). Furthermore, model validity and reproducibility are estimated. A process parameter or interaction of two parameters are deemed significant when Q^2 is larger than 0.1. Model validity should be larger than 0.25 and R^2 should be maximized to increase expressiveness of the model. However, responses are eligible for analysis when R^2 and Q^2 are high despite a model validity below 0.25. Analysis of all eligible responses is then presented in contour plots.

Wet Compression Molding

Areal share of fluorescent phase Q_1, its edge length Q_2 and the shift of centroid coordinates are the most expressive quality parameters of the study. These results differ strongly depending on how favorable the process parameters were for the press experiments. The results from segmented images, with the best quality parameters as well as with the poorest, are graphically depicted in connection with the numerical values Q_1, Q_2 and a chart of centroid shifts obtained from the segmented images, Figure 5-18.
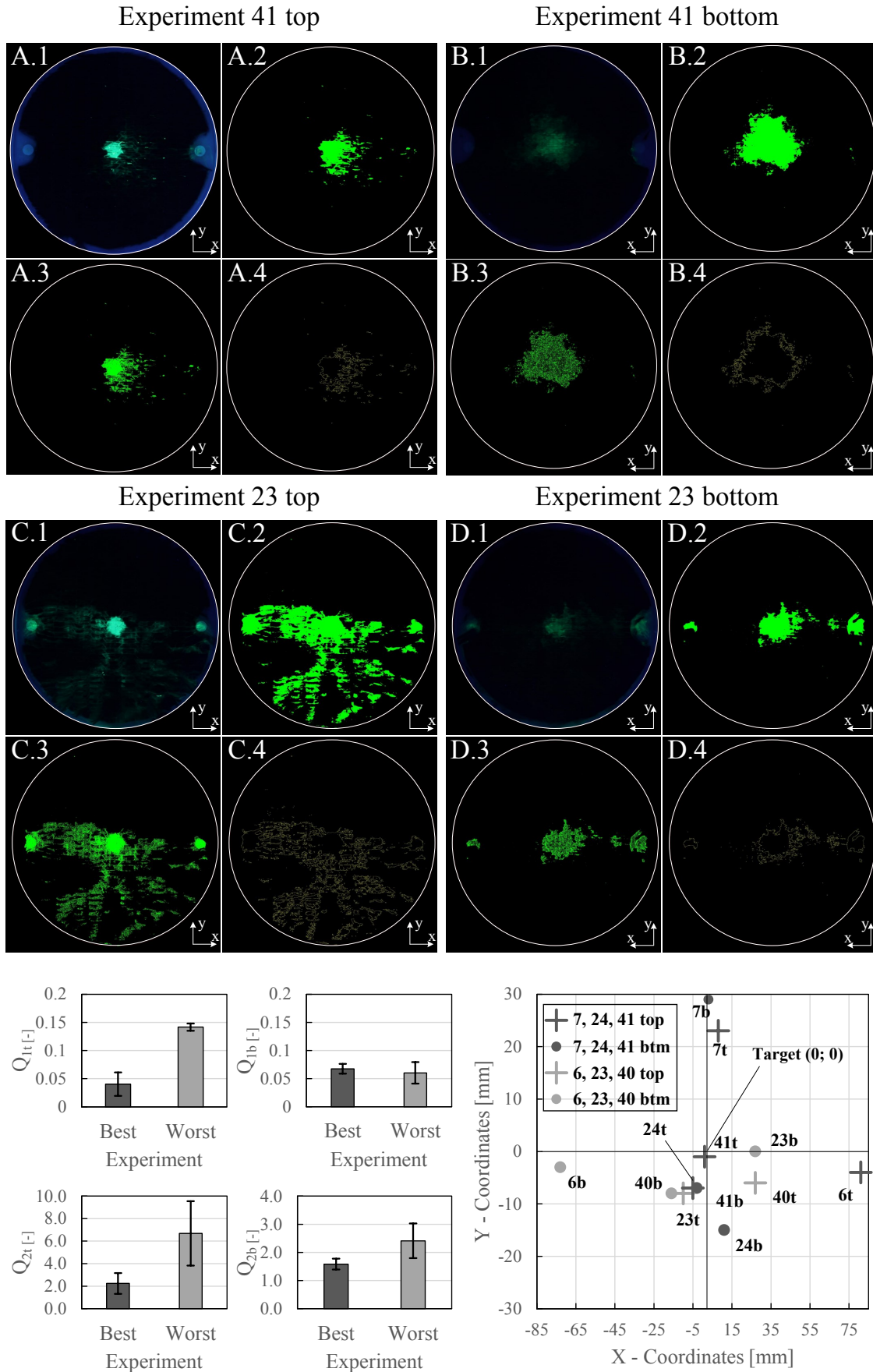
Figure 5-18 Extreme results for WCM with experiment 41 ($T_r = 35\,^\circ$C, $v_p = 9\,$mm/s, $t_{pa} = 15\,$s) beeing the best and experiment 23 ($T_r = 54\,^\circ$C, $v_p = 54\,$mm/s, $t_{pa} = 15\,$s) the poorest result. Quality parameters are shown as average and standard deviation of the respective points in the DoE (experiment 7, 24, 41 and 6, 23, 40)

The distribution of fluorescent matrix is more compact and centered around its initial center position in experiment 41 than in experiment 23. The matrix in the latter is scatterd chaotically over the lower half of the part. This difference is most apparent on the images from the top side of the part (A.1-A.4 and C.1-C.4), on which the fluorescent matrix was pre-applied in the experiment (Figure 5-13). Accordingly, Q_{1t} and Q_{2t} are lower for experiment 41 in comparison to experiment 23.

The bottom images (B.1-B.4) exhibit a bigger amount of fluorescent pixels than the top images for experiment 41, where Q_{1b} is larger than Q_{1t}. In experiment 23 (D.1-D.4) the fluorescent phase on the bottom is much lower than on the top. However, in both experiments the concentration of the fluorescence is lower on the bottom compared to the top. Q_{2b} is almost equal for both experiments but drops drastically compared to the top image of experiment 23, while it shows only a slight drop compared to the top image of experiment 41.

In compliance with the compactness of distributions, the centroid shift in x- and y-direction is much larger for experiment 23 than for experiment 41. It is important to note that the shifts in y-direction are partially due to the fact that the part is pivoted around the y-axis (marked on each image) to photograph the bottom side. But even under this consideration the areal centroid of fluorescent matrix shifts towards the outer circumference of the part on the bottom side for both experiments.

Distribution of fluorescent matrix in the cross-sections of specimen obtained via fluorescence microscopy (Figure 5-19) negatively correlates with the distribution on the top side of the pressed plates. While fluorescent matrix is widely distributed over the micrograph from experiment 42, the fluorescent photography (Scene A.2 in Figure 5-18) shows a centered distribution. This relation is inverted for experiments 6 and 23, both of which were produced with the same process parameters. Here, fluorescent matrix is scattered on the top side of the pressed plate (Scene C.2 in Figure 5-18), but centered around the right hand section of the micrograph whose right vertical edge lies close to the center of the pressed part where the matrix was initially dosed (Figure 5-10).

The qualitative description of the matrix distribution is reflected by a low I_x of 2.2828 and a slope of the fitted straight line which is tilted only slightly with $m_z = -5.0653 \cdot 10^{-5}$. In contrast, the integral over x amounts to 9.7919 and the slope of the fitted x curve is tilted with $m_z = 21.342 \cdot 10^{-5}$ for experiment 42. The micrograph images themselves, however, show mostly fluorescent phase in matrix-rich areas between fiber rovings. Within fiber rovings almost no fluorescence is detectable. When the same areas are magnified, the matrix inside the rovings is
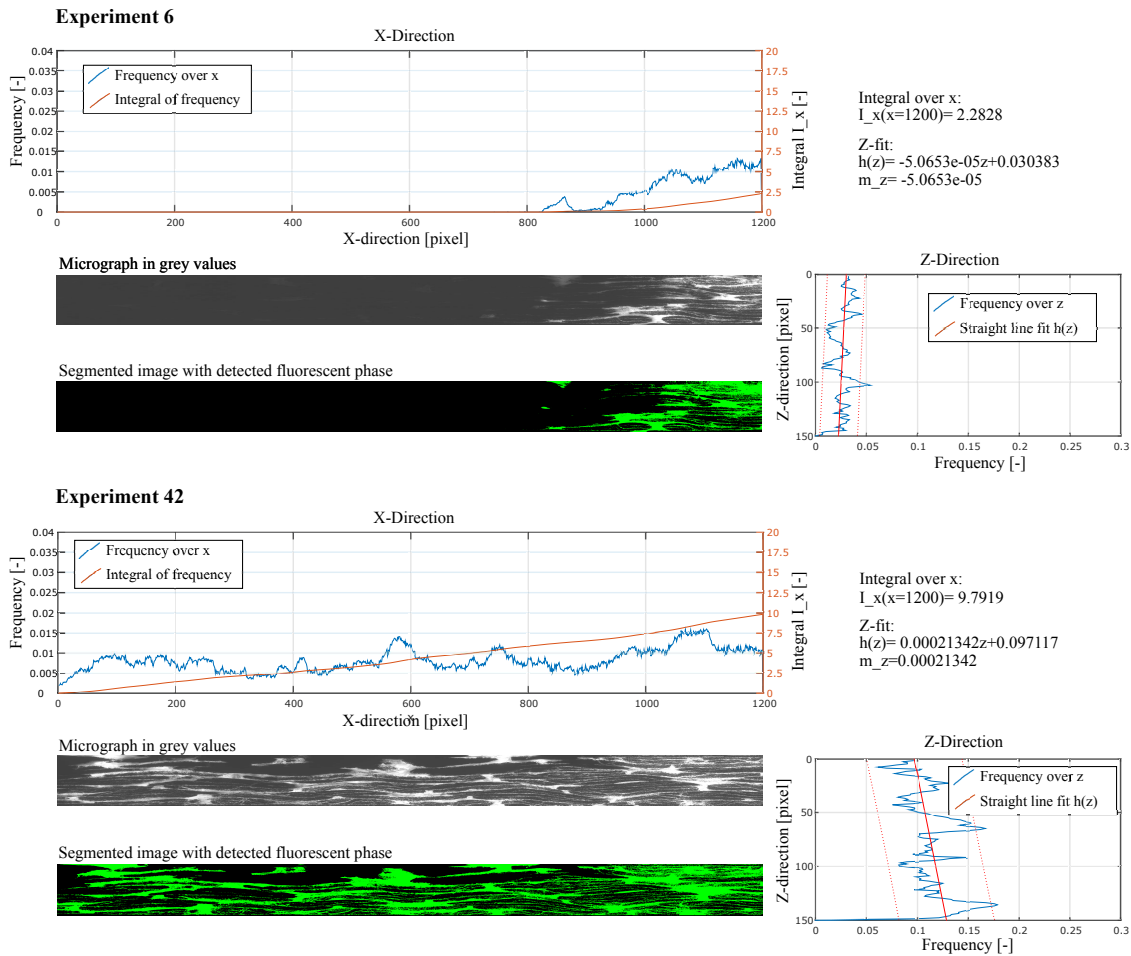
Figure 5-19 Extreme results for I_x and m_z of fluorescent micrography of WCM experiment 6 ($T_r = 54\,°\text{C}$, $v_p = 3.5\,\text{mm/s}$, $t_{pa} = 15\,\text{s}$) and experiment 42 ($T_r = 35\,°\text{C}$, $v_p = 9\,\text{mm/s}$, $t_{pa} = 15\,\text{s}$)

clearly fluorescent. Thus, the segmented images show a more heterogeneous distribution of fluorescent matrix due to the low degree of magnification (2.5x) used because of limitations from computation power.

Many plates produced in the study by WCM exhibit in plane fiber waviness of the top ply from the top plate side. In particular, the extreme results defined by quality parameters Q_{1t} and Q_{2t}, experiment 41 and experiment 6, show the range of fiber waviness encountered in the study, Figure 5-20. The bottom side of the plates did not show any dependency from the process parameters with very little fiber waviness, represented by a kurtosis t_b of 3.299 ± 0.487. However, for the top side on which the matrix was initially pre-applied in the press experiments, the kurtosis k_t averaged 1.503. Thus, these fiber angles varied much wider compared with the bottom side, with a standard deviation of 0.849 over all experiments.

Analysis of single results from the extreme points of the experiments shows a dependency of the process parameters that were varied within the study. However,
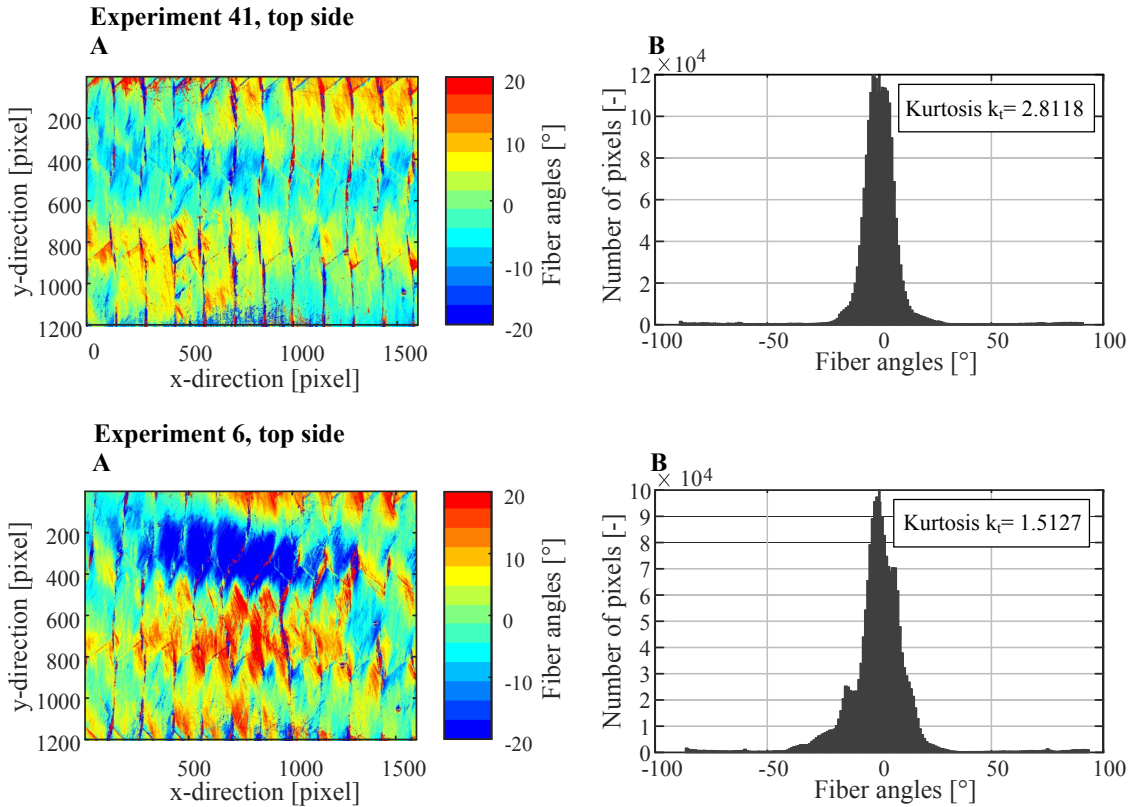
Figure 5-20 Extreme results for fiber angle distribution of WCM experiment 6 (replicate of poorest parameter combination $T_r = 54\,°C$, $v_p = 54\,\text{mm/s}$, $t_{pa} = 15\,\text{s}$) and experiment 41 (best results with $T_r = 35\,°C$, $v_p = 9\,\text{mm/s}$, $t_{pa} = 15\,\text{s}$)

to research how the parameters influence the presented quality parameters, results from all points of the DoE are integrated into the analysis. It is important to review model goodness of all responses (quality parameters) first, before detailed analysis and model fit are carried out. Model goodness for all responses in the DoE for WCM are depicted within a summary of fit, Figure 5-21.

From the summary of fit, the quality parameters of the top side Q_{1t}, Q_{2t}, p_c, $k_{\alpha t}$ and I_x are eligible for model fit and further analysis. All other parameters show a lack of accuracy for predictability with a negative Q^2 value and are not taken further into account. Model validity and reproducibility can not be computed for VC, I_x and m_z, since not all experiments were evaluated, as the parts had to be destructed for testing to obtain these parameters. Model goodness of theses responses is estimated via R^2 and Q^2 only. Thus, in this group only I_x is qualified for detailed analysis.

Overview plots, consisting of the replicate results, summary of fit, coefficients and residuals, for all quality parameters for further analysis are depicted in Appendix A.2, Figure A-5 to A-9. The plotted coefficients indicate if one of the process parameters T_r, v_p, t_{pa} or any interaction of two process parameters has a significant effect on the respective quality parameter used for analysis. This is the case if the
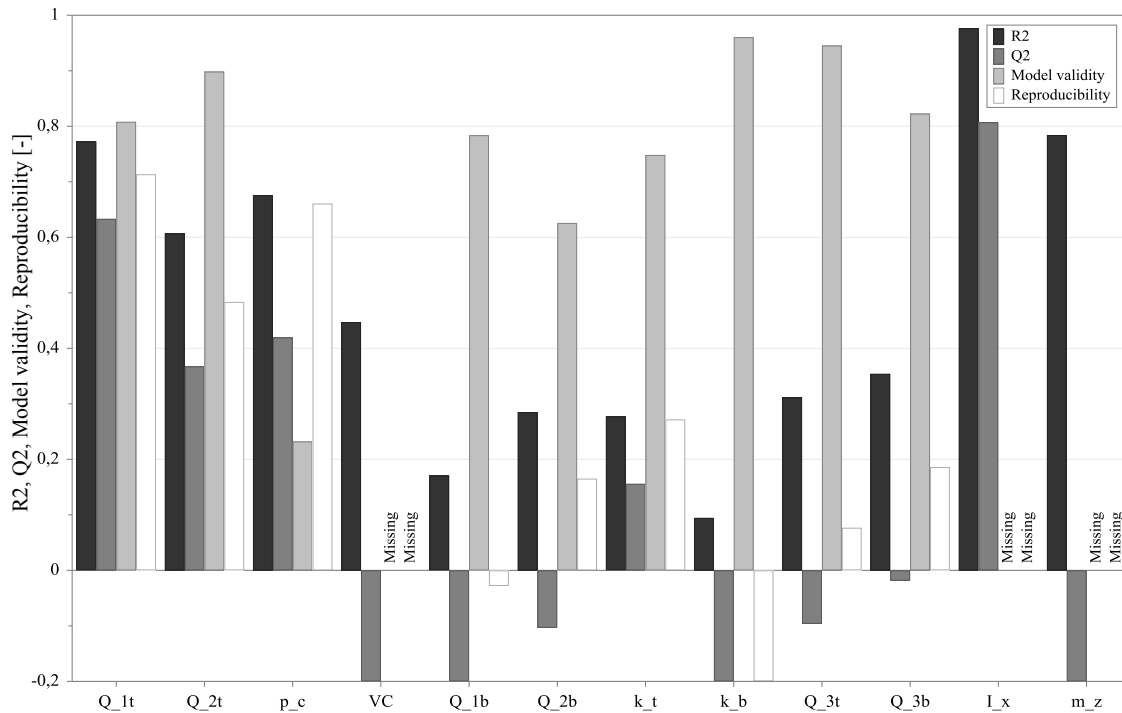
Figure 5-21 Summary of fit for responses design of experiments of WCM (Q_{1t}=Areal share of fluorescence top; Q_{2t}=Edge length of fluorescence top; p_c=Maximum pressure within cavity; VC=Void content; Q_{1b}=Areal share of fluorescence bottom; Q_{2b}=Edge length of fluorescence bottom; $k_{\alpha t}$=Kurtosis of fiber angle distribution top; $k_{\alpha b}$=Kurtosis of fiber angle distribution bottom; Q_{3t}=Absolute value of centroid shift top; Q_{3b}=Absolute value of centroid shift bottom; I_x=Integral of fluorescence in x-direction; m_z=Slope of fitted straight curve in z-direction)

standard deviation of the respective coefficient bar is smaller than the magnitude of the effect, which means the standard deviation bar does not cross zero. In case of Q_{1t} (Figure A-5), all process parameters show significant effects. Q_{2t} is also influenced by all three parameters, but strongly only by T_r (Figure A-6). T_r and t_{pa} effect the cavity pressure p_c (Figure A-7) significantly. Fiber angle distribution is weakly influenced by T_r and v_p (Figure A-8) and I_x is effected by strong interactions of T_r, v_p and t_{pa} (Figure A-9). Effects of process parameters on selected responses are depicted in two dimensional contour plots. Since the influence of t_{pa} on most responses is very weak, contour plots for T_r and v_p are shown for a constant t_{pa} of 10 s, Figure 5-22.

Areal share of fluorescent phase Q_{1t}, its relative edge length Q_{2t} and the kurtosis of fiber angle distribution k_t improved when the resin temperature T_r was minimized and the press speed v_p increased. The fluorescent matrix centered compactly around its initial pre-application spot with little scatter when the parts were produced with $T_r = 35\,°C$ and $v_p = 9\,mm/s$ (Scene A.2 in Figure 5-18). With increasing T_r and decreasing v_p, compactness successively deteriorated, which means fluorescent ma-
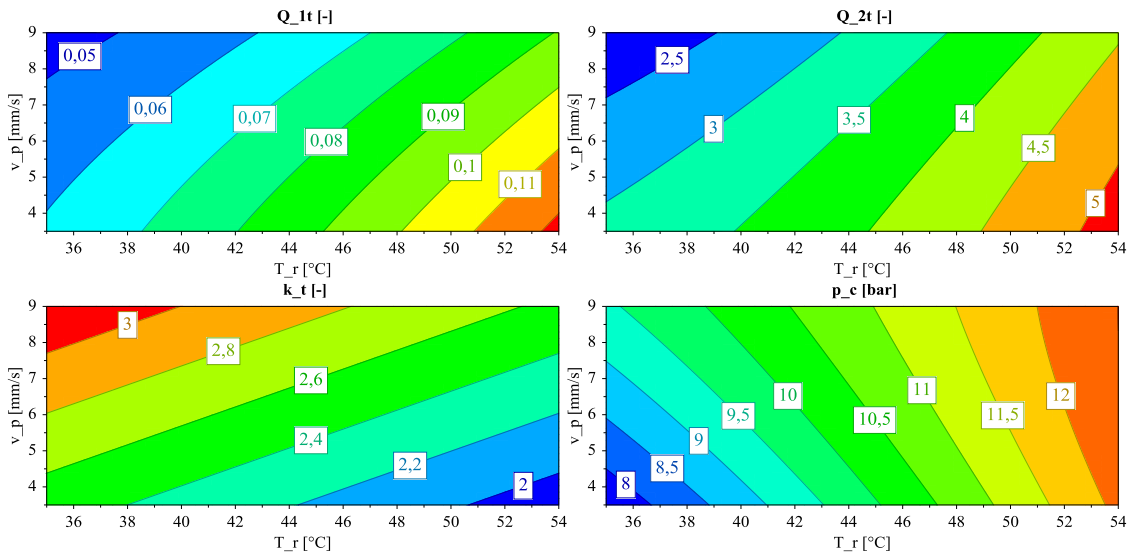
Figure 5-22 Effects of process parameters T_r and v_p on responses from areal share of fluorescence top Q_{1t}, edge length of fluorescence top Q_{2t}, kurtosis of fiber angle distribution top k_t and maximum cavity pressure p_c for WCM at a constant t_{pa} of 10 s

trix was increasingly scattered over the top side of the part with the least compact distribution at $T_r = 54\,°C$ and $v_p = 3.5\,\mathrm{mm/s}$ (Scene C.2 in Figure 5-18).

Fiber waviness shows the same correlation to the process parameters with the lowest waviness for $T_r = 35\,°C$ and $v_p = 9\,\mathrm{mm/s}$ (Scene A in Figure 5-20). However, k_t more strongly responded to the effect of press speed v_p than to resin temperature T_r compared to the compactness parameters.

Maximum cavity pressures p_c in the narrow pressure range of 8 to 12 bar are not necessarily a quality parameter that correlate with laminate quality. However, for high temperatures and fast press velocities, pressures were increasing. Lowering T_r and v_p decreased the cavity pressures. Furthermore, cavity pressures became more sensitive to resin temperature T_r and less dependent on press velocity v_p when resin temperatures were increased.

In contrast to responses discussed before, the integral I_x of amount of fluorescent pixels in x-direction is subject to interactions of all three process parameters (Figure A-9). Thus, contour plots of T_r and v_p with $t_{pa} = 5, 10$ and 15 s are presented, Figure 5-23. Extreme parameter combinations in terms of distribution of fluorescent matrix were found at 5 and 15 s pre-application time t_{pa}, while poor matrix distribution was exhibited by plates produced with $t_{pa} = 10\,\mathrm{s}$.

Fluorescent matrix distribution in X-direction improved with high temperatures and and low pressing speeds. This relation, however, changed with increasing speeds. The widest distribution of fluorescent matrix was found at $T_r = 54\,°C$, $v_p = 9\,\mathrm{mm/s}$ and $t_{pa} = 15\,\mathrm{s}$ as well as $T_r = 35\,°C$, $v_p = 3.5\,\mathrm{mm/s}$ and $t_{pa} = 5\,\mathrm{s}$. At
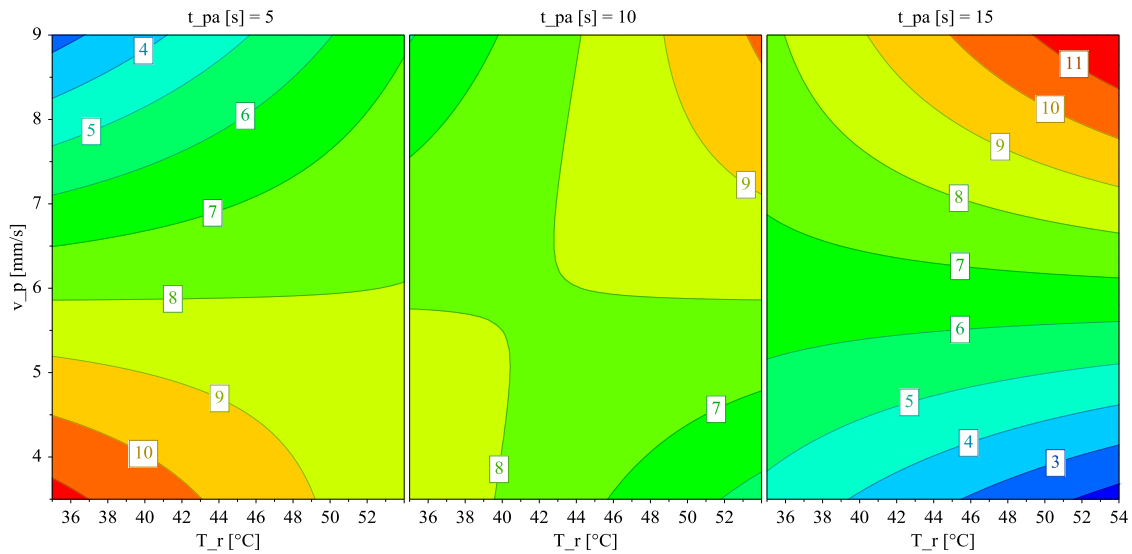
Figure 5-23 Effects of process parameters T_r, v_p and t_{pa} on integral I_x of amount of fluorescent pixels over x from microscopy for WCM

the same temperatures and pre-application times, the opposite extreme points for press velocity produced the most compact flow distribution. The extreme results for $t_{pa} = 15\,\text{s}$ of the contour plots are displayed in detail in Figure 5-19.

Carrier-Integrated Pressing

For CIP, experiment 8 and 4 exhibited the most and least compact fluorescent matrix distribution on top and bottom sides of the pressed parts. Digital image segmentation, numerical values for Q_1, Q_2 and the centroid coordinate chart for both experiments and part sides are depicted in Figure 5-24.

Fluorescent matrix on the bottom side of experiment 8 (B.2) is centered coherently around its initial pre-application region with the circular shape of the carrier cavity recognizable. On the top side of the same part (A.2), the fluorescent phase is slighty more scattered, which results in a higher areal share Q_1 and edge length Q_2. The centroid coordinates remained close to zero.

Experiment 8 showed a wider distribution of fluorescent matrix on both sides, compared to experiment 4. Respectively, Q_1 and Q_2 approximately doubled on both sides. As in experiment 8, the fluorescent phase was less compact on the top side of the part than on its bottom side. The centroids 4t and 4b underwent a larger shift, but both points moved in positive x-direction.

Experiment 8 top

Experiment 8 bottom

Experiment 4 top

Experiment 4 bottom
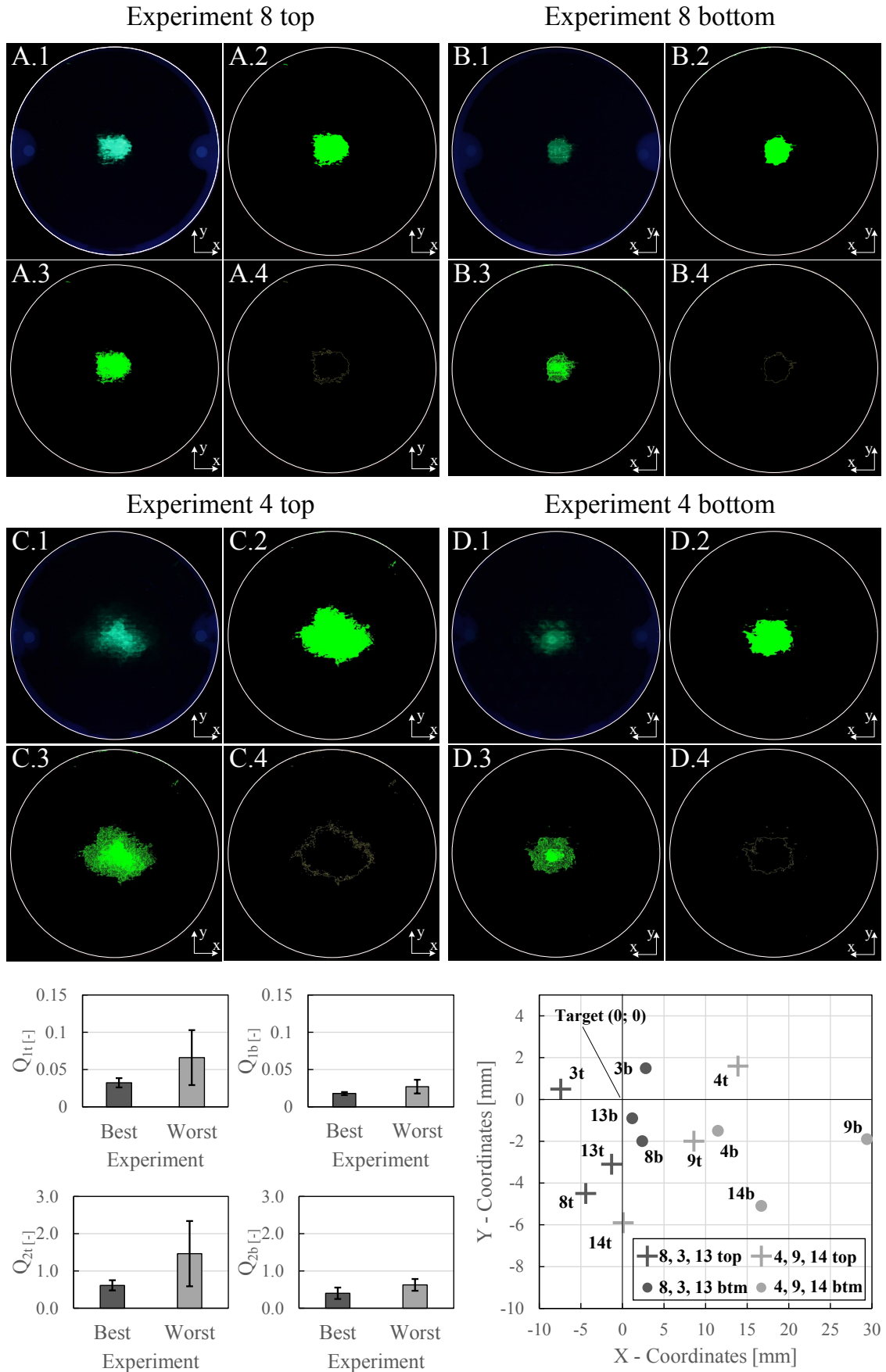
Figure 5-24 Extreme results for CIP with experiment 8 ($t_h = 5\,\text{s}$, $T_t = 100\,°\text{C}$) showed the best and experiment 4 the poorest result. Quality parameters are shown as average and standard deviation of the respective points in the DoE (experiment 8, 3, 13 and 4, 9, 14)

Compared with results for the best WCM part, experiment 41 (A.2 and B.2 in Figure 5-18), matrix distribution of CIP experiment 8 is overall more compact. However, it is important to compare the part sides of WCM and CIP from with the matrix was pre-applicated. Here, in particular Q_{1b} of 0.0158 from CIP experiment 8 is lower than Q_{1t}=0.0261 of experiment 41 produced by WCM. Relative edge length Q_2 even exhibited a difference in the magnitude of 10 between both experiments in favor of CIP.

When the poorest results from both processes are compared, CIP does not produce a flow distribution as widely scattered as WCM. While quality parameters Q_1 and Q_2 deteriorated moderately in CIP with unfavorable process parameters, flow in through-thickness direction was still dominant. In case of WCM, flow became highly unpredictable and scattered on the part top with only very little flow of fluorescent matrix in through-thickness direction.

Findings of fluorescent photography were supported by fluorescent microscopy for the extreme results, experiment 8 and 4, Figure 5-25.
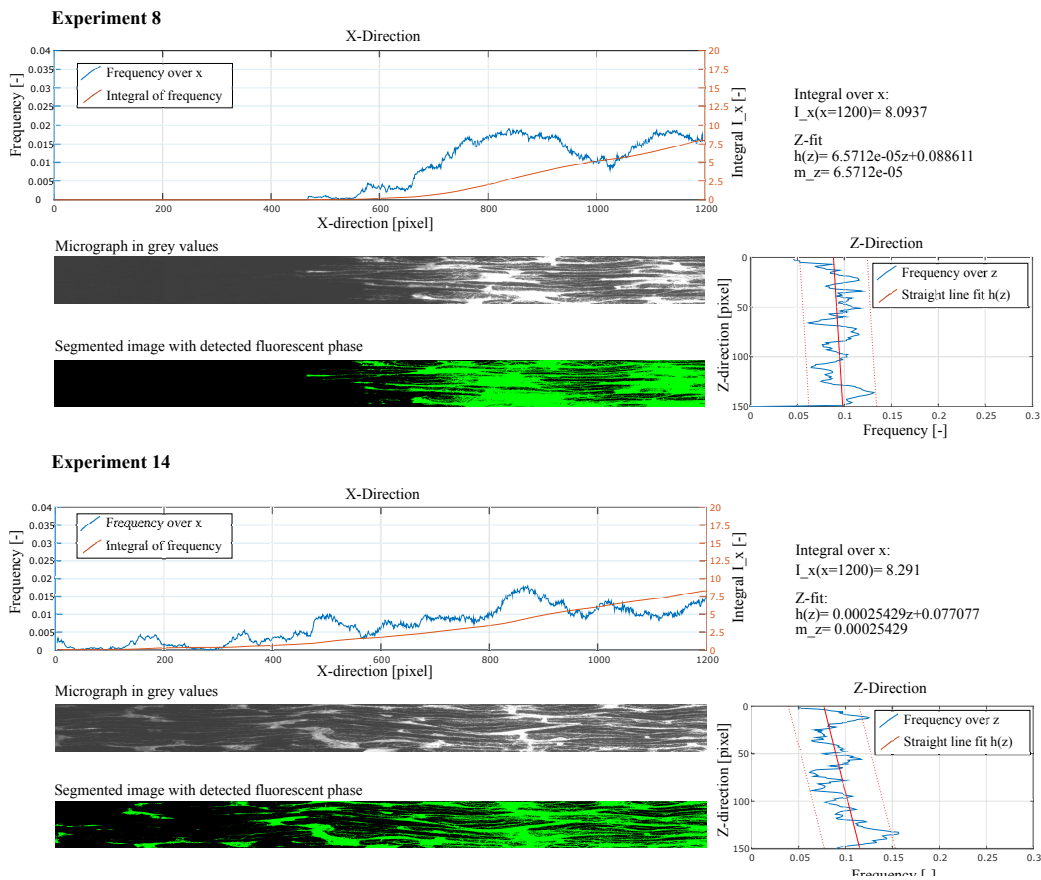
Figure 5-25 Extreme results for I_x and m_z of fluorescent microscopy of CIP experiment 4 (replicate of poorest parameter combination) and experiment 8 (best result)

Distribution of fluorescent matrix in the cross-section of experiment 8 was closely centered around the center of the part (right edge of micrograph). While at the left side of the part, no fluorescence was detected. The integral I_x of detected fluorescent pixel proceeded from approximately $x = 600$ pixels almost linear, comparable to the ideal distribution defined in Scene C of Figure 5-10.

The transition from non-fluorescent to fluorescent phase was sharp compared to experiment 14, which was also quantitatively supported by the slope of the Z-fit curve of $m_z = 6.571 \cdot 10^{-5}$.

Experiment 4 exhibited an increasing number of fluorescent pixel in positive X-direction, however fluorescent matrix was detected across the entire micrograph. I_x increased almost linear close to the worst case, Scene D of Figure 5-10. In contrast however, the straight line fitted in Z-direction was strongly tilted with $m_z = 25.429 \cdot 10^{-5}$, indicating a non-homogeneous distribution across the thickness direction of the part.

Compared to the best result in fluorescent microscopy of WCM parts, experiment 6, Figure 5-19, quality values of experiment 8 indicated a less compact matrix distribution. It must be taken into account, however, that experiment 6 exhibited a highly scattered fluorescent matrix on top of the part, comparable with C.2 of Figure 5-18, which was produced with the same process parameters. Thus, less matrix was pushed into through-thickness direction of the part, which can be detected in fluorescent microscopy.
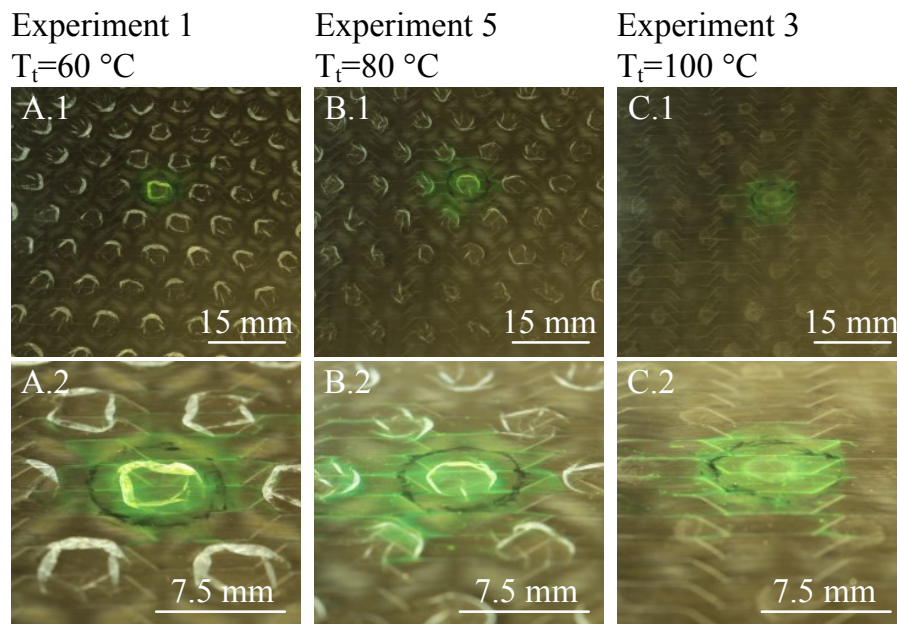
Figure 5-26 Carrier cavity elimination for $T_t = 60, 80$ and $100\,°C$ for CIP. Experiment 1 was in average awarded with 2.3 points, experiment 5 earned 4.6 and experiment 3 earned 8 points after independent subjective evaluation (n=3) after Table 5-1

In CIP fluorescent matrix flow is assumed to be influenced strongly by carrier cavity elimination within the press process. From visual inspection it was found that elimination of carrier cavities was strongly influenced by tool temperature T_t, which is reflected by evaluation results of respective experiments, Figure 5-26.

With higher tool temperatures T_t cavities were successively less likely to form wrinkles from side walls of the cavity, which collapse under normal pressure during compaction. While the carrier film processed at 60 °C (A.1 and A.2 in Figure 5-26) showed blank rings that were produced by multiple layers of carrier film, these rings were already reduced on parts pressed with medium temperature (B.1 and B.2). Experiment 3 (B.1 and B.2) exhibited only slight marks from where the cavity base had been but no build-up of film layers.

Cavities that were not well eliminated disturbed optical fiber angle measurement. Thus, no reliable distributions could be established for the bottom side of the produced parts. On the top side, however, fiber angles exhibited a less strong influence by different process parameters compared with WCM plates, Figure 5-27.
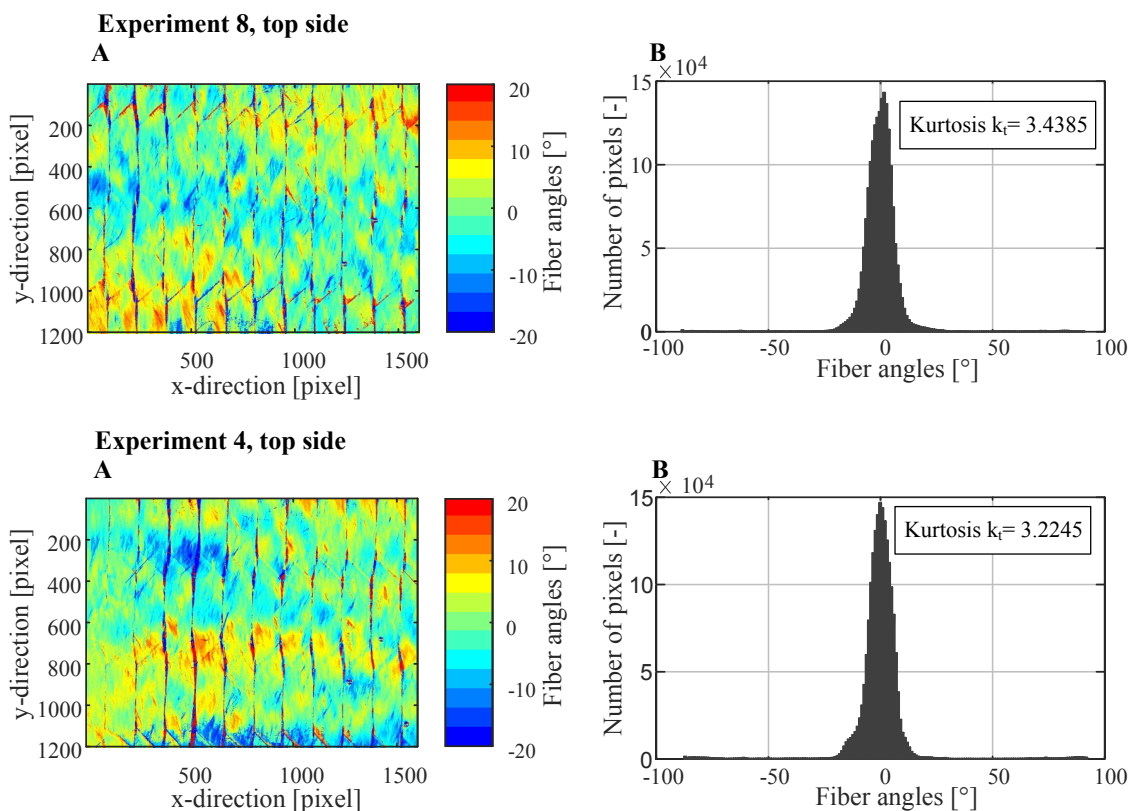
Figure 5-27 Extreme results for fiber angle distribution of CIP experiment 8 (best results with $t_h = 5$ s, $T_t = 100$ °C) and experiment 4 (poorest parameter combination $t_h = 35$ s, $T_t = 100$ °C). Fiber angles detected by Profactor sensor in the region of interest (A) and the respective histogram of pixel showing fiber angles with computed kurtosis k_t (B)

Both extreme results from flow distribution produced by CIP, experiment 8 and 4, showed comparable k_t values, with low to moderate fiber waviness. The lowest fiber waviness was achieved with experiment 11 that showed a k_t of 3.229, the worst result by experiment 1 with k_t=1.439. Over all experiments, kurtosis was computed to k_t=2.138±0.562, showing a less straight adjustment compared to all bottom sides of plates produced by WCM. Visual inspection of the bottom side of CIP plates indicated that no plate showed a fiber waviness as strong as in some WCM experiments. It is subjectively assumed that the overall fiber waviness is lower in CIP plates than in plates produced by WCM.

Evaluation of single responses showed an influence from process parameters in CIP, in particular fluorescent photography and micrography as well as cavity elimination. In the following, the entire response range for variations of the parameters heating time t_h and tool temperature T_t are presented. From statistical analysis of Modde 10.1, the summary of fit for all possible responses is depicted in Figure 5-28.
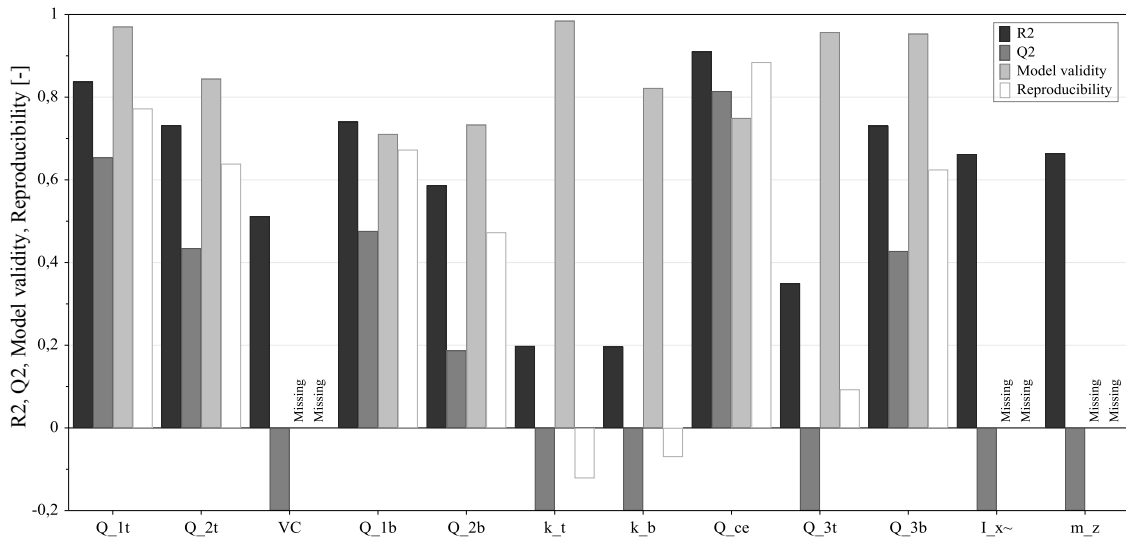
Figure 5-28 Summary of fit for responses design of experiments of CIP (Q_{1t}=Areal share of fluorescence top; Q_{2t}=Edge length of fluorescence top; VC=Void content; Q_{1b}=Areal share of fluorescence bottom; Q_{2b}=Edge length of fluorescence bottom; $k_{\alpha t}$=Kurtosis of fiber angle distribution top; $k_{\alpha b}$=Kurtosis of fiber angle distribution bottom; Q_{3t}=Absolute value of centroid shift top; Q_{3b}=Absolute value of centroid shift bottom; I_x=Integral of fluorescence in x-direction; m_z=Slope of fitted straight curve in z-direction)

In contrast to the results from WCM, CIP plates showed eligible responses from fluorescent photography from both sides. Thus, Q_{1t}, Q_{1b}, Q_{2t} and Q_{2b} were eligible for analysis. Furthermore, Q_{3t} showed high model goodness, as the evaluation of cavity elimination Q_{ce} did. Fiber angles, void content and responses from fluorescent microscopy did not show consistent results, as indicated by negative Q^2 values and thus are not discussed in the following.

From the overview plots of all eligible responses for CIP experiments (Appendix A.2, Figure A-12 to A-15), t_h had a significant influence on all responses except Q_{ce} and Q_{3b}. These latter responses were only influenced by the tool temperature T_t. Only slight interactions between both process parameters influenced Q_{1t} and Q_{2t}. The respective significant effects of process parameters on all eligible responses are depicted in Figure 5-29.
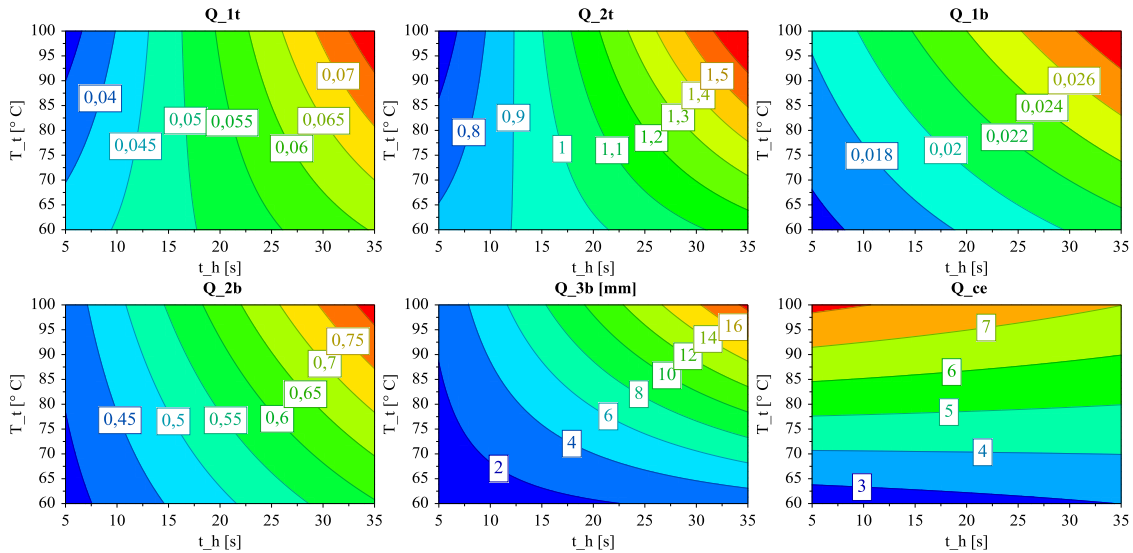
Figure 5-29 Effects of process parameters t_h and T_t on responses from areal share of fluorescence top Q_{1t}, edge length of fluorescence top Q_{2t}, areal share of fluorescence bottom Q_{1b}, edge length of fluorescence bottom Q_{2b}, centroid shift of fluorescent matrix on bottom side Q_{3b} and evaluation of elimination of carrier cavities Q_{ce} for CIP

Results have to be differentiated between top and bottom side with respect to the initial pre-application position of the fluorescent matrix on the bottom. On the top side Q_{1t} and Q_{2t} showed consistent influences from the process parameters. In particular, the heating time t_h had a strong effect on the compactness of matrix distribution. It improved with low heating times t_h with an optimum at 5 s and 100 °C tool temperature.

On the bottom side, tool temperature had a stronger effect on areal share and relative edge length of the distribution of fluorescent matrix but t_h still dominated the results. In contrast to the top side, most compact distributions were achieved with the lowest tool temperature T_t of 60 °C at minimum heating time. Worst results in terms of matrix compactness on both sides exhibited parts produced at maximum t_h of 35 s and highest tool temperatures of 100 °C.

Only the bottom centroid shift of fluorescent phase $Q3b$ was significantly influenced by process parameters and showed the same principle effect as areal share and edge length. Thus, the lowest shift occurred in parts that were produced at $t_h = 5$ s and $T_t = 60$ °C and lengthened with increasing heating time and tool temperature.

Elimination of carrier cavities were almost exclusively dependent on tool temperature. Very little influence from heating time was detected. The lowest points were awarded to parts produced at 60 °C, while quality successively increased to a maximum for films processed at 100 °C.

5.3.3 Mechanical Testing of Parts

Research question 2.3 addresses the link between matrix flow and part quality, which is known to be relevant in RTM. In order to investigate the question, void measurements (Figure 5-14) and three point bending tests after Section 5.2.3 were performed.

Measurements between experiment 8 (most compact flow) and 14 (least compact flow) for CIP showed a void content of 0.52 ± 0.21 % and 2.73 ± 1.69 %, respectively. Results for WCM revealed the same relation with 1.03 ± 0.37 % voids in experiment 41, which exhibited the most compact flow and 2.8 ± 2.7 % for experiment 6 with the most scattered flow distribution.

On average, a void content of 2.24 ± 1.17 % for WCM parts was detected, while CIP laminates contained 1.66 ± 0.89 % voids. An industrially produced WCM part from an established automotive series production that was measured for reference, yielded 2.58 ± 0.83 %. For WCM and CIP experiments however, no significant effects of process parameters were observed, since both Q^2 values in the summary of fits were negative, Figure 5-21 and 5-28.
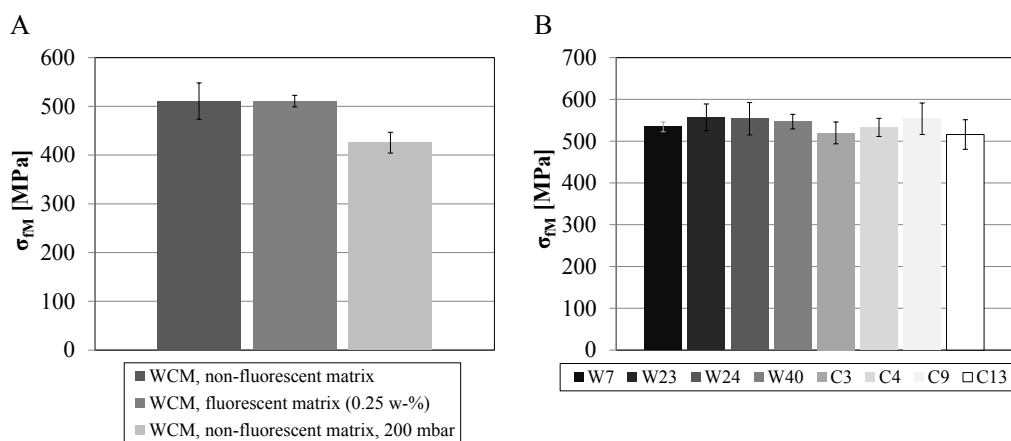
Figure 5-30 Maximum bending stress σ_{fM} from three point bending tests of WCM and CIP experiments with influence of fluorescent marker and vacuum level investigated (A; parts were produced in WCM at center point of the DoE) and tests of all process points of the DoE studies (B). All parts were tested with n=5 specimen

In addition to void measurements mechanical quality of parts was also assessed in three point bending tests. Firstly, the influence of fluorescent marker on the

maximum bending stress σ_{fM} was investigated. It was found that the marker did not effect σ_{fM}, Scene A in Figure 5-30. Thus, parts from the DoE studies which partially contained fluorescent matrix were eligible for mechanical testing, Scene B in Figure 5-30.

All parts from the DoE studies showed maximum bending stresses of above 500 Mpa, but did not show significant influences of different process parameters. In addition, no difference between WCM and CIP parts was found.

As a reference, one part produced without full evacuation of the cavity in WCM was added to the test program. The vacuum level was held at 200 mbar before full compaction of the part in contrast to all other parts produced at below 5 mbar. It was found that maximum bending stress σ_{fM} dropped to 425.37 ± 21.39 Mpa from 510.84 ± 37.38 Mpa yielded by a part produced with the same process parameters with full vacuum.

5.3.4 Influence of Draping on Matrix Flow

To investigate the influence of draping on matrix flow, complex parts (Table 4-4) were successively produced with fluorescent matrix on two slopes of the part, $40°$ and $32°$. Since materials were prepared in a flat, non-draped state and were draped and simultaneously compacted during press stroke, the influence of draping on matrix flow in comparison to pressed plates could be analyzed.

The fluorescent photographs of both fluorescent matrix positions showed a strong distribution toward the lowest point of the slope after the pressings, Figure 5-31 and 5-32. The lowest point was in case of the $40°$ slope on the left hand side for the top view and the right hand side for the bottom view of the part. In case of the $32°$ slope, the lowest point was pointing in the negative y-direction. Such an orientation was not exhibited by planar parts produced earlier, Figure 5-18 and 5-24.

Quantitative analysis of the fluorescent photographs showed that for both slopes WCM produced a more compact matrix distribution compared with the worst experiments but not compared with the best experiments (Figure 5-18). In case of CIP, compactness of matrix distribution deteriorated strongly for best and worst experiments. In comparison to WCM, results for the complex parts showed no clear differences except for the Q_{1b} value of $40°$ slope and Q_{2b} of the $32°$slope.
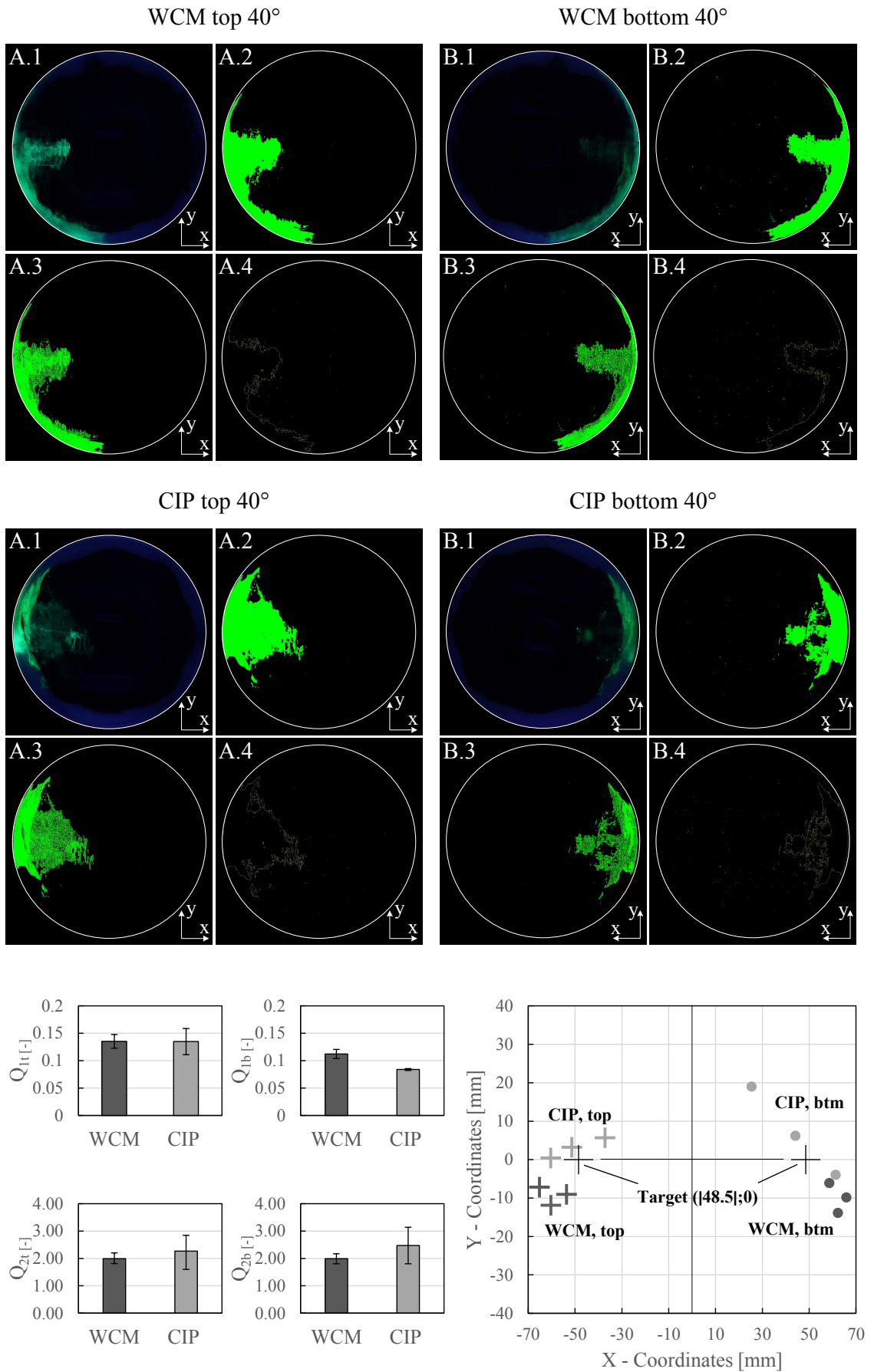
Figure 5-31 Results for WCM and CIP experiments with fluorescent matrix pre-applicated for 40° slope of complex part

WCM top 32°

WCM bottom 32°

CIP top 32°

CIP bottom 32°
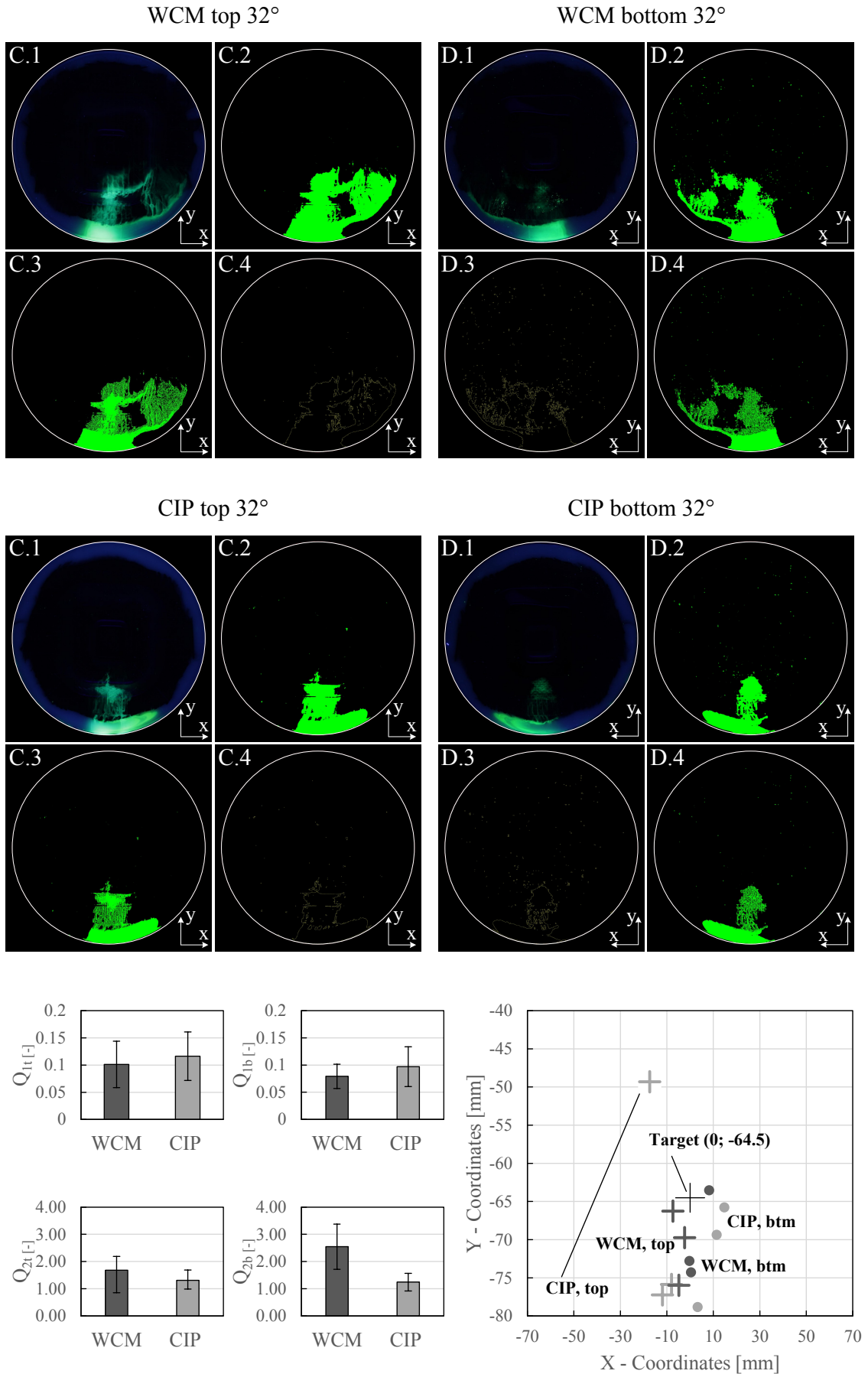
Figure 5-32 Results for WCM and CIP experiments with fluorescent matrix pre-applied for 32 ° slope of complex part

Centroid shifts became more centered with increasing slope for WCM. While even for the most compact matrix distributions (Figure 5-18) considerable shifts of up to 77 mm occurred with a high spread of replicated experiments, shifts in the complex parts were reduced. For the 40 ° slope, all experiments of WCM lay close to one another near the target. For the 32 ° slope, centroid shifts of WCM experiments increased slightly with a higher spread between experiments.

Summarized results for Q_{1t}, Q_{1b}, Q_{2t} and Q_{2b} and their standard deviation between experiments over increasing complexity for both processes are shown in Figure 5-33.
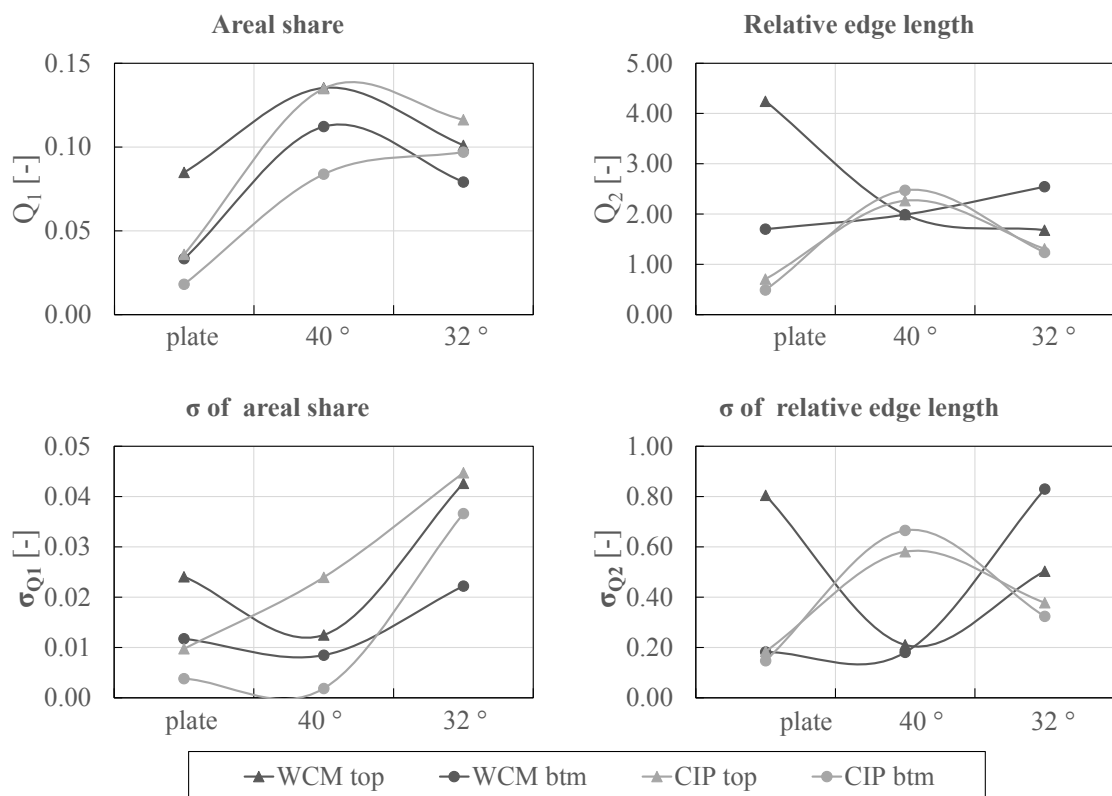
Figure 5-33 Results for WCM and CIP experiments at increasing draping complexities (plate, 40 ° and 32 ° slope)

In regard of the areal shares, Q_{1t} and Q_{1b} both processes showed an initial deterioration before the results improved slightly. The standard deviation, however, showed best results for the 40 ° slope.

Relative edge length for WCM improved overall but worsened for CIP. The least standard deviation between experiments and for both processes was achieved with a 40 ° slope. For WCM, standard deviation fluctuated strongly between the top and bottom sides of the part, while for CIP both were almost similar.

5.4 Conclusions for Matrix Flow in Compression Molding

The conclusions of the matrix flow studies are presented in regard to the initially phrased research questions in the following. The section is concluded with a summary of findings and the limitations that have to be noted in connection with the presented findings.

5.4.1 Matrix Flow in Pressing of Plates

Within the range in which process parameters were varied, the results lend evidence for the hypothetical basic matrix flows of the two processes, as introduced in Figure 3-1 for WCM and in Figure 4-2 for CIP. Thereafter, WCM is subject to matrix dislocation between the fiber material and the closing tool wall. This behavior is suggested by the scattered flow front on the top side of the part, as well as the low amount of fluorescent matrix found on the bottom side shown in fluorescent photography, Figure 5-18. This low share of flow in z-direction of the stack is further seen from fluorescent micrographs, Figure 5-19. Parts which showed a high degree of surface flow also showed compact fluorescent matrix distribution in micrographs and vice versa. In contrast, CIP parts showed a higher compactness of matrix distribution and consistent relation between bottom and top sides of the parts in fluorescent photography. Compact flow in fluorescent photography was also characterized as compact in fluorescent micrographs, Figure 5-24 and 5-25, respectively. In addition, centroid shifts were not as large and direction and magnitude of shifts were not as unpredictable over repeated experiments for CIP compared to WCM.

The different flow patterns changed only slightly with variation of parameters. In WCM, the resin temperature T_r showed the biggest effect on matrix distribution (FigureA-5 to A-7). The most scattered distributions were obtained with high temperatures. Likewise, fibers were also more distorted and cavity pressures rose. These behaviors are most likely due to the matrix viscosity in relation to the elapsed time in the process after matrix application. Early in the process, matrix of higher temperature is of low viscosity and results in higher surface flow during transport of prepared materials into the press tool. This happens because the applied matrix accumulates and forms a film atop the fiber stack, due to lower permeability in z-direction as in direction of the fiber longitudinal axis. This low viscous film is then subject to inertia during transport. Later in the process, higher matrix temperatures lead to a higher degree of cure than lower matrix temperatures. Thus, during

pressing the film is more viscous when resin temperature T_r is higher in application. When the viscous film is compressed into the fiber stack, resistance against flow is greater, which leads to higher fiber distortion as well as to higher cavity pressures. It is assumed that the same explanation is true for the press velocity v_p. Thus, with faster closing speed, the viscosity increase has not progressed as far as when the press closes slower. In case of CIP, the dominant flow in through-thickness direction of the fiber stack is not altered with different process parameters because top and bottom side responses for Q_1 and Q_2 are consistent and significant. However, centroid shift Q_{3b} is influenced by tool temperature T_t and heating time t_h. The quality of cavity elimination Q_{ce} is strongly dependent on the tool temperature. Both can be explained by the mechanism of carrier cavity elimination under heat.

When T_t and t_h is low, centroid shift is low and cavities are not eliminated from the carrier but form wrinkles on the bottom side, and vice versa. The cavities retain their initial shape to a large extend with lower temperatures. Stored matrix is then only ejected from the cavities, when the stacked materials are compressed. Therefore, matrix flow is directed strongly into the z-direction by the cavities that are intact prior to compaction. When the carrier is exposed to higher temperatures, cavities are eliminated due to relaxation of polymers that were stretched during thermoforming. This behavior is also known as creeping of thermoplastic polymers, where elongation of a polymer increases under heat and stress [94, p. 52-53]. Thus, the amount of matrix released from the cavities but also the quality of the carrier film after pressing can be controlled by the successive relapse of the carrier into its initial flat state, Figure 5-34.
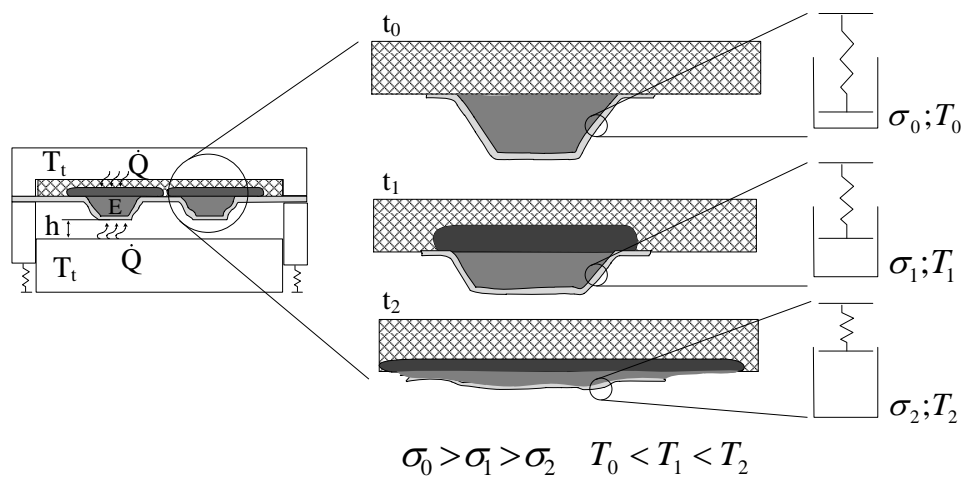
Figure 5-34 Relapse of carrier cavities due to heat influence with stages referenced to the Maxwell-model of visco-elasticity [94, p. 50]

The relapse behavior of the film cavities depends on the temperature history of the film during processing. Film temperature is mainly influenced by heat flows $\dot{Q}$ due to contact or radiation of heated tool surfaces as well as heat from exothermic

reaction of the contained matrix. The temperature of the film and the time t it is exposed to the heat sources determine how far cavity relapse has progressed before the tool is closed. When the time is too short and the cavities are still in their initial shape ($t = t_0$), they will provide a compact matrix flow but likely form wrinkles. Wrinkles cannot be eliminated after compression despite high temperatures, since the overlapping layers of the film cause pressure pikes from compression that prevent relapsing of the layers. On the other hand, when the cavities relapse to a large extend during time $t = t_2$ and eject most of the contained matrix, the flow of matrix is scattered but almost no residue from cavities remains in the film, which then forms a good surface quality of the part. This was the case in experiment 4. However, shortening of the heating time at the same, high temperatures of $100\,°\mathrm{C}$ resulted in the same film quality but much more compact flow, experiment 8 , Figure 5-24.

5.4.2 Matrix Flow and Part Quality

Results concerning the impregnation quality of the part are ambiguous. On the one hand, parts produced with both processes, WCM and CIP, showed a lower void content and lower fluctuation of voids within the laminate when the matrix flows of the parts were more compact. On average, CIP produced more compact flows and the respective parts exhibited also lower void contents than WCM parts. However, three point bending tests resulted in no differences of maximum bending stress σ_{fM} between parts, which showed least and most compact flows in both processes (Scene B in Figure 5-30). Furthermore, DoE analysis showed no significant effects on both responses, void contents and bending stresses.

However, a strong influence of the vacuum level on bending strength was detected. Thus, in comparison to traditional WCM processes where evacuation of the mold is not practiced application of films in compression molding for easy sealing may provide an advantage in regard to robust processing for better impregnation.

5.4.3 Matrix Flow under Draping

Compactness of flow considerably deteriorates when draping complexity increases due to the influence of gravity. Both processes, WCM and CIP, are currently not capable of independently draping and impregnating the part because the impregnation flow is always governed by gravitional forces that act according to the direction of drape. Partially, flow may become more compact in contrast to unfavorable process parameters in WCM because matrix is less scattered when it accumulates due to containment of the mold walls. On average however, flow becomes less compact

and also less repeatable. While for both processes robust process parameters can be found to allow for repeatable flows in plates, robustness considering the fluorescent matrix distrubution worsens with higher part complexity.

5.4.4 Conclusive Summary and Limitations in Regard to Research Questions

Matrix flow through fiber material differs in both investigated processes, WCM and CIP, in regard to matrix pre-application. Because matrix is applied on top of the fiber stack in WCM, it forms a film which is not sinking into the fiber material, also at higher temperatures and longer holding times varied in the process. This film is dislocated when the materials are transferred into the press and when the mold closes. Both causes lateral flow in agreement with the hypothetical flow situation from Figure 4-2. Only when the tool walls constrict this lateral flow, matrix is pressed into through-thickness direction of the stack as initially intended in compression molding processes. In CIP, the cavities in which the applied matrix is stored can restrict any lateral flow prior to insertion into the press. When the materials are located inside the press, matrix containment can be precisely controlled by heat flux into the film. The higher the temperature and the longer the film is exposed to the heat, the more cavities relapse and eject matrix prior to pressing. This determines how matrix flows inside the subsequent compression, but generally through-thickness flow dominates the impregnation in that process as hypothesized in Figure 3-1.

The investigations of matrix flow in compression molding were limited by the methods of fluorescence photography and microscopy as well as by the processes under investigation. While the methods were found to be sound in evaluations prior to the study presented and produced meaningful results, they do not yet provide detailed quantitative data for analysis of the processes. Fluorescent photography offered insight into part-scale flow, but is limited in terms of dilution of fluorescent matrix with neat matrix. This effect would offer more information on how the marked flow is distributed in connection with flow containment from adjacent matrix masses. Fluorescent microscopy basically supported findings from photography but computational power and the programmed script did not allow to compute micrographs with higher resolutions in the given time frame. A higher resolution gives more accurate results of fluorescent matrix distribution because the fluorescence inside the rovings can be detected, which was not the case in the micrographs used.

The processes WCM and CIP were experimentally investigated on a production system, which included manual material preparation. While the preparation was

controlled in terms of fabric and fluorescent matrix application, the neat matrix could not be monitored. In both processes, this produced a basic fluctuation of the position of matrix prior to processing, which was subject to the investigation. While the results fluctuate low enough to validly investigate the research questions, this leaves room for improvement that could be achieved with robot-led matrix application.

From the investigations it is still unclear weather or not impregnation quality is linked to matrix flow in compression molded parts. From the results of void measurements the author of this thesis assumes it is linked, for similar reasons as in RTM processing. However, it is possible that the evacuation and the small size of the mold influenced impregnation quality to a much larger degree than the matrix flow. Measurements of voids by image segmentation of micrographs can show an inaccuracy of 1% [107]. Results furthermore depend on specimen preparation and the subjective distinction between composites and voids as well as the selection of locations in the laminate from which the micrographs are used. Furthermore, three point bending does not precisely focus on void defects in the laminate but matrix as well as fiber properties. The better suited inter-laminar shear strength test could not be used, since many specimen tested prior to the study did not fail in the valid failure mode. It is likely that this can be solved with a different fiber layup, such as a unidirectional layup.

Draping overrides the basic flow situations identified for the processes in the plate study. Gravity draws the applied matrix away from their pre-application location, which results in a high degree of lateral flow rather than through-thickness flow. Results for both processes strongly resemble each other and showed a less robust process in terms of compactness. Compactness and robustness decrease with increasing draping complexity. However, these investigations are limited because only one parameter combination suitable to produce parts in both processes was used. Furthermore, the factor part complexity was only represented by the steepness of the part walls that were $40°$ and $32°$. Lower steepnesses and other part features that contribute to complexity, such as radii and edges, should be investigated to gain more detailed information on flow behavior under different geometric complexities. Also, fiber shearing should be studied in closer detail, because it can be linked to matrix flow and void content, as one study for RTM suggests [108].

Regarding all research questions investigated, it is important to note that these results are limited to the materials, fiber layup and part geometries used in the study. Furthermore, the tooling that was used was specifically designed for that study and might not be representative for other compression molding processes. The process referred to as WCM is a variation of the industrially used process, since the tool design required the use of a film. However, it is assumed that in case

of the WCM process, the film underneath the fiber stack did not alter matrix flow so that the conclusions can be transferred to other processes used under the name of WCM. The conclusions drawn are also limited in terms of the process parameters that were controlled and varied in their ranges. There may be other parameters or different parameter combinations that lead to other conclusions.

6 Carrier-Integration on Industrial Production System

Despite having demonstrated that carrier-integration does support several process functions of compression molding of small composite structures, it is yet unclear if carrier use works for industrial-sized parts, too. In order to investigate this issue, a demonstrator production line is set-up to produce the automotive seating back rest further specified in Chapter 7.3.

The principle of the industrial production system is based on the proven prototype design, especially for the press tool, which has been developed and refined during the earlier studies. The tool itself is a replication regarding function and building structure of the one detailed in Figure 4-5 and 4-6. The tool insert represents the seating back rest from Chapter 7.3 and the entire structure is made from steel. Apart from the tool, which is installed on a 250 t hydraulic press, the production system consists of a data panel for process control, a handling cart with an electromagnetic handling frame and a three component resin dosing machine with a compact mixing head, Figure 6-1.
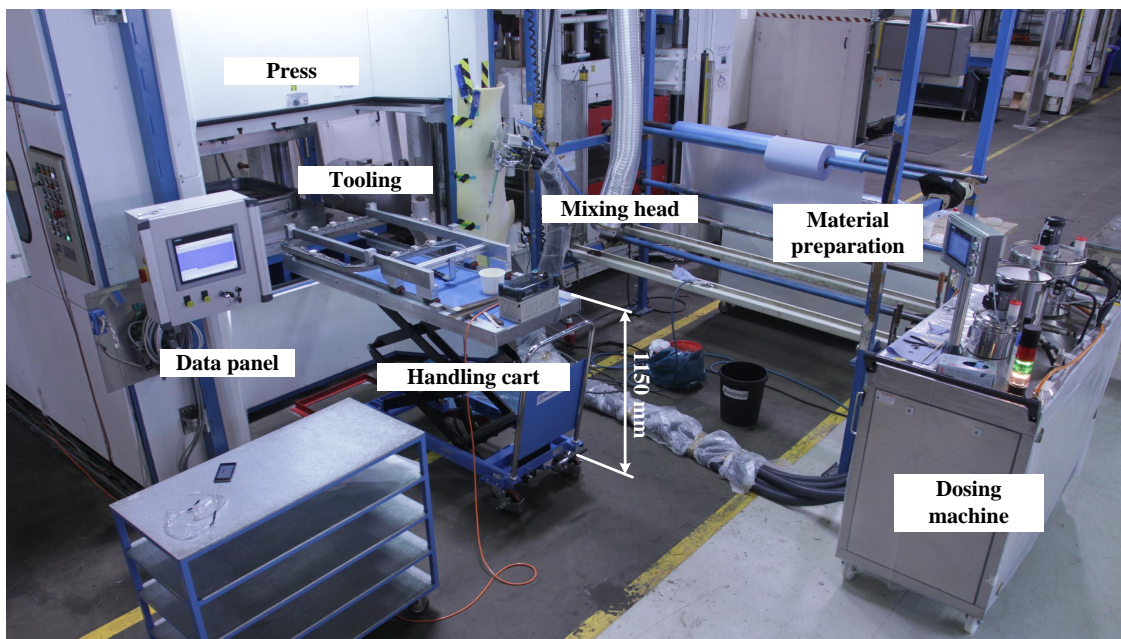
Figure 6-1 Overview of industrial production system designed after the prototype system

The carrier layout for the industrial process is based on the conic section design introduced in Table 4-7. The foundation of the complete carrier design is the total amount of resin, which needs to be stored inside the cavities. A theoretical calculation can be found in Table A-5. The conical section used in the prototype carriers is scaled larger in order to store approximately 5.9 g per cavity. The cavities are

now distributed in a rectangular pattern in order to allow better tension properties via bridges between cavities for less carrier slack. A total amount of 208 cavities are determined for that pattern, which hold approximately 748 g of resin, a surplus of 140 g in additional to the minimum amount under consideration of a film spring back rate of 0.5 after thermoforming, Table A-6.

Materials need to be handled semi-automatically with the handling cart, since the carrier clamping ring is too heavy for reliable manual transport into the tooling. Prior to resin and fiber material application onto the clamped carrier, the carrier film has to be prepared manually in several steps Figure 6-2, which resemble the same procedure as in the prototyping phase.
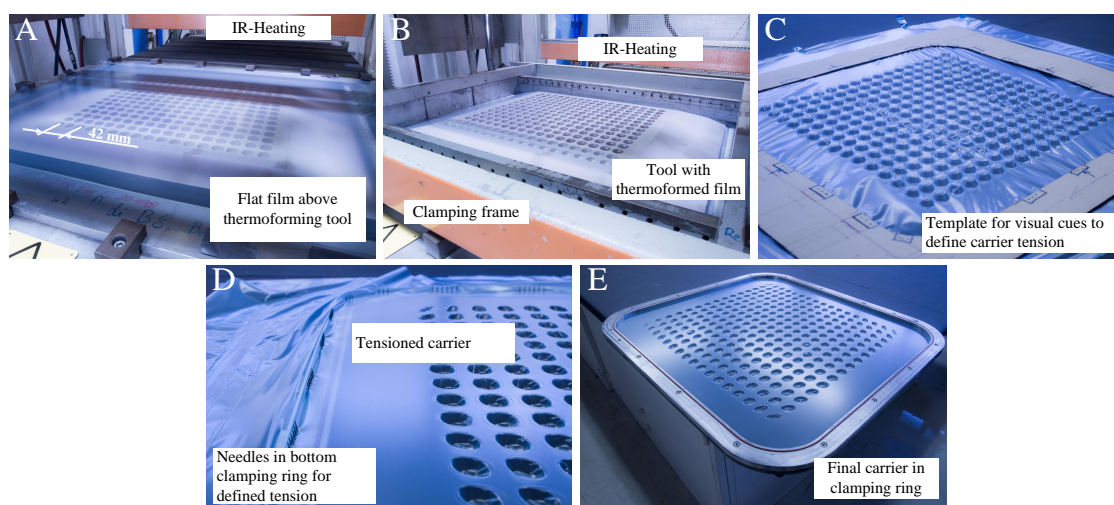
Figure 6-2 Carrier preparation for use in industrial-sized production system

The flat polymer film is manually cut and positioned above the thermoforming tool in a pre-tensioned state prior to forming. The program is set to heat the infrared heaters (IR-heaters) to 113 °C with forming immediatly after the heaters reach the temperature. Forming is initiated with the thermoforming tool driving into the heated film from below with simultaneous activation of vacuum below the film (Figure 6-2, B). After demolding, visual cues for defined carrier tension are applied with a marker pen and a template. After several trials, an elongation of 8 % was found to be optimal, in order to mitigate excessive carrier slack under material weight and to avoid elimination of cavities due to circumferential tension. The carrier is manually fastened to the bottom clamping ring using needles (Figure 6-2, D), before the top clamping ring is fitted and attached with several screws (Figure 6-2, E). The steel clamping ring with the prepared carrier can now be attached to the handling frame on the handling cart for further material preparation and transport, Figure 6-3.
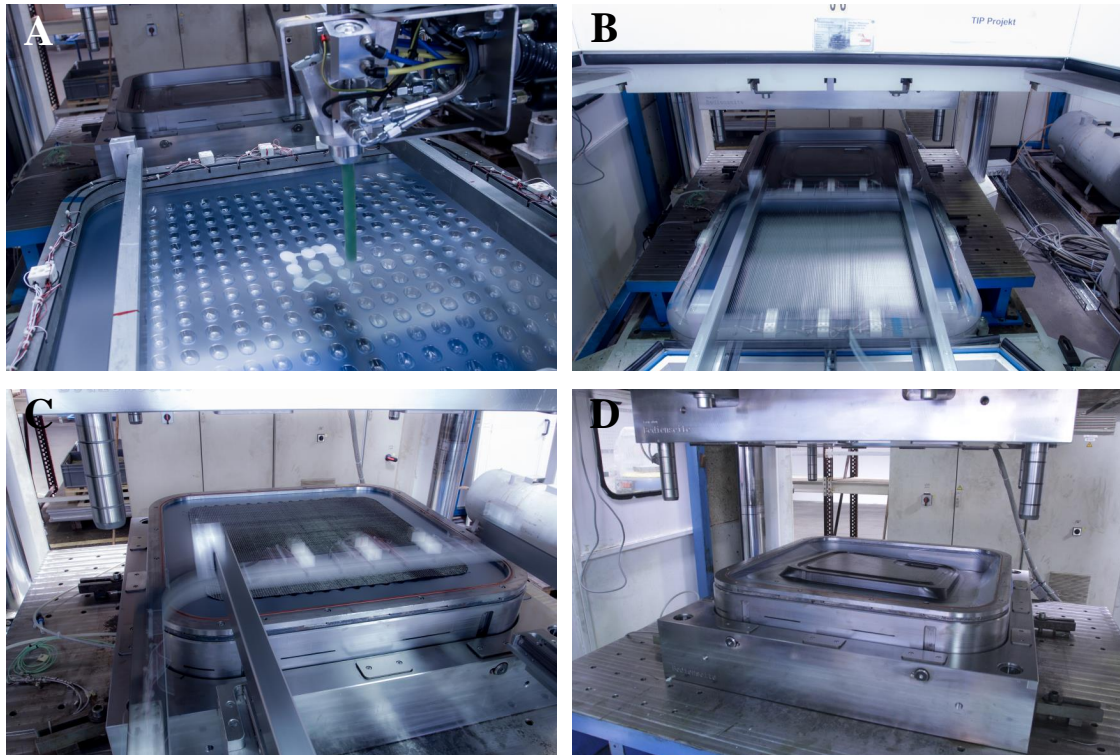
Figure 6-3 Process flow of CIP on industrial production system (A: Dosing of reactive resin into carrier cavities; B: Material transport into press tool using the electromagnetic handling frame on the handling cart; C: Positioning of materials inside press and extraction of the handling frame; D: Cured part after pressing)

The clamping ring with the tensioned carrier is temporarily held by electromagnets inside the clamping frame for manual material application. The mixing head is guided manually over the carrier cavities, circling outwardly starting at the center cavity (Figure 6-3, A). The amount of dosed resin was varied between 600 and 900 g with best results at 680 g. After application of the pre-cut and stacked NCF material (stacking pattern conforms with the ply sequence in Section 5.2.1) the clamping frame with the attached material is translationally slid into the tool (Figure 6-3, B) and lowered until the clamping ring safely sits on the tool blank holder. The electromagnets are shut off and the clamping frame can be slid back out of the tool (Figure 6-3, C) to allow the press cycle to start.

Process specifications were found to meet the optimal specifications from experiment 3 in the CIP DoE, Figure 5-15, with tool temperature T_t set to 100 °C and a holding time t_h of 5 s with films of 0.01 mm thickness. For thicker films (0.05 mm), temperatures of 120 °C and holding times of $10 - 13$ s showed the best results considering cavity elimination (Figure 6-4, A). However, these thicker films were customized by Infiana for the project and could only be provided in smaller width. Thus, they had to be welded together prior to thermoforming and the weld seam was prone to ruptures during processing under high thermal and tensional loads.

They showed superior draping capabilities in corners because of less carrier slack resulting from their higher thickness. Apart from variations in carrier films, several material combinations have been processed, Figure 6-4.
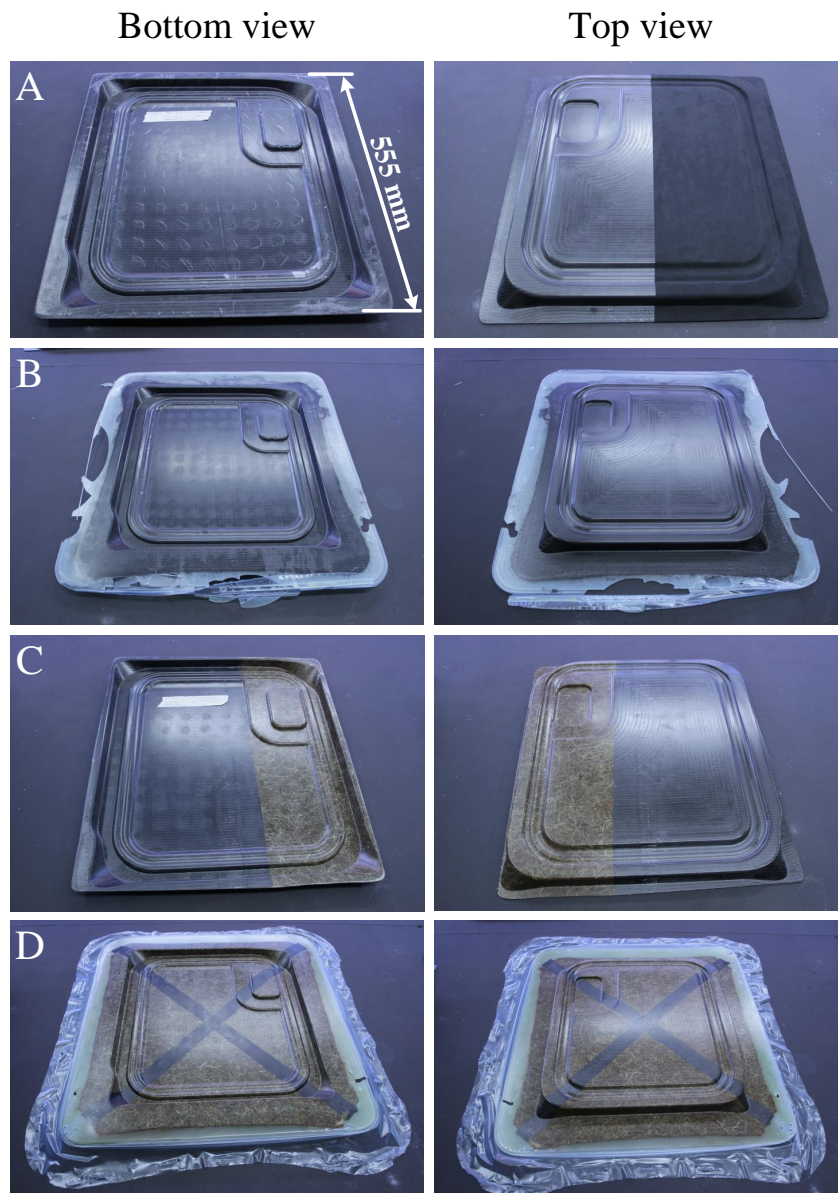
Figure 6-4 Selection of produced demonstrator parts (A: Monolithic CFRP with 0.1 mm film and partial top finish in nappa leather; B: Monolithic CFRP with 0.05 mm film; C: Partial monolithic CFRP, partial monolithic natural fiber (flax/sisal) with 0.05 mm film; D: Monolithic natural fiber (flax/sisal) with unidirectional carbon fiber reinforcements and 0.05 mm film)

The parts produced with the industrial production system showed consistently good results regarding material compaction, dry spots and impregnation defects as well as regarding cavity elimination. The carrier-integration provided the entire set of functions that were initially designed for process improvement on an industrial scale - drape fiber material, generate vacuum thightness over press stroke as well as store

and eject matrix for better process control (Figure 4-4). Thus, it can be concluded that carrier-integration works as intended on an industrial scale and may provide process improvements in respective industrial production scenarios. The designed and validated production system serves as a basis for a further investigation of the process within the scope of a comparative life cycle assessment and costing study in the next chapter.

7 Comparative Life Cycle Assessment and Costing[1]

Carrier-integrated pressing has been conceived as an LCM process applicable to serial part production similar to WCM and RTM. Since for CIP an additional carrier is introduced into production, it is not clear how this effects the material flow.

As presented in Figure 4-17, the carrier allows material draping in complex shapes without additional fiber material used for draping. However, the final parts produced by CIP are framed by a region of neat matrix, Figure 4-4. This region is generated because the fiber material is radially drawn into the mold during draping and the void in the part cavity is filled with matrix.

Due to the new circumstances under which parts can be produced with CIP, the following question should be investigated:

3. How does a composite production based on CIP impact the environment and costs per part compared to RTM and WCM?

Cost-wise, this question is particularly relevant in industrial-scale manufacturing, since development of the composite technology has lately been primarily driven by cost reductions through mass manufacturing. Process improvements are estimated to yield cost advantages between $45\,\%$ and $67\,\%$ per kg processed. This improvement is mainly due to a reduction in cycle time and changes in raw material, as one study argues [33, p. 9]. However, the extent to which shorter cycle times may still reduce costs seems limited in comparison to the cost share of about $50\text{-}75\,\%$ for carbon fiber materials alone [34, p. 14] [109, p. 269]. Because cycle time reduction is generally associated with cure kinetics of the applied polymer matrix [24, p. 4] [110, p. 1699], faster curing might not be possible because the resin still needs to impregnate fibers before cross linking. Current cycle times for RTM are $5\text{-}15\,\mathrm{min}$ [34, p. 39], fully-automated WCM reaches $3\,\mathrm{min}$[2]. On the other hand, even if fiber costs decrease by $15\text{-}25\,\%$ [34, p. 16] [33, p. 9], process adaptions can improve material efficiency. For example, through reduced scrap [111, p. 369] or better material exploitation drawing on the fiber's anisotropy [112].

Beyond costs, environmental impacts of the CFRP productions should be monitored, especially for serial production, due to harm from oil-based raw materials but also big advantages from light-weighting in the use phase.

---

[1]This chapter is based on the bachelor thesis "Setting up and Balancing of Competitive Production Lines for Carbon Fiber Composites Manufacturing" written by Marek Listl, TU Munich, 2015, supervised by Paul Bockelmann

[2]The author visited a fully automated WCM plant running on a cycle time of $3\,\mathrm{min}$ in 2015.

Carbon fiber is energy intensive due to slow graphitization of the predominantly used polyacrylonitrile (PAN) precursor [113, p. 2913] [109, p. 270]. While lighter alternatives to steel are generally found to reduce energy consumption and greenhouse gases during use, most often in the transport sector, emissions are in many cases increased due to energy consumption in production [114, p. 6089]. Das estimated that primary energy in compression molding of short, random fiber CFRP is 14 times higher than stamping a steel part [109, p. 278]. Song et. al, however, reported that pultruded composite parts saved energy against a steel baseline, also through comparative savings in manufacturing [115, p. 1264]. Production via RTM was considered more energy intensive as data from Suzuki and Takahashi suggested [116, p. 16]. Despite obvious differences of certain manufacturing processes, information on process design was too scarce to reliably discuss the reasons.

Besides details on process design, the methodology of data acquisition is critical for comprehensibility of such studies [110, p. 1705] [114, p. 6095]. To identify process differences, some studies further detail process steps due to poor data availability from databases, [117, p. 11] [110, p. 1704]. However, none has closely described series production using RTM or WCM.

7.1 Goal and Scope of Study and Assessment Outline

While most studies presented above investigated production and use of carbon fiber materials within a targeted application, this thesis aims to examine the differences in process design, process parameters and production technologies of RTM, WCM and CIP. Thus, its focus lies on the detailed and consistent process modeling and its comparative assessment without lending evidence to the general advantageous or disadvantageous nature of CFRP, neither cost- nor environmental-wise. Thus, all results for LCA and LCC are normalized on values for RTM, which are defined as 100 % within the given impact category or costs.

This study draws on the ISO 14040 framework [118] to perform a comparative process LCA in combination with LCC, with exclusion of the critical review. The combination of LCA and LCC is in line with demands for a broadening scope for sustainability studies [119, p. 93]. As no standard procedure for LCC exists, this thesis follows the LCA framework and data acquisition on considerations from process-flow simultion (PFS) and technical cost modelling (TCM), proposed by Wakeman and Månson [120, p. 366], in steady state.

The ISO 14040 framework does not specify the use of specific impact categories but states that an LCA considers three areas of protection - natural environment, human health and resources [118, p. 15]. This thesis focuses on the midpoint impact categories after Hauschild [121, p. 9] (e.g. global warming, acidifaction, eutrophication) which can be attributed to the three areas of protection. Thus, all categories provided by CML2001-April 2013 methodology are computed and the ones with particular results regarding the scope of this study are further discussed.

Data acquisition for the life cycle inventory (LCI) is generally critical for the validity of an LCA. This is particularly the case in the field of CFRP materials because no database for processes and respective machinery exists yet [117, p. 11] [110, p. 1704]. Hohmann et. al began studying industrial process characteristics [122] but work on a respective database explicitly for the use in LCA and LCC studies is ongoing.

The elementary flows considered in the study are attributed to one specific functional unit, an automotive back rest. Thus, the results obtained can only be considered as valid in regard to this part and thus, the ability to generalize the findings to other parts is limited.

7.1.1 Geographical Requirements of the Study

The study presented is grounded geographically in Germany, since automotive is primarily suited for the considered processes and the large growth of this market is attributed to ramp-up of i-model cars from BMW [123]. Consequently, the biggest machine and material suppliers are located in the region and LCI data is modeled based on their product data acquired from available sources, telephone or email correspondence. All calculations are based on facility operation in Bavaria, Germany. For energy generation, it is assumed that the German electricity mix of 2013[3] is used. Boundaries for modeling include all processing steps directly associated with CIP, WCM and RTM as well as fiber and resin production. Composite waste is not balanced, because it is unclear how it will be treated. Since incineration of CFRP is currently not practiced[4], land filling of composites is illegal in Germany [124,

---

[3]Data published by AG Energiebilanzen under the name "Bruttostromerzeugung in Deutschland ab 1990 nach Energietraegern" obtained from www.ag-energiebilanzen.de; Last accessed on 04-03-2016

[4]Newspaper article "BMW sucht neue Recyclingwege" obtained from www.mittelbayerische.de; Last accessed on 04-03-2016

p. 252] and EU legislation requires recycling[5], the biggest operator of production facilities temporarily stores waste[6].

7.2 Manufacturing Models and Specifications

Since no consistent and detailed models for RTM, WCM or CIP exist, flow-orientated function modeling [51, p. 169] [30, p. 120] is applied to define process-independent functions necessary to produce respective LCM parts. The functional structure is then specified based on the actual process to map flows of material and energy according to the overall process schemes for RTM and WCM in Figure 2-4 and CIP in Figure 4-18.

The physical process models are abstracted via designation of elementary functions that control all material and energy flows of the respective processes CIP, WCM and RTM. Use of elementary functions allows detailed break down of all processes into consistent and comparable functions, to which all necessary data are gathered for the life cycle inventory. Table 7-1 lists all necessary functions and details which functions apply to which process variation. The functions are set into a defined sequence, which is then complemented with all material and energy flows between the functions to complete the functional model. Three different models for RTM, WCM and CIP are provided in Appendix A.4, Figures A-17 to A-19. These functional models are the basis for the LCI data allocation and computation. All data are associated with one or several functions from Table 7-1.

---

[5]After Directive 2000/53/EC of the european parliament and of the council of 18 September 2000 on end-of life vehicles
[6]Interview of author with an engineer from that industrial firm on 08-17-2016

Table 7-1 Elementary functions that represent RTM, WCM and CIP as a basis for inventory analysis of the processes

Function	Function name	Sub function name	Applied in process variation		
			RTM	WCM	CIP
F1	Cut plies		x	x	x
F2	Position stack		x	x	x
F3	Heat resin and mix matrix		x	x	x
F4	Apply matrix		x	x	x
F5	Cut carrier				x
F6	Position carrier				x
F7	Prepare press and mold		x	x	x
F8	Preform stack		x		
F8.1		Heat stack	x		
F8.2		Transfer stack	x		
F8.3		Close preforming mold	x		
F8.4		Open preforming mold	x		
F9	Place material* in mold		*preform	*stack+matrix	*press blank[1]
F10	Consolidate material		x	x	x
F10.1		Close mold	x	x	x
F10.2		Evacuate mold	x		x
F10.3		Close mold		x	x
F10.4		Hold mold closed	x	x	x
F10.5		Open mold	x	x	x
F11	Release part from mold		x	x	x
F12	Place part in *		*temper oven	*cooling mold	*cooling mold
F13	Set/Temper part*		*Temper	*Set	*Set
F14	Remove part from cooling mold			x	x
F15	Trim part		x	x	x
F16	Place part in stock		x	x	x

[1]Press blank is considered the aggregate of carrier, applied resin and stack

7.3 Functional Unit, Materials and Process Parameters

An automotive seating back rest is used as the functional unit for analysis. Starting from the geometry of the back rest, Figure 7-1, the dimensions of the stack cut-out to allow for part draping, the number of plies and fiber architecture are determined. The design was verified in prototypes produced manually using vacuum assisted resin infusion (VARI).

The minimum, process-independent stack dimensions and slide length of the fabric during draping are determined from kinematic draping simulation using the CAD model and practical trials during prototyping. Stack dimensions are found to be 610x570 mm for the part itself with a sliding length of 60 mm in total for draping.
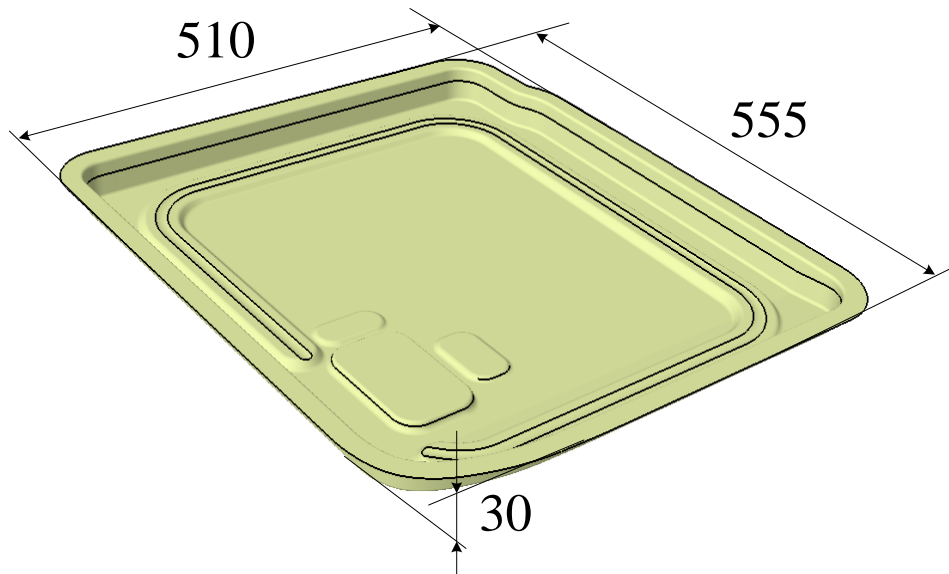
Figure 7-1 CAD model of functional unit from which tool layout in Figure 7-2 and material input data are determined

Based on the different process designs of CIP, WCM and RTM which need additional material to account for clamping and sealing, total material input data for the LCI can be determined, Figure 7-2.

For each process a circumferential seam of 10 mm is added to the stack dimensions to account for trimming after part production. In regard to CIP, no other functional surfaces are needed, since clamping and matrix sealing are provided by the carrier (Solutions 24.1 and 24.2 in Figure 4-3). For WCM and RTM it is assumed that tension during draping must be maintained with clamps that travel toward the tool cavity during the press stroke. Thus, the stack has to be designed larger to allow for the sliding length of 60 mm with respective estimations of tool dimension according to Scenes B and C in Figure 7-2. For RTM draping and trimming of the stack is performed during draping prior to injection. Scene C shows the estimated dimensions of the stack for draping and the injection tool. The WCM tool is slightly larger than for RTM to account for edge effects due to over compaction for sealing in WCM.

The part is to be produced with a nominal thickness of 2 mm and six plies with the sequence [0° /90°, +/- 45°, +/-45°]$_s$. In case of CIP, a film of 0.05 mm thickness is used as a carrier. Thus, a theoretical FVC of 0.52 for CIP and 0.51 for WCM and RTM is assumed. With the material specifications and the tool design all other material data of the functional unit are derived in Table 7-2.

Differences of the final parts produced by CIP, WCM and RTM are only marginal, concerning fiber volume content and the carrier attached to the part in case of CIP.
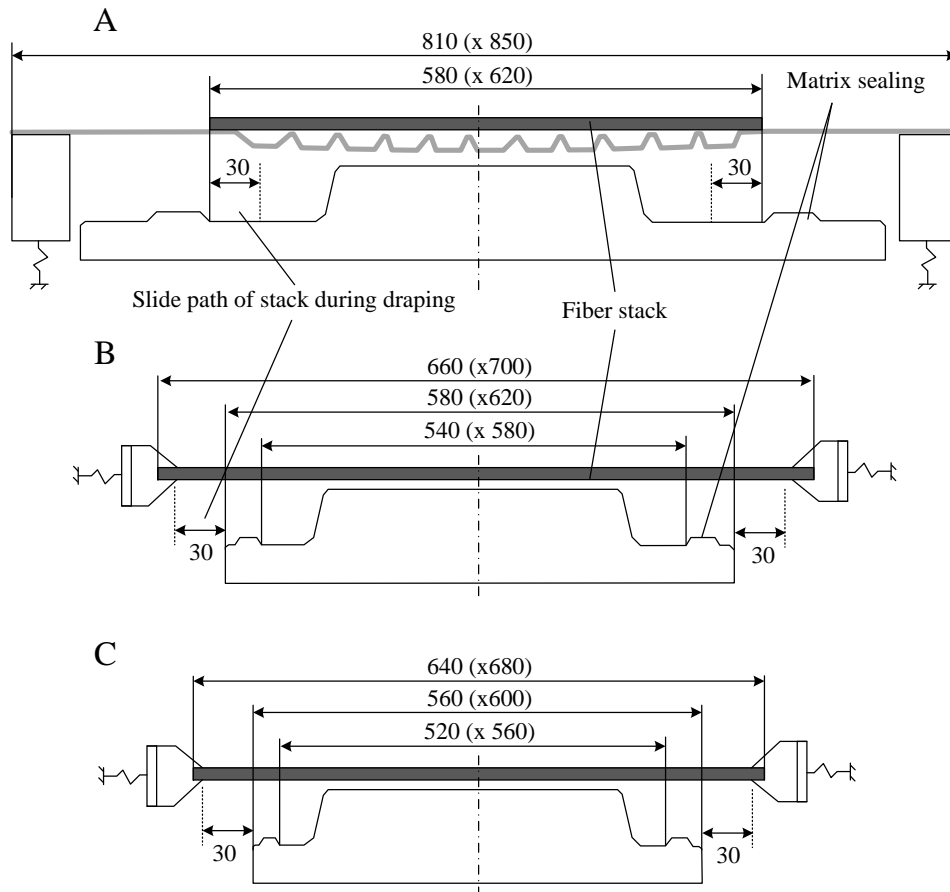
Figure 7-2 Considerations of tool design that impacts material input for CIP (A), WCM (B)
and RTM (C)

Thus no altered functionality of the part has to be considered for the LCA and
LCC.

The curing cycles for the matrix system during the primary production processes
are the limiting factor for cycle times. Concerned functions are F10, F12, F7 and F9
for all process variants. F9 and F10 are directly associated with curing. Therefore,
respective process parameters of these functions for WCM and CIP are determined
from experimental trials on the prototyping tool (Chapter 4) and a kinetic model
of the XB3585/XB3458 matrix system. Based on material handling times, press
speeds and process temperatures, Table A-7, full curing cycles for CIP and WCM
are iteratively conceived using a kinetic model from Keller and colleagues [125, p.
5].

With the given process parameters the pressings are found to yield cavity pressures
of 14.57 ± 0.72 bar and 10.33 ± 1.25 bar for WCM and CIP, respectively. To account
for an industrial environment, it is assumed that both compression molding pro-
cesses reach a maximum of 50 bar [24, p. 4]. Process parameters for RTM have
been assumed based on unpublished trials with the same matrix system but an-

Table 7-2 Material data of functional unit used as a basis for life cycle assessment and costing

Reference	Property	Value
Fiber material Hacotech C300 BX	Basis weight [g/m²]	306
	Fibers [-]	Tenax STS
	Fibers/roving [-]	24 K
	Sew [-]	PES 76 dtex hf
	Ply design [-]	biaxial
Matrix material XB3585/XB3458/Würtz PAT	Parts by weight [-]	100:19:03
	Pot life at 23 °C [min]	14-18
Carrier material Stretch-Vac 250[1]	Melt point [° C]	150
	Thickness [mm]	0.005
	Initial dimensions [mm]	850 x 810
Initial material input	Number of plies [-]	6
	Ply orientation [°]	[0/90°;+/-45°;+/-45°]s
	Ply dimensions [mm]	620x580[2] / 700x660[3] / 680x640[4]
	Stack mass [kg]	0.716[2] / 0.910[3] / 0.859[4]
	Total matrix mass [kg]	0.599[2] / 0.512[3] / 0.425[4]
Final part	Part dimensions [mm]	510 x 555 x 2
	Fiber volume content [-]	0.52[2]; 0.51[3,4]
	Weight [kg]	0.934
	Glass transition temperature [° C]	> 80

[1]Only used for CIP parts; [2]CIP; [3]WCM; [4]RTM

other NCF. Lower injection pressures of 25 bar were applied instead of up to 150 bar for current industrial press technology [24, p. 4]. The curing cycle for RTM is also defined drawing on the model of Keller et. al. [125, p. 5], adapted for temperatures and curing times from the injection experiments.

As all experiments are conducted on prototyping tools and laboratory scale presses, relevant process parameters and process times are adapted to valid parameters of respective industrial production equipment. Functions that are relevant for curing and estimation of the cycle times are given in Appendix A.4, Table A-8. Associated with these function times and the process parameters from Table A-7 is the complete definition of curing cycle for each process, Figure 7-3.

It is assumed that finished parts reach a degree of cure of 0.95, which corresponds to a glass transition temperature of approximately 106 °C after models of DiBenedetto [127] and Keller [125]. Heating of matrix within the press pior to compression is specified to 0.0368 °C and 0.0766 °C for CIP and WCM, respectively, after measurements on the prototype tool. It is assumed that the matrix takes on tooling temperature when the tool is completely closed.
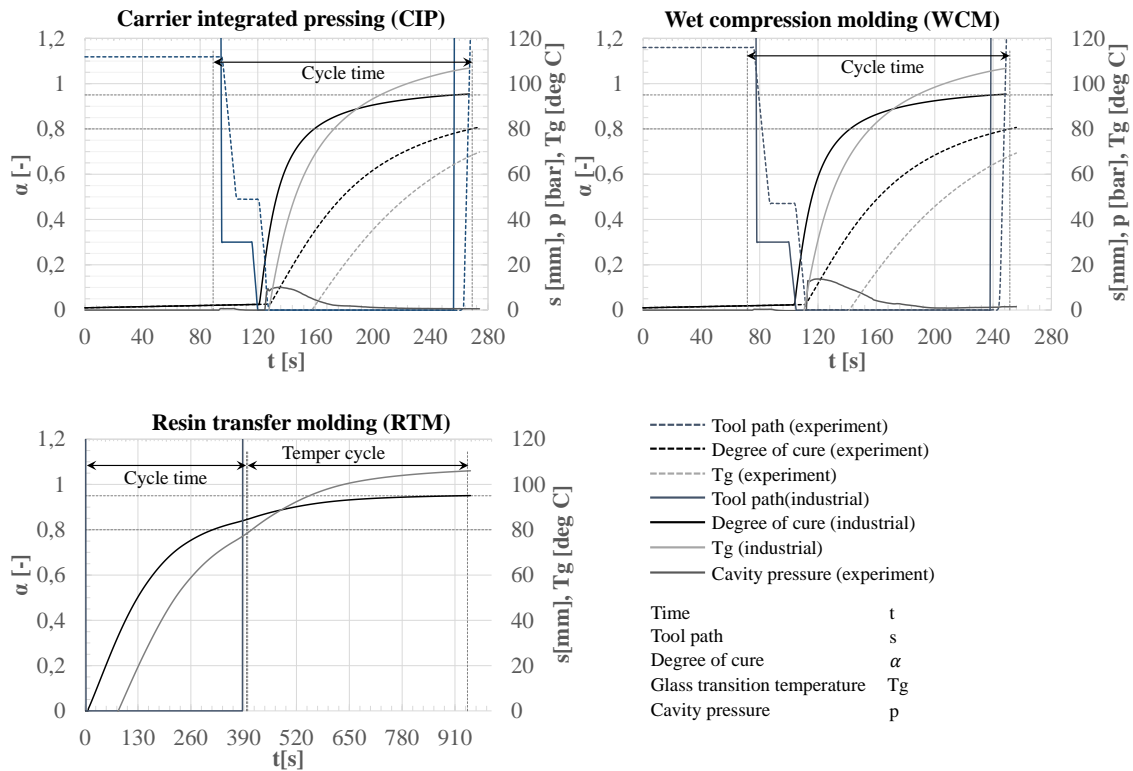
Figure 7-3 Cure cycles for CIP, WCM and RTM based on experimental results and assumptions for industrial production for pressing speeds [126] [24]. LCA and LCC are based on cycle time definition from assumptions of industrial processes

To define the RTM temper cycle, heating and cooling trials are performed with a finished prototype of the functional unit. After demolding the part cools with $0.225\,°C/s$ at an environmental temperature of $26\,°C$ during material transport to the temper oven. Heating in the temper oven set to $107\,°C$ is fitted with a 6th degree polynomial curve from measured data and used as an input for the curing model.

The curing cycles defined in Figure 7-3 in connection with the function times from Table A-8 determine the cycle times of WCM and CIP to $180\,s$ and to $397\,s$ for RTM.

Press preforming, defined in functions F8.1-8.3 in Figure A-17, is modeled after a roof production [128]. To stabilize the preform, binder material is activated with an induction oven modeled after data from Hopmann [129].

7.4 Inventory Data

Oxidization and carbonization of PAN fibers to produce carbon fibers was modeled after literature data [109, 130–132]. For all production equipment nominal power

is used for calculation, since no specific literature or data is available. Presses were modeled after an exemplary press of 500 t for RTM and scaled for CIP and WCM according to the required tonnage of 175 t. A heating power of 11.5 kVA for the press tools was assumed according to personal interviews with experts. The preforming process was modeled after data from [128] and [129]. Energy for milling of the pressed laminates was calculated from process specifications provided by Teti and Uhlmann [133, 134]. Life cycle inventory for LCA with respective references for calculations are provided in Table A-10.

LCC inventory data are attributed to machines, materials, energy and manual labor needed for part manufacturing. For cost balancing an estimated machine life of five years, 7 % rate of interest and electricity costs of 0.3 € /kWh are assumed. Production quantity is calculated to 59 892 ppa for WCM and CIP and 27 155 ppa for RTM via cycle time (Table A-8) and labor-related values (Table A-9). This yields 1582.5 h/a productive work per worker and labor costs. To assume prices and energy consumption of robots, model IRB 1600-10/1.45 is referenced and consumes 0.615 kW, has a payload of 10 kg and reach of 1.45 m according to information provided by ABB Robotics. Costs of 40 000 € per robot is assumed according to an equivalent robot RV-12SQL-S315 from Mitsubishi. Despite automation it is considered that one worker allocates 50 % of his productive time to supervise one production line of RTM, WCM and CIP.

Matrix consisting of resin, hardener and release agent is assumed to cost 5 € /kg. Fiber material and carrier cost 14.71 € /kg and 1.19 € /kg, respectively.

All inventory data, including assumptions for cost calculation for the LCC, are summarized in Table A-11.

7.5 Results from Life Cycle Assessment and -Costing

Results were obtained from computations in Gabi 6 in combination with its database "Professional 2014" based on the LCI data in Table A-11. Costs were assessed using Excel to calculate the estimations presented in Table A-11. Results from both assessments are presented in the following.

7.5.1 Results from Life Cycle Assessment

Results from all categories provided by the CML2001-April 2013 methodology were computed and compared. It became evident that the drivers of environmental impacts were mostly carbon fiber fabric and matrix and, although to a minor degree,

process energy. Process materials and especially the carrier were negligible. Results for fabric-dominated impacts and categories with strong effects from fabric and matrix were consistent among each other. Thus, only single distinguished impact categories were selected for further discussion.

From all three areas of protection - human health, natural environment and natural resources - impact categories were chosen for presentation. Global warming potential (GWP) effects human health and the natural environment. This happens through CO_2 emissions on the global ecosystem and is dominated by carbon fiber fabric use with minor contribution of matrix. Natural resources are impacted by abiotic resource depletion of elements (ADP), which was primarily driven by matrix use. This category refers to resources that are the product of past biological processes (coal, oil, gas) or physical/chemical processes (metal ores) [135, p. 48]. Terrestrial ecotoxicity potential (TETP) quantifies the influence of a substance regarding its toxicity on all species living in a terrestrial ecosystem [135, p. 73]. TETP was impacted strongly by fiber and matrix materials as well as by process energy to a minor degree. Results of the three impact categories GWP, ADP and TETP are presented in the following.

Since fabric input and thus, fabric scrap, has a big impact on GWP, this category is considered with scrap on the one hand and adjusted for fabric scrap on the other, Figure 7-4.
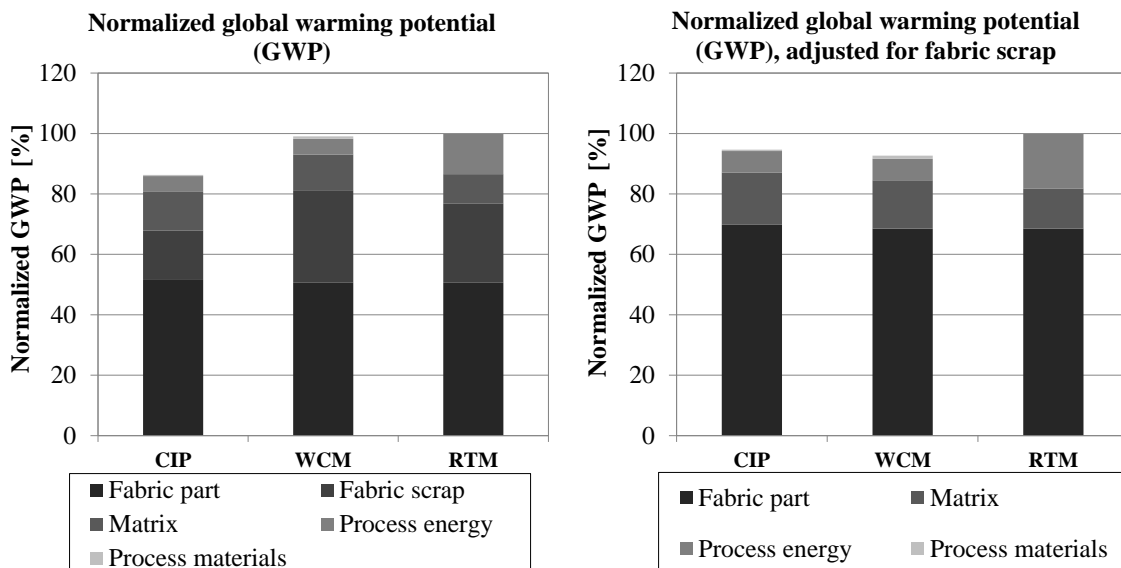
Figure 7-4 Normalized global warming potentials of CIP, WCM and RTM

Overall GWP was highest for RTM but only slightly lower in case of WCM. CIP exhibited the lowest impact because of reduced fabric scrap. The share of matrix was only marginally higher for CIP compared to WCM but lowest for RTM. While for the compression molding processes the impacts from process energy were equal,

it was found that RTM showed the highest impact on GWP from energy. Impacts from process materials, including the carrier, were negligible.

After adjustment for fabric scrap, the impact on GWP from fabric which remains within the final part was still dominant. However, WCM showed the lowest overall impact, albeit only 2 % lower compared to CIP. Due to the higher expenses of process energy, RTM still exhibited the highest impact.

The other impact categories, TETP and ADP of elements, exhibited a more balanced set of influences, where the matrix material was weightier compared to GWP, Figure 7-5.
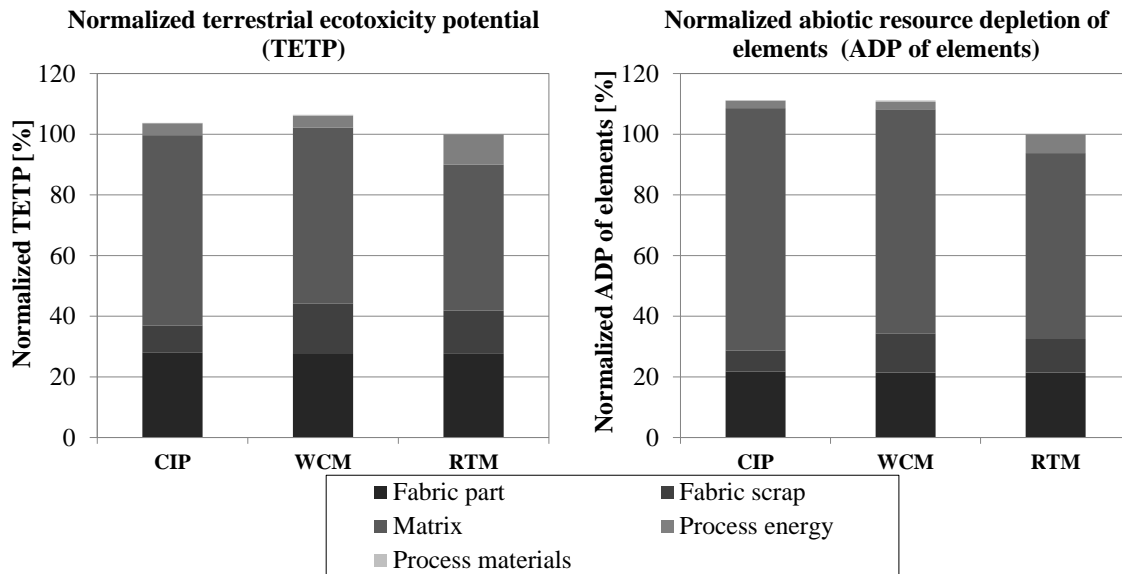
Figure 7-5 Normalized terrestrial ecotoxicity potential and abiotic resource depletion of elements of CIP, WCM and RTM

Terrestrial ecotoxicity was found to be mainly influenced by matrix and fiber use and less by process energy. Thus, RTM achieved the lowest impact in this category, while total impacts of WCM were approximately 2 % higher compared to impacts of CIP. Again, impact from process materials was very low with 0.01 %-0.3 %.

The impact from matrix materials was even higher for ADP, which resulted in almost equal overall impacts for CIP and WCM. Their impacts were approximately 11 % higher compared to RTM. Besides the lowest matrix use, RTM benefited from lower share of influence from process energy on ADP.

Results regarding GWP, ADP and TETP partially showed only marginal difference between the processes. In addition, they are directly influenced by estimations in process design, especially regarding fabric and matrix input. In order to better interpret the results in the light of said estimations, a sensitivity analysis regarding fabric input, matrix input, process materials and process energy was carried out.

The effects on the respective impact categories when each parameter was varied by ±20 % is displayed in Figure 7-6.
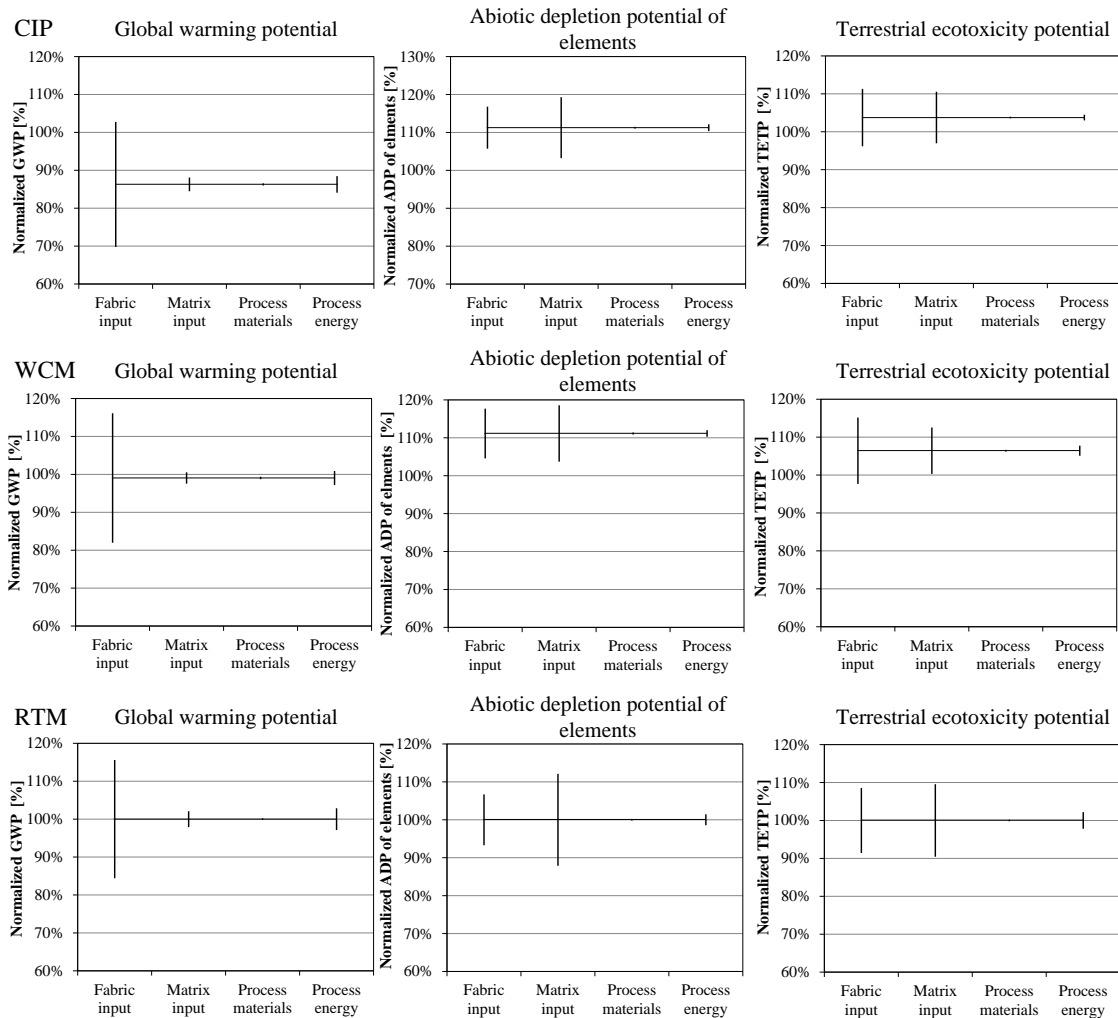
Figure 7-6 Normalized sensitivity analysis of GWP, ADP of elements and TETP regarding CIP, WCM and RTM given a 20 % variation of energy, fabric, matrix and process material input

Results of the sensitivity analysis reflected the impact shares of the parameters varied. For global warming in particular assumptions for fabric input were critical for all processes, since a variation of 20 % of the input resulted in approximately 16 % of variation of GWP. In contrast, matrix input and process energy varied only between 1 % for RTM and approximately 3 % for CIP.

ADP was particularly sensitive toward matrix input in RTM with variations of ±12 % and showed almost equal impact variations of approximately 7.5 % from matrix and fabric input for WCM and CIP.

TETP was also sensitive toward both materials, fabric and matrix. In case of WCM, matrix impact was found to be 5.9 % while RTM produced a sensitivity of 9.4 % for matrix use, slightly higher than fabric input.

In summary, the LCA results were very sensitive toward material input of both constituents of the composite, carbon fabric and duroplastic matrix. Sensitivity toward process energy was low. Contribution to the impacts from process materials, aceton, compressed air and carrier film were negligible compared to the other parameters varied.

7.5.2 Results from Life Cycle Costing

Costs were distinguished regarding materials, manipulations, machines and energy. Likewise to the LCA, fabric was divided between the amount remaining inside the final part and the amount of scrap. Since the fabric has an equally high impact on the results as in GWP, results were considered with scrap as well as adjusted for fabric scrap, Figure 7-7.
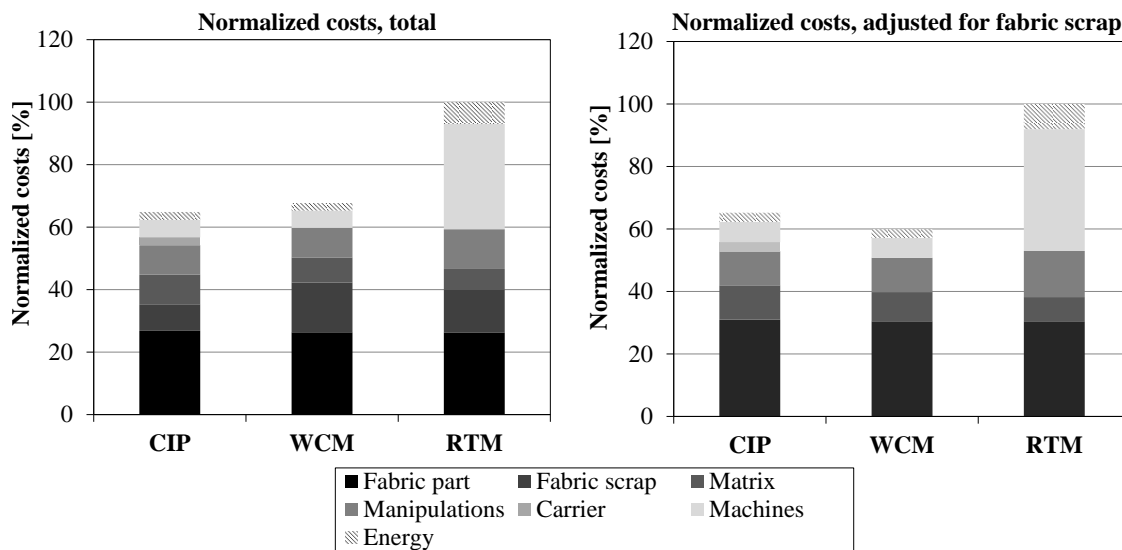
Figure 7-7 Composition of normalized costs of part production with CIP, WCM and RTM

Parts produced by RTM were considerably more expensive than parts produced with compression molding. This is mainly due to a higher expense in machines with slightly higher costs for manipulations, due to preforming and energy.

CIP was found to be less expensive than WCM despite the higher matrix input and an additional carrier film. This benefit was clearly attributed to the savings in fabric scrap.

When the costs are adjusted for fabric scrapped during processing, WCM exhibited the lowest costs, since no additional carrier and less matrix were needed for

processing. RTM, however, was still the most expensive process because of the high costs for machines and manipulations.

7.6 Conclusions from Life Cycle Assessment and -Costing

Through-thickness impregnation and draping are found to be two important aspects of compression molding processes that can be advantageous compared to RTM.

In experiments as well as in literature, through-thickness impregnation is associated with lower cavity pressures compared to RTM for high-volume manufacturing. Thus, for CIP and WCM smaller presses of 175 t can be used than for RTM (500 t) to produce the same part size. Pre-application of matrix onto the fabric, as it is enabled by through-thickness impregnation, also allows to prepare materials outside of the press. This leads to lower mold occupancy time and enables higher tool temperatures for faster curing. This becomes possible because the matrix flow path in through-thickness direction is much smaller compared to injection in longitudinal fabric direction. Faster curing in WCM and CIP reduces the cycle time considerably and makes tempering of the part obsolete. In result, RTM consumes more process energy and, thus, energy costs and environmental impacts are increased.

High pressures needed to completely fill the cavity via in-plane matrix flow can only be maintained by larger machines in case of RTM. Thus, part costs are driven considerable by higher equipment costs and the increased cycle time.

The draping mechanism offers the largest opportunity to improve environmental impacts and costs of the processes. Because RTM depends on an additional process step for draping performed by an additional press and induction oven, respective expenses for energy and machines are higher compared to WCM and CIP. In case of CIP, the approach of using a carrier film to save additional fabric for clamping can effectively reduce environmental impacts and costs. However, the part geometry must be suitable for the application and such savings are not generally possible.

The draping mechanism of CIP is also connected to higher matrix expense because regions of the cavity seam which are occupied by fabrics prior to draping must be filled with neat matrix after the fabric slides during draping. The tool layout was estimated according to the realized prototype tool, but it is likely that design improvements are possible. The results of the LCA, in particular from ADP and TETP, highlight the need to improve efficiency of matrix use for all production processes.

In the LCA, carbon fiber and matrix materials showed big impacts for different reasons. Despite the fact that carbon fiber had an impact on mineral depletion because fibers are made from oil-based PAN, the highest impact stemmed from the energy demands for graphitization, which is in line with statements from Kadla [113, p. 2913]. Thus, GWP was much more sensitive toward the fibers compared to the matrix. On the other hand, duroplastic matrix is also produced from oil but led to a higher exploitation of respective resources. The subsequent refinement, however, is not as energy-intensive and thus, GWP was not as sensitive towards matrix use. Nevertheless, process design should focus on efficiency of use of both materials in production, since elimination of scrap is the most effective way of improving environmental impacts and cost.

Within the scope of this study it is important to state that not all processes considered are suitable for the same part, like it was modeled in the study for the purpose of comparison. CIP and WCM are ideal for parts of lower geometrical complexity and size that can be produced in one press stroke. RTM provides big advantages when large and very complex parts are to be produced integratively with multiple sub-preforms. In that case, compression molding of smaller parts with subsequent joining is likely to lead to higher material expenses, costs and cycle times.

From the comparative study, however, it can be assumed that CIP can compete with WCM despite additional use of a carrier and higher matrix expense. It also provides similar advantageous toward RTM. If the part geometry is suitable, CIP may even reduce costs and CO_2 emissions due to savings of fabric. However, matrix use still has to be targeted in development to reduce TETP and ADP of elements.

7.6.1 Limitations

The LCA and LCC study presented is subject to some limitations regarding process estimations and available LCI data for carbon fiber technology.

The processes CIP, WCM and RTM have been modeled after experiments on prototyping equipment. Data had to be adjusted based on estimations for industrial processes, without validation on existing processing systems. This was particularly critical for fabric and matrix input because LCA impact categories and costs proved to be very sensitive toward these parameters.

Furthermore, data was estimated regarding one concrete part, the function unit, and thus, results are not generally applicable to other parts. Especially regarding fiber scrap, part geometry in combination with the draping mechanisms that are inherent to the respective processes plays a pivotal role.

Lastly, the data base for inventories of CFRP materials and connected manufacturing processes is very limited. LCI data for fiber production was obtained from literature but is subject to large fluctuations based on the sources. Data for most other process steps, e. g. regarding energy uptake, had to be estimated based on power ratings. This drawback, however, can only be solved in wide-ranging collaborations between industrial producers, suppliers and research institutions, as it was the case in one initial study [122].

8 Conclusions and Ongoing Work

This chapter concludes the thesis regarding its outlined purpose and reviews the contributions that can be attributed to the work. It starts with a summary and subsequently draws conclusions regarding the purpose, most notably the polylemma of superimposed draping and impregnation. The remainder of the chapter presents the possibilities for ongoing work.

8.1 Summary

This thesis focuses on compression molding of continuous CFRP for automated serial production. It is known as an alternative to RTM for less complex, smaller parts but has hitherto not been subject to scientific studies. In particular, no information on the matrix flow through the fiber material is available, as it has been and still is intensively studied for RTM. Though matrix flow seems to be especially important for compression molding because the liquid matrix is pre-applied on a planar fiber fabric prior to compression. Subsequently, the matrix flows in through-thickness direction of the fiber material simultaneously to draping of the fibers.

From an initial literature study on LCM processes, this thesis identified important functions in relation to material flow in compression molding. Furthermore, it hypothesized that the pre-applied matrix forms a film atop the fiber material which is prone to unintentional dislocation during material transport and compression. The matrix pre-application, the biggest advantage of compression molding compared to RTM, conflicts with stabilization of materials for automated handling and control of matrix flow.

Based on these hypotheses, a principle solution for spacial separation of matrix and fiber material with storage of the matrix inside cavities of a carrier was proposed. The stored matrix inside the cavities and the fiber material above the cavities can be securely transported from preparation into the press. Furthermore, cavities control the flow of matrix during compression.

By drawing on the Munich procedural model, a process and prototyping tool was designed based on the principle solution. The key issue during the design phase was to find a solution to generate vacuum tightness inside the tool cavity over the entire press stroke. A resulting technical conflict could be solved with TRIZ. It led to the design of a blank holder and using the carrier to separate matrix-flooded regions of the tool from sealings and vacuum bores. Thereby, the carrier could also mediate tensional forces onto the fiber material to support draping. In practical press trials on the designed tool it was found that a carrier made from elastic thermoplastic

polyurethane provided the highest benefit regarding to the functionality of the process. In particular, forming of cavities, cavity elimination and draping worked best with such carriers.

To research the initially hypothesized conflict between matrix flow and matrix pre-application, plates and complex parts were produced on the prototype tool in WCM and CIP. In order to visualize matrix flow, a method for tracing fluorescent matrix in photographs and micrographs was developed. Thus, the compactness and flow path of a mass of matrix that was dyed with fluorescent pigments prior to pressing could be quantified with segmentation of digital images in Matlab.

As part of a DoE study, plates were produced in WCM and CIP with respective variations of process parameters. It was found that in WCM fluorescent matrix distribution was highly scattered on the part top with little flow in through-thickness direction. Flow became more compact with lower temperatures and higher press speeds but did not reach the compactness of the distribution seen in CIP. For CIP, the temperature history of the film determined the compactness of flow because the thermoformed cavities degenerate under heat. Best results were found at high temperatures and short exposure to heat inside the tool before compression.

For complex parts, matrix was dislocated due to gravity influence during draping. The compactness of flow seen during plate pressings could not be maintained.

Whether or not more compact flow leads to higher impregnation qualities, as indicated by studies of RTM processes, could not be clearly answered. Micrographs of respective parts suggested a higher pore content inside the laminates produced with scattered flow. Three point bending trials, however, did not show any differences.

Finally, CIP was compared to WCM and RTM within a combined LCA and LCC study. It was found that CIP can provide benefits regarding CO_2 emissions during production and part costs, when the part geometry is suitable for carrier draping. In that case, less fabric is scrapped for clamping and sealing. Higher matrix expense in CIP, however, may lead to marginally higher terrestrial ecotoxicity and resource depletion compared to WCM and RTM. Due to the sensitivity of the results toward estimated material inputs, it is not reasonable to speak of clear differences between CIP and WCM. Instead, it is important to note that despite additional carrier input and higher matrix expenses, CIP can compete with WCM and provides the same advantages in comparison to RTM.

8.2 Conclusions

The research of this thesis lends evidence to the hypothesis of matrix pre-application, matrix flow control and material stabilization. Furthermore, it could be shown that a carrier with cavities can improve these three aspects and does not perform less well under circumstances of an industrial production. Matrix flow control in complex part geometries, however, is low for both processes compared, WCM and CIP.

The carrier in CIP offers a possibility to stabilize materials without the use of binder or non-isothermal processing. This also refers to the draping mechanism, which may provide valuable savings in fiber scrap, dependent on the part geometry. The carrier film also allows to draw vacuum inside the tool cavity without the danger of sealing degradation due to matrix contact - one reason that WCM does not apply vacuum despite its benefits regarding impregnation quality.

8.3 Ongoing Work

The work is a first endeavor into compression molding of CFRP for industrial series manufacturing. An important aspect, as for all LCM processes, is matrix flow. Despite the lack of scientific spadework, significant insights into matrix flow control were achieved. From this starting point, several directions for ongoing work make sense.

In respect to matrix flow, the methods of fluorescent photography and microscopy can be further developed. The method is simple, can be applied to most LCM processes and offers quickly accessible and interpretable information on the matrix flow. It would be fruitful to especially apply it to industrialized WCM, since this thesis did only consider smaller parts produced on a prototyping tool.

It is not yet clear if the matrix flow in compression molding processes is as critical to good impregnation quality as it is the case for RTM. This aspect has to be further researched, especially using more reliable indicators for impregnation quality, such as interlaminar shear strength, ultrasonic testing or CT scanning of laminates. Also, larger parts produced in compression molding should be investigated. Matrix flow might be more critical there compared to small parts considered in this thesis.

The integration of films into processing of composites has been proposed before. This thesis did not focus on expanding the functionality or surface properties of a composite part with films. In order to provide an additional benefit of a polymer film, respective industrial applications have to be considered for further film development with research into the concrete application.

Bibliography

[1] D. C. Mowery, R. R. Nelson, and B. R. Martin, "Technology policy and global warming: When new policy models are needed (or why putting new wine in old bottles won't work)," *Elsevier Research Policy*, vol. 39, no. 8, pp. 1011–1023, 2010.

[2] F. Birol and International Energy Agency, *World Energy Outlook 2014*, F. Birol, Ed. International Energy Agency, 2014, vol. 2014.

[3] BMWi, *Energie in Deutschland - Trends und Hintergründe zur Energieversorgung*, 11019 Berlin, Feb 2013.

[4] T. Altenburg, S. Bhasin, and D. Fischer, "Sustainability-oriented innovation in the automobile industry: advancing electromobility in china, france, germany and india," *Innovation and Development*, vol. 2, no. 1, pp. 67–85, Apr 2012.

[5] H. Eickenbusch and O. Krauss, "Werkstoffinnovationen für nachhaltige mobilität und energieversorgung," VDI-Platz 1, 40468 Düsseldorf, Tech. Rep., Mar 2014.

[6] H. Wallentowitz, F. A., and O. I., *Strategien in der Automobilindustrie*, 1st ed. Vieweg+Teubner, 2009, vol. 1.

[7] J. T. Black and R. A. Kohser, *DeGarmo's Materials and Processes in Manufacturing*, 11th ed. John Wiley & Sons, Aug 2011.

[8] N. Oxman, "Variable property rapid prototyping," *Virtual and Physical Prototyping*, vol. 6, no. 1, pp. 3–31, 2011.

[9] O. A. Villalobos, "Fundamentals of the design of bamboo structures," PhD thesis, Technische Universiteit Eindhoven, Eindhoven, 1993.

[10] C. Mattheck, *Verborgene Gestaltgesetze der Natur: Optimalformen ohne Computer*, 1st ed. Karlsruhe: Forschungszentrum Karlsruhe, 2006.

[11] P. Ermanni, Zürich, 2007, ch. Composites Technologien: Skript zur ETH-Vorlesung.

[12] K. Potter, "Design of composite products - a personal viewpoint," *Composites Manufacturing*, vol. 3, no. 3, pp. 173–182, 1992.

[13] D. Biermann, W. Hufenbach, and G. Seliger, *Serientaugliche Bearbeitung und Handhabung moderner faserverstärkter Hochleistungswerkstoffe: Untersuchungsbericht zum Forschungs- und Handlungsbedarf*, 2008.

[14] P. Potluri and J. Atkinson, "Automated manufacture of composites: handling, measurement of properties and lay-up simulations," *Composites Part A: Applied Science and Manufacturing*, vol. 34, no. 6, pp. 493–501, 2003.

[15] K. Drechsler, Ed., *CFK-Technologie im Automobilbau: Was man von anderen Märkten lernen kann*, 2010.

[16] J. P. M. W. L. Michaeli, W.; Wessels, "New process technology for high volume production of composites," *Journal for Polymer Engineering*, vol. 31, no. 1, pp. 63–68, 2011.

[17] C. D. Rudd and K. N. Kendall, "Towards a manufacturing technology for high–volume production of composite components," *ARCHIVE: Proceedings of the Institution of Mechanical Engineers, Part B: Journal of Engineering Manufacture 1989-1996 (vols 203-210)*, vol. 206, no. 22, pp. 77–91, 1992.

[18] BMW, "Annual report 2014," 80788 München, Tech. Rep., 2014.

[19] D. Hofbauer, L. Kroll, J. Kaufmann, A. Repper, and H. Pfitzer, "Faserverbundtechnologien für automobilkomponenten in der großserie," *Lightweight Design*, vol. 7, no. 6, pp. 40–45, 2014.

[20] F. Dirschmid, "Die cfk-karosserie des bmw i8 und deren auslegung," in *Karosseriebautage Hamburg*, ser. Proceedings, G. Tecklenburg, Ed. Wiesbaden: Springer Fachmedien Wiesbaden, 2014, pp. 217–231.

[21] A. Endruweit, "Investigation of the influence of local inhomogeneities in the textile permeability on the resin flow in liquid composites moulding processes," Ph.D. dissertation, ETH, Zürich, 2003.

[22] J. . Z. C. . L. R. . W. B. Li, "Statistical characterization and robust design of rtm processes," *Composites Part A: Applied Science and Manufacturing*, vol. 36, no. 5, pp. 564–580, 2005.

[23] E. . S. S. . B. M. Fries, "Hochdruck-rtm-technologie gewinnt an flexibilität," *MM Compositesworld*, pp. 12–14, Sep 2012.

[24] R. Zirn, "Anforderungen an die pressentechnik bei der produktion von cfk-karosserieteilen," in *Leichtbau-Technologien im Automobilbau*, W. Siebenpfeiffer, Ed. Wiesbaden: Springer Fachmedien Wiesbaden, 2014, pp. 4–10.

[25] G. Wolfsberger, "Fiber composite modules: Crushcore - wetpressing technology with class-a surface out of tool," Sep 2014.

[26] B. R. Lundstroem, T. S.; Gebart, "Influence from process parameters on void formation in resin transfer molding," *Polymer Composites*, vol. 15, no. 1, pp.

25–33, 1994.

[27] D. Abraham and McIlhagger, "A review of liquid injection techniques for the manufacture of aerospace composite structures," *Polymers & Polymer Composites*, vol. 4, no. 6, pp. 437–444, 1996.

[28] V. Michaud and A. Mortensen, "Infiltration processing of fibre reinforced composites: governing phenomena," *Composites Part A: Applied Science and Manufacturing*, vol. 32, no. 8, pp. 981–996, 2001.

[29] P. Bockelmann, K. Drechsler, and A. Chakrabarti, Eds., *ICoRD'15 - Research into Design Across Boundaries Volume 2: Creativity, Sustainability, DfX, Enabling Technologies, Management and Applications*, aufl. 2015 ed.   New Delhi: Springer India, 2015.

[30] U. Lindemann, *Methodische Entwicklung technischer Produkte: Methoden flexibel und situationsgerecht anwenden*, 3rd ed.   Berlin and Heidelberg: Springer, 2009.

[31] K. Drechsler and P. Bockelmann, *Handbuch Produktentwicklung.*   Hanser Verlag, 2016, ch. Produktentwicklung mit Neuen Materialien am Beispiel der Carbon Composites, pp. 877–904.

[32] H. Schürmann, *Konstruieren mit Faser-Kunststoff-Verbunden: Mit 39 Tabellen*, 2nd ed.   Springer Berlin Heidelberg, 2007.

[33] R. Heuss, N. Müller, W. van Sintern, A. Starke, and A. Tschiesner, "Light weight, heavy impact," 2012.

[34] R. Laessig, M. Eisenhut, A. Mathias, R. Schulte, F. Peters, T. Kuehmann, T. Waldmann, and W. Begemann, "Series production of high-strength composites," Tech. Rep., Sep 2012.

[35] G. W. Ehrenstein, *Faserverbund-Kunststoffe: Werkstoffe - Verarbeitung - Eigenschaften.*   Hanser, 2006.

[36] J. Krollmann, "Design and development of a hybrid, shape adaptive key safety structure in the fuzzy front end of the automotive industry," Sep 2014.

[37] W. A. Walbran, "Experimental validation of local and global force simulations for rigid tool liquid composite moulding processes," Ph.D. dissertation, The University of Auckland, Auckland, 2011.

[38] M. . R. S. Flemming, *Faserverbundbauweisen Eigenschaften.*   Springer-Verlag Berlin Heidelberg New York, 2003.

[39] L. Herbeck, "Von der manufaktur zur produktion - herausforderungen für die faserkunststoffverbunde," pp. 1–20, Jun 2010.

[40] H. Darcy, *Les fontaines publiques de la ville de Dijon: Exposition et application des principes à suivre et des formules à employer dans les questions de distrubtion d'eau*, Paris, 1856.

[41] S. Bickerton, E. M. Sozer, P. J. Graham, and S. G. Advani, "Fabric structure and mold curvature effects on preform permeability and mold filling in the rtm process. part i. experiments," *Composites Part A: Applied Science and Manufacturing*, vol. 31, no. 5, pp. 423–438, 2000.

[42] E. Fries, "Hochdruck-rtm technologie für die großserienproduktion von carbonfaserverstärkten kunststoffbauteilen," in *Materialica 2010*.

[43] V. D. Ingenieure, *VDI 2014 Blatt 1 - Entwicklung von Bauteilen aus Faser-Kunststoff-Verbund; Grundlagen*, Verein Deutscher Ingenieure Std., 1989.

[44] A. C. Long, *Design and manufacture of textile composites.* Cambridge: Woodhead Pub., 2005.

[45] M. F. Ashby, Y. J. M. Bréchet, D. Cebon, and L. Salvo, "Selection strategies for materials and processes," *Materials & Design*, vol. 25, no. 1, pp. 51–67, 2004.

[46] M. V. Gandhi, B. S. Thompson, and F. Fischer, "Manufacturing-process-driven design methodologies for components fabricated in composite materials," *Composites Manufacturing*, vol. 1, no. 1, pp. 32–40, 1990.

[47] K. M. Eisenhardt, "Building theories from case study research," *Academy of Management Review*, vol. 14, no. 4, pp. 532–550, 1989.

[48] M. Q. Patton, *Qualitative research and evaluation methods*, 3rd ed. Thousand Oaks and Calif: Sage Publications, 2002.

[49] J. G. March, "Exploration and exploitation in organizational learning," *Organization Science*, vol. 2, no. 1, pp. 71–87, 1991.

[50] D. Maffin, "Engineering design models: Context, theory and practice," *Journal of Engineering Design*, vol. 9, no. 4, pp. 315–327, 1998.

[51] G. Pahl, K. Wallace, and L. Blessing, *Engineering design: A systematic approach*, 3rd ed. London: Springer, 2007.

[52] V. D. Ingenieure, *VDI 2221 - Methodik zum Entwickeln und Konstruieren technischer Systeme und Produkte*, Verein Deutscher Ingenieure Std., 1993.

[53] M. J. Benders, "Methodik der kombinierten werkstoff-, fertigungsverfahrens- und geometriesynthese," Ph.D. dissertation, Rheinisch-Westphälische Technische Hochschule, Aachen, 2011.

[54] N. Patel, V. Rohatgi, and L. J. Lee, "Micro scale flow behavior and void formation mechanism during impregnation through a unidirectional stitched fiberglass mat," *Polymer Engineering and Science*, vol. 35, no. 10, pp. 837–851, 1995.

[55] K. M. Pillai, "Modeling the unsaturated flow in liquid composite molding processes: A review and some thoughts," *Journal of Composite Materials*, vol. 38, no. 23, pp. 2097–2118, 2004.

[56] J. S. Leclerc and E. Ruiz, "Porosity reduction using optimized flow velocity in resin transfer molding," *Composites Part A: Applied Science and Manufacturing*, vol. 39, no. 12, pp. 1859–1868, 2008.

[57] S. Bickerton and S. G. Advani, "Characterizatrion and modeling of racetracking in liquid composite molding processes," *Composites Science and Technology*, vol. 59, pp. 2215–2229, 1999.

[58] S. Bickerton, H. C. Stadtfeld, K. V. Steiner, and S. G. Advani, "Design and application of actively controlled injection schemes for resin-transfer molding," *Composites Science and Technology*, vol. 61, no. 11, pp. 1625–1637, 2001.

[59] M. K. Kang, J. J. Jung, and W. I. Lee, "Analysis of resin transfer moulding process with controlled multiple gates resin injection," *Composites Part A: Applied Science and Manufacturing*, vol. 31, no. 5, pp. 407–422, 2000.

[60] K.-T. Hsiao and S. G. Advani, "Flow sensing and control strategies to address race-tracking disturbances in resin transfer molding. part i: design and algorithm development," *Composites Part A: Applied Science and Manufacturing*, vol. 35, no. 10, pp. 1149–1159, 2004.

[61] O. Restrepo, K.-T. Hsiao, A. Rodriguez, and B. Minaie, "Development of adaptive injection flow rate and pressure control algorithms for resin transfer molding," *Composites Part A: Applied Science and Manufacturing*, vol. 38, no. 6, pp. 1547–1568, 2007.

[62] B. A. E. T. F. Ruiz, E.; L., "Flexible injection: A novel lcm technology for low cost manufacturing of high performance composites. part i - experimental investigation," in *The 9th International Conference on Flow Processes in Composite Materials (FPCM-9)*, Montréal, Quebec, Canada, July 2008.

[63] B. Deryck, N.; Graham, "Method of producting advanced composite components," U.S. Patent US2012/0 135 219 A1, 02 17, 2012.

[64] R. D. Hawkins, "Controlled delta pressure bulk resin infusion system apparatus and method," U.S. Patent US 2007/0 090 562 A1, 04 26, 2007.

[65] C.-Y. Chang, "Effect of process variables on the quality of compression resin transfer molding," *Journal of Reinforced Plastics and Composites*, vol. 25, no. 10, pp. 1027–1037, 2006.

[66] H. Kong, A. P. Mouritz, and R. Paton, "Tensile extension properties and deformation mechanisms of multiaxial non-crimp fabrics," *Composite Structures*, vol. 66, no. 1-4, pp. 249–259, 2004.

[67] R. Loendersloot, S. V. Lomov, R. Akkerman, and I. Verpoest, "Carbon composites based on multiaxial multiply stitched preforms. part v: geometry of sheared biaxial fabrics," *Composites Part A: Applied Science and Manufacturing*, vol. 37, no. 1, pp. 103–113, 2006.

[68] S. Bel, N. Hamila, P. Boisse, and F. Dumont, "Finite element model for ncf composite reinforcement preforming: Importance of inter-ply sliding," *Composites Part A: Applied Science and Manufacturing*, vol. 43, no. 12, pp. 2269–2277, 2012.

[69] J. S. Lee, S. J. Hong, W.-R. Yu, and T. J. Kang, "The effect of blank holder force on the stamp forming behavior of non-crimp fabric with a chain stitch," *Composites Science and Technology*, vol. 67, no. 3-4, pp. 357–366, 2007.

[70] S. G. Pantelakis and E. A. Baxevani, "Optimization of the diaphragm forming process with regard to product quality and cost," *Composites Part A: Applied Science and Manufacturing*, vol. 33, no. 4, pp. 459–470, 2002.

[71] D. Leutz, M. Kluepfel, F. Dumont, R. Hinterhoelzl, K. Drechsler, and C. Weimer, "Fe-simulation of the diaphragm draping process for ncf on a macro-scale level," in *The 14th International Esaform Conference on Material Forming (ESAFORM 2011)*, ser. AIP Conference Proceedings. AIP, 2011, pp. 1019–1024.

[72] D. Haeffelin, P. Lachner, S. Sattler, J. Krollmann, M. Freiberger, T. Pump, F. Knoblich, and S. Schmidhuber, *Folienintegrierter RTM-Prozess (resin transfer molding) für endlosfaserverstärkte Schalenbauteile (Film-RTM): [... Forschungs- und Entwicklungsprojekt ... mit*, ser. Fortschritt-Berichte VDI: Reihe 5, Grund- und Werkstoffe, Kunststoffe. Düsseldorf: VDI-Verl., 2014, vol. 754.

[73] G. Reinhart, G.; Straßer, "Flexible gripping technology for the automated handling of limp technical textiles in composites industry," *Production Engineering*, vol. 5, no. 3, pp. 301–306, June 2011.

[74] F. C. N. V. Fleischer, J.; Förster, "Intelligent gripper technology for the handling of carbon fiber material," *Production Engineering*, vol. 8, no. 6, pp. 691–700, 2014.

[75] P. Simacek, S. G. Advani, and S. A. Iobst, "Modeling flow in compression resin transfer molding for manufacturing of complex lightweight high-performance automotive parts," *Journal of Composite Materials*, vol. 42, no. 23, pp. 2523–2545, 2008.

[76] D. Pradhan, A. K.and Das, R. Chattopahdyay, and S. N. Singh, "Effect of 3d fiber orientation distribution on transverse air permeability of fibrous porous media," *Powder Technology*, vol. 221, pp. 101–104, May 2012.

[77] M. Steyer, A. Schuette, K. Fischer, L. WInkelmann, and T. Grundmann, "Mass production of fibre-reinforced plastic components for structural applications," *Automobiltechnische Zeitschrift ATZ*, no. 4, pp. 76–79, 2009.

[78] W. Michaeli and K. Fischer, "Analysis of the gap impregnation process," vol. 2009.   Baltimore: SAMPE, May 2009.

[79] M. B. Roller, "Characterization of the time-temperature-viscosity behavior of curing b-staged epoxy resin," *Polymer Engineering and Science*, vol. 15, no. 6, pp. 406–414, 1975.

[80] P. R. Goppel, J. M.; Chant, "Verfahren zur herstellung von gegenständen aus wärmehärtenden harzend," German Patent 2 131 472, January 05, 1972.

[81] L. T. M. Blessing and A. Chakrabarti, *DRM, a design research methodology.* Dordrecht, New York: Springer, 2009.

[82] G. S. Altshuller, L. Shulyak, and S. Rodman, *The innovation algorithm: TRIZ, systematic innovation and technical creativity*, 1st ed.   Worcester, Mass.: Technical Innovation Center, 1999.

[83] G. S. Altshuller, L. Shulyak, S. Rodman, and D. W. Clarke, *40 principles: TRIZ keys to technical innovation*, 2nd ed., ser. TrizTools.   Worcester, Mass.: Technical Innovation Center, 2005, vol. v. 1.

[84] E. Witten, Ed., *Handbuch Faserverbundkunststoffe: Grundlagen, Verarbeitung, Anwendungen*, 3rd ed.   Wiesbaden: Vieweg + Teubner, 2010.

[85] U. Lindemann, "Triz basiskurs," TUM Graduate School Seminar, March 2012.

[86] S. V. Lomov, M. Barburski, T. Stoilova, I. Verpoest, R. Akkerman, R. Loendersloot, and R. ten Thije, "Carbon composites based on multiaxial multiply stitched preforms. part 3: Biaxial tension, picture frame and compression tests of the preforms," *Composites Part A: Applied Science and Manufacturing*, vol. 36, pp. 1188–1206, 2005.

[87] P. Harrison, W.-R. Yu, and A. C. Long, *Modelling the deformability of biaxial non-crimp fabric composites*, 1st ed. Woodhead Pub., April 2011, ch. 7, pp. 144–165.

[88] F. J. Schirmaier, K. A. Weidenmann, L. Kärger, and F. Henning, "Characterisation of the draping behaviour of unidirectional non-crimp fabrics (ud-ncf)," *Composites Part A: Applied Science and Manufacturing*, vol. 80, pp. 28–38, 2016.

[89] S. Thumfart, W. Palfinger, S. M., and C. Eitzinger, *Accurate Fibre Orientation Measurement for Carbon Fibre Surfaces*, ser. Computer Analysis of Images and Patterns. Springer-Verlag Berlin Heidelberg, August 2013, vol. 8048, book 10, pp. 75–82.

[90] M. Bauer, P. Friede, and C. Uhlig, "Sandwiches mit noppenwabenkern," *Kunststoffe*, no. 8, pp. 95–97, August 2006.

[91] P. Rinza and H. Schmitz, *Nutzwert-Kosten-Analyse*, 1st ed. Springer Verlag Berlin Heidelberg, 1992.

[92] A. Birkert, S. Haage, and M. Straub, *Umformtechnische Herstellung komplexer Karosserieteile*, 1st ed. Springer Vieweg, 2013.

[93] P. Schwarzmann, *Thermoformen in der Praxis*, 2nd ed. Carl Hanser Verlag, München 2008, October 2008.

[94] W. Michaeli, H. Greif, L. Wolters, and F.-J. Vossebuerger, *Technologie der Kunststoffe*, 2nd ed. Carl Hanser Verlag München Wien, 1998.

[95] T. Centea and P. Hubert, "Measuring the impregnation of an out-of-autoclave prepreg by micro-ct," *Composites Science and Technology*, vol. 71, no. 5, pp. 593–599, March 2011.

[96] M. Nordlund, S. P. Fernberg, and T. S. Lundstroem, "Particle deposition mechanisms during processing of advanced composite materials," *Composites Part A: Applied Science and Manufacturing*, vol. 38, pp. 2182–2193, June 2007.

[97] J. W. C. Pang and I. P. Bond, "'bleeding composites' - damage detection and self-repair using a biomimetic approach," *Composites Part A:*, vol. 36, pp. 183–188, 2005.

[98] P. Klauth, B. R., C. Ralfs, P. Ustohal, J. Vanderborght, H. Vereecken, and E. Klumpp, "Fluorescence macrophotography as a tool to visualise and quantify spatial distribution of deposited colloid tracers in porous media," *Colloids and Surfaces A: Physiochemical and Engineering Aspects*, vol. 306, pp. 118–125, 2007.

[99] B. Jaehne, *Digitale Bildverarbeitung*, 7th ed. Springer Vieweg, 2012.

[100] S. Hesse and G. Schnell, *Sensoren für die Prozess- und Fabrikautomation*, 6th ed. Springer Vieweg, 2014.

[101] R. Winter and F. Noll, *Methoden der Biophysikalischen Chemie*, 1st ed. Tebner, May 1998.

[102] H. Frey, "Die verarbeitung von farbbildern nach helligkeit, sättigung und buntton," in *Mustererkennung 1990*, R. E. Großkopf, Ed., vol. 12, DAGM-Symposium. Springer-Verlag, 1990, pp. 324–331.

[103] R. Yuste, "Fluorescence microscopy today," *Nature Methods*, vol. 2, no. 12, pp. 902–904, December 2005.

[104] K. Siebertz, D. van Bebber, and T. Hochkirchen, *Design of Experiments (DoE)*, 1st ed. Springer Berlin Heidelberg, 2010.

[105] A. Field, *Discovering Statistics using SPSS (and sex and drugs and rock 'n' roll)*, 3rd ed. Sage Publications Ltd, 2009.

[106] DIN, *Fibre-reinforced plastic composites - Determination of flexural properties*, DIN Deutsches Insitut für Normung e. V. Std. DIN EN ISO 14 125, May 2011.

[107] J. E. Little, X. W. Yuan, and M. I. Jones, "Voids characterizsation in carbon fibre/epoxy composite laminates," in *18th International conference on composite materials*, 2011.

[108] B. Yang, T. Jin, F. Bi, Y. Wei, and J. Li, "Influence of fabric shear and flow direction on void formation during resin transfer molding," *Composites Part A: Applied Science and Manufacturing*, no. 68, pp. 10–18, September 2015.

[109] S. Das, "Life cycle assessment of carbon fiber-reinforced polymer composites," *International Journal Of Life Cycle Assessment*, vol. 16, no. 3, pp. 268–282, Mar 2011. [Online]. Available: http://dx.doi.org/10.1007/s11367-011-0264-z

[110] R. A. Witik, J. Payet, V. Michaud, C. Ludwig, and J.-A. E. Månson, "Assessing the life cycle costs and environmental performance of lightweight materials in automobile applications," *Composites Part A: Applied Science and Manufacturing*, vol. 42, no. 11, pp. 1694–1709, Nov 2011. [Online]. Available: http://dx.doi.org/10.1016/j.compositesa.2011.07.024

[111] G. A. Keoleian and J. L. Sullivan, "Materials challenges and opportunities for enhancing the sustainability of automobiles," *MRS Bull.*, vol. 37, no. 04, pp. 365–373, Apr 2012. [Online]. Available: http://dx.doi.org/10.1557/mrs.2012.52

[112] M. G. Bader, "Selection of composite materials and manufacturing routes for cost-effective performance," *Composites Part A: Applied Science and Manufacturing*, vol. 33, no. 7, pp. 913–934, Jul 2002. [Online]. Available: http://dx.doi.org/10.1016/S1359-835X(02)00044-1

[113] J. F. Kadla, S. Kubo, R. A. Venditti, R. Gilbert, and A. Compere, "Lignin-based carbon fibers for composite fiber applications," *Carbon*, vol. 40, no. 15, pp. 2913–2920, 2002.

[114] H. C. Kim and T. J. Wallington, "Life-cycle energy and greenhouse gas emission benefits of lightweighting in automobiles: Review and harmonization," *Environmental Science & Technology*, p. 130528153844008, May 2013. [Online]. Available: http://dx.doi.org/10.1021/es3042115

[115] Y. S. Song, J. R. Youn, and T. G. Gutowski, "Life cycle energy analysis of fiber-reinforced composites," *Composites Part A-applied Science And Manufacturing*, vol. 40, no. 8, pp. 1257–1265, Aug 2009. [Online]. Available: http://dx.doi.org/10.1016/j.compositesa.2009.05.020

[116] T. Suzuki and J. Takahashi, "Prediction of energy intensity of carbon fiber reinforced plastics for mass-produced passenger cars," in *The 9th Japan International SAMPE symposium*, T. Suzuki and J. Takahashi, Eds. SAMPE, Dec 2005, pp. 14–19.

[117] J. R. Duflou, J. D. Moor, I. Verpoest, and W. Dewulf, "Environmental impact analysis of composite use in car manufacturing," *CIRP Annals - Manufacturing Technology*, vol. 58, no. 1, pp. 9–12, 2009. [Online]. Available: http://dx.doi.org/10.1016/j.cirp.2009.03.077

[118] *Environmental management - Life cycle assessment - Principles and framework (ISO 14040)*, International Organization for Standardization Std., 2006.

[119] J. B. Guinée, R. Heijungs, G. Huppes, A. Zamagni, P. Masoni, R. Buonamici, T. Ekvall, and T. Rydberg, "Life cycle assessment: Past, present, and future †," *Environmental Science & Technology*, vol. 45, no. 1, pp. 90–96, Jan 2011. [Online]. Available: http://dx.doi.org/10.1021/es101316v

[120] M. D. Wakeman and J.-A. E. Månson, *Design and Manufacture of Textile Composites*, 1st ed. Woodhead Publishing Limited, 2005, ch. 10, pp. 364–404.

[121] M. Z. Hauschild and M. Huijbregts, *Introducing Life Cycle Impact Assessment*, 1st ed., ser. LCA Compendium - The Complete World of Life Cycle Assessment. Springer, 2015, ch. 1, pp. 1–16.

[122] A. Hohmann, B. Schwab, D. Wehner, A. S., R. Ilg, T. Schueppel, and T. v. Reden, "Mai enviro - vorstudie zur lebenszyklusanalyse mit oekobilanzieller bewertung relevanter fertigungsprozessketten für cfk-strukturen," Fraunhofer Gesellschaft, Technology report, 2015.

[123] E. Witten, T. Kraus, and M. Kuehnel, "Composites-market report 2014," Tech. Rep., Oct 2014.

[124] J. Rybicka, A. Tiwari, P. A. D. Campo, and J. Howarth, "Capturing composites manufacturing waste flows through process mapping," *Journal of Cleaner Production*, vol. 91, pp. 251–261, Mar 2015. [Online]. Available: http://dx.doi.org/10.1016/j.jclepro.2014.12.033

[125] A. Keller, K. Masania, A. C. Taylor, and C. Dransfeld, "Fast-curing epoxy polymers with silica nanoparticles: properties and rheo-kinetic modelling," *Journal of Material Science*, Jul 2015. [Online]. Available: http://dx.doi.org/10.1007/s10853-015-9158-y

[126] C. Fais, "Lightweight automotive design with hp-rtm," *Reinforced Plastics*, 2011.

[127] A. T. DiBenedetto, "Prediction of the glass transition temperature of polymers: A model based on the principle of corresponding states," *Journal of Polymer Science: Part B: Polymer Physics*, vol. 25, pp. 1949–1969, 1987.

[128] C. Sorg, "Data mining as a method of industrialization and qualification of new manufacturing processes for cfrp components in automotive mass production," PhD thesis, Technical University Munich, 2014.

[129] C. Hopmann, "Aushärten per induktion," *Der Plastverarbeiter*, vol. 65, pp. 86–89, 2014.

[130] E. Griffing, "Carbon fiber from pan," Wichita Sate University, Technical Report, May 2009.

[131] P. Morgan, *Carbon fibers and their composites*, 1st ed. CRC Press, 2005.

[132] O. M. DeVegt and W. G. Haije, "Comparative environmental life cycle assessment of composite materials," Technical Report, December 1997.

[133] R. Teti, "Machining of composite materials," in *CIRP Annals - Manufacturing Technology*, vol. 51, no. 2. Elsevier, 2002, pp. 611–634.

[134] E. Uhlmann, F. Sammler, S. Richarz, F. Heitmueller, and M. Bilz, "Machining of carbon fibre reinforced plastics," in *Procedia CIRP*, vol. 24, 2014, pp. 19–24.

[135] J. B. Guinée, "Development of a methodology for the environmental life-cycle assessment of products," PhD thesis, Rijkuniversiteit te Leiden, March 1995.

A Appendix

A.1 to Chapter 4

Table A-1 Semi-quantitative effect matrix of functions relevant to press processing of composites established from team discussion. Criticality = Active Sum x Passive Sum

	Store/eject matrix	Transfer tension to fibers	Attach carrier to laminate	Functionalize part surface	Generate vacuum tightness o. press stroke	Generate resin tightness	Transfer tension to carrier	Convey carrier material during drape	Active sum	Activity	Criticality
Store/eject matrix		2	2	2	0	1	2	1	10	2.00	50
Transfer tension to fibers	1		0	0	2	1	1	3	8	1.14	56
Attach carrier to laminate	0	0		3	0	0	0	0	3	0.60	15
Functionalize part surface	0	0	3		0	0	0	0	3	0.60	15
Generate vacuum tightness o. press stroke	0	2	0	0		2	2	2	8	0.89	72
Generate resin tightness	0	0	0	0	2		0	0	2	0.40	10
Transfer tension to carrier	2	1	0	0	3	0		3	9	1.80	45
Convey carrier material during drape	2	2	0	0	2	1	0		7	0.78	63
Passive sum	5	7	5	5	9	5	5	9			

Point definition: 0 = No effect; 1 = Weak effect; 2 = Medium effect; 3 = Strong, immediate effect

HACOTECH

Stand: 2009

Technisches Datenblatt / Technical Data Sheet

_____

C300BX
Biaxial-Carbongelege 300 g/m², 2.540 mm breit

Konstruktion	Flächengewicht g/m²	Toleranz + / - %	Material	tex
-45°	150	5	Tenax STS	24 K
+45°	150	5	Tenax STS	24 K
Nähfaden	6	5	PES 76 dtex hf	
Gesamt	**306**			

Stabilisierung in 0° (E-Glas 34tex) und 90° (E-Glas 68 tex)

Breite   2.540 mm

Rollenlänge   ca. 50 lfm

HANSEATIC COMPOSITES TECHNOLOGIES
HACOTECH GmbH, Randersweide 1, 21035 Hamburg   info@hacotech.com, www.hacotech.com

Figure A-1 Datasheet of fiber material C300BX from Hacotech

HUNTSMAN

Enriching lives through innovation

Advanced Materials

Araldite® LY 1564 / Resin XB 3585 / Hardener XB 3458*

WARM CURING EPOXY SYSTEM

Araldite® LY 1564 is a low viscosity epoxy resin
Resin XB 3585 is an epoxy resin
Hardener XB 3458 is an amine hardener

APPLICATIONS	Industrial composites		
PROPERTIES	High reactivity system for composite parts		
PROCESSING	• Wet lay-up • Resin Transfer Moulding		
PRODUCT DATA	**Araldite® LY 1564**		
	Aspect (visual)	clear liquid	
	Viscosity at 25 ℃ (ISO 12058-1)	1200 – 1400 **	[mPa s]
	Density at 25 ℃ (ISO 1675)	1.1 - 1.2	[g/cm³]
	Epoxy index (ISO 3001)	5.8 - 6.05 **	[Eq/kg]
	Resin XB 3585		
	Aspect (visual)	clear liquid	
	Viscosity at 25 ℃ (ISO 12058-1)	6500 – 9000 **	[mPa.s]
	Density at 25 ℃ (ISO 1675)	1.15 - 1.20	[g/cm³]
	Epoxy index (ISO 3001)	5.45 – 5.65**	[Eq/kg]
	Hardener XB 3458		
	Aspect (visual)	clear to slightly yellow / red liquid	
	Viscosity at 25 ℃ (ISO 12058-1)	190 – 250 **	[mPa.s]
	Density at 25 ℃ (ISO 1675)	0.98 - 1.02	[g/cm³]
	Amine value (ISO 9702)	17.0 – 17.8 **	[Eq/kg]

** Specified data are on a regular basis analysed. Data which is described in this document as 'typical' is not analysed on a regular basis and is given for information purposes only. Data values are not guaranteed or warranted unless if specifically mentioned.

STORAGE	Provided that Araldite® LY 1564, Resin XB 3585 or Hardener XB 3458 are stored in a dry place in their original, properly closed containers at the storage temperatures mentioned in the MSDS they will have the shelf lives indicated on the labels. Partly emptied containers should be closed immediately after use. Epoxy Resin XB 3585 which has crystallized and looks cloudy can be restored to its original state by heating to 60 - 80 ℃.

* In addition to the brand name product denomination may show different appendices, which allows us to differentiate between our production sites: e.g. BD = Germany, US = United States, IN = India,CI = China, etc. These appendices are in use on packaging, transport and invoicing documents. Generally the same specifications apply for all versions. Please address any additional need for clarification to the appropriate Huntsman contact.

Figure A-2 Datasheet of XB3585 (resin) and XB3458 (hardener) from Huntsman 1/2

HUNTSMAN
Enriching lives through innovation

TYPICAL SYSTEM DATA
PROCESSING DATA

MIX RATIO	Components		Parts by weight	Parts by volume
	Araldite® LY 1564		100	100
	Hardener XB 3458		20	24
	Resin XB 3585		100	100
	Hardener XB 3458		19	23

We recommend that the components are weighed with an accurate balance to prevent mixing inaccuracies which can affect the properties of the matrix system. The components should be mixed thoroughly to ensure homogeneity. It is important that the side and the bottom of the vessel are incorporated into the mixing process.

When processing large quantities of mixture the pot life will decrease due to exothermic reaction. It is advisable to divide large mixes into several smaller containers.

INITIAL MIX VISCOSITY (CONE-PLATE VISCOSIMETER)			LY 1564 XB 3458	XB 3585 XB 3458
	at 40 °C	[mPa.s]	450 - 550	220 - 320
	at 60 °C	[mPa.s]	100 - 160	50 - 110
	at 70 °C	[mPa.s]	40 - 70	30 - 60
	at 80 °C	[mPa.s]	30 - 60	20 - 50

POT LIFE (TECAM 100 G)			LY 1564 XB 3458	XB 3585 XB 3458
	at 23 °C	[min]	13 - 17	14 - 18

GEL TIME (HOT PLATE)			LY 1564 XB 3458	XB 3585 XB 3458
	at 40 °C	[min]	30 - 37	23 - 30
	at 50 °C	[min]	16 - 22	12 - 17
	at 60 °C	[min]	6 - 11	6 - 10
	at 70 °C	[min]	4 - 8	3 - 7
	at 80 °C	[min]	2 - 4	2 - 4
	at 100 °C	[min]	0.5 - 1.5	0.5 - 1.5

GELATION AT 28 °C (IN THIN LAYERS: 0.4-0.7 MM)			LY 1564 XB 3458	XB 3585 XB 3458
	Start	[min]	90 - 100	70 - 90
	End	[min]	95 - 125	95 - 125

The values shown are for small amounts of pure resin/hardener mix. In composite structures the gel time can differ significantly from the given values depending on the fibre content and the laminate thickness.

Figure A-3 Datasheet of XB3585 (resin) and XB3458 (hardener) from Huntsman 2/2

Richmond
Aircraft Products
TECHNICAL DATA

8/30/2006

STRETCH-VAC™ 250

Copolymer, Medium Temperature Bagging Film

DESCRIPTION:

STRETCH-VAC™ 250 is a highly conformable, light blue tinted copolymer bagging film. STRETCH-VAC™ 250 is designed for cures up to 250°F (121°C) and will remain soft and pliable.

APPLICATION:

STRETCH-VAC™ 250 is engineered for use with all standard 250°F (121°C) curing epoxy resin systems. It is particularly suited for de-bulking and hot compaction cycles where softness and elongation is essential. STRETCH-VAC™ 250 can be heat seamed to meet any custom shape requirements.
This film is not suited for use with polyester or vinyl ester resins.

MECHANICAL PROPERTIES	TYPICAL VALUES	
Tensile strength:	> 8000 PSI	562 kg/cm²
Elongation:	> 800 %	

THERMAL PROPERTIES	°F	°C
Maximum use temperature:	275	135
Melt point (DSC):	302	150

STRETCH-VAC™ 250 is available in sheeting and v-sheeting (centerfold) in standard roll sizes at:
.002" x 60" sheeting x 940'   .051mm x 1.52m sheeting x 286.5m
.002" x 60" v-sheeting (centerfold opens   .015mm x 1.52m v-sheeting (centerfold opens
to 120") x 470'   to 3.04m) x 143.3m

13503 Pumice Street, Norwalk, California 90650 · TEL 562-404-2440 · FAX 562-404-9011

-14-

Figure A-4 Datasheet of Stretch-Vac 250 from Richmond

Table A-2 Objectives measurement from benefit analysis in Section 4.5.2

| Objectives | | Unit | Fixed fibers | | | Non-fixed fibers | | Polymer films | | |
| | | | | | | | | Inelastic | Elastic | |
			Knob paper	Nap core	Tissue paper	Suction fleece	Peel ply	Polypropylene	Silicone	Polyurethane
Z11	Technological criteria									
Z111	Flexibility of carrier									
Z1111	Number of wrinkles	-	4	3	3	4	4	1	4	3
Z1112	Number of ruptures	-	1	2	4	2.5	3	4	4	4
Z112	Increased part weight by carrier	g	4.47	0.43	3.86	8.25	2.82	0.69	0.00	1.88
Z113	Transfer tension on fibers									
Z1131	Deviation of fiber angle	°	6.42	2	7.11	7.11	5.5	6.72	6.78	6.22
Z1132	Deviation from target geometry	%	16.2	14	10.3	6	8.7	9.3	7.5	7
Z114	Seal tool with carrier	points [0;4]	1	0	1	2	1	4	4	4
Z115	Storage/ejection of resin by carrier									
Z1151	Defined position of resin on carrier	points [0;4]	3	3	2	2	1	4	4	4
Z1152	Forming of cavities into carrier	points [0;4]	2	1	1	4	0	4	2	4
Z1153	Elimination of cavities	points [0;4]	2	1	3	3	1	2	2	4
Z12	Economic criteria									
Z121	Material costs	€	0.7	120	0.4	7	3	2	1	3
Z122	Processing costs	points [0;4]	0	0	0	0	0	4	4	4

Table A-3 Objectives values from benefit analysis in Section 4.5.2

| Objectives | | Global weighting factor | Max. points | Fixed fibers | | | Non-fixed fibers | | Polymer films | | |
| | | | | | | | | | Inelastic | Elastic | |
				Knob paper	Nap core	Tissue paper	Suction fleece	Peel ply	Polypropylene	Silicone	Polyurethane
Z11	Technical criteria	0.850	4	0.00	0.00	0.00	0.00	0.00	0.00	0.00	0.00
Z111	Flexibility of the carrier material	0.272	4	2.50	2.50	3.50	3.25	3.50	2.50	4.00	3.50
Z1111	Number of wrinkles	0.136	4	4.00	3.00	3.00	4.00	4.00	1.00	4.00	3.00
Z1112	Number of ruptures	0.136	4	1.00	2.00	4.00	2.50	3.00	4.00	4.00	4.00
Z112	Increased part weight by carrier	0.068	4	1.83	3.79	2.13	0.00	2.63	3.66	4.00	3.09
Z113	Transfer tension on fibers	0.247	4	1.28	1.43	2.03	2.88	3.29	2.46	2.78	3.20
Z1131	Deviation of fiber angle	0.123	4	2.56	2.00	1.75	1.75	3.65	2.21	2.14	2.80
Z1132	Deviation from target geometry	0.123	4	0.00	0.86	2.31	4.00	2.94	2.71	3.41	3.61
Z114	Seal tool with carrier	0.043	4	1.00	0.00	1.00	2.00	1.00	3.00	4.00	4.00
Z115	Storage/ejection of resin by carrier	0.221	4	2.33	1.67	2.00	3.00	0.67	3.33	2.67	4.00
Z1151	Defined position of resin on carrier	0.074	4	3.00	3.00	2.00	2.00	1.00	4.00	4.00	4.00
Z1152	Forming of cavities into carrier	0.074	4	2.00	1.00	1.00	4.00	0.00	4.00	2.00	4.00
Z1153	Elimination of cavities	0.074	4	2.00	1.00	3.00	3.00	1.00	2.00	2.00	4.00
Z12	Economic criteria	0.150	4	2.00	0.00	2.10	0.00	1.27	3.59	3.90	3.27
Z121	Material costs	0.120	4	4.00	0.00	4.19	0.00	2.54	3.17	3.81	2.54
Z122	Processing costs	0.030	4	0.00	0.00	0.00	0.00	0.00	4.00	4.00	4.00

Table A-4 Benefit values from benefit analysis in Section 4.5.2

| Objectives | | Global weighting factor | Max. points | Fixed fibers | | | Non-fixed fibers | | Polymer films | | |
| | | | | | | | | | Inelastic | Elastic | |
				Knob paper	Nap core	Tissue paper	Suction fleece	Peel ply	Polypropylene	Silicone	Polyurethane
Z11	Technological criteria	0.850	3.40	1.68	1.66	2.08	2.34	2.13	2.40	2.80	3.01
Z111	Flexibility of carrier	0.272	1.09	0.68	0.68	0.95	0.88	0.95	0.68	1.09	0.95
Z1111	Number of wrinkles	0.136	0.54	0.54	0.41	0.41	0.54	0.54	0.14	0.54	0.41
Z1112	Number of ruptures	0.136	0.54	0.14	0.27	0.54	0.34	0.41	0.54	0.54	0.54
Z112	Increased part weight by carrier	0.068	0.27	0.12	0.26	0.14	0.00	0.18	0.25	0.27	0.21
Z113	Transfer tension on fibers	0.247	0.99	0.32	0.35	0.50	0.71	0.81	0.61	0.68	0.79
Z1131	Deviation of fiber angle	0.123	0.49	0.32	0.25	0.22	0.22	0.45	0.27	0.26	0.35
Z1132	Deviation from target geometry	0.123	0.49	0.00	0.11	0.29	0.49	0.36	0.33	0.42	0.44
Z114	Seal tool with carrier	0.043	0.17	0.04	0.00	0.04	0.09	0.04	0.13	0.17	0.17
Z115	Storage/ejection of resin by carrier	0.221	0.88	0.52	0.37	0.44	0.66	0.15	0.74	0.59	0.88
Z1151	Defined position of resin on carrier	0.074	0.29	0.22	0.22	0.15	0.15	0.07	0.29	0.29	0.29
Z1152	Forming of cavities into carrier	0.074	0.29	0.15	0.07	0.07	0.29	0.00	0.29	0.15	0.29
Z1153	Elimination of cavities	0.074	0.29	0.15	0.07	0.22	0.22	0.07	0.15	0.15	0.29
Z12	Economic criteria	0.150	0.60	0.48	0.00	0.50	0.00	0.30	0.50	0.58	0.42
Z121	Material costs	0.120	0.48	0.48	0.00	0.50	0.00	0.30	0.38	0.46	0.30
Z122	Processing costs	0.030	0.12	0.00	0.00	0.00	0.00	0.00	0.12	0.12	0.12
Z1	**Overall evaluation**	**1.000**	**4.00**	**2.16**	**1.66**	**2.59**	**2.34**	**2.44**	**2.90**	**3.38**	**3.43**

A.2 to Chapter 5
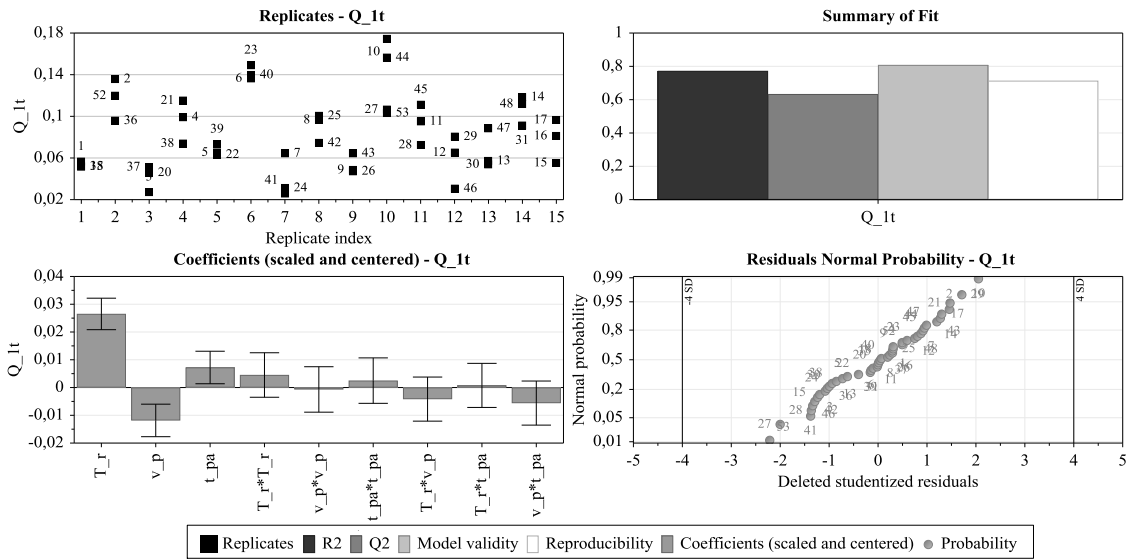
Figure A-5 Overview plot for areal share of fluorescence phase Q_{1t} for top side of WCM experiments
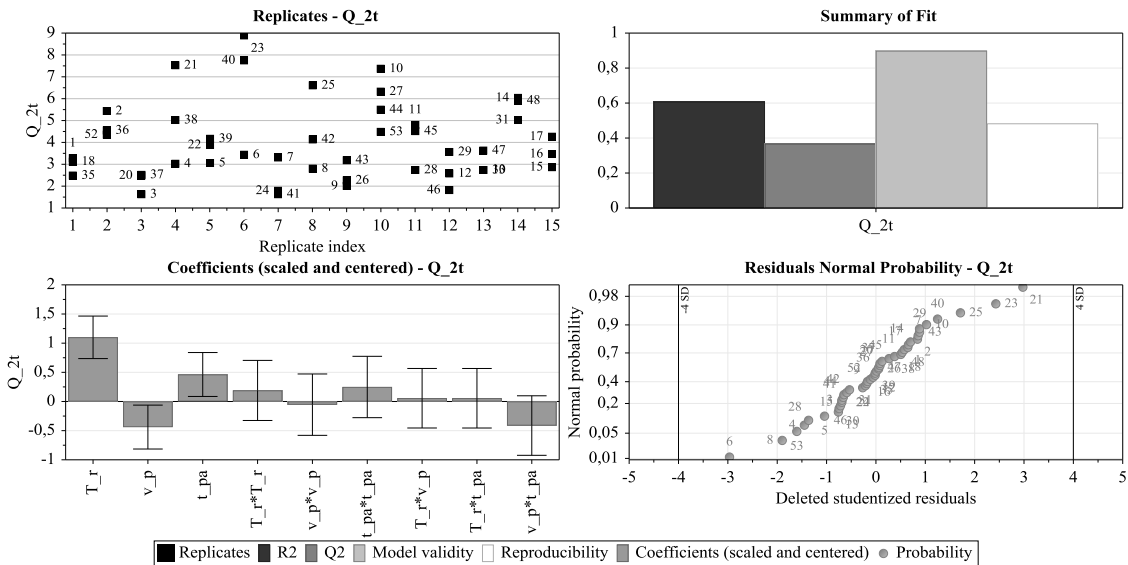

Figure A-6 Overview plot for edge length of fluorescence phase Q_{2t} for top side of WCM experiments

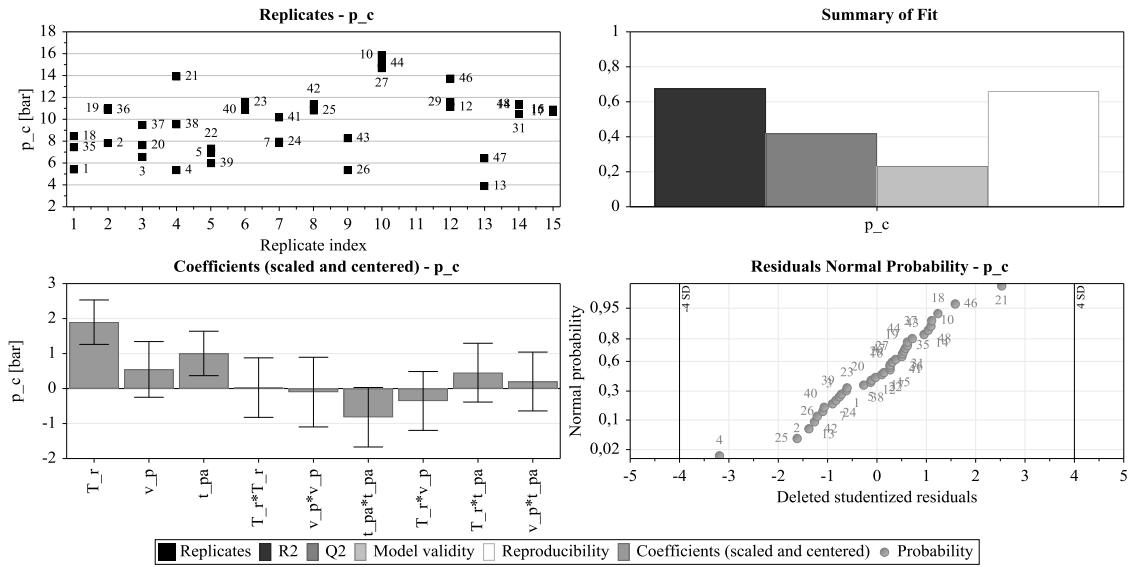**Figure A-7** Overview plot for cavity pressure p_c for WCM experiments
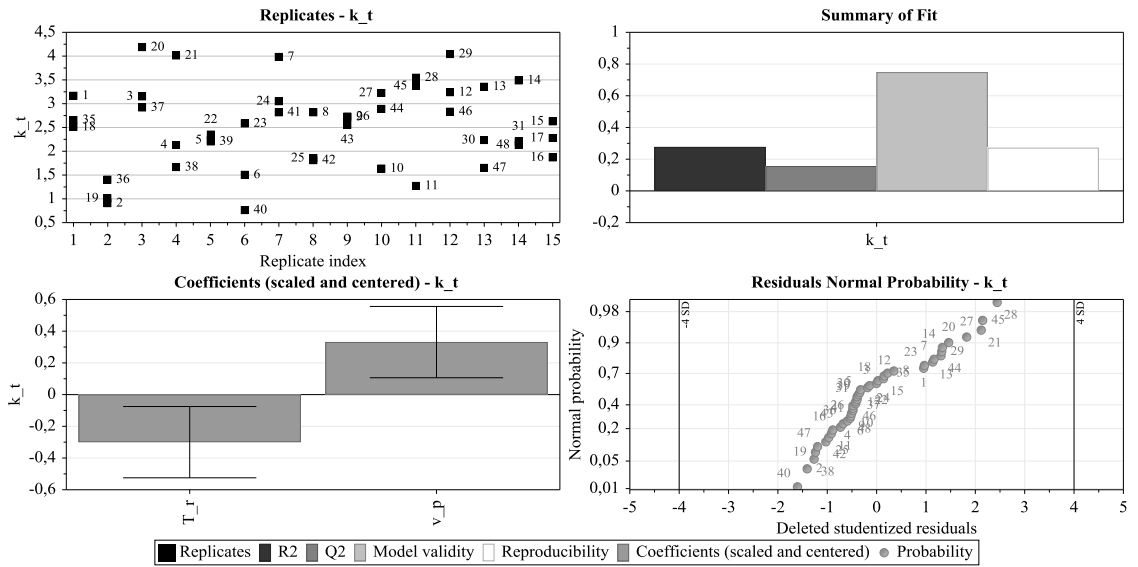
Figure A-8 Overview plot for kurtosis of fiber angle distribution $k_{\alpha t}$ for top side of WCM experiments
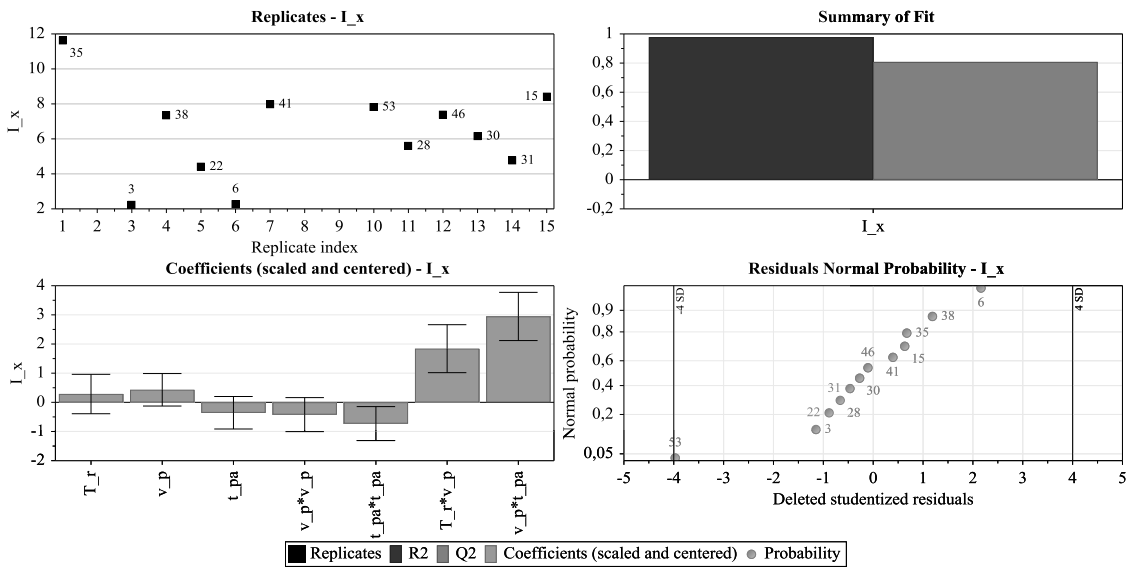
Figure A-9 Overview plot for integral of fluorescent phase in x-direction I_x for WCM experiments
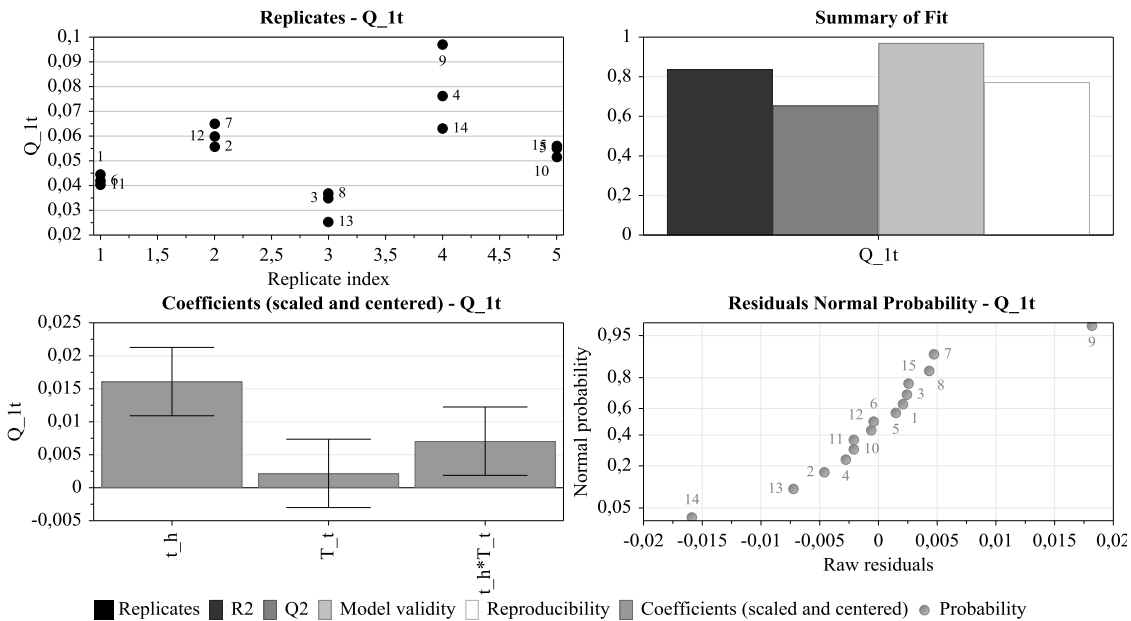
Figure A-10 Overview plot for areal share of fluorescence phase Q_{1t} for top side CIP experiments
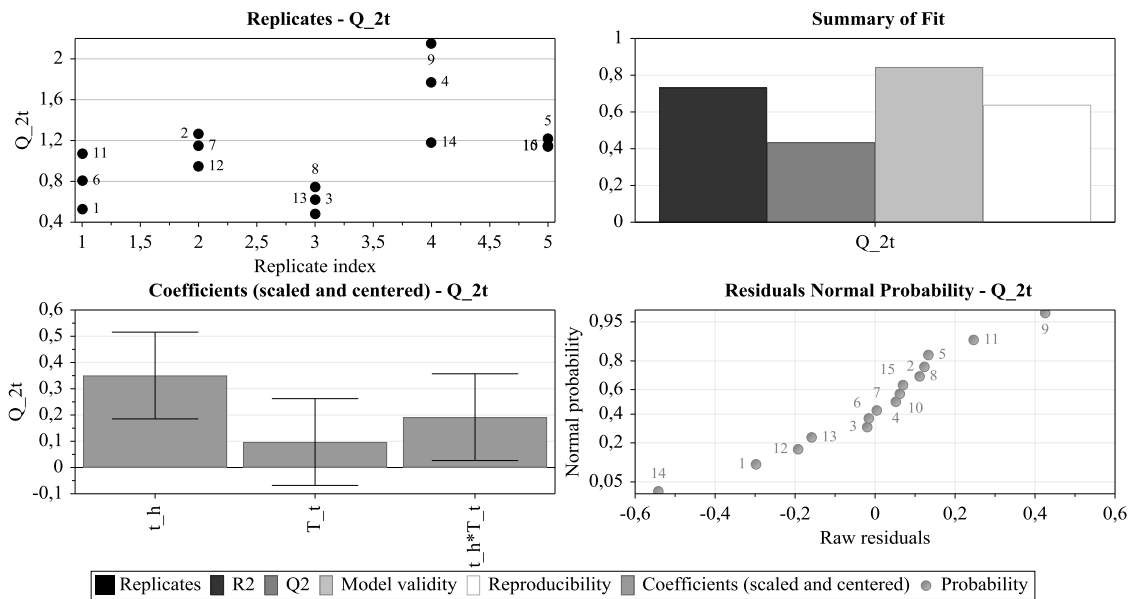
Figure A-11 Overview plot for relative fluorescent edge length Q_{2t} for top side of CIP experiments
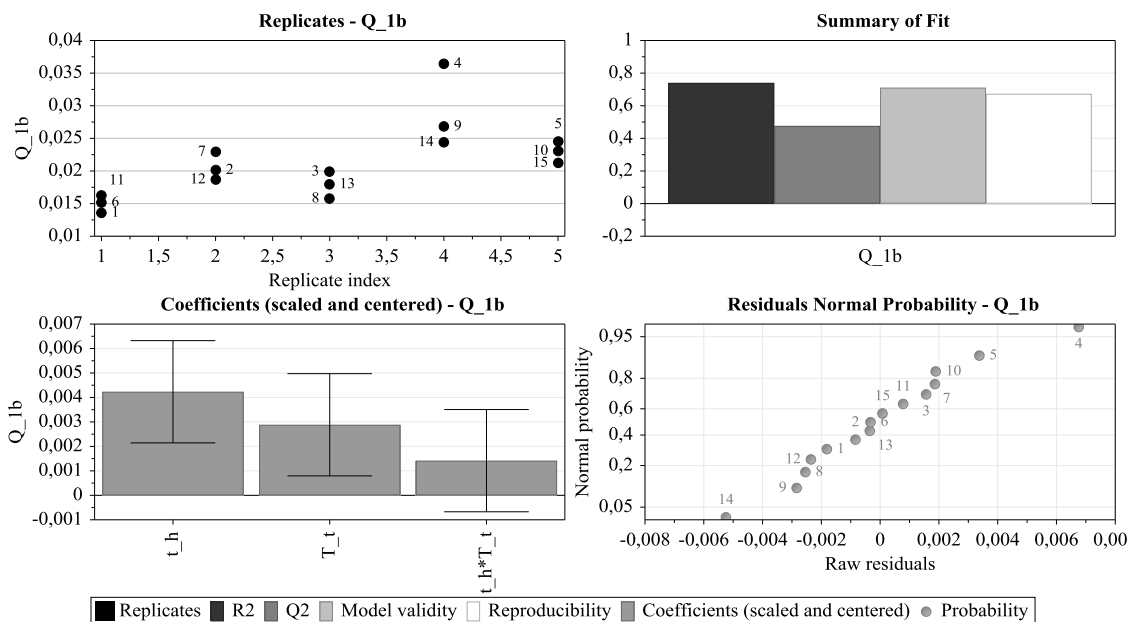
Figure A-12 Overview plot for areal share of fluorescence phase Q_{1b} for bottom side CIP experiments
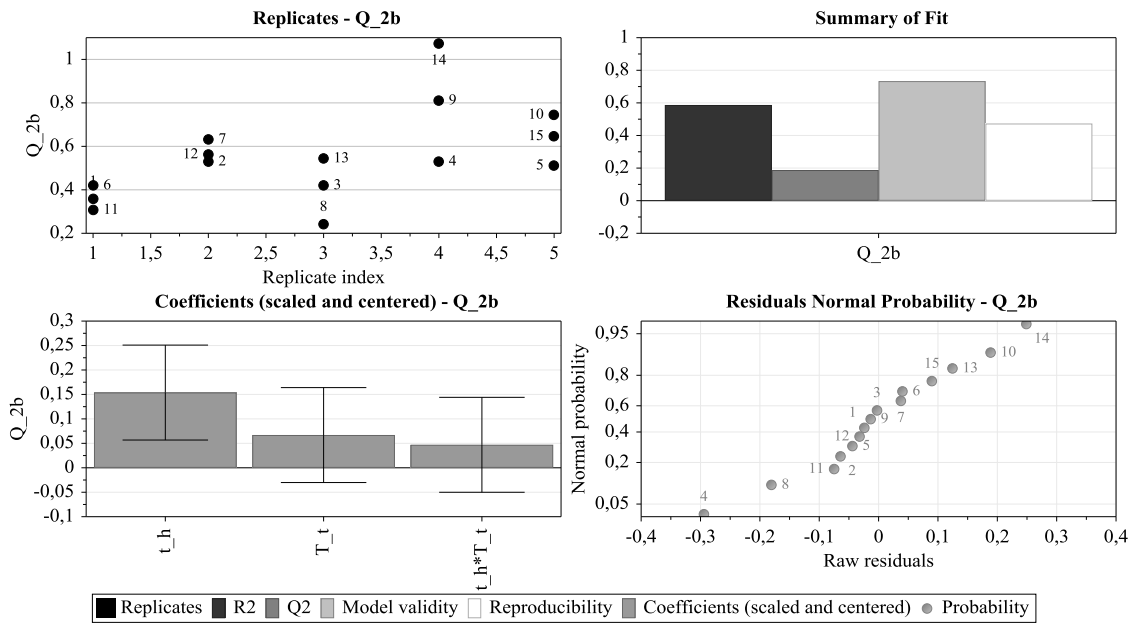
Figure A-13 Overview plot for relative fluorescent edge length Q_{2b} for bottom side of CIP experiments
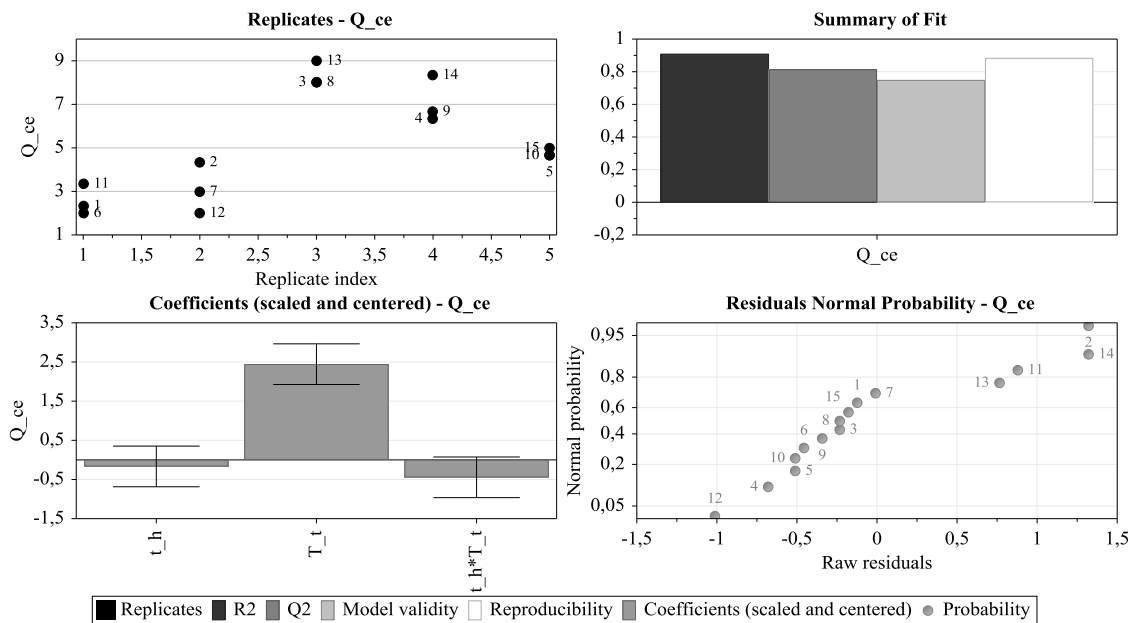
Figure A-14 Overview plot for evaluation of carrier cavitiy elimination Q_{ce} of CIP experiments
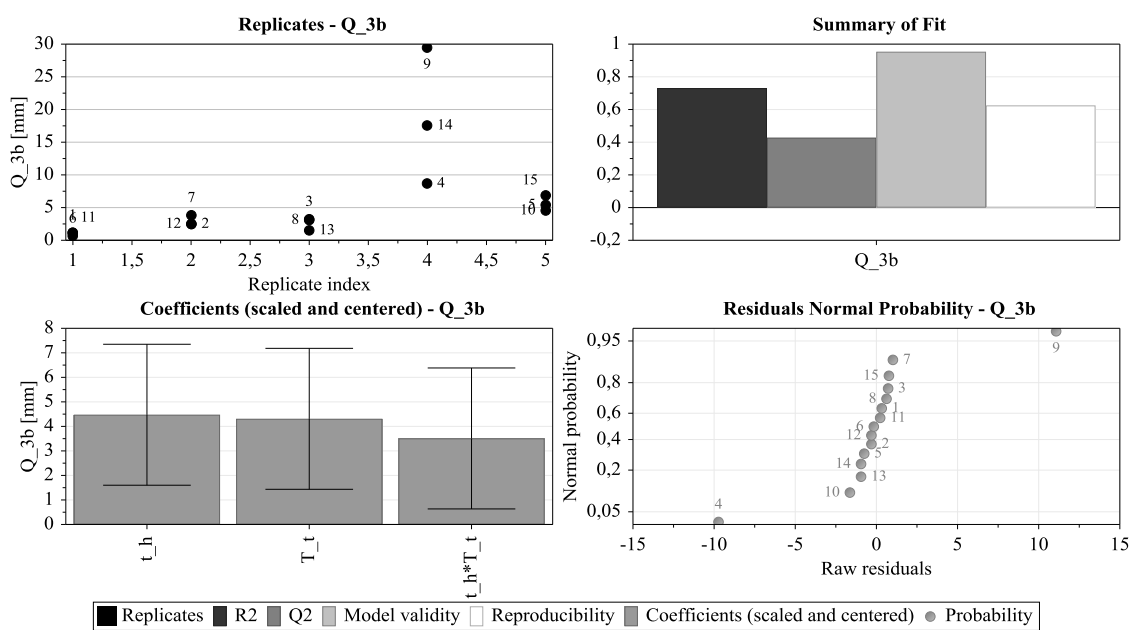
Figure A-15 Overview plot for centroid shift of fluorescent matrix Q_{3b} for bottom side of CIP experiments

Figure A-16 Quality parameters of manual material preparation from all DoE experiments for WCM (index W) and CIP (index C)

A.3 to Chapter 6

Table A-5 Calculation of material masses inside tool cavity

Design data	Value	Unit
Total volume of part cavity	9.08E-04	[m^3]
Volume of cavity filled with fibers	0.000763708	[m^3]

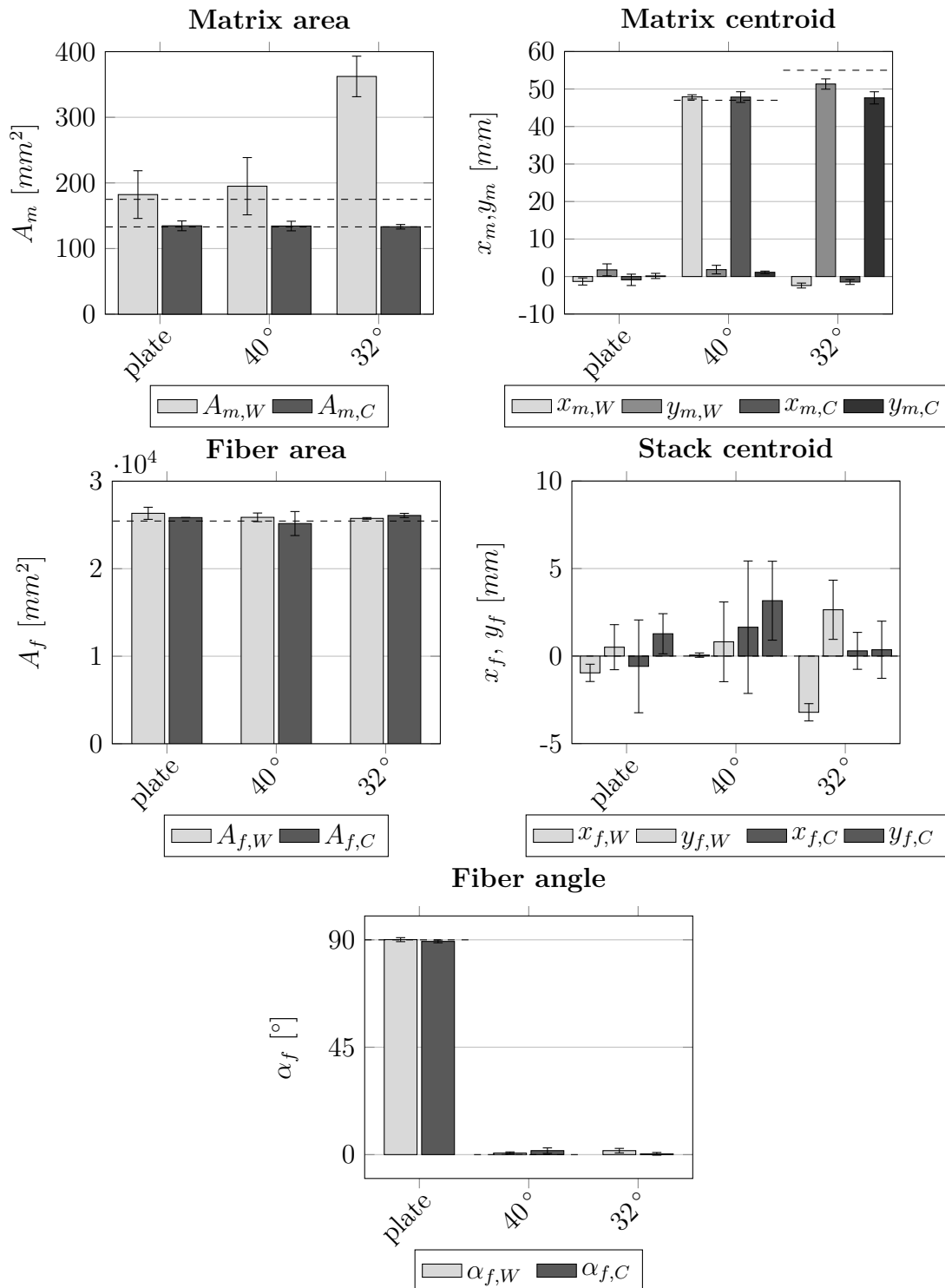| Material values	Value	Unit
Density of resin	1.17	[g/cm^3]
Density of carbon fibers	1.77	[g/cm^3]
Material	Carbon, NCF	[-]
Areal mass of NCF	300	[g/m^2]
Area of NCF cut-out	3.82E-01	[m^2]
Edge length of NCF cut-out	3.336637061	[m]
Thickness of carrier film	0.05	[mm]

Real amounts of materials	Value	Unit
Number of plies	6	[-]
Length of NCF cut-out, x-direction	0.64	[m]
Length of NCF cut-out, y-direction	0.6	[m]
Volume of fiber material	3.88E-04	[m^3]
Mass of fiber material	6.87E+02	[g]
Fiber volume content	0.508475	-
Volume of resin to wet fibers	3.75E-04	[m^3]
Mass of resin to wet fibers	439.20	[g]
Volume of resin to fill circumference	1.45E-04	[m^3]
Mass of resin to fill circumference	169.3	[g]
Total volume of resin	608.53	[g]
Total mass of resin	0.000520109	[m^3]
Total material mass	1295.86	[g]

NCF cut-out
Y 600 x 640 mm **X**

Area of fibers/resin
Circumference (no fibers)

Total part volume 908.4 cm³

X **Y**
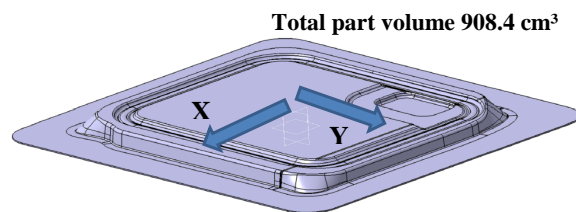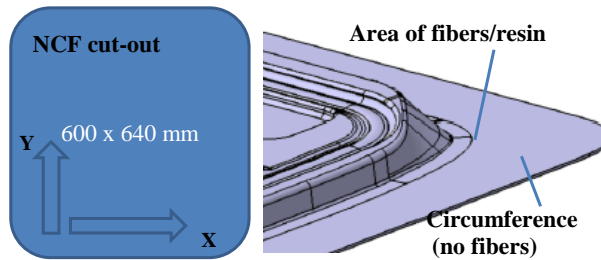
Table A-6 Carrier layout in reference to Table A-5

Geometry of single cavity (sc)	Value	Unit
Radius top r_0	13	[mm]
Depth h	12	[mm]
Radius bottom r_1	10	[mm]

Resin stored in single cavity (sc)	Value	Unit
Volume theoretically V_sc	5.013981875	[cm³]
Mass theoretically m_sc	5.866358794	[g]

Film spring back after thermoforming	Value	Unit
	0.5	[-]

Aggregated cavities	Value	Unit
Minimum amount from mass in CAD model	208	[-]
Number of cavities in x-direction	15	[-]
Number of cavities in y-direction	17	[-]
Total number of cavities	255	[-]
Total mass of resin	747.9607462	[g]
Minimum total mass of resin	608.53	[g]

Cavity distribution on carrier	Value	Unit
Length covered by fiber material, x-direction	600	[mm]
Length covered by fiber material, y-direction	640	[mm]
-10 % tensioning compensation of film, x	540	[mm]
-10 % tensioning compensation of film, y	576	[mm]
Width of bridge, x-direction	10	[mm]
Width of bridge, y-direction	7.88	[mm]

r_0
V
h
r_1

$$V = \frac{h \cdot \pi}{12} \cdot (D^2 + d^2 + D \cdot d)$$

1 mm chamfering

Length covered by cavities

Width of bridge

Y **X**
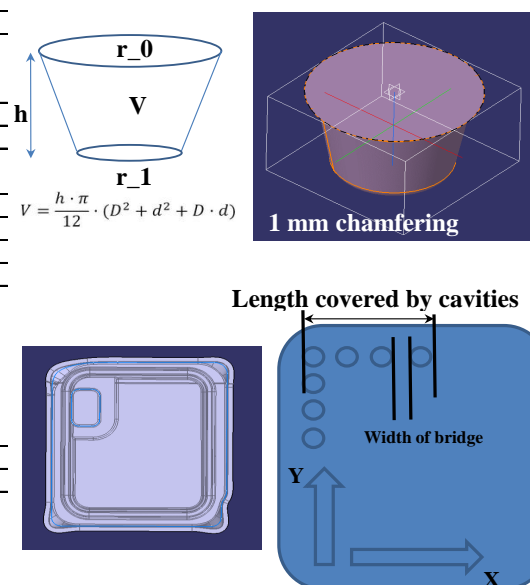
A.4 to Chapter 7

Figure A-17 Functional model of the RTM process after general function definition from Figure 7-1

MATRIX

F3

Resin

Hardener

Heat resin

Mix matrix

Apply matrix

FIBERS

F1

Cut plies

Fibers

F2

Position stack

Finished part

Stack + matrix

Legend

Function #

F

Material flow

Function description

Changed material status

F16

Place part in stock

F9

Place stack+matrix in press

MOLD

F7

Prepare press and mold

F15

Trim part

F10.1

Close mold

F10

F14

Remove part from cooling mold

F10.2

Hold mold closed

F13

Set part in cooling mold

F10.5

Open mold

F12

Place part in cooling mold

F11

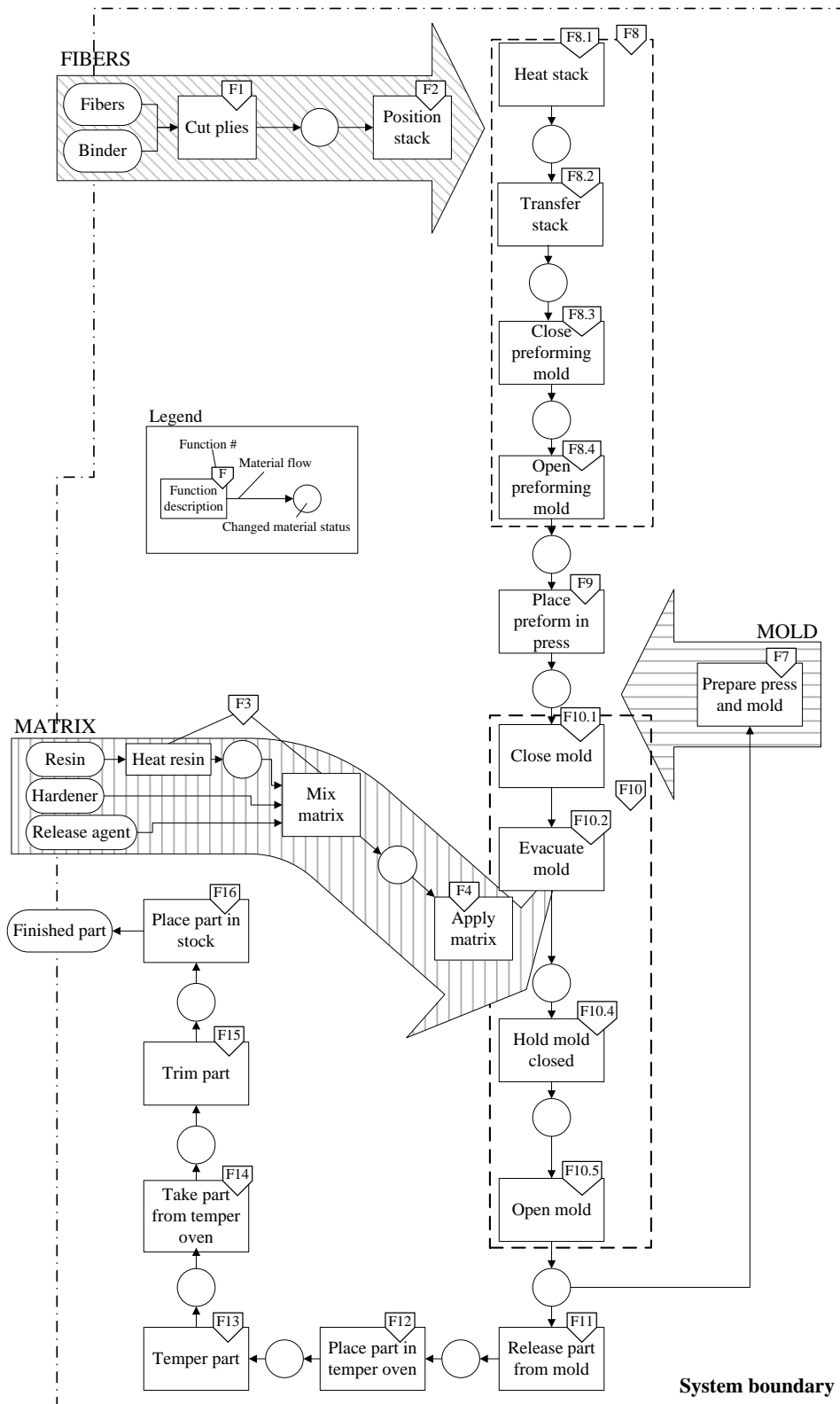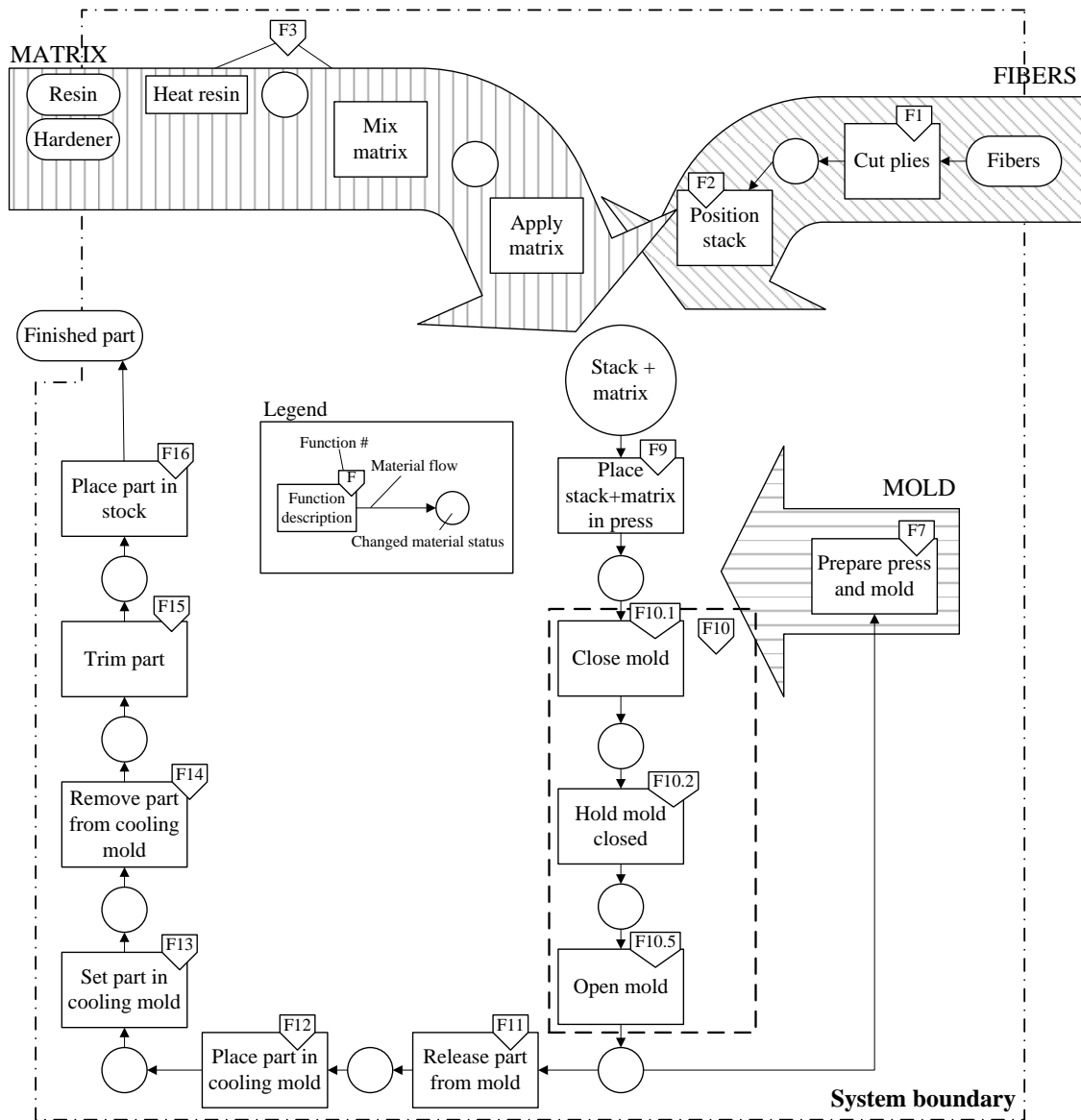Release part from mold

System boundary

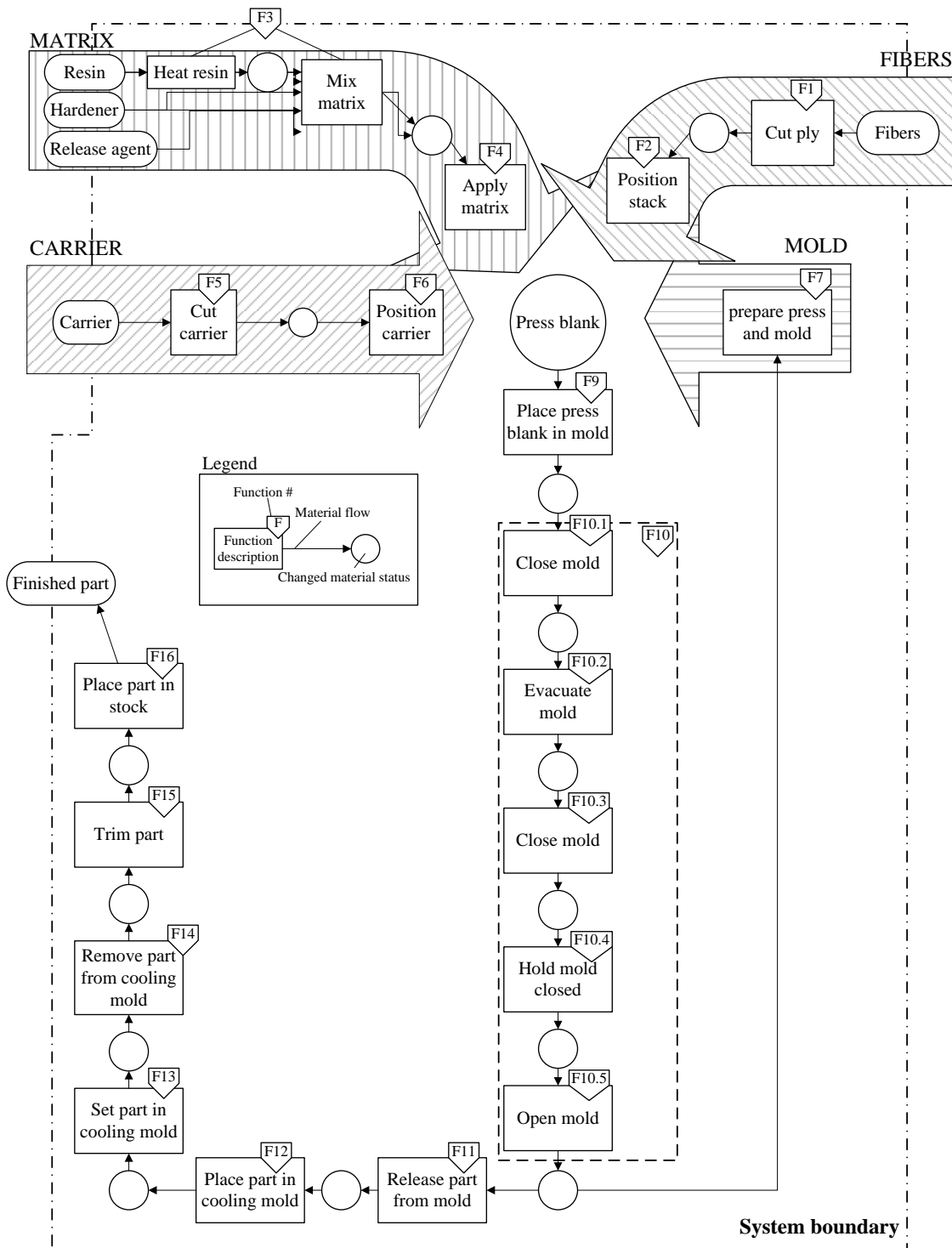**Figure A-18** Functional model of the WCM process after general function definition from Figure 7-1

Figure A-19 Functional model of the CIP process after general function definition from Figure 7-1

Table A-7 Process parameters of experiments and derived assumptions for industrial processes used for LCA and LCC

Process parameter	Unit	RTM	WCM	CIP	Function
Resin temperature	[°C]	85	42	42	F3
Hardener temperature	[°C]	26	26	26	F3
Applied matrix mass	[g]	400	55.52	55.52	F4
Tool temperature	[°C]	85	100*/128**	100*/128**	F10
Total press stroke	[mm]	500	500	500	F10
Mold pre-closing velocity	[mm/s]	-	5*/250**	5*/250**	F10.1
Mold closing velocity	[mm/s]	30	5	5	F10.3
Max. cavity pressure	[bar]	25*/150**	14.57*/50**	10.33*/50**	F10.4
Mold opening velocity	[mm/s]	300	250	250	F10.5

*Experiments; **Assumptions for industrial equipment from Fais (2011), Zirn (2014)

Table A-8 Times to perform functions in experiments (measured) and derived assumptions for industrial processes used for LCA and LCC

Process		Time to perform							Cycle time
		F2+F4+F9	F7	F10.1	F10.2	F10.3	F10.4	F10.5	F12	F7+F9+F10+F12
						[s]				
Experiments	RTM	120 (F4); 4 (F9)	-	-	15	10	370.66	10	3	397
	WCM	75.5	-	11.17	15.8	9.2	133	11	3	193
	CIP	92.75	-	11.75	14.71	9.43	133	11	3	193
Industrial*	RTM	120 (F4); 4 (F9)	10	2.77	5	-	370.66	1.57	3	397
	WCM	75.5; 4 (F9)	10	1.9	20.53	6	133	1.57	3	180
	CIP	92.75; 4 (F9)	10	1.9	20.53	6	133	1.57	3	180

*Assumtions for industrial equipment from Fais (2011), Zirn (2014)
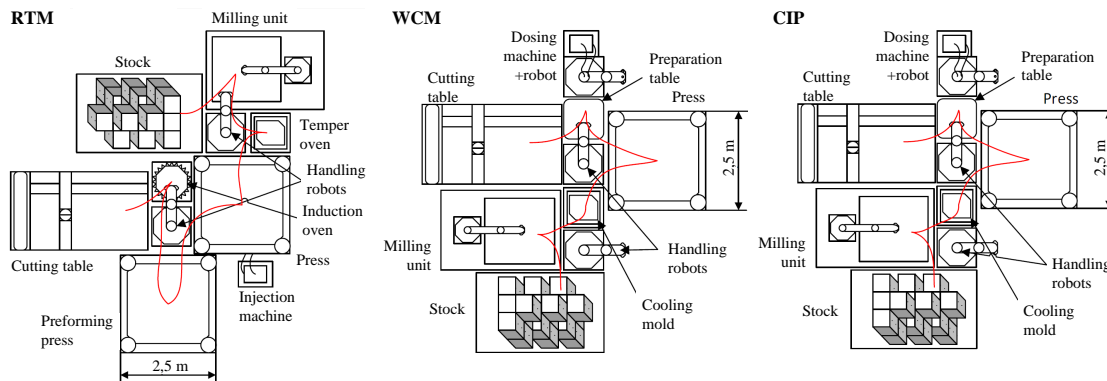
Figure A-20 Process-flow simulation chart for production layout of RTM, WCM and CIP

Table A-9 Labor costs per year in South Bavaria. Reference "Other surcharges" includes extras like work clothes and training courses

Reference	Value*
Monthly income [€]	2482
Annual income [€]	29784
Christmas bonus [€]	1241
Vacation bonus [€]	992.8
Contributions for pension schemes [€]	319.08
Employer's social security contributions [€]	6249.1
Company pension scheme [€]	1191.36
Other surcharges [€]	2233.8
Total costs [€]	42011.14

* After collective labor agreement of South Bavaria for for metal and electrical industry from www.igmetall.de

Table A-10 Life cycle inventory data for all RTM, WCM and CIP

Function	Type	Flow	RTM	WCM	CIP	References / Assumptions
	Energy [MJ]	In	0.238	0.243	0.221	
F1	Fibers [kg]	In	0.8597	0.91	0.716	Zünd G3 XL[1] / Table 2
	Fiber scrap [kg]	Out	0.0642	0.0657	0.060	
F2	Energy [MJ]	In	0.005	0.005	0.005	8 s actuation of robot[2]
	Energy [MJ]	In	4.76	1.44	1.44	Dosing machines[3]
	Matrix [kg]	In	0.425	0.5122	0.599	Material input data
F3	Matrix waste [kg]	Out	0	0.059	0.025	Material input data; Nozzle[3]
	Release agent [kg]	In	0.011	0.013	0.015	3 % of resin mass
	Aceton [kg]	In	0	0.126	0.054	3 flushings with nozzle[3]
	Compressed air [nm³]	In	0	0.336	0.336	3 flushings with nozzle[3, 4]
F4	Energy [MJ]	In	0	0.01	0.011	Robot[2] driven acc. function times
	Energy [MJ]	In	0	0	0.114	
F5	Carrier [kg]	In	0	0	4.33E-06	Zünd G3 XL[1]
	Carrier scrap [kg]	Out	0	0	1.556E-07	
F6	Energy [MJ]	In	0	0	0.007	Robot[2], 8 s actuation, 4 s clamp
F7	Energy [MJ]	In	0	0	0	Manual preparation[5]
	Compressed air [nm³]	In	0.533	0.533	0.533	
F8	Energy [MJ]	In	2.291	0	0	Press preforming[6]
	Fiber scrap [kg]	Out	0.190	0	0	
F9	Energy [MJ]	In	0.005	0.005	0.005	8 s actuation of robot[2]
F10	Energy [MJ]	In	9.7	3.8	4	Tool actuation and heating[6]
F11	Compres. air [nm³]	In	0.014	0.014	0.014	Pneumatic stamps[7]
F12	Energy [MJ]	In	0.004	0.004	0.004	6 s actuation of robot[2]
F13	Energy [MJ]	In	2.194	0.624	0.624	Setting tools[8], temper oven
F14	Energy [MJ]	In	0.005	0.005	0.005	8 s actuation of robot[2]
	Energy [MJ]	In	0.714	0.714	0.714	
F15	Fiber scrap [kg]	Out	0.0384	0.2775	0.075	Part trimming[9]
	Matrix scrap [kg]	Out	0.0583	0.0862	0.221	
	Carrier scrap [kg]	Out	0	0	2.136E-06	
F16	Energy [MJ]	In	0.005	0.005	0.005	6 s actuation of robot[2]

Technical data for [1] obtained from email from Rebstock Consulting GmbH; cutting speed assumed to 200 mm/s based on trials. Scrap estimated to be 10 mm surcharge from stack dimensions; [2] from email from ABB for IRB 1600-10/1.45. [3]Energy demand for machines estimated with average power rating of 8 kW for dosing machine for WCM and CIP driven for 180 s amd of 12 kW for injection machine for RTM driven for 397 s, nozzle geometry obtained from www.tartler.com, volume of 0.031 dm³, static mixer volume estimated to 0.023 dm³ in trials; [4]320 L/min from compr. air gun EB-13112 from www.kindustrie.com (accessed 2015-07-28) ; [5]Manual preparation for 10 s as measured from BMW roof production in www.youtube.com/watch?v=qZrOxQ1V6bQ (accessed 2015-07-28); Press preforming moddeled after Sorg (2015), where binder activation at 160 deg C after 30 s in an 1.4 kVA induction oven after industrial expert. Preforming on press with 175 t and 22 kVA actuating power after Sorg (2015), with 200 mm/s actuation velocity and 500 mm stroke; [6]Heating power for tools calculated for 0.319 m² projected tool surface and 128 °C for WCM/CIP and 85 °C for RTM after unpublished results for industrial tool heating and curing layout. Actuation energy from data from email correspondence with Maschinenfabrik Lauffer GmbH & Co. KG for industrial press with 22 kW power and use of support pump with 5.5 kW power during closed state. Energy demand for presses is calculated as proportional to press force with cavity pressures for RTM of 150 bar and for WCM/CIP of 50 bar after Zirn (2014). Driving speeds of 700 mm/s for pre-closing and 70 mm/s for the last 30 mm in WCM and CIP after Zirn (2014). Pneumatic stamps demold part through use of 2.01 L air volume at 7 bar, 50 cm² stamp surface, 8 stamps and 50 mm stroke; [8]Heating energy for setting mold for CIP/WCM at 50 °C and projected surface of 0.319 m² after unpublished results for industrial tool heating. Actuation energy calculated via linear actuators LM80-V from http://www.thomsonlinear.com (last accessed 2015-07-28) with a velocity of 100 mm/s, 800 N and stroke of 500 mm for setting tools for WCM and CIP, RTM part tempered in industrial oven at 115 °C for 397 s; [9]Milling cell with robot equipped with high-speed cutting (HSC) spindle and PKD-ZS-0800-8-100-0150-50 cutter from shop.vhf.de (accessed on 2015-07-28). Process runs with 800 m/min cutting speed, 31000 rpm, 0.02 mm width per revolution from Teti (2002) and a feeding speed of 21.2 mm/s. In experiments for prototype production, 2700 mm trimming length from Table 2 are obtained. Spindle power is 5 kVA and robot use from [2] is assumed.

Table A-11 Inventory data for Life cycle costing for RTM, WCM and CIP with respect to produced volumes (RTM: 27 155 ppa; WCM/CIP: 59 892 ppa), depreation period of five years and interest rate of 7 %

Reference/Function	Costs [€]
Cutting table[1] (F1, F5)	15000
Dosing/injection machine[2] (F3)	100000 (RTM), 50000 (WCM, CIP)
Induction oven[3] (F8)	30000
Preforming press+tooling[4] (F8)	186000 + 35000
Main press+tooling[5] (F10)	186000 + 70000 (CIP)/60000 (WCM); 533000 + 70000 (RTM)
Cooling mold[6], temper oven[7] (F13)	35000 (WCM, CIP); 60000 (RTM)
Milling unit[8] (F15)	100000
Robot[9] (F2, 4, 6, 9, 12, 14, 16)	40000

[1]15000 € for Zünd G3 XL after personal interviews;[2]100000 for 3-component low pressure dosing machine and dosing head for RTM and 50000 € for respective dosing machine for WCM/CIP from quotes obtained 07/2009, mixing is performed by static mixer with aceton cleaning;[3]After interviews with experts on preforming processes, 30000 € is assumed for an induction oven;[4]Preforming press (175t after Sorg (2015)) for 186000 € and preforming tool for 35000 € according to expert interview;[5]For WCM/CIP press (175t) 186000 € and for RTM press (500t) 533000 € is assumed from quotes obtained 07/2009 with prices scaled according to tonnage needed due to cavity pressure. Tooling is assumed to cost 70000 € for CIP and RTM and 60000 € for WCM from quotes received 09/2015;[6]Aluminum setting mold with pressure cylinders is assumed to cost 35000 €;[7]Temper oven with 120 kW heating power is assumed to cost 60000 € after a quote of an industrial oven obtained 07/2009;[8]Completely housed and ventilated milling unit with robot is estimated to cost 100000 €; [9]Acc. to price list for IRB 1600-10/1.45 industrial robot from ABB

B Publications

Printed Publications

[P1] P. Bockelmann, D. Häffelin, K. Drechsler, "B72195 WO2014075812A1: Method for producing a component from a fibre composite material, pressing blank therefor and component", *Patent*, 2014.

[P2] P. Bockelmann, K. Drechsler, A. Chakrabarti, "Research on Development of Liquid Composite Molding Parts: Situation & Framework", *ICoRD'15 Research into Design Across Boundaries; Smart Innovation, Systems and Technology*, vol. 2, pp. 495 – 505, 2016.

[P3] P. Bockelmann, K. Drechsler, "Produktentwicklung mit Neuen Materialien am Beispiel der Carbon Composites", *Handbuch Produktentwicklung, Ed. U. Lindemann, Hanser*, vol. 2, pp. 877 – 904, 2016.

Conferences and Talks

[C1] P. Bockelmann, D. Häffelin, K. Drechsler, "Carrier-Integrated Pressing: An Alternative Impregnation Process for Automated Processing of Thermoset Continueous Fiber-Reinforced Laminates", *2nd International Symposium on Automated Composites Manufacturing*, 2015.

[C2] P. Bockelmann, E. Ladstätter, "A Case from Germany: How and Why Cooperation can Promote Composite Manufacturing", *German CFRP Composite Latest Technology Movement, Nagoya University, Japan*, 2015.

[C3] P. Bockelmann, J. Maierhofer, J. Krollmann, S. Zaremba, K. Drechsler, P. Mertiny, "Resin Flow in Compression Molding Processes", *17th European Conference on Composite Materials ECCM17*, 2016.

C Supervised student theses

[S1]   C. Wechselberger, "Development of a novel press process for the production of composite parts", Term paper, 2013.

[S2]   F. Weikl, "Werkzeugentwicklung für einen neuartigen Pressprozess zur automatisierten Faserverbundverarbeitung", Bachelor thesis, 2013.

[S3]   A. Nieratschker, "Experimental Characterization of Materials for Carrier-Integrated Pressing in Automated Composite Manufacturing", Term paper, 2015.

[S4]   M. Listl, "Setting up and balancing of competitive production lines for carbon fiber composites manufacturing", Bachelor thesis, 2015.

[S5]   J. Maierhofer, "Entwicklung und Anwendung einer makroskopischen Analysemethode zur Charakterisierung des Harzflusses in Nasspressverfahren", Student thesis, 2015.

[S6]   F. Krause, "Harzflussanalyse in Abhängigkeit von Prozess und Parameterkombination innerhalb eines statistischen Versuchsplanes", Student thesis, 2016.

[S7]   A. Sodji, "Simulative Untersuchung des Drapierverhaltens unfixierter, trockener Fasertextilien im Trägerintegrierten Pressen", Master thesis, 2016.

Eidesstattliche Erklärung

Ich erkläre hiermit ehrenwörtlich, dass ich die vorliegende Arbeit selbstständig und ohne Benutzung anderer als der angegebenen Hilfsmittel angefertigt habe; die aus fremden Quellen (einschließlich elektronischer Quellen) direkt oder indirekt übernommenen Gedanken sind ausnahmslos als solche kenntlich gemacht.

Die Arbeit wurde in gleicher oder ähnlicher Form noch keiner anderen Prüfungsbehörde vorgelegt.

....
Ort, Datum

....
Unterschrift